Control of the Heart by Neurones of the Dorsal Motor Nucleus of the Vagus Nerve (DVMN) in Health and Disease

By

Asif Machhada*†

Supervised by

Professor Alexander V Gourine*

Professor Mark F Lythgoe†

& Doctor Daniel Stuckey†

*Centre for Cardiovascular and Metabolic Neuroscience, Department of Neuroscience, Physiology and Pharmacology, Division of Biosciences

†UCL Centre for Advanced Biomedical Imaging,
Division of Medicine

Submitted for a Doctorate of Philosophy in Cardiovascular Neuroscience with Medical Physics

UNIVERSITY COLLEGE LONDON

Declaration

I, Asif Machhada confirm that the work presented in this thesis is my own. Where information has been derived from other sources, I confirm that this has been indicated in the thesis.

Asif Machhada

28/08/2015

Abstract

The strength, functional significance and origins of parasympathetic (vagal) control of left ventricular function remain controversial. Experimental studies conducted on rats and mice using methods of genetic neuronal targeting, functional neuroanatomical mapping, and pharmaco- and optogenetics were employed to test the hypothesis that parasympathetic control of the left ventricle is provided by vagal preganglionic neurones of the dorsal motor nucleus (DVMN). The results of the experiments described in this thesis suggest that (i) activity of the DVMN vagal preganglionic neurones are responsible for tonic parasympathetic control of ventricular excitability, likely to be mediated by nitric oxide; (ii) synuclein deficiency (a model relevant to Parkinson's disease) results in a reduction in the activity of the DVMN neurones affecting the electrophysiological properties of the ventricle; (iii) tonic muscarinic influence on left ventricular contractility is provided by a subpopulation of vagal preganglionic neurones located in the caudal region of the left DVMN; (iv) reduced activity of the DVMN neurones is associated with a severely compromised aerobic exercise capacity; (v) increased activity of the DVMN neurones improves left ventricular performance and exercise capacity; and (vi) recruitment of the DVMN activity is sufficient to preserve exercise capacity and left ventricular function in heart failure developing after a myocardial infarction. These findings provide the first insight into the central nervous substrate that underlies functional parasympathetic innervation of the ventricles and highlight its importance in controlling cardiac function. The data obtained suggest that the DVMN neuronal projections provide tonic restraining influence on the ventricular arrhythmic potential and contractility, and have a trophic effect maintaining the ability of the heart to mount an appropriate inotropic response during exercise. As such, DVMN activity has a significant beneficial effect on the healthy left ventricle as well as ventricular myocardium compromised by occlusion of a major coronary artery.

Acknowledgements

I would first and foremost like to thank my principal supervisor Professor Alexander V. Gourine for his invaluable support and guidance, especially with genetic targeting of the DVMN. I am also grateful to Professor Mark F. Lythgoe and Dr. Daniel Stuckey for their supervision and for the opportunity to expand my physiological investigations with medical imaging.

I would like to thank Dr. Svetlana Mastitskaya, who performed many procedures with me to establish a protocol for myocardial infarction and whose early work on the DVMN mediation of remote preconditioning formed the basis of many of my hypotheses. My gratitude also extends to the collaborating labs of Professor Andrew Tobin for breeding of the M_3 knock-in mice, Dr. Stefan Trapp for the electrophysiological recordings of the DVMN and of Dr. Gareth Ackland, who provided me with immunoblots to better understand the underlying molecular mechanisms. Finally, I would like to thank Professor Andrew Ramage, Dr. Nephtali Marina and Dr. Patrick Hosford for their guidance and support.

Publications

Machhada A, Sanchez J, Whittle J, Gutierrez AA, Stephens RCM, Stuckey D, Bradley S, Kasparov S, Tobin AR, Gourine AV & Ackland GL. Parasympathetic regulation of PKD1 glucose uptake in skeletal muscle regulates exercise capacity through the muscarinic M3 receptor. In Submission.

Machhada A, Mastitskaya S, Hosford P, Stuckey DJ, Lythgoe MF, & Gourine AV. Optogenetic targeting of unmyelinated vagal efferents in heart failure. In Submission.

*Harrison IF, ***Machhada A,** *Colgan N, Lythgoe MF, Ozama I, O'Callaghan J, Holmes HE, Wells J, Murray T, Ahmed Z, Johnson RA, Collins EC, O'Neill MJ, Gourine AV Lythgoe MF. Glymphatic Clearance Impaired in a Mouse Model of Tauopathy: Captured Using Contrast-Enhanced MRI. In Submission.

Ackland GL, Whittle J, Toner A, Gutierrez AA. Sanchez J, **Machhada A**, Stephens RCM, Reddy S, Dyson A, Sneyd R, Struthers R, Minto G Singer M, Shah A & Gourine AV. (2015). Impaired baroreflex sensitivity induces Nox-2 mediated cardiac dysfunction through over-expression of GRK2. *Critical Care Medicine* In Press.

Machhada A, Marina N, Stuckey DJ, Lythgoe MF, & Gourine AV. (2015). Origins of the vagal drive controlling left ventricular contractility. *The Journal of Physiology* In Press.

Machhada A, Gourine AV, Ackland GL. (2015). Vagal modulation of atrial fibrillation. *Journal of the American College of Cardiology* 66**,** 977-978.

Machhada A, Ang R, Ackland GL, Ninkina N, Buchman VL, Lythgoe MF, Trapp S, Tinker A, Marina N & Gourine AV. (2015). Control of ventricular excitability by neurons of the dorsal motor nucleus of the vagus nerve. *Heart Rhythm* 12, 2285-93.

Marina N, Ang R, **Machhada A,** Kasymov V, Karagiannis A, Hosford PS, Mosienko V, Teschemacher AG, Vihko P, Paton JF, Kasparov S & Gourine AV. (2015). Brainstem hypoxia contributes to the development of hypertension in the spontaneously hypertensive rat. *Hypertension* 65, 775-783.

Deas E, Piipari K, **Machhada A,** Li A, Gutierrez-del-Arroyo A, Withers DJ & Abramov AY. (2014). PINK1 deficiency in β-cells increases basal insulin secretion and improves glucose tolerance in mice. *Open biology* 4, 140051.

Conference proceedings

Machhada A, Lythgoe MF, & Gourine AV. (2015). Using high resolution ultrasound to assess direct parasympathetic control of ventricular contractility: A comparison with a pressure-clamped model. *Proceedings of The World Molecular Imaging Congress*.

*Machhada A, *Harrison IF, *Colgan N, Lythgoe MF, Ozama I, O'Callaghan J, Holmes HE, Wells J, Murray T, Ahmed Z, Johnson RA, Collins EC, O'Neill MJ, Gourine AV Lythgoe MF. (2015). Glymphatic Clearance Impaired in a Mouse Model of Tauopathy: Captured Using Contrast-Enhanced MRI. *Proceedings of The World Molecular Imaging Congress*.

*Harrison IF, *Machhada A, *Colgan N, Lythgoe MF, Ozama I, O'Callaghan J, Holmes HE, Wells J, Murray T, Ahmed Z, Johnson RA, Collins EC, O'Neill MJ, Gourine AV Lythgoe MF. (2015). Glymphatic Clearance Impaired in a Mouse Model of Tauopathy: Captured Using Contrast-Enhanced MRI. *Alzheimer's Association International Conference*.

*Harrison IF, *Machhada A, *Colgan N, Lythgoe MF, Ozama I, O'Callaghan J, Holmes HE, Wells J, Murray T, Ahmed Z, Johnson RA, Collins EC, O'Neill MJ, Gourine AV Lythgoe MF. (2015). Glymphatic Clearance Impaired in a Mouse Model of Tauopathy: Captured Using Contrast-Enhanced MRI. *Proceedings of the British Chapter of The International Society for Magnetic Resonance in Medicine.*

Machhada A, Ang R, Ackland GL, Ninkina N, Buchman VL, Lythgoe MF, Trapp S, Tinker A, Marina N & Gourine AV. (2015). Reduced activity of dorsal vagal preganglionic neurones associated with synuclein pathology predisposes the heart to ventricular arrhythmia. *European Society for Cardiology Congress.*

Machhada A, Marina N, Lythgoe MF, & Gourine AV. (2014). Direct load- and heart rate-independent control of ventricular contractility by a distinct population of vagal preganglionic neurones. *European Heart Journal* 35, 450-451.

Machhada A, Ang R, Ninkina N, Buchman VL, Ackland GL, Lythgoe MF, Marina N & Gourine AV. (2014). A CNS cell group that controls electrical stability of the heart. *European Heart Journal* 35, 435.

Machhada A, Lythgoe MF, Gourine AV & Ackland GL. (2014). Vagal mechanisms controlling exercise capacity. *European Heart Journal* 35, 953.

Machhada A, Marina N, Lythgoe MF, & Gourine AV. (2013). Identification of vagal preganglionic neurones that control ventricular contractility using transoesophageal atrial pacing (TAP) and spinal cord transection. *Proceedings of The Physiological Society,* PCC058.

Machhada A, Marina N, Wells J, Lythgoe MF, & Gourine AV. (2013). New evidence for vagal control of the left heart. *Heart* 99, A135.

Butt AB, Haidry RJ, Oukrif D, Dunn J, Gupta A, Bhatt A, Hrynkiewicz, Waheed A, Owen C, Machhada A, Rodriguez JM, Banks MR, Lovat LB, Novelli M. (2012). Polo-like kinase 1 expression predicts aneuploidy in the Barret's metaplasia-dysplasia-carcinoma sequence. *Gut* 61, A302.

Butt AB, Haidry RJ, Oukrif D, Dunn J, Gupta A, Bhatt A, Hrynkiewicz, Waheed A, Owen C, Machhada A, Rodriguez JM, Banks MR, Lovat LB, Novelli M. (2012). Polo-like kinase 1 expression predicts aneuploidy in the Barret's metaplasia-dysplasia-carcinoma sequence. *Digestive Diseases Week*. 142, Su1877.

Table of Contents

Table of Tables

Table of Figures

List of Abbreviations

7-NI	7-Nitroindazole
A	peak atrial filling velocity
ABP	arterial blood pressure
ACh	acetylcholine
aCSF	artificial cerebrospinal fluid
AlstR	allatostatin receptor
AMN	atropine methylnitrate
AN	afferent neurones
AV	atrioventricular
AVNERP	atrioventricular node effective recovery period
cGMP	cyclic guanosine monophosphate
ChAT	choline acetyl-transferase
ChIEF	chimeric channelrhodopsin variant
ChR	channelrhodopsin
CHT1	High affinity choline transporter
DBP	diastolic blood pressure
DMSO	dimethyl sulfoxide
DT	deceleration time
DVMN	dorsal vagal motor nucleus
E	peak early filling velocity
Ees	end-systolic elastance
eGFP	enhanced green fluorescent protein
eNOS	endothelial nitric oxide synthase

EPN	efferent parasympathetic neurones
ESN	efferent sympathetic neurones
GIRK	G protein inwardly rectifying potassium channels
GLUT4	glucose transporter
GRK	G protein-receptor kinase
HR	heart rate
HRP	horseradish peroxidase
HRR	heart rate recovery
HRV	heart rate variability
If	pacemaker current
IN	interneurones
iNOS	inducible nitric oxide synthase
IVCT	isovolumetric contraction time
IVRT	isovolumetric relaxation time
KI	knock-in
KO	knockout
LAD	left anterior descending artery
LV	left ventricle
LV ET	left ventricular ejection time
LV MPI	left ventricular myocardial performance
LV$dP/dt_{max}$	maximum of the first differential of LVP
LV$dP/dt_{min}$	minimum of the first differential of LVP
LVEDP	left ventricular end diastolic pressure
LVESP	left ventricular end systolic pressure
LVP	left ventricular pressure

LVV	lentiviral vector
MAP	mean arterial pressure
MI	myocardial infarction
NA	nucleus ambiguus
nNOS	neuronal nitric oxide synthase
NO	nitric oxide
PES	programmed electrical stimulation
PKD1	protein kinase D1
PP	pulse pressure
QTc	corrected QT interval
RSA	respiratory sinus arrhythmia
RV	right ventricle
SA	sinoatrial
SBP	systolic blood pressure
SN	sympathoexcitatory neurones
SNRT	sinus node recovery time
td-Tomato	tandem dimer Tomato red fluorescent protein
vERP	ventricular effective refractory period
VF	ventricular fibrillation
VIP	vasoactive intestinal peptide
VNS	vagus nerve stimulation
VPNs	vagal preganglionic neurones
V_T	ventricular tachycardia
WT	wild-type
XII	hypoglossal

Chapter 1 Background

1.1 Evolution of the parasympathetic nervous system

In the seventeenth century, William Harvey suggested a link between the brain and heart when he wrote:

> *"Every affection of the mind that is attended with either pain or pleasure, hope or fear, is the cause of an agitation whose influence extends to the heart"* (Harvey, 1628).

Over the last century, there have been numerous anatomical and physiological studies of the autonomic nervous system, principally responsible for the integrated cardiovascular control involving sympathetic (facilitatory) and parasympathetic (inhibitory) arms. Complex interactions between them at different levels of the brain and spinal cord (the neuraxis) as well as on the periphery ensure effective control of cardiac function to meet ever changing behavioural and physiological demands (Ondicova & Mravec, 2010).

It appears that evolutionary development of the parasympathetic nervous system preceded the development of its sympathetic counterpart (Kuntz, 1911). Significant work on the phylogenetic history of the nervous system has concluded that ancestral vertebrates did not possess a nervous structure equivalent to any part of the mammalian sympathetic nervous system, and bodily functions were largely controlled by the vagi (Marcus, 1909). In the evolution of the parasympathetic nervous system itself, unmyelinated vagal fibres appeared first.

1.2 Neurochemical transmission of the vagus

1.2.1 A brief history

Since the discovery of the inhibitory influence of the vagus nerve on the heart in 1845 by Ernst and Eduard Weber, the vagal control of cardiac function has been a topic of intense scrutiny. Earlier attempts to understand the role of both the left and right vagi began with electrical stimulation and characterisation of the resultant effects on the rate of atrial and ventricular contraction and velocities of measured potentials in conducting tissues.

With the discovery of acetylcholine (ACh) and its major role in parasympathetic chemical transmission, various methods were developed to detect the presence of key enzymes involved in its metabolism. While these methods allowed identification of the vagal innervation of the atria, the sinoatrial (SA) and atrioventricular (AV) nodes and conducting tissue, the significance of the parasympathetic innervation of the ventricles always remained an area of ambiguity. Physiological experiments conducted to better understand vagal control of the ventricular function all had varying levels of success (Coote, 2013). Vagus nerve stimulation (VNS) has been shown to have an effect on contractility, automaticity and electrical stability of the ventricles (Degeest *et al.*, 1965c; Vassalle *et al.*, 1967; Zuanetti *et al.*, 1987). Moreover, both ACh and nitric oxide (NO) have been suggested to mediate vagal effects on the ventricle. On the other hand, *in vitro* studies on isolated ventricular cardiomyocytes demonstrated changes in their contractile behaviour following the application of ACh and NO.

The central nervous sites harbouring vagal preganglionic neurones (VPNs) projecting to the heart have been identified in many mammalian species (Spyer, 1994) although the nature of their anatomical and functional organisation has yet to be fully realised.

1.2.2 Acetylcholine

Walter Dixon was one of the first to focus on the mechanisms of how vagal nerve stimulation inhibits the heart. At the time of Dixon's medical training in London, Bayliss and Starling demonstrated intestinal production of secretin which triggered the release of digestive enzymes (Bayliss & Starling, 1902). Dixon extrapolated this observation to the heart and proposed that VNS results in the conversion of intracardiac stores of proinhibitin to inhibitin. Later he described the results of an experiment in which purified extract obtained from a vagally inhibited dog's heart (the donor) slowed a frog's heart (the recipient) and this effect was inhibited by atropine (Dixon, 1906; Dixon, 1907).

This was then followed by the classical work of Otto Loewi. He isolated two frog hearts (one with vagal innervation intact) and perfused them with a salt solution which mimicked the composition of extracellular fluid (Ringer, 1883). Following a few minutes of VNS, Ringer's solution was transferred from the donor to the recipient; the heart rate (HR) was reduced mimicking the effect of VNS. This demonstrated that the vagus nerve produces its effect through the release of an inhibitory substance which Loewi named "Vagusstoff" or "vagus substance" (Loewi, 1921). Atropine was found to abolish these effects by a mechanism other than inhibition of release (Loewi, 1926; Loewi & Navratil, 1926). Vagusstoff was then characterised as a choline ester exhibiting effects similar to those of ACh (Dale, 1934a; Dale, 1934b; Dale & Feldberg, 1934). This was accepted by Loewi and he agreed to refer to it as such in his Nobel Prize lecture (Loewi, 1936). This work laid the foundations of modern concepts of neurohumoral (now neurochemical) transmission and the investigation of its role in the autonomic control of many organs.

1.2.3 Nitric Oxide

NO was first identified as "nitrous air" by Joseph Priestly (Priestley, 1775) and has long been considered an air pollutant. In 1980, Robert Furchgott investigated the role of ACh on vasculature and found that relaxation of blood vessels only occurred when endothelial cells were present in the preparation. He observed that in

the absence of endothelia ACh was not able to cause vasodilation, suggesting that endothelial cells produce a substance that mediates the effects of ACh. This substance was subsequently named “endothelial derived relaxing factor” (Furchgott & Vanhoutte, 1989). Moreover, in 1977, Ferid Murad independently investigated the mechanism underlying nitroglycerin (used widely for the treatment of angina) and discovered that it relaxes smooth muscle cells. In 1986, Louis Ignarro identified endothelial-derived growth factor as having the same properties as the NO gas. This was the first time a gas was demonstrated to have a physiological role. For this discovery, Furchgott, Murad and Ignarro were awarded the Nobel Prize in Physiology or Medicine in 1998 (SoRelle, 1998).

NO is produced by the enzyme nitric oxide synthase (NOS), which exists in inducible as well as in constitutive endothelial (eNOS) and neuronal (nNOS) isoforms (Moncada *et al.*, 1991). The physiological effects of NO are predominantly mediated through activation of cytosolic guanylate cyclase, resulting in an increased production of cyclic guanosine monophosphate (cGMP) and leading to the activation of many downstream signalling pathways (Ignarro, 1991). NO is released by many cells in virtually all tissues of the body (Danson & Paterson, 2005). There is evidence that NO may mediate some vagal effects on the heart (Conlon *et al.*, 1998; Patel *et al.*, 2008) in addition to its characteristic role in the control of coronary circulation (Paterson, 2001; Rastaldo et al., 2007). NO-induced stimulation of cGMP production has been demonstrated to have an effect on pacemaker current (If) in nodal tissue leading to increases in HR (Musialek et al., 1997). Presynaptic actions of NO generated by nNOS within the intrinsic cardiac ganglia (Tanaka et al., 1993; Choate et al., 2001) have also been demonstrated to potentiate the magnitude of bradycardia (Herring et al., 2000) during VNS through the facilitation of ACh release (Herring & Paterson, 2001).

1.2.4 Functional interactions of vagal signalling molecules

The functional interactions between NO- and ACh-mediated signalling pathways in the context of cardiac innervation has been difficult to fully discern (Danson & Paterson, 2005). nNOS is expressed by intracardiac cholinergic neurones in many species (Klimaschewski *et al.*, 1992; Mawe *et al.*, 1996; Choate *et al.*, 2001;

Pauza *et al.*, 2014). Inhibition of nNOS has been found to result in a substantial reduction of vagally-mediated bradycardia *in vivo* in the ferret and guinea pig (Conlon & Kidd, 1999) tested, while a smaller effect was observed in the dog (Elvan *et al.*, 1997). No effect of nNOS blockade was reported in the rabbit heart (Liu *et al.*, 1996; Sears *et al.*, 1998).

NO donors have been shown to increase the high frequency component of heart rate variability (HRV) - an index of cardiac vagal tone (Chowdhary & Townend, 1999). Both NO donors and the cGMP analogue 8-bromo-cGMP were reported to potentiate bradycardia induced by vagal nerve stimulation (Sears *et al.*, 1999). However, application of NOS or guanylate cyclase inhibitors had no effect on bradycardia induced by carbamylcholine (the stable analogue of ACh), supporting the view of NO as an important presynaptic modulator of vagal neurotransmission (Hebeiss & Kilbinger, 1996; Morot Gaudry-Talarmain *et al.*, 1997; Sears *et al.*, 1999; Herring *et al.*, 2000).

Certain neuropeptides are expressed through cardiac postganglionic vagal neurones (Weihe & Reinecke, 1981; Weihe *et al.*, 1984; Lundberg & Hökfelt, 1986). ACh is well established to co-localise with vasoactive intestinal peptide [(VIP); (Lundberg *et al.*, 1979; Bartfai *et al.*, 1988)]. ACh and VIP were first demonstrated to be co-localised in vagal postganglionic neurones of cats, where VIP was found to potentiate ACh release in preparation for the submandibular gland (Polak, 1969; Szerb, 1979). ACh co-release with other neurotransmitters paints a complicated picture of autonomic regulation of HR (Christophe *et al.*, 1984). For example, in conditions of combined β-adrenoceptor and muscarinic blockade, tachycardia induced by VNS was found to be blocked by VIP antagonism (Henning, 1992). Voltage clamp experiments demonstrated an increased magnitude of I_f in response to VIP (Shvilkin *et al.*, 1994). This has been suggested to be an endogenous mechanism to prevent excess bradycardia during periods of increased vagal activity (Shvilkin *et al.*, 1994).

1.3 Vagal innervation

1.3.1 The vagal nuclei

Unmyelinated parasympathetic fibres originating from the dorsal vagal motor nucleus [(DVMN); (Figure 1-1; Figure 1-2] possess pre- and postganglionic muscarinic receptors. Only mammals have myelinated vagal fibres which originate from the nucleus ambiguus [(NA); (Figure 1-1)] and possess preganglionic nicotinic receptors and postganglionic muscarinic receptors (Porges, 2009). The ontogenesis of the DVMN in metamorphosing amphibians undergoing anatomical and physiological changes during the shift from water to air breathing helps identify the DVMN as the primary vagal nucleus. Developing cardiorespiratory interactions introduces a phasic component in cardiac vagal tone and this required migration of a subset of the DVMN neurones ventrally giving rise to a compact formation of the NA (Burggren & Infantino, 1994; Smatresk, 1994; Burggren, 1995). DVMN neurones with C fibre axons (Ciriello & Calaresu, 1980; Nosaka et al., 1982; Jones et al., 1998) are therefore considered to be phylogenetically older and provide the tonic vagal supply. The intermediate zone between them is a likely remnant of the migrating population post nuclear division (Taylor et al., 1999; Jones, 2001).

The majority of studies that have applied tracers, such as horseradish peroxidase (HRP), identified that cardiac vagal innervation is provided by VPNs residing in the NA and the DVMN, with some isolated neurones scattered in the intermediate zone. This has been demonstrated in rats (Nosaka *et al.*, 1979; Nosaka *et al.*, 1982; Stuesse, 1982; Izzo *et al.*, 1993), cats (Sugimoto *et al.*, 1979; Ciriello & Calaresu, 1980; Geis & Wurster, 1980b; Kalia & Mesulam, 1980; Bennett *et al.*, 1981; Geis *et al.*, 1981; Miura & Okada, 1981; Ciriello & Calaresu, 1982), dogs (Bennett *et al.*, 1981; Hopkins & Armour, 1982, 1984; Plecha *et al.*, 1988) and pigs (Hopkins *et al.*, 1984; Hopkins *et al.*, 1997).

Recordings of antidromic potentials generated by electrical stimulation of the cardiac vagal branch have identified significant cardiac innervation by neurones residing in the NA (McAllen & Spyer, 1976; McAllen & Spyer, 1978b, a; Ciriello & Calaresu, 1982). These neurones were shown to be activated by pulmonary C-fibre

afferent stimulation (Wang *et al.*, 2000). Subsequently, neurones of the NA have been found to have rhythmic, respiratory-related patterns of discharge (Gilbey *et al.*, 1984) with B fibre axons innervating nodal tissue. Rhythmic activity of the NA neurones underlies the respiratory sinus arrhythmia [(RSA); (McAllen & Spyer, 1978b; Neff *et al.*, 2003)]. The relative proportion of DVMN neurones projecting to the heart is believed to be lower (Jones, 2001), and their functional significance in the control of cardiac function remains unknown. DVMN neurones have long latency C fibre (unmyelinated) axons (Ciriello & Calaresu, 1980; Nosaka *et al.*, 1982; Jones *et al.*, 1995). It has been suggested from anterograde tracing studies that vagal control of the heart involves the convergence and integration of distinct projections from both nuclei projecting to cardiac plexuses (Cheng *et al.*, 1999; Cheng & Powley, 2000).

1.3.2 The effect of vagal nerve stimulation

Studies involving VNS established that it controls HR (the chronotropic state) and AV conduction velocity (the dromotropic state). The left vagus mostly innervates the AV node with the corresponding negative dromotropic effect, whilst the right vagus mainly innervates the SA node exerting a profound negative chronotropic effect (Gaskell, 1882; Cohn, 1912; Gesell, 1916; Haney *et al.*, 1943).

Many of these studies concluded that there is no effect of the vagus nerve on the ventricular function (Roy & Adami, 1891; Bayliss & Starling, 1892; Henderson & Barringer, 1913; Drury, 1923; Rothberger & Scherf, 1930; Ullrich *et al.*, 1954; Carlsten *et al.*, 1957; Schreiner *et al.*, 1957; Denison & Green, 1958; Sarnoff *et al.*, 1960; Reeves & Hefner, 1961). It was still evident to some, however, that inhibition of the ventricular rhythm was different in mammals compared to those of lower vertebrates such as the eel, frog or tortoise, where ventricular asystole would arise if the atria were arrested, i.e. the mammalian ventricle had a more powerful independent rhythmic action inherent to the ventricular tissue (McWilliam, 1888; Howell & Duke, 1906; Patterson *et al.*, 1914; Wiggers & Katz, 1922). In other studies involving mammals, a reduced ventricular automaticity and rate were observed in dogs with complete atrioventricular block (Eliakim *et al.*, 1961) and in the area of the His bundle (Gonzalas-Serrato & Alanis, 1962; Higgins *et al.*, 1973).

Left VNS has been shown to reduce ventricular contractility independent of HR changes and β-adrenergic input (Degeest *et al.*, 1965c; Lewis *et al.*, 2001). In cats, VNS (Gatti *et al.*, 1997) and electrical stimulation of the DVMN (Geis & Wurster, 1980a) produced similar effects.

1.3.3 The cardiac ganglia

VPNs project from the medulla oblongata to vagal postganglionic neurones within the cardiac ganglia (Randall & Wurster, 1994; Rossi, 1994; Spyer *et al.*, 1994). The postganglionic neurones project to the atrial and ventricular musculature in addition to SA and AV nodes (Carlson *et al.*, 1992; Randall & Wurster, 1994). Activation of them triggers chronotropic, dromotropic and inotropic effects (Levy & Martin, 1984; Carlson *et al.*, 1992). Sympathetic preganglionic neurones of the spinal cord receive excitatory inputs from the hypothalamus and the brainstem and project to paravertebral ganglia innervating the heart (Gilbey, 2007). Sensory afferent neurones are located in the dorsal root ganglia, nodose ganglia and in the cardiac ganglia (Ardell, 1994; Armour, 1994; Randall & Wurster, 1994; Spyer *et al.*, 1994) and mediate long- and short-distance (local) reflexes (Ardell, 1994; Randall & Wurster, 1994; Spyer *et al.*, 1994).

Cardiac ganglia are typically found in fat pads at the level of the SA and AV nodes (McFarland & Anders, 1913; Francillon, 1928; Davies *et al.*, 1952; Navaratnam, 1965; Smith, 1971b; Rossi, 1994). Cardiac ganglia near the SA node have been reported to be located near the superior left atrial surface (Leonhardt, 1986; Singh *et al.*, 1996), the interatrial groove and the coronary sulcus junction (King & Coakley, 1958). Ganglia have also been found on the aorta, left pulmonary veins (Leonhardt, 1986; Singh *et al.*, 1996) and caval surfaces (Leonhardt, 1986). Although some studies have reported the absence of ganglia at the level of the ventricles (Davies *et al.*, 1952), many other studies have found ganglia within this vicinity (Lee, 1849; Blackhall-Morison, 1926; Smith, 1971b, a). Collections of cardiac ganglia have also been found near the ventricular coronary vasculature (Singh *et al.*, 1996).

1.4 The controversy: vagal innervation of the ventricle

1.4.1 Immunohistochemical evidence

Sympathetic nerves innervate the SA and AV nodes, the atria, ventricles and the conducting tissue. While the vagal innervation of the atria, the SA and AV nodes and conducting tissues has been well established, the terminal parasympathetic innervation of the ventricles has been a subject of on-going controversy (Levy, 1971a; Coote, 2013). Some of the first histological (Cullis & Tribe, 1913; Nonidez, 1939, 1941) and physiological (Carlsten *et al.*, 1957) data indicated that the mammalian ventricles lack any significant parasympathetic innervation except at the AV junction (Roy & Adami, 1891).

Acetylcholinesterase staining was one of the first methods applied to provide indirect histological evidence of ventricular parasympathetic innervation (Karnovsky & Roots, 1964; Broderson *et al.*, 1974). ACh release results in either muscarinic or nicotinic receptor activation at either pre- or post-synaptic membranes, where ACh is hydrolysed into choline and acetate by acetylcholinesterase (Kuhar & Murrin, 1978). The staining methods operated on the basis that parasympathetic fibres would stain more deeply than sympathetic fibres and therefore may not be entirely specific to parasympathetic innervation (Nilsson, 1976). Initial reports found no vagal innervation of the ventricular myocardium using this method (Carbonell, 1956; James, 1967). In other studies, moderate ventricular cholinesterase activity was detected. Some (Nonidez, 1939; Tcheng, 1951; Higgins *et al.*, 1973) but not all (Robb & Kaylor, 1945; Stotler & Mc, 1947) silver impregnation techniques were able to visualise low-density cholinergic fibres in the canine and feline ventricles beyond the extensive plexuses found in the atria. Rich cholinergic innervation of epicardial and endocardial ventricular surfaces has since been found in human (Kent *et al.*, 1974; Pauza *et al.*, 2000), pig (Crick *et al.*, 1999; Ulphani *et al.*, 2010) and rat hearts (Mastitskaya *et al.*, 2012).

The high-affinity choline transporter (CHT1) is specifically expressed in cholinergic neurones and constitutes a rate-limiting step for acetylcholine synthesis. Choline undergoes reuptake into the presynaptic terminals by via CHT1 in Na^+-

dependant process (Kobayashi *et al.*, 2002; Okuda & Haga, 2003). Techniques involving northern blot and *in situ* hybridisation have demonstrated that CHT1 protein is expressed specifically by cholinergic neurones (Misawa et al., 2001; Kobayashi et al., 2002; Lips et al., 2002) and has since been found in the murine myocytes (Kakinuma *et al.*, 2012).

1.4.2 In vitro evidence

A direct effect of ACh has been described in isolated cardiomyocytes in the rat (McMorn *et al.*, 1993), cat (Hommers *et al.*, 2003), guinea-pig (Zang *et al.*, 2005b) and ferret (Ito *et al.*, 1995). Ferret myocytes displayed a 10% reduction in their twitch shortening in response to the application of ACh (Dobrzynski *et al.*, 2002). It was proposed that ACh mediates its action on ventricular myocytes via phosphorylation of the G protein-coupled inwardly rectifying K^+ channels (GIRK/Kir), in particular Kir3.1 and Kir3.4, which are abundant throughout the heart (Dobrzynski *et al.*, 2001), and reducing basal Ca^{2+} currents (Belardinelli *et al.*, 1995; Dobrzynski *et al.*, 2002).

Ventricular myocytes have also been shown to express eNOS as well as soluble guanylate cyclase (Balligand *et al.*, 1993; Kojda *et al.*, 1997). In isolated electrically stimulated (contracting) guinea pig myocytes, NO has been shown to attenuate the magnitude of contractions by >20% via the production of cGMP (Patel *et al.*, 2008). Complementary to this, non-specific NOS blockade has demonstrated a potentiation of contraction (Balligand *et al.*, 1995; Kaye *et al.*, 1996). This effect was not observed in mice with genetic deletion of eNOS (Vandecasteele *et al.*, 1999). nNOS has been found to be associated with sarcolemmal proteins (Sears *et al.*, 2003) and the sarcoplasmic reticulum (Xu *et al.*, 1999), and may also play a role in inhibition of contraction (Ashley *et al.*, 2002) through the inhibition of an L-type calcium current (Sears *et al.*, 2003). However, this effect is not consistently observed (Barouch *et al.*, 2002). Despite this, a preparation has yet to be developed that isolates the role of nNOS to establish the true integrative role (Danson & Paterson, 2005).

1.5 Resolving this controversy: Targeting the DVMN

In the context of the existing controversial evidence of vagal innervation of the cardiac ventricle, this thesis aims to determine the functional significance of vagal innervation of the ventricle through a comprehensive programme of carefully designed experiments using the latest advances in molecular neuroscience and *in vivo* animal models. Studies of the ontogenesis of the dorsal vagal column in metamorphosing amphibians (such as in the axolotl) undergoing anatomical and physiological changes during transition from water to air breathing identified the DVMN as the primary vagal nucleus. Indeed, in the neotenous axolotl, all VPNs are located in the DVMN (Taylor, 1994). The developing mechanisms of cardiorespiratory coupling requires a phasic vagal component, therefore migration of a subpopulation of DVMN VPNs closer to the ventral respiratory group is essential to acquire respiratory modulation of activity (Burggren & Infantino, 1994; Smatresk, 1994; Burggren, 1995).

Based on these previous studies, the DVMN, being evolutionarily older, are hypothesised to be the main group of VPNs that innervate cardiac ventricle. Indeed, a recent study has shown that when DVMN VPNs are selectively recruited using an optogenetic approach has a potent cardioprotective effect (via a muscarinic mechanism) on ventricular cardiomyocytes against acute ischemia/reperfusion injury (Mastitskaya *et al.*, 2012), thus suggesting that this may be the case. This study on the DVMN is consistent with the evidence of a potent cardioprotective effect of ACh (which is as potent as adenosine in reducing myocardial injury) reported previously (Richard *et al.*, 1995; Qian *et al.*, 1996; Yamaguchi *et al.*, 1997; Cohen *et al.*, 2001).

1.6 Main Hypothesis and Aims

Experimental studies described in this thesis tested the hypothesis that functionally significant parasympathetic control of the left ventricle (LV) of the heart is provided by VPNs of the DVMN. Methods of genetic neuronal targeting, functional neuroanatomical mapping, pharmaco- and optogenetics applied in *in vivo* animal (rat and mouse) models were used to address the following specific aims:

1. To determine the role of DVMN VPNs in controlling electrical properties of the ventricle (Chapter 2);
2. To determine the role of DVMN VPNs in controlling LV contractility (Chapter 3);
3. To determine the role of DVMN VPNs in controlling exercise capacity (Chapter 4);
4. To determine the effect of DVMN stimulation on progression of LV dysfunction developing after a myocardial infarction [(MI); (Chapter 5)].

1.7 Distribution of choline acetyl-transferase-expressing neurones along the rostro-caudal extent of the brainstem

The candidate's own atlas showing distribution of VPNs in the dorsal vagal complex was generated by immunostaining of coronal sections of an adult rat brainstem for choline acetyl-transferase (ChAT). Adult Sprague-Dawley rats (400 g) were terminally anaesthetised with pentobarbitone sodium (200 mg kg^{-1}, i.p) perfused through the ascending aorta with 0.9% saline followed by 4% phosphate-buffered (0.1 M, pH 7.4) paraformaldehyde. After 12 hours of post-fixation and subsequent cryoprotection (30% sucrose), the brainstem was isolated and sliced. 30-μm-thick coronal sections were collected along the rostro-caudal extent of the medulla oblongata. Sections were processed for immunohistochemical detection of ChAT. Tissue was incubated in goat anti-ChAT antibody (1:500, Chemicon) followed by incubation with donkey anti-goat antibody conjugated with Alexa Fluor568 (1:500, Abcam).

ChAT-positive DVMN and NA neurones were distinctly identifiable on the coronal sections of the rat brainstem (Figure 1-2). On the caudal brainstem sections, the DVMN shows as a discrete group of neurones located in proximity to the central canal and dorsally to the hypoglossal (XII) nucleus containing large motor neurones also expressing ChAT (Paxinos & Watson, 1998). Rostral groups of DVMN neurones are found near the dorsomedial edge of the brainstem (Figure 1-2).

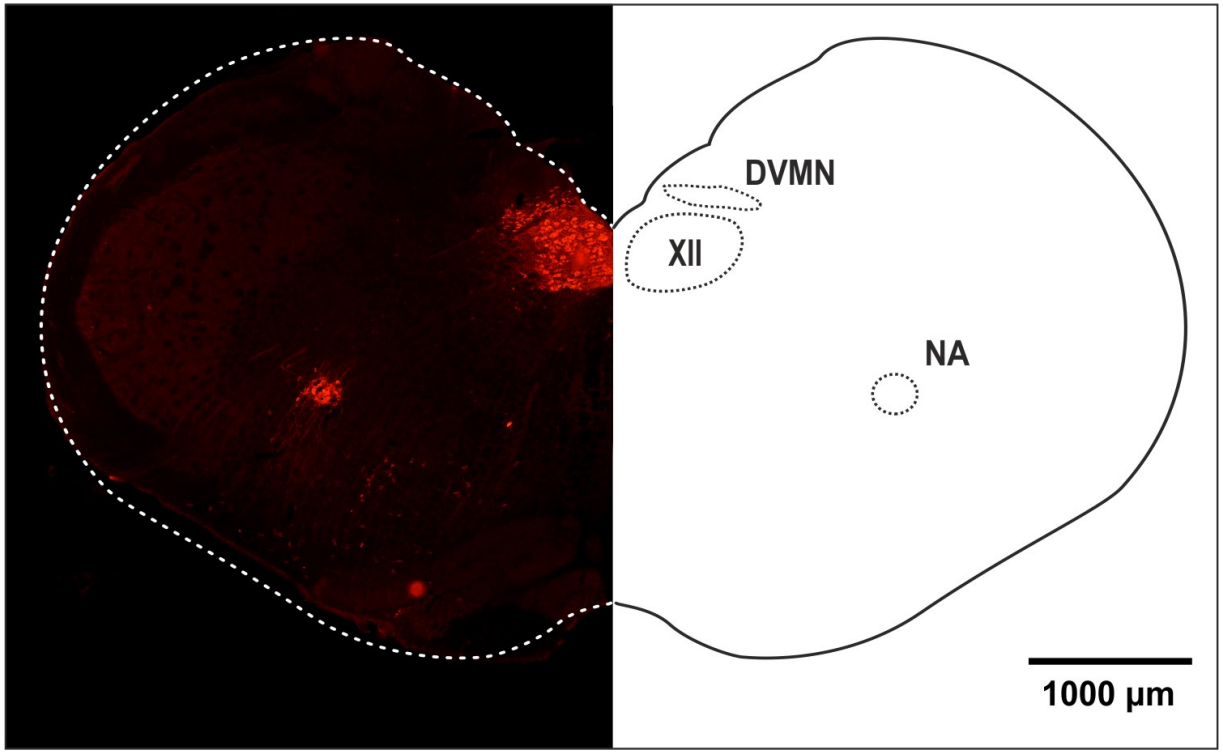

Figure 1-1: Identification of choline acetyltransferase (ChAT) expressing neurones in the coronal section of the rat medulla oblongata

Confocal image of a coronal section of the rat brainstem illustrating the location of the DVMN and NA vagal preganglionic neurones. Immunohistochemistry identified the ChAT-positive, i.e. cholinergic (red) neurones. XII, hypoglossal motor nucleus.

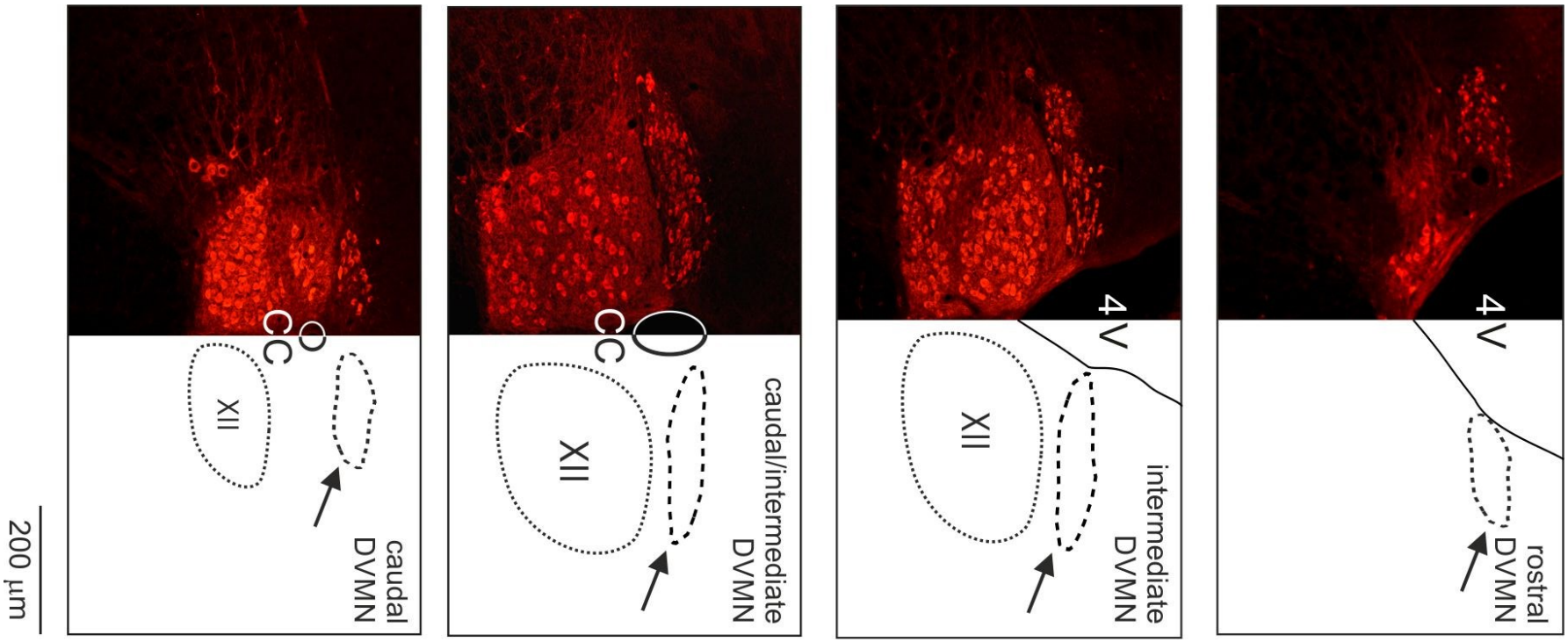

Figure 1-2: Distribution of choline acetyltransferase (ChAT)-expressing neurones in the dorsal aspect of the rat medulla oblongata

Confocal images of the coronal sections of the rat brainstem illustrating the distribution of the DVMN VPNs. Immunohistochemistry identified ChAT-positive, i.e. cholinergic (red) neurones. 4V, fourth ventricle; XII, hypoglossal motor nucleus; CC, central canal.

Chapter 2 Control of Ventricular Excitability

2.1 Introduction

Sudden circulatory collapse is often due to malignant arrhythmias, such as ventricular tachycardia (V_T). Predictors of sudden cardiac death include conventional coronary risk factors and conditions, such as congestive heart failure, as well as markers of vagal dysfunction, including reduced HRV and reduced baroreflex sensitivity (La Rovere *et al.*, 1998; Olshansky *et al.*, 2008).

Atrial arrhythmias such as atrial fibrillation also have a well-established relationship with both sympathetic and parasympathetic signalling (Coumel *et al.*, 1978). This association has been extended to primary ventricular arrhythmias (which predispose to sudden death) in addition to the modulation of arrhythmia risk within the context of inherited dysfunction of cardiac ion channels, i.e. cardiac channelopathies. These studies have mainly focused on evaluating the effect of increased sympathetic activity. It has been well documented that reduced HRV and a raised HR develop before V_T in humans (Shusterman *et al.*, 1998). Furthermore, stimulation of the left stellate sympathetic ganglia in dogs to increase sympathetic activity induced QT prolongation and preceded ventricular arrhythmia and sudden death (Zhou *et al.*, 2008). More recently, the role of the vagus in ventricular arrhythmias, particularly in specific channelopathies, such as idiopathic ventricular fibrillation (VF), is more recoginised. Patients with idiopathic VF with J-wave syndrome were associated with high vagal tone. This manifested as potentiated J-wave elevation during bradycardia and increased propensity to sleeping VF events, each associated with an increased vagal tone (Mizumaki *et al.*, 2012). The predisposition of the ostensibly normal heart to potentially fatal V_T with loss of vagal regulation, however, has remained unexplored.

With regard to conditions of raised sympathetic activity, it is not surprising that VNS is being explored as a therapeutic option in heart failure and one component of its potential benefit may be an antiarrhythmic effect (Hauptman *et al.*, 2012; Shen & Zipes, 2014). Experimental studies on animal models have demonstrated profound antiarrhythmic effects of VNS (Waxman *et al.*, 1989; Vanoli

et al., 1991; Ng *et al.*, 2007). It effectively reduces the restitution slope, prevents alternans and increases the ventricular effective refractory period [(vERP); (Ng *et al.*, 2007)]. VNS also decreases the incidences of ventricular arrhythmia associated with heightened sympathetic activity during myocardial infarction (MI) (Vanoli *et al.*, 1991). There is clinical evidence that vagal tone suppresses an accelerated ventricular rhythm (Waxman *et al.*, 1988), and experimental data showing that the vagal influence on ventricular refractoriness and arrhythmia threshold is tonic and could be abolished by bilateral vagotomy or systemic muscarinic receptor blockade (Schwartz *et al.*, 1977). Studies from a collaborating laboratory demonstrated that global genetic deletion of the inhibitory G-protein $G\alpha_{i2}$ (which mediates muscarinic influences on the heart) in mice is associated with a reduced vERP, prolonged corrected QT interval (QT_C) and a predisposition to V_T (Zuberi *et al.*, 2010). There is also evidence that the protective vagal influence on cardiac electrical stability might be mediated by NO, which is produced by nNOS (Brack *et al.*, 2009; Brack *et al.*, 2011).

Despite this evidence, there has been no attempt to study the central nervous mechanisms underlying parasympathetic antiarrhythmic influences thus far. In this study the aim was to identify a population of VPNs that provide functional parasympathetic innervation of the ventricles and control the ventricular excitability. VPNs projecting to cardiac ganglia are located in the brainstem. Neuronal tracing experiments in different species (Hopkins *et al.*, 1997; Jones *et al.*, 1998) have identified the DVMN as one such population of neurones with long latency C-fibre axons converging upon cardiac plexuses (Jones *et al.*, 1998). Since the activities of the DVMN neurones appear to protect ventricular cardiomyocytes against acute ischemia/reperfusion injury (Mastitskaya *et al.*, 2012), it is hypothesised that functional ventricular innervation is provided by the DVMN neuronal projections.

Autonomic dysfunction is of increasing clinical importance as it contributes to the pathogenesis of Parkinson's disease (Goldberg *et al.*, 2012; Greene, 2014). Parkinson's disease is the second most common neurodegenerative disorder (de Lau & Breteler, 2006) characterised by a loss of dopaminergic neurones, with consequent motor impairment as well as DVMN dysfunction, resulting in a host of autonomic

abnormalities (Braak *et al.*, 2002; Goldberg *et al.*, 2012). Aggregation of α-synuclein is a major molecular event in the development of this disease due to the toxicity of certain intermediate products of this process. Age-dependent decline of substantia nigra pars compacta synaptic function has been reported in α-synuclein deficient mice (Al-Wandi *et al.*, 2010). These changes appeared to be even more pronounced in triple-synuclein-null ($\alpha\beta\gamma^{-/-}$) mice that have been generated to limit functional compensation by other members of the synuclein family (Anwar *et al.*, 2011). In this study $\alpha\beta\gamma^{-/-}$ mice are used to determine whether synuclein deficiency leads to a reduction in the activity of the DVMN neurones and is associated with changes in ventricular electrophysiology.

2.2 Methods

All the experiments were performed in accordance with the European Commission Directive 2010/63/EU (European Convention for the Protection of Vertebrate Animals used for Experimental and Other Scientific Purposes) and the United Kingdom (UK) Home Office (Scientific Procedures) Act (1986), with project approval from the Institutional Animal Care and Use Committee.

2.2.1 Cardiac Electrophysiology

Cardiac pacing using extrastimulation was performed using S88-Grass stimulator. Adult male Sprague-Dawley rats (380–450 g), wild-type (WT) and $\alpha\beta\gamma^{-/-}$ mice were under urethane anaesthesia (1.3 g kg^{-1}, i.p.), and an octapolar electrophysiology catheter (1.6 F for rats and 1.1 F for mice) was positioned in the right atrium and the right ventricle (RV) via the jugular vein, or in the LV via the right common carotid artery. For the assessment of vERP, 10 paced beats (10xS1) were applied, using a cycle length of 85 ms in mice and 100 ms in rats, followed by a gradually shortened extra single paced beat (S2) until failure of ventricular capture. The maximum S1-S2 coupling interval was measured as the vERP. V_T threshold (in rats only) was evaluated by application of 15 paced beats (15xS1), shortening the cycle length from 100 ms to 20 ms in 4 ms increments (10 to 60 Hz burst pacing). One episode of V_T was defined as at least 10 consecutive broad complex systoles (all of which were noted to self cardiovert). The definitions of V_T were similar to that in recent publications (Zuberi *et al.*, 2010).

For the assessment of the AV node effective refractory period (AVNERP) in rats, 10 paced beats (10xS1) using a cycle length of 141 ms were applied followed by a gradually shortened extra single paced beat (S2) until failure of ventricular capture. Wenkebach point was determined by shortening the cycle length (from 150 ms) until a 2:1 block was observed. The sinus node recovery time (SNRT) was measured as the period between the last paced beat and the onset of the first P wave after 30 s of atrial pacing (cycle length 141 ms).

2.2.2 Pharmacological Study

To determine the presence of tonic parasympathetic influence on cardiac electrical stability in the main experimental model used in the present study (rat under urethane anaesthesia) systemic β-adrenoceptor blockade was applied (atenolol, 2 mg kg^{-1} h^{-1} i.v.). The effects of sequential systemic muscarinic (atropine methyl nitrate, 2 mg^{-1} kg^{-1} h^{-1} i.v.) and nNOS (7-Nitroindazole [7-NI], 20 mg^{-1} kg^{-1} i.p.) blockade on AVNERP, SNRP, Wenkebach point, left and right vERP and left and right V_T were determined.

2.2.3 Genetic targeting of the DVMN vagal preganglionic neurones

VPNs of the DVMN characteristically express the transcriptional factor Phox2 and can be targeted to express the gene of interest using viral vectors with Phox2 activated promoter – PRSx8 (Lonergan *et al.*, 2005). DVMN neurones along the whole rostro-caudal extent of the left and right nuclei were transduced with lentiviral vectors (LVV) to express either the G_i-protein-coupled *Drosophila* allatostatin receptor (AlstR) or enhanced green fluorescent protein (eGFP, control). The original PRSx8-AlstR-eGFP-LVV construct was thoroughly validated in previous studies (Marina *et al.*, 2010; Marina *et al.*, 2011). Validation of the transgene specificity in targeting DVMN neurones to express AlstR and efficacy of the natural ligand of AlstR, the insect peptide allatostatin, to produce a highly selective, rapid and reversible silencing of neurones expressing AlstR have been described in detail previously (Mastitskaya *et al.*, 2012).

Male Sprague-Dawley rats (50 g) were anaesthetised with ketamine (60 mg kg^{-1}, i.m.) and medetomidine (250 μg kg^{-1}, i.m.). Adequate depth of surgical anaesthesia was confirmed by the absence of a withdrawal response to a paw pinch. With the head fixed prone in the stereotaxic frame the dorsal surface of the brainstem was exposed. DVMN neurones were targeted on each side with two microinjections (0.25 μl; 0.05 μl min^{-1}) of a solution containing viral particles of PRSx8-AlstR-eGFP-LVV (Figure 2-1) or PRSx8-eGFP-LVV (Figure 2-2). The established titres at the time of production were within the range of 1 x 10^9 and 1 x 10^{10} transducing units ml^{-1}. The injections were made at 0.5 mm rostral, 0.6 mm lateral, 0.8 mm

ventral and at 1.0 mm rostral, 0.8 mm lateral, 0.6 mm ventral from the *calamus scriptorius*. Anaesthesia was reversed with atipemazole (1 mg kg^{-1}, i.m.). For post-operative analgesia, rats were administered with buprenorphine (0.05 mg kg^{-1} d^{-1}, s.c.) for three days and caprofen (4 mg kg^{-1} d^{-1}, i.p.) for five days. One rat injected with PRSx8-AlstR-eGFP-LVV developed a middle ear infection and was excluded from the study. Rats weighed 300-400g at the time of the experimentations.

The activity of VPNs transduced to express AlstR along the left and the right extent of the DVMN was reduced by allatostatin infusion into the *cisterna magna.* The effects of this treatment on vERP and V_T threshold were determined in conditions of intact sympathetic tone.

In a separate experiment, conducted in conditions of systemic β-adrenoceptor (atenolol) and muscarinic (atropine) blockade, atrial and ventricular pacing protocols were applied before and after acute bilateral silencing of the DVMN neurones by targeted microinjections of a potent $GABA_A$ receptor agonist muscimol. Rats (n=8) were anaesthetised, instrumented for cardiac electrophysiology as described above and the head was fixed in the stereotaxic frame with the dorsal side up. An occipital craniotomy was performed to expose dorsal brainstem. A multi-barrelled glass micropipette (tip size 20-25 μm) was used for microinjections of a vehicle (saline) or muscimol (0.1 M; 40 nl; pH 7.4) into the left and right DVMN (coordinates: 0.3 mm rostral, 0.7 mm lateral, 0.8 mm ventral from the *calamus scriptorius*). The injections were made using pressure over a period of 5-10 s and were monitored using a dissecting microscope with a calibrated micrometer disk.

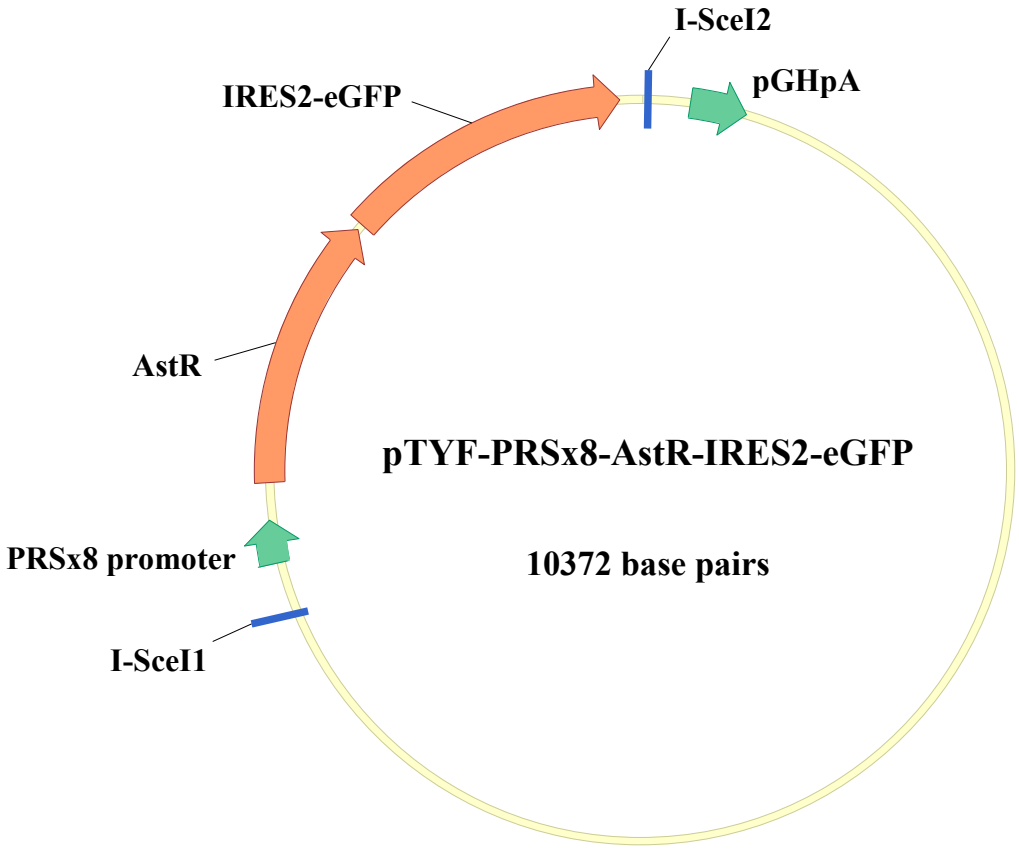

Figure 2-1: PRSx8-AlstR-eGFP-LVV Vector circle map

A vector circle map showing the proteins involved in the construction of the viral plasmid.

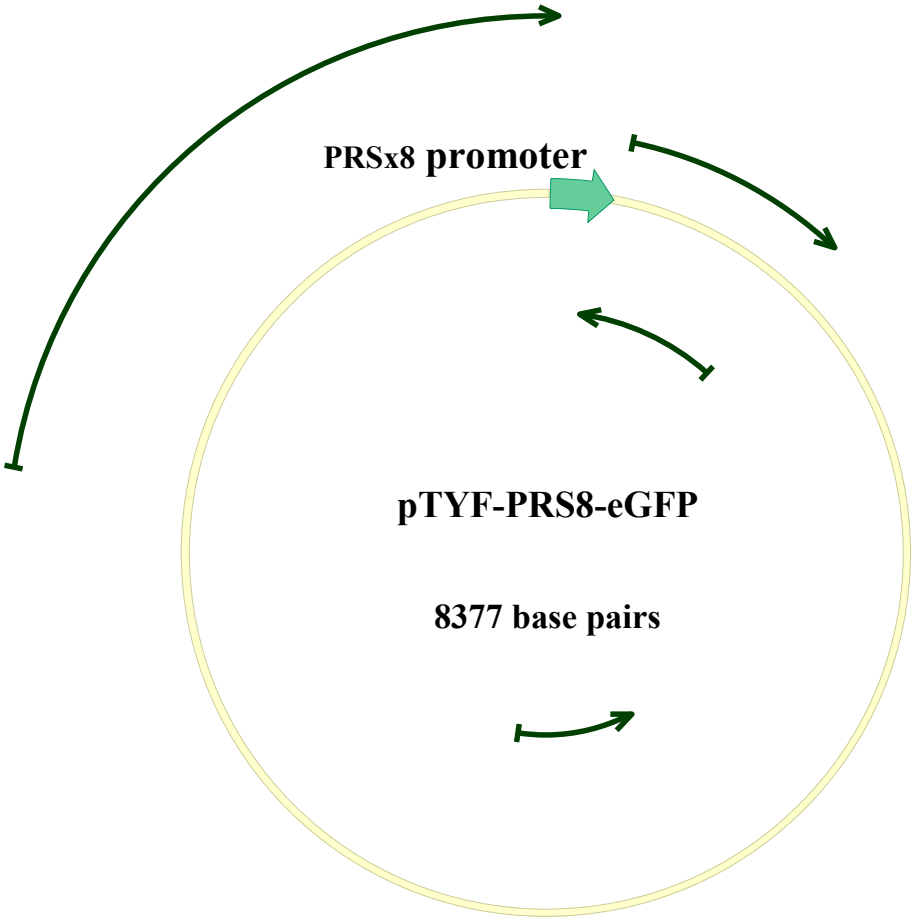

Figure 2-2: PRSx8-eGFP-LVV Vector circle map

A vector circle map showing the proteins involved in the construction of the viral plasmid.

2.2.4 Derivations of QT interval

Needle electrodes were used to acquire lead II ECG. ECG was acquired for 15 minutes prior to programmed electrical stimulation and 15 minutes after allatostatin applications in rats expressing AlstR or eGFP in the DVMN, 15 minutes after saline or muscimol microinjections into the DVMN and in $\alpha\beta\gamma^{-/-}$ and WT mice at baseline. In the pharmacological experiments, ECG was acquired for 15 minutes before and after the administration of each drug.

Three different approaches to deriving QT_C were used due to the established controversies concerning its derivation in rodents (Hayes *et al.*, 1994; Karjalainen *et al.*, 1994). Corrected QT interval (QT_C) was derived using (i) Bazett's formula $QT_{BC} = QT \div \sqrt{(RR \div F)}$ (where RR is in ms and f=100 ms for mice and f=150 ms for rats) (Kmecova & Klimas, 2010; Zuberi *et al.*, 2010); (ii) Fridericia cubic root formula $QT_{FC} = QT \times \sqrt[3]{(RR \div F)}$ (where f=100 ms for mice and f=150 ms for rats); and (iii) nomogram correction $QT_{NC} = QT + 0.384 \times (150 - RR)$ for rats and $QT + 0.156 \times (100 - RR)$ for mice (Hayes *et al.*, 1994; Karjalainen *et al.*, 1994). QT_C was analysed using a Tukey-Kramer multiple comparison test following a three-way ANOVA, comparing the effects of constructs (rats) or genotype (mice), allatostatin/vehicle (rats), age (mice) and QT_C derivation formula. As a surrogate measure of ventricular repolarisation avoiding rate dependency, raw QT measurements from vERP measurements were also analysed.

2.2.5 Humane end-points

At the end of the experiments the animals were euthanised with an overdose of pentobarbitone sodium (200 mg kg^{-1}, i.p.).

2.2.6 Recording the activity of the DVMN neurones

The electrophysiological recordings were kindly conducted by the collaborating lab of Dr. Stefan Trapp. Coronal (200 μm) brainstem slices were obtained from 12-18 month old WT (n=5) and $\alpha\beta\gamma^{-/-}$ (n=4) mice terminally anaesthetised with halothane. Brains were dissected in ice-cold low $[Na^+]$ solution

containing 200 mM sucrose, 2.5 mM KCl, 28 mM $NaHCO_3$, 1.25 mM NaH_2PO_4, 3 mM pyruvate, 7 mM $MgCl_2$, 0.5 mM $CaCl_2$ and 7 mM glucose (pH 7.4). After recovery at 34 °C for 30 minutes in a solution containing 118 mM NaCl, 3 mM KCl, 25 mM $NaHCO_3$, 1.2 mM NaH_2PO_4, 7 mM $MgCl_2$, 0.5 mM $CaCl_2$ and 2.5 mM glucose (pH 7.4), slices were kept at 34 °C in artificial cerebrospinal fluid (aCSF) containing 118 mM NaCl, 3 mM KCl, 25 mM $NaHCO_3$, 1 mM $MgCl_2$, 2 mM $CaCl_2$, and 10 mM glucose saturated with 95% O_2 and 5% CO_2 (pH 7.4).

Recording pipettes (3-6 MΩ) were pulled from thin-walled borosilicate capillaries and recordings were performed in the cell-attached mode using an EPC-9 amplifier and Pulse/Pulsefit software (Heka Elektronik, Lambrecht, Germany). Electrodes were filled with 120 mM K-gluconate, 5 mM HEPES, 5 mM BAPTA, 1 mM NaCl, 1 mM $MgCl_2$, 1 mM $CaCl_2$, and 2 mM K_2ATP (pH 7.2). Recordings were carried out in aCSF saturated with 95% O_2 and 5% CO_2 at 28-32 °C. Currents were filtered at 1 kHz and digitised at 3 kHz. Mean action potential frequency was determined by taking the average frequency over a period of three minutes. Recordings were analysed using Strathclyde Electrophysiology Software (WinEDR/WinWCP; University of Strathclyde).

2.2.7 Histology

At the end of the experiments the rats were perfused through the ascending aorta with 0.9% NaCl solution followed by 500 ml 4% phosphate-buffered (0.1 M, pH 7.4) paraformaldehyde; the brains were removed and stored in the same fixative overnight at 4 °C. After cryoprotection in 30% sucrose, the brainstem was isolated and a sequence of transverse slices (30 μm) was cut. The extent of AlstR-eGFP or eGFP expression and the sites of microinjections were identified histologically using confocal microscopy and mapped using a stereotaxic atlas (Paxinos & Watson, 1998). All drugs and reagents were sourced from SigmaAldrich (UK) unless stated otherwise.

2.2.8 Data analysis

Data are expressed as means ± standard errors. Interactions between groups and/or treatments were analysed using an ANOVA with a Tukey-Kramer multiple comparison test, non-parametric Mann-Whitney-*U* test or paired *t*-test as appropriate. DVMN neuronal recordings from each animal were averaged and analysed using a Wilcoxon Rank-Sum test for difference in the medians.

2.3 Results

2.3.1 Experiment 1. The effects of systemic muscarinic receptor and nitric oxide blockade on cardiac excitability

Parasympathetic control of cardiac excitability mediated by ACh and NO is preserved under urethane anaesthesia. In conditions of β-adrenoceptor blockade (atenolol), atropine administration reduced AVNERP (62±6 *vs* 77±3 ms at baseline; p=0.003, Tukey-Kramer; Figure 2-3A), SNRT (171±7 *vs* 219±5 ms at baseline; p=0.002, Tukey-Kramer; Figure 2-3B) and lowered the S1 coupling interval required to achieve 2:1 heart block (64±1 *vs* 73±2 ms at baseline; p=0.0008, Tukey-Kramer; Figure 2-3C). No significant changes were observed following subsequent systemic nNOS blockade with 7-NI or during the course of the experiment in the group of time/vehicle control animals (Figure 2-3).

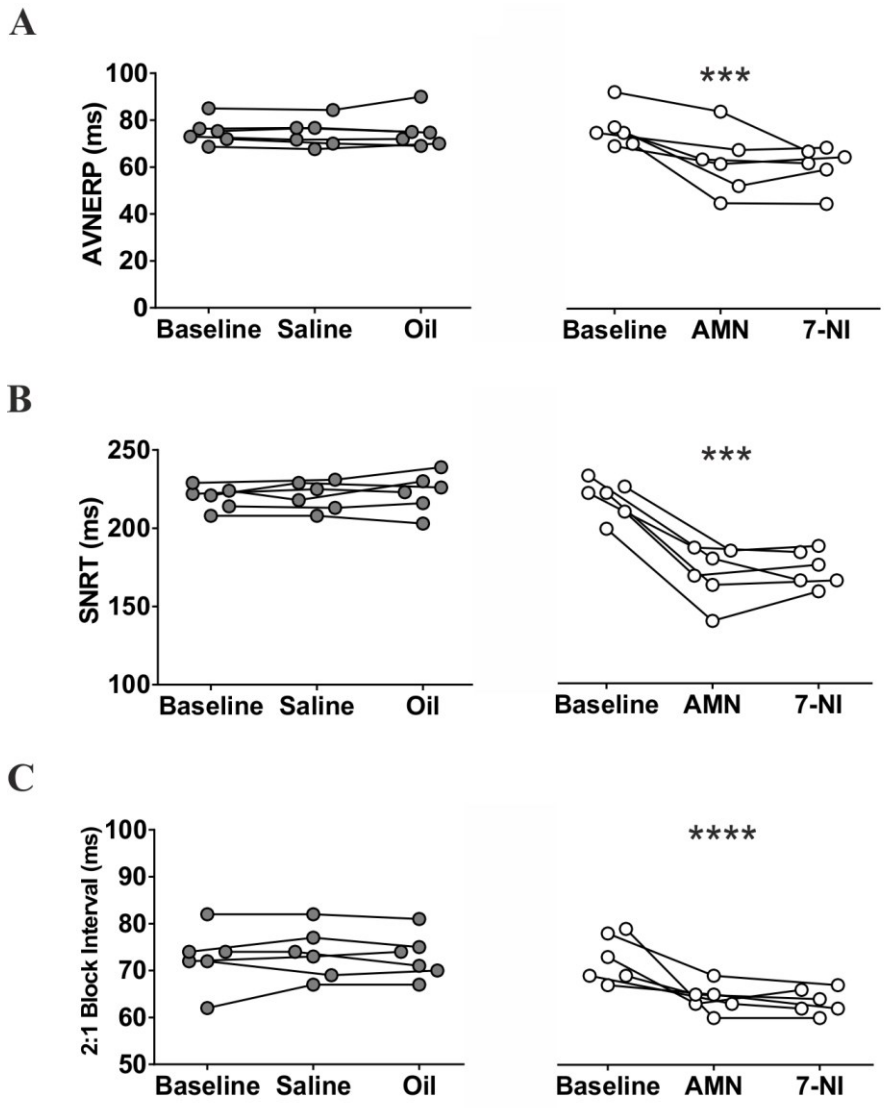

Figure 2-3: Tonic muscarinic influence on the electrical properties of nodal tissue

Summary data obtained in rats under urethane anaesthesia in conditions of systemic β-adrenoceptor blockade illustrating changes in **A**), AV node effective refractory period (AVNERP); **B**) SA node recovery time (SNRT) and **C**) coupling interval required to achieve 2:1 heart block after sequential systemic administration of atropine methyl nitrate (AMN) and neuronal nitric oxide synthase inhibitor 7-Nitroindazole (7-NI), or respective control vehicles (saline for AMN and peanut oil for 7-NI). *Asterisk* denotes significance with respect to baseline. ***P<0.001; ****P<0.0001.

In the ventricular pacing paradigm (in conditions of systemic β-adrenoceptor blockade), atropine had no effect on the left or right vERP and V_T threshold (Figure 2-4). Addition of systemic nNOS blockade was associated with a reduction of both left (40±2 *vs* 49±2 ms at baseline; p=0.001, Tukey-Kramer; Figure 2-4A) and right (41±2 *vs* 49±2 ms at baseline; p=0.03, Tukey-Kramer; Figure 2-4B) vERP. 7-NI administration produced a modest QT_C prolongation measured during vERP assessment protocols in the LV only (74±2 *vs* 67±3 ms at baseline; p=0.02, Tukey-Kramer; Figure 2-4B). This was concordant with the surface ECG data pooled from all atrial and ventricular pacing experiments, revealing a modest prolongation in two derivations of QT_C (Table 2-1). nNOS blockade also resulted in lowering of the left (28±3 *vs* 54±3 ms at baseline; p=0.0002, Tukey-Kramer; Figure 2-4C) and right (45±6 *vs* 60±0 ms at baseline; p=0.001, Tukey-Kramer; Figure 2-4C) V_T thresholds.

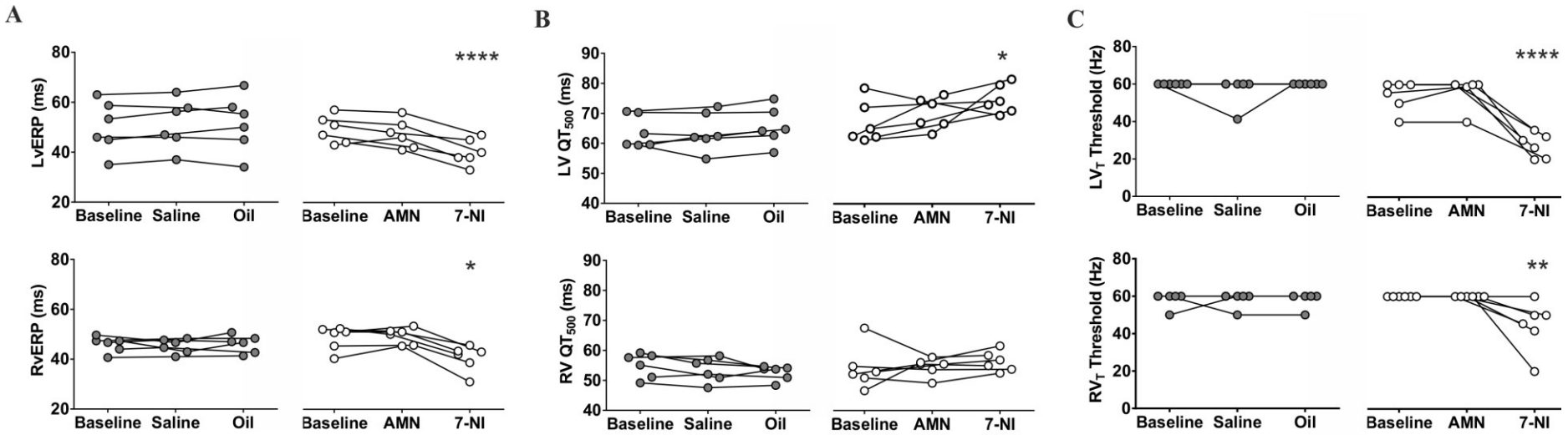

Figure 2-4: Tonic nitric oxide-mediated influence on the electrical properties of the ventricles

Summary data obtained in rats under urethane anaesthesia in conditions of systemic β-adrenoceptor blockade illustrating changes in **A**) left and right ventricular effective refractory period (LvERP and RvERP); **B**) left ventricle (LV) and right ventricle (RV) raw QT (QT_{500}, measurements taken during vERP assessment protocol), and **C**) left and right ventricular tachycardia (LVT and RVT) thresholds after sequential systemic administration of AMN and 7-NI, or respective control vehicles (saline for AMN and peanut oil for 7-NI). *Asterisk* denotes significance with respect to baseline. *P<0.05; **P<0.01; ****P<0.0001.

Table 2-1 The effects of muscarinic and nNOS blockade on ECG Morphology

Parameters of ECG morphology recorded in rats under urethane anaesthesia in conditions of systemic β-adrenoceptor blockade following sequential systemic administration of atropine methyl nitrate and neuronal nitric oxide synthase inhibitor 7-Nitroindazole (7-NI) or respective control vehicles (saline for atropine and peanut oil for 7-NI).

	R-R (ms)	P-R (ms)	QT_{BC} (ms)	QT_{FC} (ms)	QT_{NC} (ms)
Time/Vehicle Controls					
(n=18)					
Baseline	187 ± 3	45 ± 1	89 ± 1	106 ± 2	85 ± 2
Saline	186 ± 3	45 ± 1	90 ± 2	107 ± 2	86 ± 2
Oil	184 ± 3	44 ± 1	88 ± 1	105 ± 1	84 ± 2
Muscarinic/nNOS blockade					
(n=18)					
Baseline	184 ± 3	45 ± 1	89 ± 1	106 ± 1	85 ± 2
AMN	154 ± 3*	48 ± 1	92 ± 1	94 ± 2	86 ± 2
7-NI	170 ± 14	46 ± 2	96 ± 4*	110 ± 14	110 ± 15*

Values are presented as means ± SEM.

7-NI = 7-Nitroindazole; AMN = atropine methyl nitrate; QT_{BC} = QT correction using Bazett's formula; QT_{FC} = QT correction using Fridericia's formula; QT_{NC} = QT correction using the nomogram formula. *Asterisk* denotes significance with respect to baseline and control values. *P<0.05.

2.3.2 Experiment 2. The effects of reduced DVMN activity on ventricular excitability

Application of allatostatin in rats expressing AlstR in the DVMN (Figure 2-5) resulted in vERP shortening (33±1 *vs* 42±1 ms at baseline; p=0.002, Tukey-Kramer; Figure 2-6A, B) in the absence of HR changes (p=0.8; Table 2-2). vERP reduction is known to be pro-arrhythmic in situations of both re-entry and triggered activity. Analyses of averaged ECG waveforms have demonstrated a prolongation of QT_C according to all three correction formulae (p=0.028, Tukey-Kramer; Table 2-2; Figure 2-6C). Measurements obtained during the vERP assessment protocol have also demonstrated QT prolongation in conditions of DVMN inhibition (60±4 *vs* 52±2 ms at baseline; p=0.04, Tukey-Kramer; Figure 2-6D). V_T threshold (manifesting in this case as either monomorphic or polymorphic tachycardia) was lowered following DVMN inhibition (22±4 *vs* 44±9 Hz at baseline; p=0.007, Tukey-Kramer; Figure 2-6E, F). Application of allatostatin in rats expressing eGFP in the DVMN had no effect on vERP (42±4 *vs* 44±0.4 ms at baseline), V_T threshold (51±6 *vs* 52±5 Hz at baseline) or QT_C (Table 2-2). Four rats expressing eGFP remained negative for V_T (up to 60 Hz) throughout the course of the experiment. Three animals expressing AlstR in the DVMN, which were negative for V_T before allatostatin administration, displayed reduced V_T thresholds 30 min after application of the peptide.

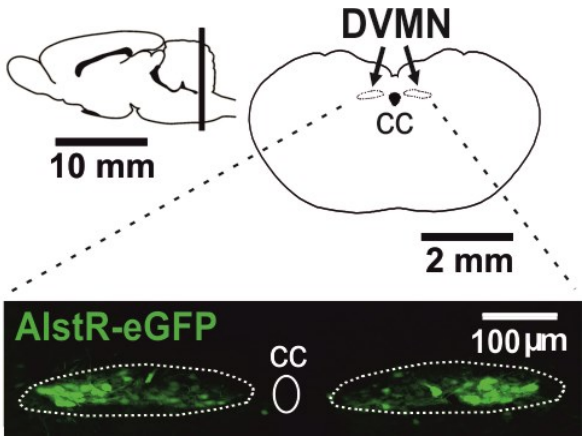

Figure 2-5: Targeting DVMN neurones to reduce their activity

Schematic drawings showing the location of the DVMN in the rat brain. **Below**: a confocal image of a coronal section of the rat brainstem, targeted to express allatostatin receptor (AlstR) in the DVMN. DVMN neurones are transduced to express AlstR-eGFP. CC, central canal.

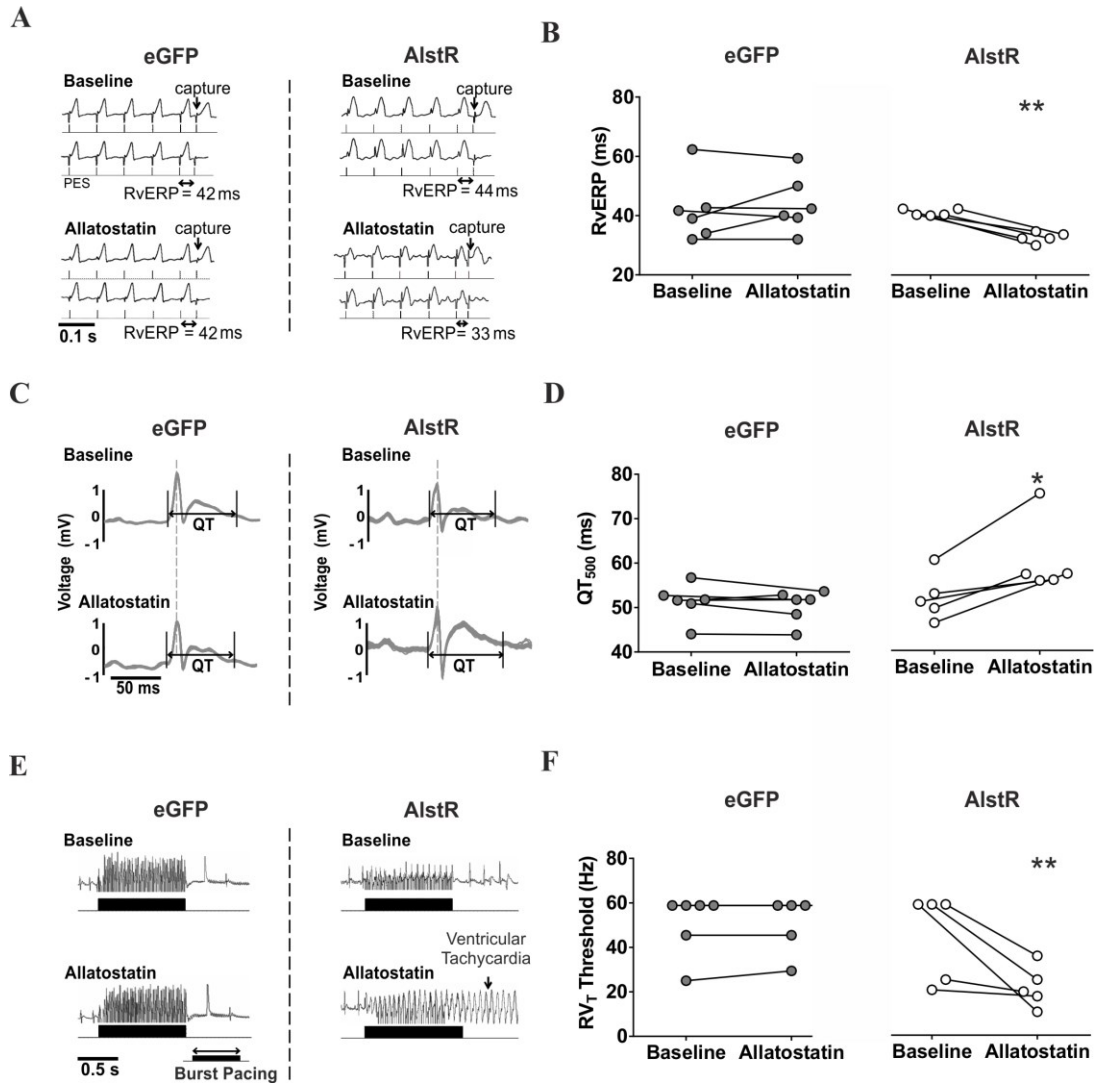

Figure 2-6: The effects of reducing the activity of the DVMN VPNs on the electrical properties of the heart

A) Representative *in vivo* cardiac electrophysiology data produced by programmed electrical stimulation (PES) showing an example of vERP shortening in rats expressing AlstR in the DVMN after administration of allatostatin; **B**) Summary data illustrating vERP shortening after inhibition of the DVMN neurones; **C**) Representative signal averaged ECG recordings illustrating QT prolongation in rats expressing AlstR in the DVMN after administration of allatostatin; **D**) Summary data showing QT_{500} prolongation after inhibition of the DVMN neurones; **E**) Representative *in vivo* cardiac electrophysiology data produced by burst pacing in increasing frequencies showing an example of a lower V_T threshold in rats expressing AlstR in the DVMN after allatostatin application; **F**) Summary data illustrating decreased V_T threshold in rats after DVMN activity is reduced. eGFP - rats expressing enhanced green fluorescent protein in the DVMN. *Asterisk* indicates significance of allatostatin with respect to baseline. *P<0.05; **P<0.01.

Table 2-2 The effects of reducing DVMN activity on ECG morphology

Parameters of ECG morphology in rats expressing eGFP or AlstR in the neurones of the DVMN before and after administration of allatostatin

	R-R (ms)	P-R (ms)	QT_{BC} (ms)	QT_{FC} (ms)	QT_{NC} (ms)
eGFP (n=6)					
Baseline	149 ± 9	51 ± 3	67 ± 4	66 ± 4	70 ± 4
Alst	146 ± 8	49 ± 6	66 ± 4	65 ± 5	70 ± 4
AlstR (n=5)					
Baseline	152 ± 6	50 ± 3	67 ± 4	67 ± 4	71 ± 4
Alst	145 ± 4	47 ± 2	83 ± 5*	80 ± 6*	85 ± 5*

Values are presented as means ± SEM.

Alst = allatostatin (ligand for AlstR); AlstR = allatostatin receptor (animals transduced to express AlstR in the DVMN), eGFP = enhanced green fluorescent protein (animals transduced to express eGFP in the DVMN); QT_{BC} = QT correction using Bazett's formula, QT_{FC} = QT correction using Fridericia's formula; QT_{NC} = QT correction using the nomogram formula. *Asterisk* denotes significance with respect to baseline considering gene-treatment-QT correction interactions. *P<0.05.

In conditions of systemic β-adrenoceptor and muscarinic blockade, inhibition of the DVMN neurones by bilateral microinjections of muscimol reduced left vERP (45±22 *vs* 54±2 ms at baseline; p=0.02, Tukey-Kramer) and V_T threshold (51±4 *vs* 60±0 Hz at baseline; p=0.03, Tukey-Kramer) (Figure 2-7). In the conditions of β-adrenoceptor and muscarinic blockade, DVMN inhibition resulted in a small increase of SNRT (169±2 *vs* 162±2 ms at baseline; p=0.02, Tukey-Kramer) and had no effect on AVNERP, the coupling interval required to achieve 2:1 heart block or QT_C (Figure 2-7).

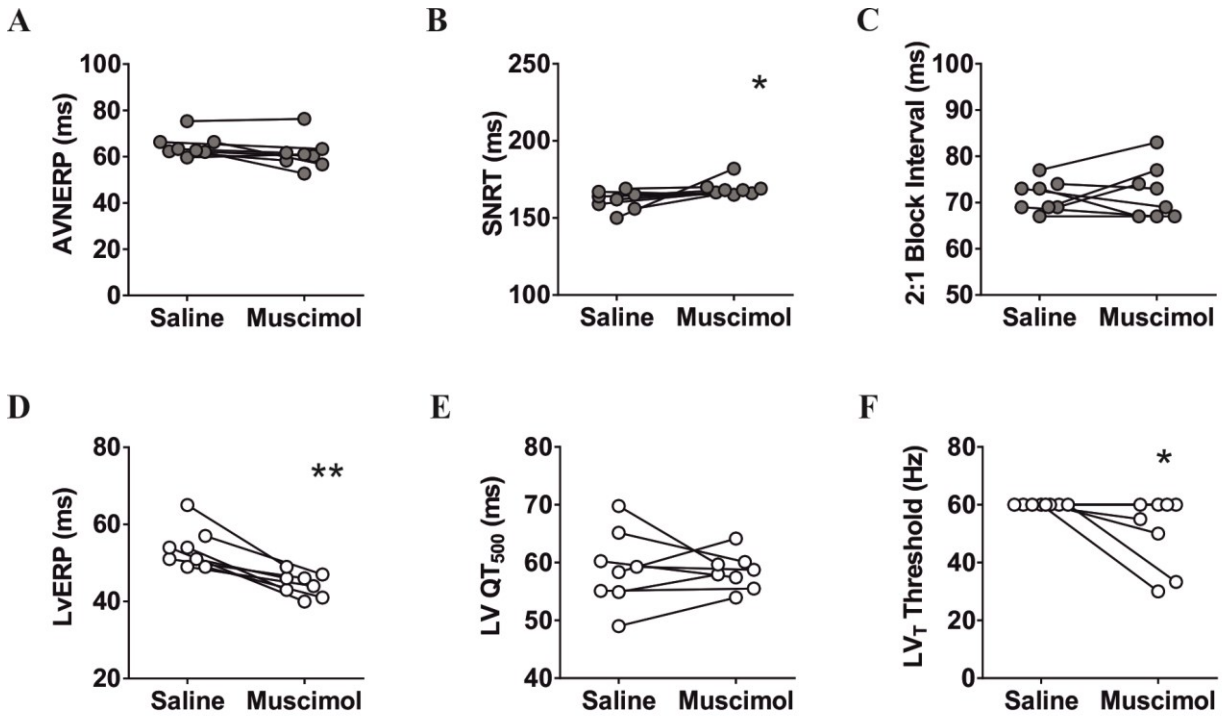

Figure 2-7: The effects of bilateral inhibition of the DVMN neurones by targeted microinjections of muscimol on the electrical properties of the heart in conditions of combined β-adrenoceptor and muscarinic blockade

Summary data illustrating AVNERP, SNRT, the coupling interval required to achieve 2:1 heart block, left vERP, left ventricular QT_{500} and left V_T threshold values after bilateral saline and muscimol microinjections into the DVMN. *Asterisk* denotes significance of muscimol with respect to saline. *P<0.05; **P<0.01.

2.3.3 Experiment 3. The effects of synuclein pathology on DVMN neurones and ventricular electrophysiology

Reduced activity of the DVMN neurones in aging αβγ-/- mice is associated with altered electrical properties of the heart. Six-month old αβγ-/- mice and their WT counterparts showed no significant differences in cardiac electrophysiology: both vERP (37±5 *vs* 37±3 ms; Figure 2-8A) and ECG features including QT_C were similar. In contrast, 12 to18-month old αβγ-/- mice displayed a shorter vERP (31±1 *vs* 43±3 ms in the WTs; p=0.002, Mann-Whitney-*U*; Figure 2-8B) and a prolonged QT_C ($P<0.05$; Table 2-3 Figure 2-8C). Electrophysiological recordings taken from the DVMN neurones in acute brainstem slices showed a markedly reduced level of DVMN activity (~60%) in older αβγ-/- mice (1.2±0.1 *vs* 2.3±0.2 Hz in the WTs; p=0.04, Wilcoxon Rank-Sum test; Figure 2-8D, E).

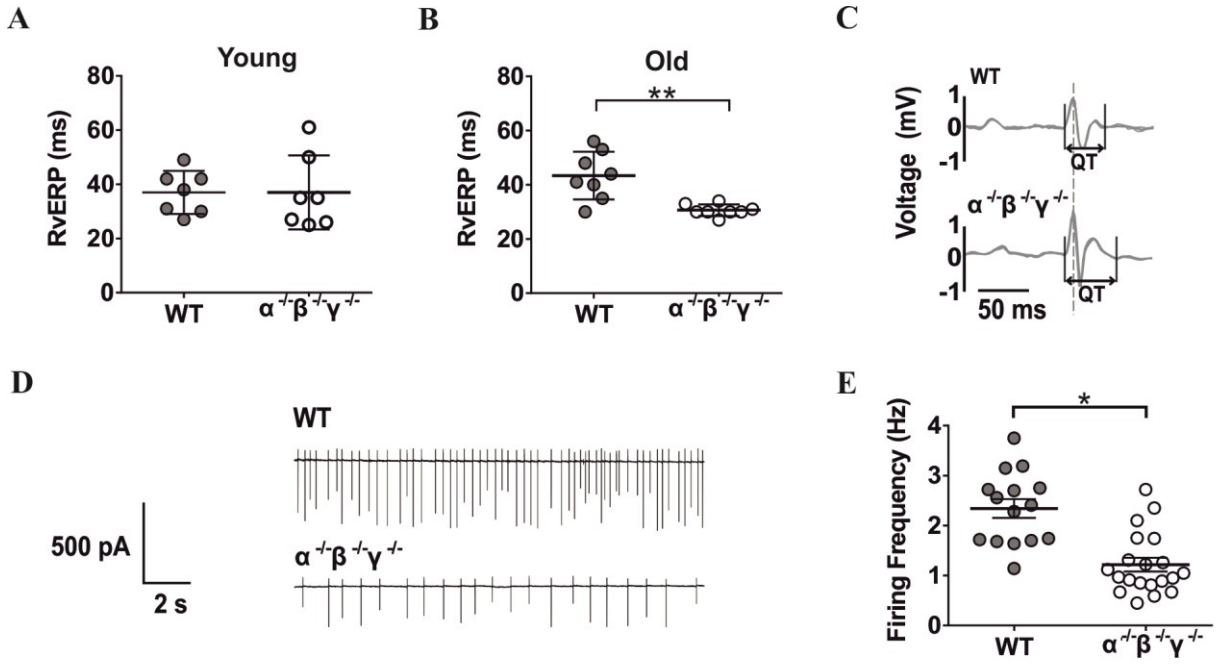

Figure 2-8: Reduced activity of the DVMN neurones in aging triple-synuclein-null ($\alpha\beta\gamma^{-/-}$) mice is associated with altered electrical properties of the heart

A) At 6 months of age there is no difference in vERP between wild type (WT) and $\alpha\beta\gamma^{-/-}$ mice; **B**) At 12-18 months, $\alpha\beta\gamma^{-/-}$ mice had a significantly shorter vERP than WT animals; **C**) Representative signal averaged ECG recordings illustrating QT prolongation in $\alpha\beta\gamma^{-/-}$ mice; **D**) Representative recordings of the electrical activity of the DVMN neurones in WT and $\alpha\beta\gamma^{-/-}$ mice; **E**) DVMN neurones of older $\alpha\beta\gamma^{-/-}$ mice have a significantly reduced firing frequency compared to age- and sex-matched WT counterparts. *Asterisk* denotes significance with respect to WT. *P<0.05; **P<0.01.

Table 2-3 The effects of synuclein pathology on ECG morphology

Parameters of ECG morphology in young and aging wild type and αβγ synuclein deficient mice**.**

	R-R (ms)	**P-R (ms)**	**QT_{BC} (ms)**	**QT_{FC} (ms)**	**QT_{NC} (ms)**
6 month old					
WT (n=6)	94 ± 1	32 ± 2	22 ± 2	20 ± 1	40 ± 18
$\alpha\beta\gamma^{-/-}$ (n=6)	108 ± 10	38 ± 3	21 ± 1	22 ± 1	21 ± 2
12-18 month old					
WT (n=6)	101 ± 4	33 ± 2	22 ± 1	22 ± 1	21 ± 1
$\alpha\beta\gamma^{-/-}$ (n=6)	92 ± 2	39 ± 3	26 ± 2*	24 ± 2*	26 ± 2*

Values are presented as means ± SEM.

WT = wild type mice; $\alpha\beta\gamma^{-/-}$ = triple α,β,γ synuclein protein knockout mice; QT_{BC} = QT correction using Bazett's formula; QT_{FC} = QT correction using Fridericia's formula; QT_{NC} = QT correction using the nomogram formula. *Asterisk* denotes significance with respect to WT considering age-phenotype-QT correction interactions. *P<0.05.

2.4 Discussion

The data obtained in the present study demonstrate that reduced activity of the DVMN VPNs has a significant impact on cardiac electrical properties with changes consistent with a potential for ventricular arrhythmia. Targeted reduction of DVMN activity in a rat model is associated with vERP shortening and a reduced V_T threshold. The absence of changes in R-R and P-R intervals, vERP shortening and reduced V_T threshold with no associated lowering of AVNERP or SNRT, observed during reduced DVMN activity in conditions of β-adrenoceptor and muscarinic blockade, would suggest preferential innervation of the ventricles by the DVMN neuronal projections.

Tonic parasympathetic influence on cardiac electrical stability is preserved in experimental animals kept under urethane anaesthesia. In conditions of β-adrenoceptor blockade, sequential systemic muscarinic and nNOS inhibition confirmed that vagal effects are mediated by the actions of ACh and NO. Systemic atropine administration led to a reduction in AVNERP, SNRT and coupling interval required to achieve 2:1 heart block and had no effect on vERP and V_T. Systemic 7-NI treatment had no further effect on AVNERP, SNRT and coupling interval, but led to a significant reduction in both left and right vERP and V_T. These data suggest that the vagal effects are mediated by a muscarinic mechanism at the level of atria/nodal tissue and by NO at the level of the ventricles. The latter conclusion is concordant with the most recent academic literature (Brack *et al.*, 2009; Brack *et al.*, 2011).

This NO-mediated parasympathetic influence on the heart appears to stem from the activity of the DVMN neurones. Indeed, when the activity of the DVMN was reduced in conditions of combined muscarinic and β-adrenoceptor blockade, only reductions in vERP and VT (and not in AVNERP or SNRT) were observed. The cholinergic component is established to largely originate from the population of VPNs of the NA, which are believed to provide the most important source of phasic parasympathetic control of the SA and AV nodes (Taylor *et al.*, 1999).

Having previously demonstrated that synuclein deficiency results in age-dependent synaptic abnormalities by a collaborating laboratory (Anwar *et al.*, 2011), $\alpha\beta\gamma^{-/-}$ mice were used as a model of age-dependent autonomic dysfunction relevant to Parkinson's disease. In aging $\alpha\beta\gamma^{-/-}$ mice reduced activity of the DVMN neurones was found to be associated with altered electrical properties of the heart similar to that observed in rats following acute DVMN inhibition.

2.5 Study Limitations

In both models (rats and mice), changes in the QTc interval were measured and a prolongation associated with vagal withdrawal was found. The magnitude of the recorded QTc changes, however, was variable depending on the experimental protocol. There are a number of considerations concerning the interpretation of these findings. The combination of shortened vERP and prolonged QTc is paradoxical although this has been observed previously in mice with global genetic deletion of $G\alpha i_2$ (Zuberi *et al.*, 2010). These differences have been explained by the rate dependence of changes in the dynamics of repolarisation. In addition, it is worth noting that vERP and action potential duration are not always strictly correlated (Coronel *et al.*, 2012). Finally, there is some debate with regards to the nature of the T wave in rodents and how it exactly relates to ventricular repolarisation (Zhang *et al.*, 2014).

The use of anaesthesia can also alter ventricular excitability and predisposition to arrhythmia (Wong *et al.*, 1993; Lorente *et al.*, 2000). Arrhythmias were observed only during electrical stimulation designed to evoke arrhythmia, i.e. the rodents did not develop spontaneous arrhythmias. Replication of these findings in conscious rats or mice with cardiac telemetry monitoring to evaluate the native cardiac rhythm would enhance the clinical applicability of these results. Future experiments should thus employ techniques for chronic DVMN inhibition in conscious rodents in longitudinal studies.

Allatostatin does not cross the blood-brain barrier however and cannulation is required for brainstem access, making chronic inhibition and *in vivo* conscious studies difficult. Transducing the DVMN with inhibitory G-protein coupled receptor based DREADD receptors would overcome the need to deliver the ligand via an intrathecal cannula, as clozapine N-oxide can be administered via intraperitoneal injection or drinking water (Armbruster *et al.*, 2007). DREADDs further open the possibility of combinatorial experiments by using inhibitory and excitatory receptors that have been differentially targeted to either a subset of sympathetic or parasympathetic neurones through combinations of viral and transgenic approaches. This would allow *in vivo* analyses of models with selective functional silencing and

excitation of autonomic neurones, as well as expanded mapping of key central neural circuits influencing autonomic output (Armbruster *et al.*, 2007). The viral titres for the constructs used were not reliably known. Acceptable expression was predetermined by injection in test subjects allowing four weeks prior to conducting histology. The extent of expression could have instead been evaluated via polymerase chain reaction as titres would inevitably vary, given the titre loss of the lentiviral constructs immediately after thawing.

Also, rodents are not the ideal models for studying disorders of cardiac repolarisation as the K^+ currents affected differ according to the species tested (Davis *et al.*, 2011). Various murine models of cardiac arrhythmia have been developed, such as those with Na^+ channel defects and autonomically driven arrhythmias associated with engineered defects in Ca^{2+} handling (Cerrone *et al.*, 2005). However, the basic organisational, developmental and signalling pathways between the brain and the heart are broadly conserved across small and large mammals, which gives the fundamental observations based on the reported data from these experiments a clear translational relevance (Yutzey & Robbins, 2007). Also, as rats and mice are both identified as being largely sympathetic animals, establishing a significant parasympathetic component to the functional innervation of the ventricles should be regarded as an important finding given that it may have a larger contribution within humans and other larger mammals.

In summary, a rat model was employed in this study to determine the effects of acute DVMN inhibition and a mouse model was used to study the effects of age-dependent decline in DVMN activity, relevant to the development of Parkinson's disease. Both models demonstrated that reduced activity of DVMN neurones have a significant impact on cardiac electrical properties, with changes consistent with the development of a ventricular pro-arrhythmic phenotype. Vagal influence on ventricular excitability generated by the DVMN is likely to be mediated by NO. These findings are the first of their kind to provide a fundamental insight into the central nervous substrate that underlie functional parasympathetic innervation of the ventricles and thus highlight its vulnerability in the context of neurodegenerative diseases.

Chapter 3 Control of Ventricular Contractility

3.1 Introduction

The heart is controlled by the parasympathetic and sympathetic limbs of the autonomic nervous system. Sympathetic nerves innervate the sinoatrial and atrioventricular nodes, the atria, ventricles and the conducting tissue. Parasympathetic efferent fibres are known to control nodal tissues and atria. The role of the vagal innervation of the ventricles, however, remains controversial (Coote, 2013). The majority of physiology textbooks state that the vagal innervation of the ventricle is sparse and direct parasympathetic control of ventricular contractility is insignificant. This view persists in both the scientific and educational literature despite evidence obtained in various species (from mouse to man) demonstrating the presence of ChAT-positive nerve fibres, acetylcholinesterase and muscarinic receptors in both ventricles (for a recent review, see Coote, 2013). Rich cholinergic innervation of epicardial and endocardial ventricular surfaces was demonstrated in human (Kent *et al.*, 1974; Pauza *et al.*, 2000), pig (Crick *et al.*, 1999; Ulphani *et al.*, 2010), and rat hearts (Zang *et al.*, 2005a; Mastitskaya *et al.*, 2012).

Although the functional significance of direct parasympathetic influence on ventricular contractility at resting condition remains unknown, data obtained from dogs, pigs and humans have demonstrated that VNS decreases the force of ventricular contraction independent of HR changes (Eliakim *et al.*, 1961; Degeest *et al.*, 1965c; Lewis *et al.*, 2001). These data are also supported by the results of the *in vitro* studies conducted on isolated rat (McMorn *et al.*, 1993), cat (Hommers *et al.*, 2003), guinea pig (Zang *et al.*, 2005b) and ferret (Ito *et al.*, 1995) cardiomyocytes. For example, ferret ventricular cardiomyocytes respond to a prototypical effector molecule of the parasympathetic nervous system - ACh - with a reduction in the magnitude of their muscle twitch shortening (Dobrzynski *et al.*, 2002). These effects of ACh are mediated via rapid phosphorylation of certain inwardly rectifying potassium channels (in particular Kir3.1 and Kir3.4, expressed throughout the heart including the ventricles) (Dobrzynski *et al.*, 2001) potentiating K^+ currents and/or reduction of Ca^{2+} currents (Belardinelli *et al.*, 1995; Dobrzynski *et al.*, 2002).

Neuronal tracing studies conducted in rats (Nosaka *et al.*, 1979; Nosaka *et al.*, 1982; Stuesse, 1982; Izzo *et al.*, 1993), cats (Sugimoto *et al.*, 1979; Ciriello & Calaresu, 1980; Geis & Wurster, 1980b; Kalia & Mesulam, 1980; Bennett *et al.*, 1981; Geis *et al.*, 1981; Miura & Okada, 1981; Ciriello & Calaresu, 1982; Jones *et al.*, 1995), dogs (Bennett *et al.*, 1981; Hopkins & Armour, 1982, 1984; Plecha *et al.*, 1988), and pigs (Hopkins *et al.*, 1984; Hopkins *et al.*, 1997) identified the anatomical locations of cardiac VPNs primarily residing within the brainstem NA and the DVMN. Neurones of the NA have rhythmic, respiratory-related patterns of discharge with B fibre axons innervating nodal tissue (McAllen & Spyer, 1976; McAllen & Spyer, 1978b, a; Ciriello & Calaresu, 1982). The relative proportion of DVMN neurones projecting to the heart is believed to be low (Jones, 2001) and their functional significance in the control of cardiac function remains unknown. DVMN neurones have slowly conducting C fibre (unmyelinated) axons (Ciriello & Calaresu, 1980; Nosaka *et al.*, 1982; Jones *et al.*, 1995) and are not modulated by respiratory networks. There is evidence that the activities of these neurones protect (via a muscarinic mechanism) ventricular cardiomyocytes against acute ischemia/reperfusion injury (Mastitskaya *et al.*, 2012) and control ventricular excitability (Chapter 2), which suggests that the DVMN contains a population of VPNs that innervate the LV.

In the present study, an anaesthetised rat model was used to test the hypothesis that DVMN VPNs contribute to the control of LV contractility. First, the presence of tonic vagal influence on LV inotropy was confirmed (demonstrated by systemic muscarinic receptor blockade). Next, the effects of reducing the activity of DVMN neurones on LV contractility were determined and finally the anatomical location of the functional subpopulation of the DVMN neurones was identified, which are responsible for parasympathetic control of LV contractility.

3.2 Methods

All the experiments were performed in accordance with the European Commission Directive 2010/63/EU (European Convention for the Protection of Vertebrate Animals used for Experimental and Other Scientific Purposes) and the UK Home Office (Scientific Procedures) Act (1986) with project approval from the Institutional Animal Care and Use Committee.

3.2.1 Animal preparation

Adult male Sprague-Dawley rats (Charles River Laboratories, Oxford, UK) weighing 380–450 g were anaesthetised with urethane (1.3 g^{-1} kg^{-1}; i.p.; following 4% isoflurane induction) or pentobarbitone sodium (Animalcare, York, UK) (induction 60 mg kg^{-1} i.p.; maintenance 10-15 mg kg^{-1} h^{-1} i.v.). Since anaesthesia is known to have a significant impact on vagal activity, experiments designed to reveal tonic parasympathetic influence on the LV (Experiments 1, 2 and 3) were conducted on animals anaesthetised with urethane, which has been shown to preserve the level of chronotropic vagal tone similar to that in decerebrate animals (O'Leary & Jones, 2003). Experiments designed to recruit vagal activity (Experiment 3) were conducted in rats anaesthetised with pentobarbital, which reduces vagal tone (O'Leary & Jones, 2003).

Adequate anaesthesia was ensured throughout the experiment through continuous monitoring of HR and arterial blood pressure (ABP) stability and the absence of a withdrawal response to a paw pinch. With the animal in a supine position, the femoral artery and both femoral veins were cannulated for measurement of the systemic ABP, fluid infusion and administration of drugs. A 2F Millar pressure catheter (SPR-320NR, Millar instruments, Texas, USA) was advanced via the right carotid artery and positioned within the chamber of the LV to monitor changes in LV pressure (LVP) (Figure 3-1A). The trachea was cannulated and the animal was ventilated with room air using a small rodent ventilator (Model 683, Harvard Apparatus, Massachusetts, USA) with a tidal volume of ~8-10 ml kg^{-1} set at a normal respiratory frequency of ~60 strokes min^{-1}. Body temperature was maintained with a servo-controlled heating pad at 37.0±0.5 °C. Partial pressures of

O_2 and CO_2 as well as pH of the arterial blood were measured every hour (RAPIDLab 348EX, Siemens, Surrey, UK). The rate and volume of mechanical ventilation were adjusted and oxygen was added to the respiratory gas mixture (if required) to maintain blood gases within the physiological ranges. ABP, LVP, tracheal pressure and standard lead II ECG were recorded using a Power1401 interface and *Spike2* software (Cambridge Electronic Design, Cambridge, UK). Average waveforms were used to determine systolic blood pressure (SBP), diastolic blood pressure (DBP), mean arterial blood pressure (MAP), LV end systolic pressure (LVESP), and LV end diastolic pressure (LVEDP). The differential of LV pressure (LVd*P*/dt) was derived from the LVP recording using the slope function.

3.2.2 Assessment of left ventricular contractility

The atria were paced at a rate of 10 or 20% above the resting HR using silver wire electrodes advanced via the oesophagus to the level of the heart (Figure 3-1A). To remove sympathetic influences, β-adrenoceptor blocker atenolol was administered (initial bolus dose 2 mg kg^{-1} i.v., followed by 3 mg^{-1} kg^{-1} h^{-1} i.v. infusion) and the spinal cord was transected at the cervical level (C1). To restore arterial blood pressure (MAP ~100 mmHg) after C1 transection, vasopressin (0.15 nM in saline) was infused intravenously at a rate of 10 µl min^{-1} (Figure 3-1B). The maximum of the first differential of LVP (LV*dP*/dt_{max}, mmHg s^{-1}) measures the inotropic state but with a caveat of load dependency. Systemic β-adrenoceptor blockade, C1 transection and vasopressin infusion remove sympathetic influences, provide constant loading conditions and fixed filling times (whilst pacing), allowing the use of LVd*P*/dt_{max} as a measure of LV contractility (further assessment of the LV contractile function by indexing of the maximum of the first differential to instantaneous LVP [(LV*dP*/dt_{max})/LVP] or deriving the maximum instantaneous ratio of this $[(LVdP/dt)/LVP]_{max}$ was not used due to known limitations (Van den Bos *et al.*, 1973)).

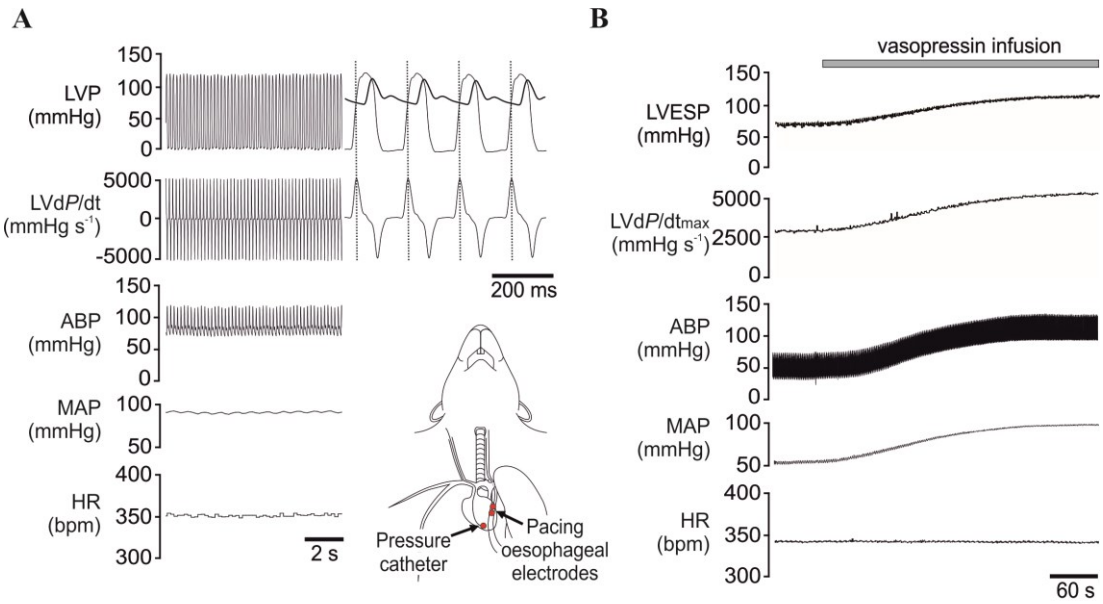

Figure 3-1: Experimental approaches used for the assessment of left ventricular contractility in anaesthetised rats

A) Representative recordings obtained in pentobarbital-anaesthetised rat illustrating simultaneous monitoring of heart rates (HR), arterial blood pressure (ABP), left ventricular pressure (LVP), derived mean arterial blood pressure (MAP) and the first differential of left ventricular pressure (LVdP/dt); Inset: Scheme illustrating placement of a 2F Millar pressure catheter in the LV chamber (advanced via the right common carotid artery) and positioning of atrial pacing electrodes in the lumen of the oesophagus at the level of the right atrium; **B)** Representative example of simultaneous monitoring of HR, MAP, ABP, LV end-systolic pressure (LVESP) and maximum of the first differential of the LV pressure ($LVdP/dt_{max}$) in conditions of systemic β-adrenoceptor blockade and spinal cord transection at C1 level before and during intravenous infusion of vasopressin (0.15 nM, 10 µl min^{-1}) to restore MAP to ~100 mmHg. Normal arterial pH, PCO_2 and PO_2 were maintained by adjusting parameters of mechanical ventilation and providing supplemental oxygen in the inspired gas mixture. Sympathetic blockade and vasopressin infusion provide constant loading conditions and fixed filling times whilst pacing, allowing the use of $LVdP/dt_{max}$ as a measure of LV contractility.

3.2.3 Ultrasound imaging of the LV

LV pressure-area loop analysis was performed by a combined measurement of LVP using a 2F Millar pressure catheter and LV imaging using a Vevo® 2100 ultrasound system (VisualSonics, Amsterdam, The Netherlands). A MS250 13-24MHz linear array transducer was used to provide a parasternal long-axis view (Figure 3-2A). Precautions were taken to minimise the effects of cardiac preload using the approach previously described (Lewis *et al.*, 2001). With a suture positioned sub-diaphragmatically around the inferior vena cava as a snare to lower SBP by ~25 mmHg while pacing at a rate of 10% above resting HR, LVP-area data were acquired in segments each comprised of 15 heart beats (Figure 3-2B). Measurements were made before and after systemic β-adrenoceptor blockade with atenolol (3 mg kg^{-1} i.v.) and again following systemic muscarinic receptor blockade with atropine methyl nitrate (2 mg kg^{-1}; i.v.). Using LV cross-sectional area (mm^2) as a surrogate measure of LV volume, the regression slope of the end-systolic LVP-area relationship was used to determine the end-systolic elastance (Ees, mmHg mm^{-2}; Figure 3-2B) – an index of LV inotropic state which is insensitive to loading conditions.

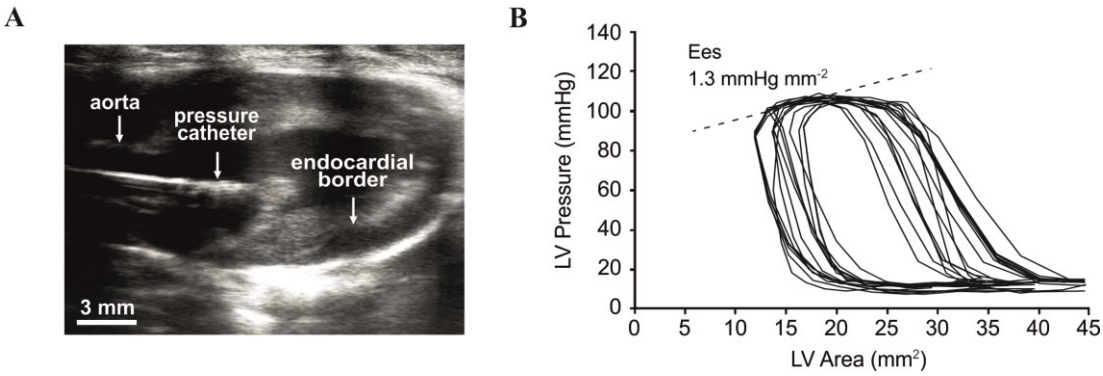

Figure 3-2: An ultrasound approach combined with invasive measurements for the assessment of left ventricular contractility in anaesthetised rats

A) A B-Mode ultrasound image of a parasternal long axis view of the LV with a Millar pressure catheter placed in the LV chamber for simultaneous recordings of the LVP and LV area; **B**) Representative LV pressure-area relationships obtained in a urethane-anaesthetised rat in conditions of systemic β-adrenoceptor blockade (atenolol). Atrial pacing at 400 bpm was combined with occlusion of the inferior vena cava to provide a family of pressure-area loops. To determine end-systolic elastance (Ees), a regression line was drawn between the LVESP-area points of each loop ensuring $r^2>0.9$.

3.2.4 Genetic targeting of the DVMN vagal preganglionic neurones

Young male Sprague-Dawley rats (50-60 g) were anaesthetised with ketamine (Vetalar, Zoetis, London, UK) (60 mg kg^{-1} i.m.) and medetomidine (Domitor, Elanco, Animal Health, Hampshire, UK) (250 μg kg^{-1} i.m.). Adequate depth of surgical anaesthesia was confirmed by the absence of a withdrawal response to a paw pinch. With the head fixed prone in a stereotaxic frame, lignocaine (Norbrook, Cumbria, UK) (2 ml of 0.2% solution) was injected subcutaneously before a midline dorsal neck incision was made to expose the atlanto-occipital membrane and then the dorsal surface of the brainstem. DVMN was targeted bilaterally with two microinjections per side (0.25 μL at a rate of 0.05 μL min^{-1}) of a solution containing viral particles of PRSx8-AlstR-eGFP-LVV or PRSx8-eGFP-LVV. The established titres at the time of production were within the range of 1 x 10^9 and 1 x 10^{10} transducing units ml^{-1}. Taking the *calamus scriptorius* as the reference point, the injections were made at 0.5 mm rostral, 0.6 mm lateral, 0.8 mm ventral and at 1.0 mm rostral, 0.8 mm lateral, 0.6 mm ventral. Anaesthesia was reversed with atipemazole (Antisedan, Elanco, Animal Health, Hamspshire, UK) (1 mg kg^{-1}; i.m.). For post-operative analgesia, the rats were administered with buprenorphine (Vetergesic, York, UK) (0.05 mg^{-1} kg^{-1} d^{-1}; s.c.) for three days and caprofen (Caprieve, Norbrook, Cumbria, UK) (4 mg^{-1} kg^{-1} d^{-1}; i.p.) for five days. The rats weighed 380-450 g at the time of the experiments.

3.2.5 Glutamate and muscimol microinjections into the DVMN

The animals were anaesthetised and instrumented as described above, and the head was fixed in the stereotaxic frame dorsal side up. An occipital craniotomy was performed and the cerebellum was partially removed to expose the dorsal surface of the brainstem. A three-barrelled glass micropipette (tip size 20-25 μm) was used for microinjections of either glutamate or muscimol in discrete locations along the rostro-caudal extent of the left and right DVMN. Microinjections were randomised and inserted into the three DVMN locations separated by distances of 0.5 mm. Taking the *calamus scriptorius* as the reference point, the microinjections were made at 1.5 mm rostral, 0.8 mm lateral, 0.9 mm ventral (*rostral* area), 1.0 mm rostral, 0.75 mm lateral, 0.7 mm ventral (*intermediate* area), and 0.3 mm rostral, 0.7 mm lateral,

0.8 mm ventral (*caudal* area). The barrels of the micropipette contained glutamate or muscimol, with vehicle and saline containing 5% of fluorescent beads (Invitrogen, Paisley, UK). The injections were made using pressure over a period of 5-10 s and were monitored using a dissecting microscope with a calibrated micrometer disk.

3.2.6 Histology

At the end of the experiments the rats were perfused through the ascending aorta with 0.9% NaCl solution followed by 500 ml 4% phosphate-buffered (0.1 M, pH 7.4) paraformaldehyde; the brains were removed and stored in the same fixative overnight at 4 °C. After cryoprotection in 30% sucrose, the brainstem was isolated and a sequence of transverse slices (30 μm) was cut. The extent of AlstR-eGFP or eGFP expression and the sites of microinjections were identified histologically using confocal microscopy and mapped using a stereotaxic atlas (Paxinos & Watson, 1998). All drugs and reagents were sourced from SigmaAldrich (UK) unless otherwise stated.

3.2.7 Experiment 1. The effects of systemic muscarinic receptor blockade on left ventricular contractility

The animals were anaesthetised with urethane (maintains a level of vagal tone) or pentobarbital (reduces vagal tone), prepared as described above and left to stabilise for 15-30 min before measurements of baseline cardiovascular variables were taken. The effects of systemic muscarinic receptor blockade (atropine methyl nitrate, 2 mg kg^{-1} i.v.) on LV contractility was evaluated during atrial pacing (10% above resting HR) in conditions of systemic β-adrenoceptor blockade (atenolol) combined with C1 transection to remove sympathetic influences (sympathetic blockade). In a separate cohort of animals, LV pressure recordings and ultrasound LV area imaging were conducted followed by LV pressure-area loop analysis to determine the effects of atropine methyl nitrate on LV end-systolic elastance.

3.2.8 Experiment 2. The effects of reduced DVMN activity on left ventricular contractility

The animals transduced to express AlstR-eGFP or eGFP by the DVMN neurones were anaesthetised with urethane and prepared as described above. To

achieve acute and selective inhibition of DVMN neurones expressing AlstR, a small occipital craniotomy was performed and a miniature polyethylene catheter was placed in the *cisterna magna* to deliver allatostatin (4 µl of 100 µM solution in aCSF). The animals were left to stabilise for 15-30 min. The measurements of cardiovascular variables were taken before and after allatostatin application in rats expressing AlstR-eGFP (reduced DVMN activity) or eGFP (control).

3.2.9 Experiment 3. To identify the region of the DVMN responsible for the control of left ventricular contractility

The animals were anaesthetised with pentobarbital (reduces vagal tone) and prepared as described above. The dorsal surface of the brainstem was exposed (to allow microinjections into the DVMN) and the animals were left to stabilise for 15-30 min. Neurones in discrete locations along the rostro-caudal extent of the left and right DVMN were activated following microinjections of an excitatory amino-acid L-glutamate (10 mM; 40 nl; pH 7.4) and the effects of these treatments on cardiovascular variables were assessed at resting HR conditions, during atrial pacing (10% above resting HR) and after systemic β-adrenoceptor blockade (atenolol) combined with C1 transection to remove sympathetic influences. In a separate cohort of animals anaesthetised with urethane, caudal DVMN areas (identified as having a significant impact on LV contractility as a result of studies with the use of glutamate microinjections) were inhibited by microinjections of a potent $GABA_A$ receptor agonist muscimol (0.1 M; 40 nl; pH 7.4), and the effects of this treatment on LV contractility was assessed. Microinjections of a vehicle (0.9% NaCl; 40 nl) were used to determine the effects of the delivery of a given volume. The order of DVMN microinjections was randomised between the left and right sites.

3.2.10 Humane end-points

At the end of the experiments the animals were euthanised with an overdose of pentobarbitone sodium (200 mg kg^{-1}, i.p.).

3.2.11 Data analysis

Recordings of the cardiovascular variables were analysed using *Spike2* software (Cambridge Electronic Design). LV pressure-area loop analysis was performed using Lab Chart 8 software (ADInstruments, Oxford UK). Differences between the experimental groups were assessed for statistical significance using GraphPad Prism 6 software (GraphPad Software, California, USA). Comparisons were made using a two-way ANOVA (followed by Sidak's p value correction for multiple comparisons) or Student's paired or unpaired *t* test, as appropriate. Data are reported as individual values and means ± s.e.m. Differences with $P<0.05$ were considered to be significant.

3.3 Results

3.3.1 Experiment 1. The effects of systemic muscarinic receptor blockade on left ventricular contractility

In rats anaesthetised with urethane and in conditions of systemic β-adrenoceptor blockade (atenolol) combined with C1 transection (to remove sympathetic influences), intravenous administration of atropine methyl nitrate (2 mg kg^{-1}) led to significant increases in HR, ABP, LVESP and LVd*P*/dt_{max} (Table 3-1). Increases in MAP, LVESP and LVd*P*/dt_{max} following atropine administration were also observed during atrial pacing (Figure 3-3A; Table 3-1). On the other hand, in rats anaesthetised with pentobarbital, systemic atropine had no effect on cardiovascular variables during atrial pacing in conditions of sympathetic blockade (Figure 3-3A; Table 3-1).

In a separate series of experiments, LV pressure-area loop analysis has demonstrated decreases in LV contractility following systemic atenolol administration both in urethane-anaesthetised animals (decrease in Ees from 2.5±0.2 to 1.4±0.2 mmHg mm^{-2}; p=0.0004; Figure 3-3B), as well as in animals anaesthetised with pentobarbital (decrease in Ees from 2.3±0.2 to 1.3±0.2; p=0.0001; Figure 3-3B). Subsequent systemic administration of atropine increased end-systolic elastance in urethane- (increase in Ees from 1.3±0.2 to 1.7±0.2 mmHg mm^{-2}; p=0.007; Figure 3-3C), but not in pentobarbital- (1.1±0.1 *vs* 1.0±0.1 mmHg mm^{-2}; p=0.3; Figure 3-3C) anaesthetised animals. These data confirm the existence of a tonic inhibitory muscarinic influence on LV contractility, which in rats is preserved under urethane anaesthesia and is suppressed by pentobarbital.

Table 3-1 The effects of systemic muscarinic receptor blockade with atropine methyl nitrate on cardiovascular variables in conditions of β-adrenoceptor blockade and C1 transection to remove sympathetic influences

Anaesthesia	**Urethane**		**Pentobarbital**
	Unpaced	**Paced**	**Paced**
n	6	6	7
LVdP/dt max (mmHg s-1)			
Saline	5500 ± 487	4642 ± 127	4708 ± 184
AMN	6894 ± 664	5253 ± 215	4760 ± 203
Mean difference	1394 ± 224	611 ± 95	50 ± 79
p	0.002	0.001	0.5
LVESP (mmHg)			
Saline	120 ± 3	118 ± 4	120 ± 3
AMN	138 ± 5	132 ± 6	119 ± 3
Mean difference	18 ± 4	14 ± 3	1 ± 2
p	0.006	0.004	0.5
LVEDP (mmHg)			
Saline	4 ± 2	5 ± 1	6 ± 1
AMN	5 ± 2	5 ± 1	5 ± 1
Mean difference	1 ± 1	0 ± 1	0 ± 1
p	0.8	0.4	0.7
MAP (mmHg)			
Saline	98 ± 2	95 ± 2	103 ± 4
AMN	110 ± 3	108 ± 3	101 ± 3
Mean difference	12 ± 2	13 ± 3	2 ± 2
p	0.003	0.004	0.4
HR (bpm)			
Saline	353 ± 6		
AMN	374 ± 8		
Mean difference	21 ± 6		
p	0.01		

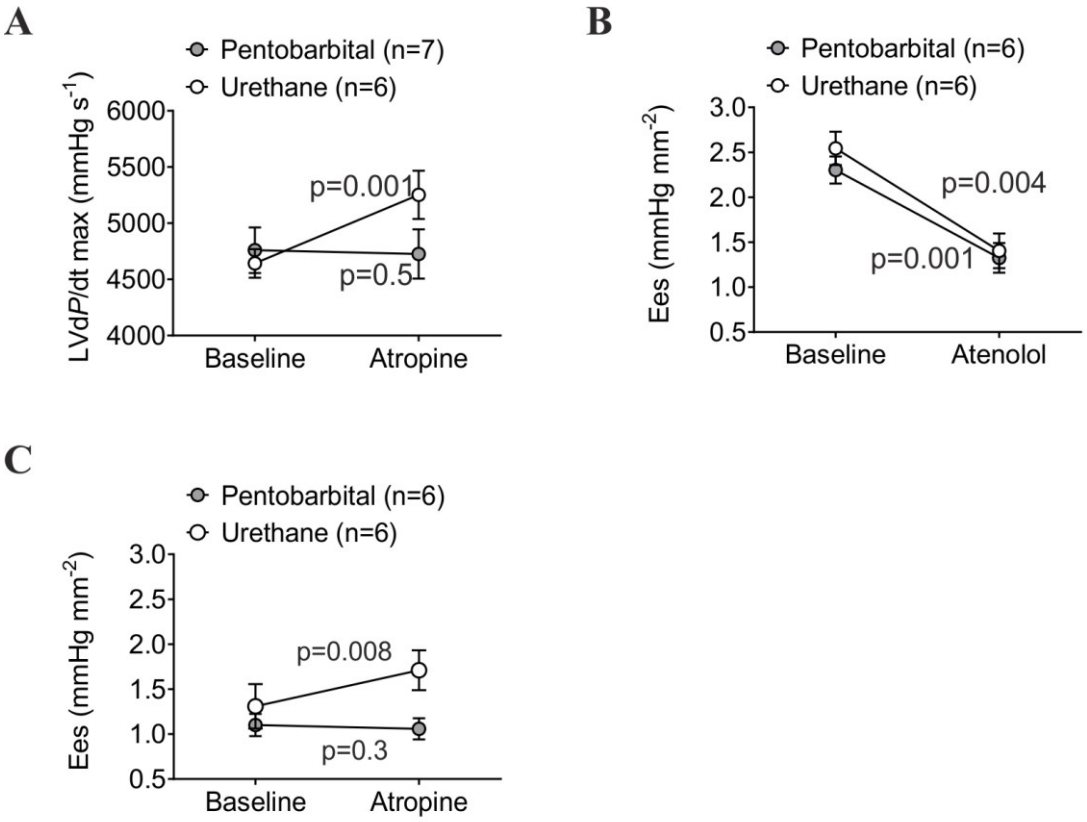

Figure 3-3: Tonic restraining muscarinic influence on LV contractility is preserved under urethane anaesthesia and is abolished by pentobarbital

A) Summary data illustrating average (means ± SEM) values of $LVdP/dt_{max}$ obtained in conditions of atrial pacing and systemic β-adrenoceptor blockade (atenolol) combined with C1 transection (to remove sympathetic influences) before and after intravenous administration of atropine methyl nitrate (2 mg kg^{-1}) in rats anaesthetised with pentobarbital or urethane; **B**) Summary data illustrating average (means ± SEM) values of end-systolic elastance (Ees) before and after intravenous administration of atenolol (2 mg kg^{-1}) in rats anaesthetised with pentobarbital or urethane; **C)** Summary data illustrating average (means ± SEM) values of Ees in conditions of β-adrenoceptor blockade (atenolol) before and after intravenous administration of atropine methyl nitrate (2 mg kg^{-1}) in rats anaesthetised with pentobarbital or urethane.

3.3.2 Experiment 2. The effects of reduced DVMN activity on left ventricular contractility

In rats (urethane anaesthesia), bilateral inhibition of the DVMN VPNs transduced to express AlstR (Figure 3-4) was achieved by application of allatostatin in the *cisterna magna*. This experiment was conducted on animals with intact sympathetic tone. Inhibition of the DVMN neurones increased LVESP (by 16±2 mmHg; P<0.001; Table 3-2), LVd*P*/dt_{max} (by 922±232 mmHg s^{-1}; p=0.001; Table 3-2) and MAP (by 7±4 mmHg; p=0.009; Table 3-2; Figure 3-5A, B). DVMN inhibition had no effect on HR or LVEDP (Table 3-2). No significant changes in all recorded cardiovascular variables were observed following allatostatin application into the *cisterna magna* in rats expressing control transgene (eGFP) in the DVMN (Table 3-2; Figure 3-5A, B). These data suggest that tonic activity of the DVMN VPNs have a significant inhibitory effect on LV contractile function.

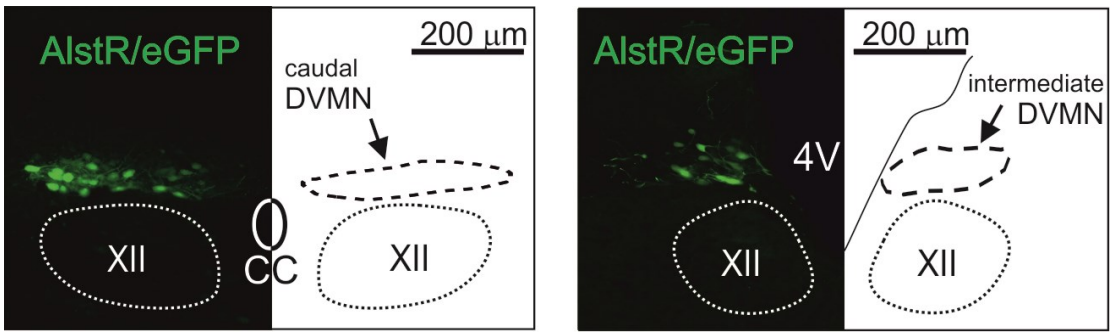

Figure 3-4: Targeting DVMN neurones to reduce their activity

Confocal images of the coronal sections of the rat brainstem targeted to express allatostatin receptor (AlstR) in the DVMN neurones. Figure 3-4 illustrates a representative example of the distribution of VPNs transduced to express AlstR/eGFP in the caudal and intermediate regions of the nucleus. 4V, fourth ventricle. XII, hypoglossal motor nucleus. CC, central canal.

Table 3-2 The effects of reducing DVMN activity (allatostatin application) on cardiovascular variables in anaesthetised (urethane) rats

Transgene	**eGFP (control)**	**AlstR**
n	6	6
LVd*P*/d*t* max (mmHg s^{-1})		
Baseline	9099 ± 969	10914 ± 537
Allatostatin	9170 ± 991	11837 ± 388
Mean difference	71 ± 113	922 ± 232
p	0.7	0.001
LVESP (mmHg)		
Baseline	146 ± 10	156 ± 6
Allatostatin	149 ± 10	172 ± 5
Mean difference	4 ± 1	16 ± 2
p	0.1	<0.0001
LVEDP (mmHg)		
Baseline	3 ± 1	3 ± 1
Allatostatin	3 ± 1	3 ± 1
Mean difference	0 ± 1	0 ± 0
p	0.7	0.9
MAP (mmHg)		
Baseline	91± 4	102 ± 3
Allatostatin	98± 8	109 ± 2
Mean difference	6 ± 4	7 ± 4
p	0.2	0.2
HR (bpm)		
Baseline	430 ± 18	461 ± 8
Allatostatin	430 ± 18	466 ± 10
Mean difference	0 ± 2	5 ± 4
P	0.9	0.2

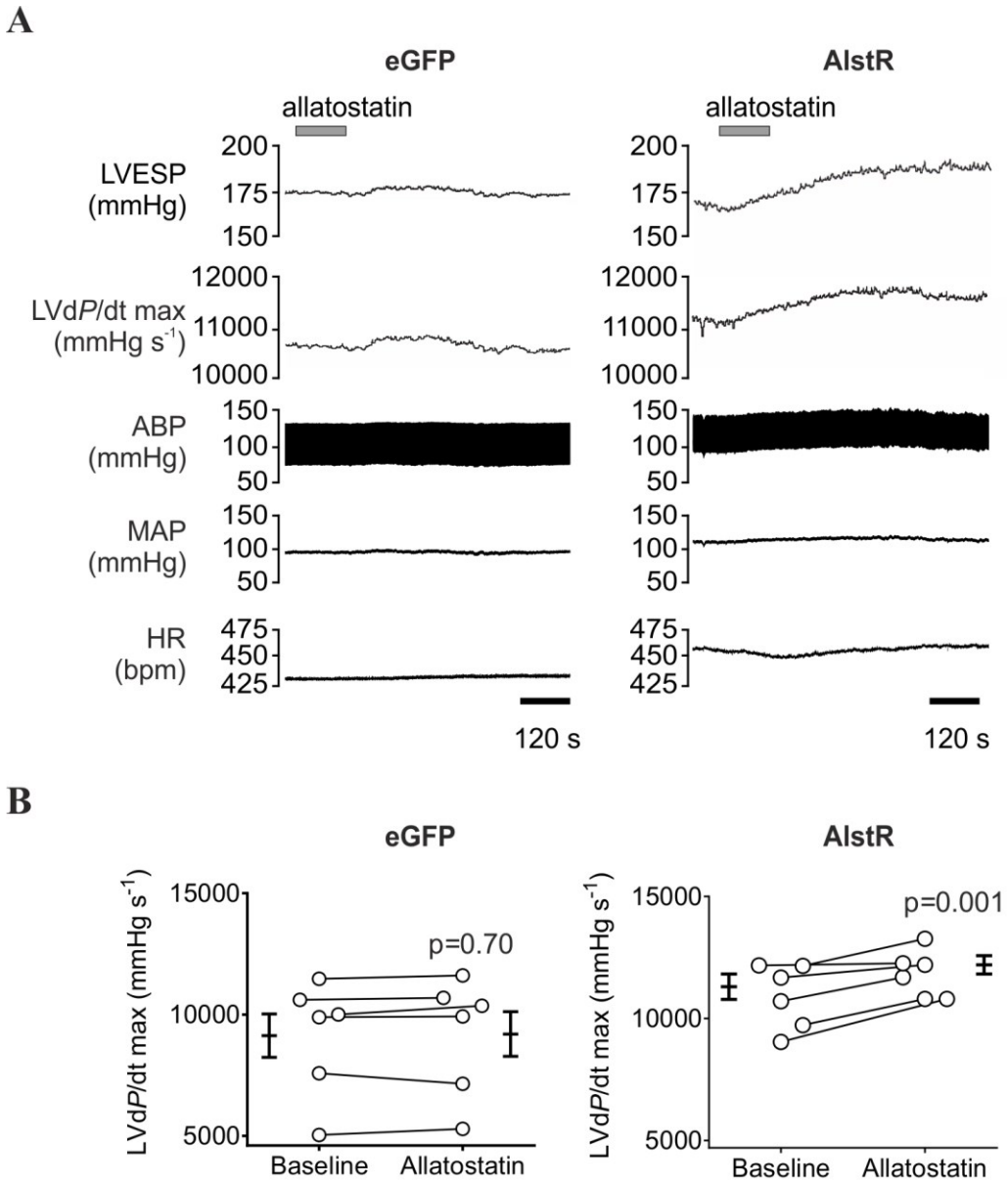

Figure 3-5: Inhibition of VPNs in the dorsal motor nucleus of the vagus nerve (DVMN) increases left ventricular contractility

A) Raw traces illustrating the recordings of HR, MAP, ABP, LVESP and LVdP/dt_{max} before and after allatostatin application into the cisterna magna of rats expressing eGFP or AlstR in the DVMN (urethane anaesthesia). No significant changes in all recorded cardiovascular variables were observed following allatostatin application in rats expressing eGFP. Inhibition of the DVMN neurones increases LVESP and LVdP/dt_{max}. eGFP, animal transduced to express eGFP in the DVMN. AlstR, animal transduced to express AlstR/eGFP in the DVMN; **B)** Summary data illustrating individual and average (means ± SEM) values of LVdP/dt_{max} obtained before and after allatostatin application into the cisterna magna of rats expressing eGFP (n=6) or AlstR (n=6) in the DVMN (urethane anaesthesia, intact sympathetic tone).

3.3.3 Experiment 3. To identify the region of the DVMN responsible for the control of left ventricular contractility

In rats anaesthetised with pentobarbital, neurones in discrete locations along the rostro-caudal extent of the left and right DVMN (Figure 3-6) were activated by glutamate microinjections; the effects of these treatments on cardiovascular variables were first assessed at resting HR conditions (Table 3-3;). Activation of neurones in the left caudal area of the DVMN (Table 3-3) induced profound decreases in LVdP/dt_{max}, LVESP, ABP and HR (Figure 3-6; Table 3-3). Activation of the intermediate DVMN area located 0.5 mm rostrally (Figure 3-6) decreased LVdP/dt_{max} and MAP (Table 3-3); however, the magnitude of the evoked changes was smaller compared to the responses elicited by glutamate actions at the caudal site. Activation of the most rostral area of the left DVMN or any area along the rostro-caudal extent of the right DVMN had no effect on cardiovascular variables (Table 3-3; Table 3-4). Sites of microinjections were marked by fluorescent beads and were confirmed to lie within the targeted DVMN regions (Figure 3-6B, C).

Under constant HR conditions (pacing at 10% above resting HR), activation of neurones in the left caudal DVMN area was also associated with significant decreases in LVdP/dt_{max}, LVESP and MAP with no effect on LVEDP (Table 3-5; Figure 3-7; Figure 3-8). Smaller yet significant decreases in LVdP/dt_{max}, LVESP and MAP were evoked by stimulation of neurones in the left caudal DVMN under constant HR conditions, combined with systemic β-adrenoceptor blockade and C1 transection (Table 3-5; Figure 3-7; Figure 3-8). Responses triggered by glutamate-induced activation of the left caudal DVMN were abolished by atropine (Table 3-5).

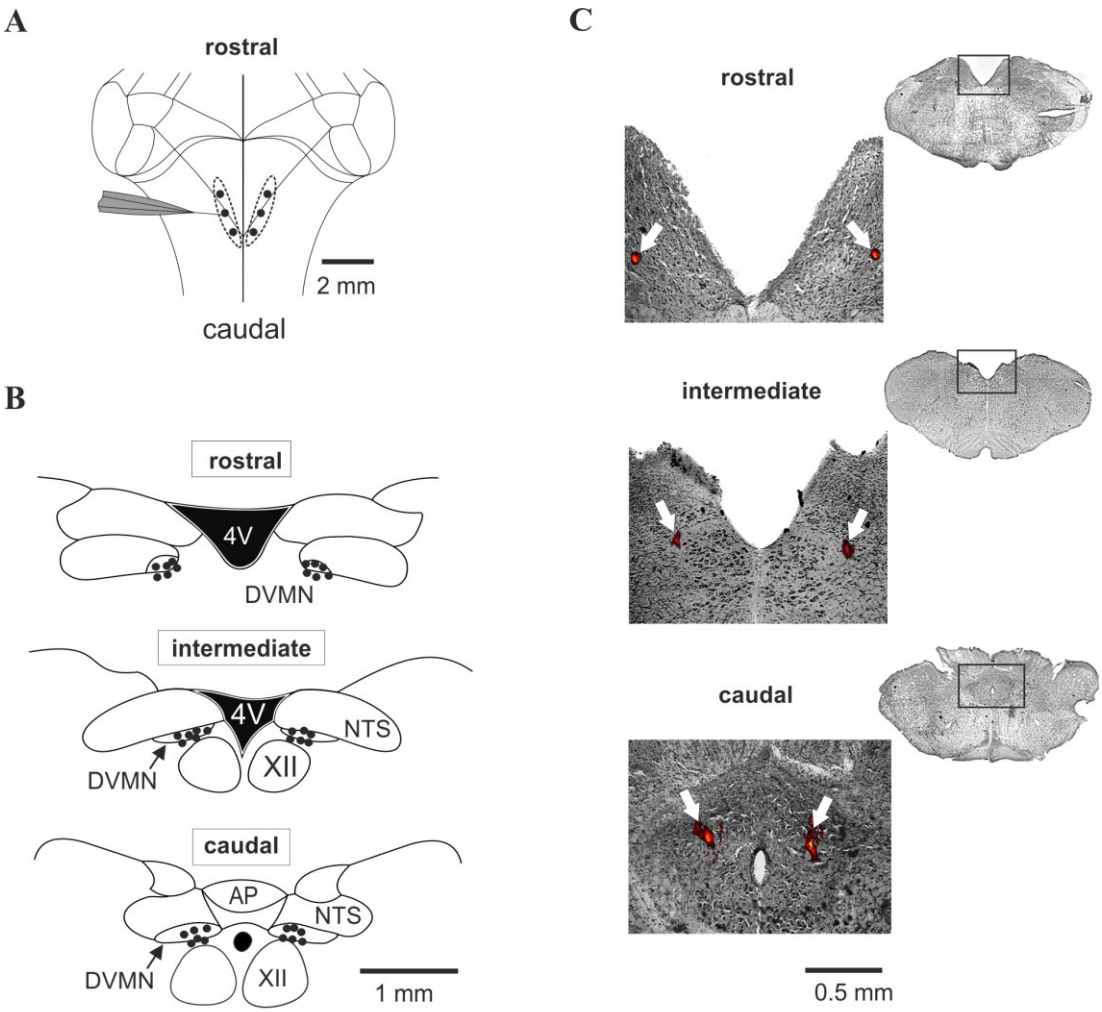

Figure 3-6: Histological identification of microinjection sites along the rostro-caudal extent of the left and right DVMN

A) Scheme of the rat brainstem viewed from its dorsal surface illustrating targeting of the rostral, intermediate and caudal aspects of the left and right DVMN; **B**) Schemes of the coronal sections of the rat brainstem illustrating the locations of the rostral, intermediate and caudal microinjection sites identified by deposition of fluorescent beads. AP, area postrema. NTS, nucleus of the solitary tract. S, solitary tract; **C**) Microphotographs of the coronal sections of the rat brainstem illustrating microinjection sites targeting rostral, intermediate and caudal regions of the left and right DVMN.

Table 3-3 The effects of left DVMN activation in discrete locations along the rostro-caudal extent of the left and right nuclei (glutamate microinjections) on cardiovascular variables in anaesthetised (pentobarbital) rats

	Left DVMN		
	Rostral	**Intermediate**	**Caudal**
n	6	6	11
LVd*P*/d*t* max (mmHg s^{-1})			
Saline	4999 ± 186	5232 ± 222	5671 ± 225
Glutamate	4845 ± 176	4813 ± 252	4030 ± 333
Mean difference	154 ± 74	420 ± 112	1641 ± 134
p	0.6	0.01	<0.0001
LVESP (mmHg)			
Saline	124 ± 3	127 ± 5	125 ± 2
Glutamate	122 ± 4	121 ± 5	97 ± 5
Mean difference	3 ± 1	6 ± 2	28 ± 3
p	0.8	0.2	<0.0001
LVEDP (mmHg)			
Saline	4 ± 0	5 ± 1	4 ± 1
Glutamate	4 ± 0	5 ± 1	4 ± 1
Mean difference	0 ± 0	0 ± 0	1 ± 0
p	>0.9	0.9	0.2
MAP (mmHg)			
Saline	95 ± 2	99 ± 5	98 ± 3
Glutamate	94 ± 3	89 ± 7	72 ± 3
Mean difference	1 ± 1	10 ± 3	26 ± 3
p	0.9	0.001	<0.0001
HR (bpm)			
Baseline	385 ± 14	396 ± 17	398 ± 11
Glutamate	383 ± 14	396 ± 18	378 ± 9
Mean difference	0 ± 1	1 ± 3	20 ± 6
p	>0.9	>0.9	0.01

Table 3-4 The effects of right DVMN activation in discrete locations along the rostro-caudal extent of the left and right nuclei (glutamate microinjections) on cardiovascular variables in anaesthetised (pentobarbital) rats

	Right DVMN		
	Rostral	**Intermediate**	**Caudal**
n	6	6	6
LVd*P*/d*t* max (mmHg s^{-1})			
Saline	5132 ± 191	5168±219	5190 ± 293
Glutamate	4930 ± 219	4987 ± 195	4879 ± 457
Mean difference	203 ± 61	180 ± 109	312 ± 179
p	0.3	0.4	0.08
LVESP (mmHg)			
Saline	125 ± 2	127 ± 4	120 ± 2
Glutamate	122 ± 3	123 ± 6	115 ± 3
Mean difference	2 ± 1	3 ± 1	5 ± 2
p	0.8	0.5	0.3
LVEDP (mmHg)			
Saline	5 ± 0	5 ± 1	5 ± 1
Glutamate	4 ± 0	5 ± 0	5 ± 1
Mean difference	1 ± 0	1 ± 0	2 ± 2
p	0.9	0.9	>0.9
MAP (mmHg)			
Saline	98 ± 3	101 ± 5	102 ± 3
Glutamate	96 ± 3	101 ± 6	98 ± 2
Mean difference	2 ± 3	1 ± 2	4 ± 3
p	0.6	>0.9	0.3
HR (bpm)			
Baseline	389 ± 18	401 ± 15	392 ± 19
Glutamate	393 ± 15	402 ± 14	393 ± 19
Mean difference	3 ± 4	0 ± 2	0 ± 1
p	0.3	>0.9	>0.9

Table 3-5. The effect of neuronal activation in the left caudal DVMN (glutamate microinjections) on cardiovascular variables at resting conditions, during atrial pacing at 10% above resting HR, and during pacing in conditions of β-adrenoceptor blockade combined with C1 transection (sympathetic blockade, SB) before and after systemic administration of atropine methyl nitrate (AMN) (pentobarbital-anaesthetised rats)

	Left DVMN			
	Unpaced	**Paced**	**Paced/SB**	**Paced/SB/ Atropine**
n	11	8	11	7
LVd*P*/d*t* max (mmHg s^{-1})				
Saline	5671 ± 225	6043 ± 327	5141 ± 261	4759 ± 203
Glutamate	4030 ± 333	4506 ± 252	4667 ± 201	4726 ± 219
Mean Differenc	1641 ± 134	1536 ± 164	475 ± 140	33 ± 175
p	<0.0001	<0.0001	0.004	0.9
LVESP (mmHg)				
Saline	125 ± 2	126 ± 4	126 ± 6	119 ± 3
Glutamate	97 ± 5	107 ± 3	118 ± 5	118 ± 3
Mean Differenc	28 ± 3	19 ± 4	9 ± 4	0 ± 5
p	<0.0001	0.0002	0.04	0.9
LVEDP (mmHg)				
Saline	4 ± 1	4 ± 1	4 ± 1	5 ± 1
Glutamate	4 ± 1	6 ± 1	5 ± 1	5 ± 1
Mean Differenc	1 ± 0	2 ± 2	1 ± 2	0 ± 2
p	0.2	0.8	0.9	>0.9
MAP (mmHg)				
Saline	98 ± 3	96 ± 6	108 ± 4	101 ± 3
Glutamate	72 ± 3	73 ± 3	100 ± 4	101 ± 3
Mean Differenc	26 ± 3	23 ± 3	8 ± 3	0 ± 4
p	<0.0001	<0.0001	0.02	>0.9

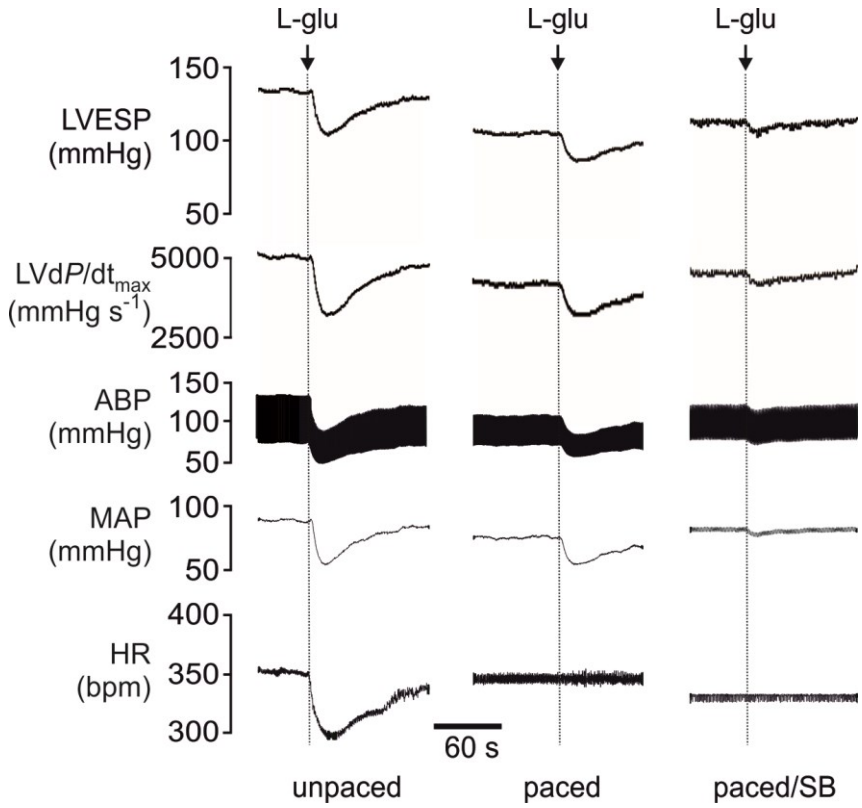

Figure 3-7: Raw traces showing activation of neurones in the caudal region of the left DVMN decreases left ventricular contractility

Raw traces illustrating recordings of HR, MAP, ABP, LVESP and LVdP/dt$_{max}$ before and after glutamate microinjections into the caudal region of the left DVMN at resting HR conditions, during atrial pacing (10% above resting HR) and after systemic β-adrenoceptor blockade (atenolol) combined with spinal cord (C1) transection to remove sympathetic influences (pentobarbital anaesthesia). L-glu, L-glutamate. SB, sympathetic blockade.

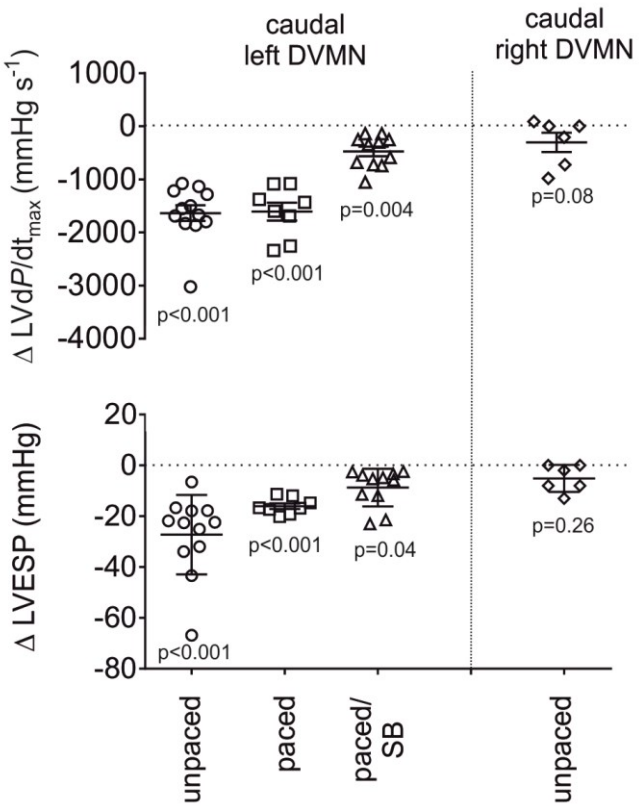

Figure 3-8: Summary data showing activation of neurones in the caudal region of the left DVMN decreases left ventricular contractility

Summary data illustrating individual and average (means ± SEM) values of peak changes in LVESP and LVdP/dt_{max} induced by glutamate microinjections into the caudal regions of DVMN at resting HR conditions, during atrial pacing and during atrial pacing combined with sympathetic blockade (SB). No significant changes in all recorded cardiovascular variables were observed following activation of the right DVMN. Therefore, the effects of glutamate microinjections were only assessed at resting condition.

In animals anaesthetised with urethane (under systemic β-adrenoceptor blockade combined with C1 transection), inhibition of the left caudal DVMN following microinjections of muscimol increased LVd*P*/dt_{max}, LVESP, MAP and HR (Figure 3-9; Figure 3-10). Since silencing of the DVMN neurones transduced to express AlstR by allatostatin application was not associated with changes in HR, the cardiovascular response profile recorded after muscimol microinjections suggested potential diffusion and actions of the drug on neurones of the neighbouring brainstem structures (e.g. nucleus of the solitary tract). Smaller yet significant increases in LVd*P*/dt_{max} and LVESP in response to inhibition of the left caudal DVMN were also observed during atrial pacing (Table 3-6; Figure 3-9; Figure 3-10). Inhibition of the right caudal DVMN following microinjections of muscimol produced no changes in cardiovascular variables (Table 3-6; Figure 3-9; Figure 3-10). These data indicate that neurones residing in the caudal region of the left DVMN exert direct load- and HR-independent tonic control of LV contractility.

Table 3-6 The effects of neuronal inhibition in the caudal DVMN regions (muscimol microinjections) on cardiovascular variables in conditions of β-adrenoceptor blockade combined with C1 transection (urethane-anaesthetised rats)

	Left caudal DVMN		Right caudal DVMN
	Unpaced	Paced	Unpaced
n	10	6	10
LVd*P*/d*t* max (mmHg s^{-1})			
Saline	5487 ± 286	4445 ± 196	5582 ± 308
Muscimol	6360 ± 303	4686 ± 197	5882 ± 368
Mean Difference	873 ± 151	240 ± 44	299 ± 224
p	0.0005	0.003	0.3
LVESP (mmHg)			
Baseline	118 ± 3	113 ± 3	117 ± 4
Muscimol	134 ± 4	116 ± 3	121 ± 5
Mean Difference	17 ± 4	3 ± 1	5 ± 5
p	0.001	0.008	0.5
LVEDP (mmHg)			
Baseline	4 ± 0	7 ± 1	5 ± 1
Muscimol	4 ± 0	7 ± 1	4 ± 1
Mean Difference	0 ± 1	0 ± 1	0 ± 1
p	0.8	0.7	0.9
MAP (mmHg)			
Baseline	93 ± 1	95 ± 2	92 ± 1
Muscimol	103 ± 1	98 ± 2	93 ± 4
Mean Difference	10 ± 1	2 ± 1	1 ± 3
p	0.001	0.06	0.8
HR (mmHg)			
Baseline	343 ± 11		358 ± 11
Muscimol	356 ± 10		363 ± 11
Mean Difference	13 ± 5		5 ± 2
p	0.004		0.4

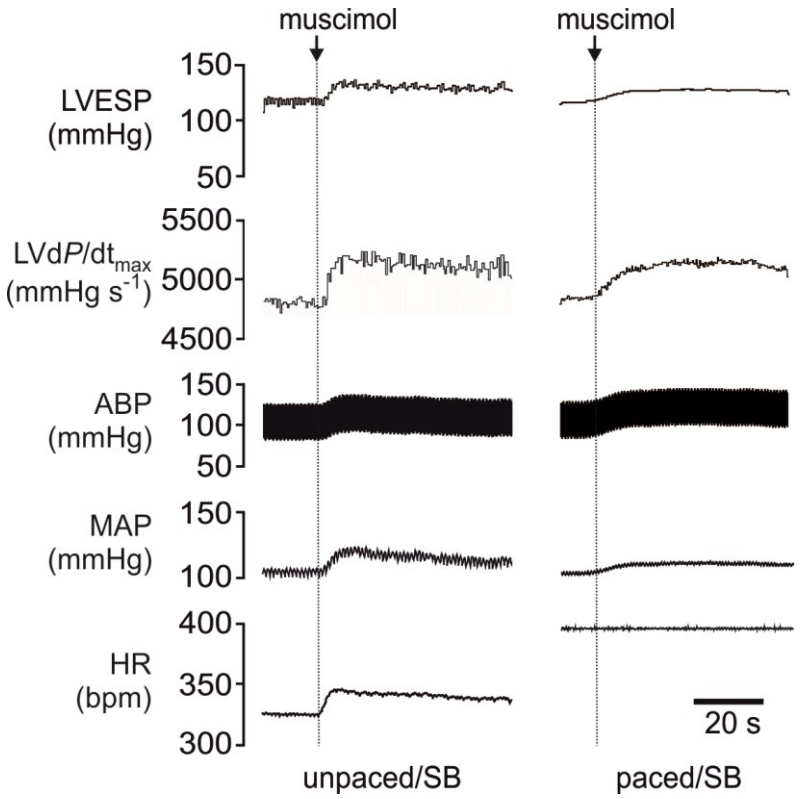

Figure 3-9: Raw traces showing inhibition of neurones in the caudal region of the left DVMN increases left ventricular contractility

Raw traces illustrating recordings of HR, MAP, ABP, LVESP and LVd*P*/dt$_{max}$ before and after muscimol microinjections into the caudal region of the left DVMN in conditions of systemic β-adrenoceptor blockade (atenolol) combined with spinal cord (C1) transection at resting HR and during atrial pacing (urethane anaesthesia).

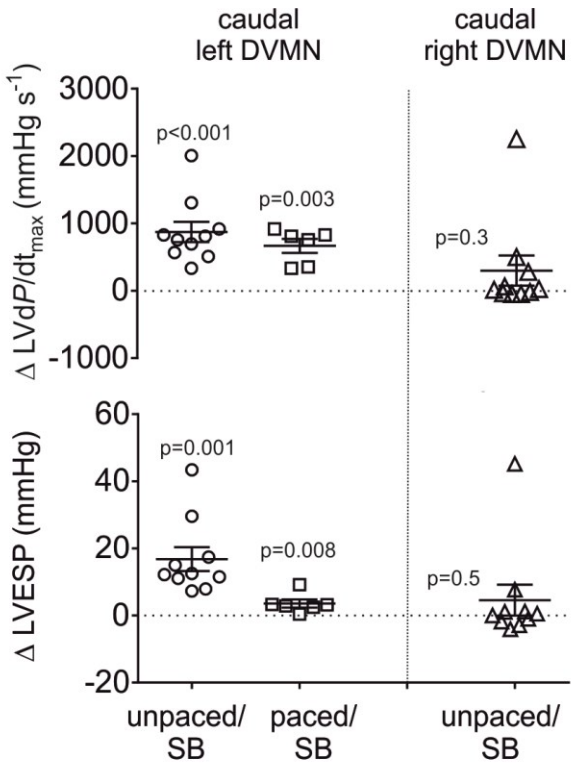

Figure 3-10: Summary data showing inhibition of neurones in the caudal region of the left DVMN increases left ventricular contractility

Summary data illustrating individual and average (means ± SEM) values of peak changes in LVESP and LVd*P*/dt_{max} resulting from muscimol microinjections into the caudal regions of DVMN in conditions of sympathetic blockade at resting HR and during atrial pacing. No significant changes in all recorded cardiovascular variables were observed following muscimol microinjections into the right caudal DVMN.

3.4 Discussion

The study in this chapter tested the hypothesis that tonic parasympathetic control of LV contractility is provided by the activity of VPNs, which reside in the DVMN. First, using an anaesthetised rat model, the presence of tonic restraining muscarinic influence on LV inotropy was confirmed. Next, DVMN neurones were targeted to express inhibitory G-protein coupled receptors from insects; their targeted reduction in activity following application of the insect peptide allatostatin (Mastitskaya *et al*., 2012) was found to be associated with significant increases in LV contractility. Although VPNs residing in the NA are likely to have an impact on the LV function, the data obtained in the present study support the hypothesis that a significant component of the parasympathetic control of the LV inotropy is indeed provided by tonically active neurones of the DVMN. Functional neuroanatomical mapping, using glutamate and muscimol microinjections to activate and inhibit neuronal cell bodies in distinct locations along the rostro-caudal extent of the left and right DVMN, identified the precise anatomical location of VPNs that have an impact on LV contractility. These neurones appear to be concentrated in the caudal region of the left DVMN.

The strength and significance of direct tonic parasympathetic control of LV inotropic state has remained unknown. Earlier studies conducted using dogs, pigs and humans demonstrated that VNS leads to load-independent decreases in LV contractility (Eliakim *et al.*, 1961; Degeest *et al.*, 1964; Degeest *et al.*, 1965c; Lewis *et al.*, 2001). The evidence of changes in LV inotropy observed in a *reverse* experimental paradigm, i.e. when acute bilateral vagotomy is performed or systemic muscarinic receptor blockade is applied, is limited. De Geest *et al.* reported that bilateral vagotomy blocks the negative inotropic effect of peripheral chemoreceptor stimulation (Degeest *et al.*, 1965a, b; Lewis *et al.*, 2001). In humans, intracoronary administration of ACh attenuated inotropic responses to β-adrenoceptor stimulation (dobutamine infusion) (Landzberg *et al.*, 1994). Interestingly, intracoronary atropine potentiated dobutamine-induced inotropic responses, and this effect of atropine was absent in transplanted (i.e. denervated) hearts (Landzberg *et al.*, 1994). Consequently, these findings have demonstrated the existence of a tonic restraining parasympathetic influence on LV contractility in humans.

A more recent study reported increases in LVESP after acute bilateral vagotomy in the arterially perfused working heart-brainstem rat preparation (Nalivaiko *et al.*, 2010). Here, using two different measures, the existence of tonic negative muscarinic influence on LV contractility in a rat model was confirmed. In conditions of systemic β-adrenoceptor blockade, intravenous administration of atropine increased LV Ees and LVd*P*/dt_{max} (at constant filling times and loading conditions). Systemic muscarinic receptor blockade increased LV contractility only in animals anaesthetised with urethane, confirming previous reports that urethane preserves and pentobarbital reduces (chronotropic) vagal tone (O'Leary & Jones, 2003). These data illustrate a tonic restraining muscarinic influence on LV contractility and sensitivity of this influence to anaesthetic agents which suppress the parasympathetic drive.

In an earlier study it was found that the increased activity of DVMN VPNs protects LV cardiomyocytes against acute ischemia/reperfusion injury. This cardioprotective effect was found to be mediated by a muscarinic mechanism (Mastitskaya *et al.*, 2012). Based on these findings, it was hypothesised that the same population of DVMN neurones that exerts powerful cardioprotection may also contribute to the control of ventricular contractility. Acute bilateral inhibition of AlstR-expressing DVMN neurones along the rostro-caudal extent of the nuclei (by allatostatin infusion) increased LV end-systolic pressure and LVd*P*/dt_{max}. This effect indicated an increase in LV contractility since no changes in LVEDP, HR and MAP were observed. Functional neuroanatomical mapping (using microinjections of glutamate and muscimol to activate and inhibit DVMN neuronal cell bodies, respectively) has further demonstrated that preganglionic neurones responsible for parasympathetic control of LV inotropic state are concentrated in the caudal region of the left DVMN.

At resting HR conditions (prior to β-adrenoceptor blockade and spinal cord transection), microinjections of glutamate into the left caudal DVMN induced profound changes in HR and the MAP, indicative of a sympathetic withdrawal. These effects could be explained by glutamate diffusion from the site of microinjection and its impact on neurones of the neighbouring nucleus of the solitary

tract, which receives inputs from all cardiorespiratory afferents (Spyer, 1994), and/or acute recruitment of the inhibitory presynaptic vagal influences, which control noradrenaline release from sympathetic terminals innervating the heart. The magnitude of the parasympathetic effect on HR is known to depend on the strength of the sympathetic tone, indicative of the effective presynaptic interactions (Levy, 1971b).

Activation of neurones in the caudal region of the left DVMN led to a significant decrease in LV contractility, including in conditions of systemic β-adrenoceptor blockade and spinal cord transection, suggesting that parasympathetic control of LV inotropy originates from this region of the brainstem. Microinjections of glutamate trigger transient activation of the neuronal cell bodies in the targeted brain area and have no effect on fibres of passage (Goodchild *et al.*, 1982). This was important for the design of the current study since axons of VPNs of the NA form hairpin loops in the vicinity of the DVMN (Jones, 2001).

The short duration and unimodal cardiovascular response profile after microinjections of glutamate suggested that activation of neurones in neighbouring brainstem structures is unlikely. To minimise the likelihood of this, a fifth of glutamate concentration originally described in Goodchild *et al.* (1982) and a tenth of glutamate concentration used to recruit VPNs of the NA (Sampaio *et al.*, 2003) were used. Interestingly, relative decreases in LV contractility, triggered in response to activation of the neuronal cell bodies in the left caudal DVMN, were quantitatively similar (~20%) to those observed in rabbits when VNS was combined with the anodal block technique for selective stimulation of unmyelinated efferent fibres (Garcia Perez & Jordan, 2001). These data support the conclusions of the present study; since only DVMN VPNs have C fibre axons (neurones of the NA have B fibre axons).

There is evidence that cardiomyocytes themselves are able to synthesise ACh, and ACh synthesis by cardiomyocytes is facilitated by muscarinic receptor activation (Kakinuma *et al.*, 2009; Kakinuma *et al.*, 2012; Sun *et al.*, 2013). Despite on-going debates on the density of vagal innervation of the LV myocardium, there is

strong evidence that VNS is associated with significant increases in LV ACh content (Eliakim *et al.*, 1961; Akiyama *et al.*, 1994; Akiyama & Yamazaki, 2001). If cardiomyocytes are capable of producing physiologically significant amounts of ACh in an autocrine/paracrine manner (sensitive to muscarinic receptor agonism), activation of even sparse vagal efferent innervation may have a significant impact on LV function. LV cardiomyocytes are protected against ischemia/reperfusion injury when the activity of DVMN neurones is selectively recruited using an optogenetic approach (Mastitskaya *et al.*, 2012); the data is thus consistent with the evidence of a potent cardioprotective effect of ACh (which is as potent as adenosine in reducing myocardial injury) reported previously (Richard *et al.*, 1995; Qian *et al.*, 1996; Yamaguchi *et al.*, 1997; Cohen *et al.*, 2001).

3.5 Study Limitations

Inhibition of neurones in the left caudal area of the DVMN using microinjections of a potent $GABA_A$ receptor agonist muscimol increased LV contractility, although the magnitude of the observed effects was smaller compared to that induced by systemic muscarinic receptor blockade. These data suggest that either muscimol microinjections were not sufficient to inhibit the same population of DVMN neurones recruited by the actions of glutamate, or VPNs residing in other areas of the brainstem (NA, intermediate zone) also contribute to the parasympathetic control of LV inotropy, or both.

With regards to the gene transfer work to silence the DVMN neurones, the viral titres for the constructs used were not reliably known. Acceptable expression was predetermined by injection in test subjects allowing four weeks prior to conducting histology. The extent of expression could have instead been evaluated via polymerase chain reaction as titres would inevitably vary, given the titre loss of the lentiviral constructs immediately after thawing.

In summary, the findings of the present study confirm the existence of tonic restraining muscarinic influence on LV contractility, which is preserved under urethane anaesthesia and is abolished by pentobarbital. Functionally significant parasympathetic control of LV contractile function originates from the activity of a group of VPNs residing in the caudal region of the left DVMN.

Chapter 4 The Vagal mechanisms Controlling Exercise Capacity

4.1 Introduction

There is significant evidence indicating that the activity of the parasympathetic nervous system correlates with exercise capacity (Goldsmith *et al.*, 1997). Endurance exercise training has been shown to be associated with a lower resting HR (al-Ani *et al.*, 1996; Carter *et al.*, 2003) accompanied by changes in baroreflex sensitivity, HRV and heart rate recovery (HRR), which are all suggestive of a higher vagal tone (Aubert *et al.*, 2003; Niemela *et al.*, 2008; Filliau *et al.*, 2015).

Higher baroreflex sensitivity, enhanced power of the high frequency component of the HRV and rapid HRR following cessation of exercise in athletes in training would suggest that there is indeed some degree of plasticity in the central nervous control of the heart (Merati *et al.*, 2015), however, the mechanisms underlying the effects of exercise and physical activity on vagal tone have never being explored. The established concept postulating that exercise training enhances vagal tone has been challenged recently by the experimental data obtained through rats and mice, showing that exercise alters the expression of the funny channel (HCN4) in the SA node (lengthening the hyperpolarisation between action potentials) and this process underlies development of bradycardia (at rest) in athletes (D'Souza *et al.*, 2014).

Although this and other data would suggest the effect of exercise training on nodal tissue remodelling (D'Souza *et al.*, 2015), an overwhelming body of evidence indicates that trained individuals and especially elite athletes exhibit incredibly high parasympathetic tone (Sacknoff *et al.*, 1994; Carter *et al.*, 2003). This established association between high vagal tone and enhanced exercise capacity suggests that *either* parasympathetic tone can be enhanced by exercise training *or* high vagal tone (due to genetic factors) makes one more tolerant to endurance training regimes, or both. Although the mechanisms underlying plasticity of the central parasympathetic circuits are unknown, there is significant evidence supporting the first hypothesis, e.g. Hepburn *et al.* (2005) demonstrated that respiratory training, independent of physical exercise, increased the high frequency component of HRV at rest. This was

accompanied by a decrease in the low frequency peak (an index of sympathetic tone). Improvement in HRR was also reported in this study. Consequently, it is clear that intact neural pathways are necessary for resting bradycardia and heightened baroreflex sensitivity associated with exercise training (Ordway *et al.*, 1982; Ceroni *et al.*, 2009).

There is also evidence supporting the second hypothesis. In a study involving adolescent twins (aged 13-22), a significant association was found between RSA and exercise behaviour that was concluded to derive entirely from a genetic factor (De Geus *et al.*, 2003). For all the measures, correlations in monozygotic twin pairs were larger than those in dizygotic twin pairs, indicating significant genetic influences on all traits. This study also concluded that genetic factors determine high levels of aerobic fitness causing adolescents to have a higher affinity for and more reliable adherence to exercise. Amplitude of the RSA may be used as an indicator of how trainable an individual is and there is evidence supporting this hypothesis. For example it was shown that individuals with high amplitude RSA display larger VO_{2max} during exercise (Boutcher & Stein, 1995). Exercise training could thus be more rewarding and less aversive to those with a genetic make-up that results in higher vagal tone.

This experimental study was designed to directly test the hypothesis that the strength of parasympathetic tone determines exercise capacity. If this hypothesis is correct, then vagal withdrawal should decrease and vagal recruitment should enhance ability to exercise. An experimental model of forced exercise in rodents was used. Exercise capacity was determined using specified conditions: (i) unilateral cervical vagotomy; (ii) acute and chronic (four hours) systemic muscarinic receptor blockade with atropine; (iii) systemic M_2 and M_3 muscarinic receptor blockade; (iv) nNOS blockade; (v) genetic targeting and silencing of VPNs of the DVMN, demonstrated in 0 and 2 to control electrical and contractile properties of the ventricle) using a pharmacogenetic approach; and (vi) optogenetic activation of the DVMN neurones. A separate experiment was conducted in mice with genetically engineered impairment of the M_3 signalling pathway. The results obtained demonstrate that reduced activity of the DVMN neurones dramatically impairs, whereas increased

activity of the DVMN enhances exercise capacity and contractile function of the LV via downregulation of GRK2 and β-arrestin expression by cardiomyocytes. In conclusion, the vagus nerve exerts trophic cardiac effects maintaining the ability of the heart to mount an appropriate inotropic response during exercise.

4.2 Methods

All the experiments were performed on rats and mice in accordance with the European Commission Directive 2010/63/EU (European Convention for the Protection of Vertebrate Animals used for Experimental and Other Scientific Purposes) and the UK Home Office (Scientific Procedures) Act (1986) with project approval from the Institutional Animal Care and Use Committee.

4.2.1 Exercise model

Exercise capacity of rats and mice was determined using a single lane treadmill (Panlab Harvard Apparatus, Cambridge, UK) with an electrical shock grid set at a minimum threshold of 0.1 mA. The animals were selected for their exercise compliance after a three-day recruitment protocol. Animals were subjected to daily recruitment sessions involving running speeds of 20-30 cm s^{-1} over a five minutes period after 15 minutes of acclimatisation to the treadmill environment. To determine exercise capacity, treadmill speed was raised from 20 cm s^{-1} in increments of 5 cm s^{-1} every five minutes in rats and every three minutes in mice until the hind limbs made contact with the grid four times within a two-minute period - the humanely defined point of exhaustion. The distances covered by the animals were recorded and exercise capacity was expressed in joules (J or kg m^2 s^{-2}).

4.2.2 Blood pressure and heart rate recordings in conscious animals

ABP and HR in conscious rats were recorded using tail cuff plethysmography method or biotelemetry monitoring. Blood pressure measurements by tail cuff plethysmography were performed at the same time each day for all the rats. Briefly, the rats were placed on a heated platform at 37 °C in a quiet, temperature controlled (~30 °C) area. The tail was instrumented with a cuff and a volume pressure-recording sensor (CODA system, Kent Scientific, USA) and a total of 20-30 measurements were taken over a period of 15 minutes. All animals used in this study were acclimatised to the recording environment with 10 control blood pressure measurements at the beginning of each recording session. At least 10 additional measurements were subsequently taken and recorded values were averaged to determine the resting level of the ABP.

Biotelemetry was also used to record systemic ABP and HR in conscious freely moving animals. The rats were anaesthetised with ketamine (60 mg kg^{-1}; i.m.) and medetomidine (250 µg kg^{-1}; i.m.). Laparotomy was performed and the cannula connected to the telemetric pressure transducer (model TA11PA-C40, Data Science International, USA) was secured within the lumen of the abdominal aorta. The muscle and skin levels of the abdomen were separately sutured. Anaesthesia was reversed with atipemazole (1 mg kg^{-1}; i.m.) and the animals were allowed to recover for at least seven days. For post-operative analgesia, rats were administered with buprenorphine (0.05 mg kg^{-1} d^{-1}; s.c.) for three days and caprofen (4 mg kg^{-1} d^{-1}; i.p.) for five days.

4.2.3 Ultrasound assessment of ejection fraction

Left ventricular (LV) function was assessed using a Vevo® 2100 high-resolution ultrasound system with an MS250 13-24MHz linear array transducer (VisualSonics, Amsterdam, The Netherlands). Under isoflurane anaesthesia (2% isoflurane), baseline ejection fraction and HR (lead II ECG) were determined. Dobutamine (0.5 mg kg^{-1}; i.p.) was administered to determine cardiac responses to β-adrenoceptor stimulation. Ejection fraction was determined using B-mode acquisition of a parasternal long-axis view of the ventricle (in plane so as to dissect across the aorta) in order to measure the length of the ventricle during systole and diastole. Three short-axis images perpendicular to this were acquired along the length of the ventricle to segment the endocardial border. By applying Simpson's rule to approximate ventricular volume, ejection fraction was determined and expressed as the percentage of blood at diastole ejected during systole (Figure 4-1) (Schiller *et al.*, 1989).

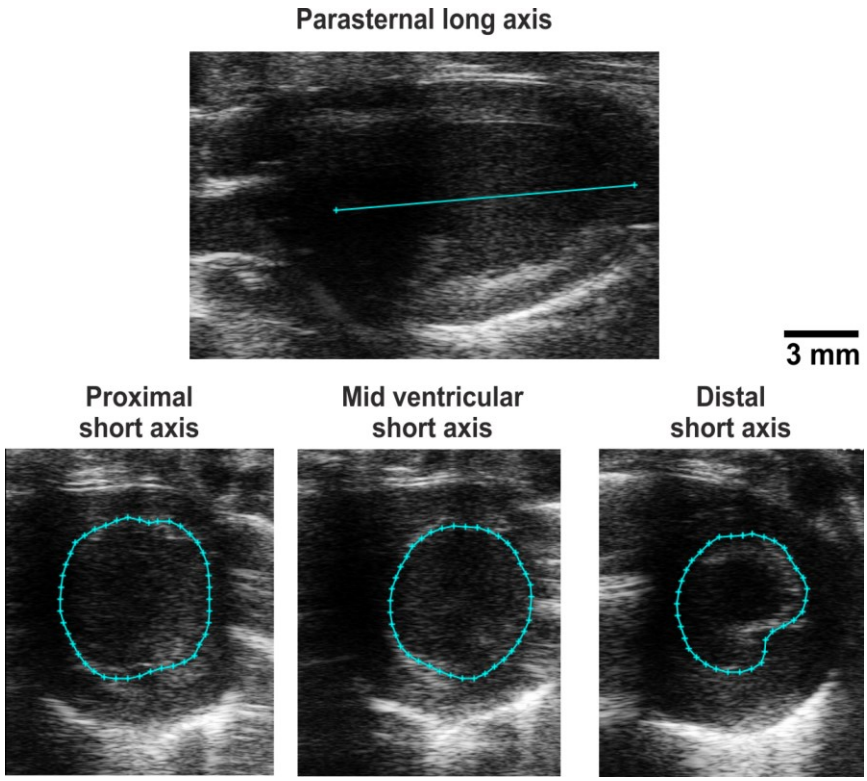

Figure 4-1: Ultrasound imaging of the left ventricle

Example of a B-Mode LV acquisition made to determine the ejection fraction. A parasternal view of the long axis was used to determine the length at the LV at systole and diastole. This was used in combination with three short axis slices allowing approximation of LV volume at these two time points using Simpson's rule.

4.2.4 Haemodynamic measurements

The animals were anaesthetised with urethane (1.3 g^{-1} kg^{-1}; i.v.; following 4% isoflurane induction). Adequate anaesthesia was ensured throughout the experiment by continuous monitoring of HR and ABP stability and the absence of a withdrawal response to a paw pinch. With the animals in a supine position, the femoral artery and both femoral veins were cannulated for the measurements of the systemic ABP, fluid infusion and administration of drugs. The trachea was cannulated and the animals were allowed to freely breathe a supplied gas mixture. Body temperature was maintained with a servo-controlled heating pad at 37.0±0.5 °C. Partial pressures of O_2 and CO_2 as well as pH of the arterial blood were measured every hour (RAPIDLab 348EX, Siemens, UK). Oxygen was added to the respiratory gas mixture (if required) to maintain blood oxygenation within the physiological range. A 2F Millar pressure catheter (SPR-320NR, Millar instruments, USA) was advanced via the right carotid artery and positioned within the chamber of the LV to monitor changes in LVP. Average waveforms of LVP and ABP were used to determine LVESP, and the MAP. LVdP/dt_{max} was derived from the LVP recording using the slope function. Atrial pacing at 20% above baseline HR was performed using a 1.6 F octapolar electrophysiology catheter (EPR-802, Millar instruments, UK) positioned in the right atrium via the jugular vein. Dobutamine (0.5 mg kg^{-1}; i.p.) was administered to determine cardiac responses to β-adrenoceptor stimulation. Cardiovascular variables were recorded using a Power1401 interface and analysed off-line using *Spike2* software (Cambridge Electronic Design).

4.2.5 Genetic targeting of the DVMN vagal preganglionic neurones

Young male Sprague-Dawley rats (50-60 g) were anaesthetised with ketamine (60 mg kg^{-1}; i.m.) and medetomidine (250 µg kg^{-1}; i.m.). Adequate depth of surgical anaesthesia was confirmed by the absence of a withdrawal response to a paw pinch. With the head fixed prone in a stereotaxic frame, lidocaine (2% solution) was injected subcutaneously for pre-operative analgesia before a midline dorsal neck incision was made to expose the atlanto-occipital membrane and then the dorsal surface of the brainstem. The DVMN was targeted bilaterally with two microinjections per side (0.25 µl at a rate of 0.05 µl min^{-1}) of a solution containing

viral particles of PRSx8-AlstR-eGFP-LVV or PRSx8-eGFP-LVV. The established titres at the time of production were within the range of 1 x 10^9 and 1 x 10^{10} transducing units ml^{-1}.Taking the *calamus scriptorius* as the reference point, the injections were made at 0.5 mm rostral, 0.6 mm lateral, 0.8 mm ventral and at 1.0 mm rostral, 0.8 mm lateral, 0.6 mm ventral.

For optogenetic activation, a mutant of channelrhodopsin (ChR) – ChIEF – fused with the tandem dimer Tomato (tdTomato) red fluorescent protein was used. ChIEF is a chimeric ChR variant constructed from the N-terminal part of the ChR1 and the C-terminal part of the ChR2 and also incorporates an isoleucine 170 to valine mutation. ChIEF combines the reduced inactivation characteristics of ChR1 with more favourable cation permeability properties conferred by ChR2 (Lin *et al.*, 2009). The I170V mutation further improves the channel closure kinetics. ChIEF therefore allows a greater temporal control of neuronal activation by blue light pulses resulting in cation flow and depolarisation. Its spectral properties are similar to those of ChR2, but it shows more efficient membrane expression and trafficking in the mammalian cells (Lin *et al.*, 2009). DVMN neurones were targeted using the same approach but with one microinjection of PRSx8-ChIEF-tdTomato-LVV (Figure 4-2) on each side using the caudal set of coordinates. The established titres at the time of production were within the range of 1 x 10^9 and 1 x 10^{10} transducing units ml^{-1}. Caudal DVMN neurones were targeted as they have been found to affect LV function most significantly (Chapter 2). Anaesthesia was reversed with atipemazole (1 mg kg^{-1}; i.m.). For post-operative analgesia, rats were administered with buprenorphine (0.05 mg kg^{-1} d^{-1}; s.c.) for three days and caprofen (4 mg kg^{-1} d^{-1}; i.p.) for five days.

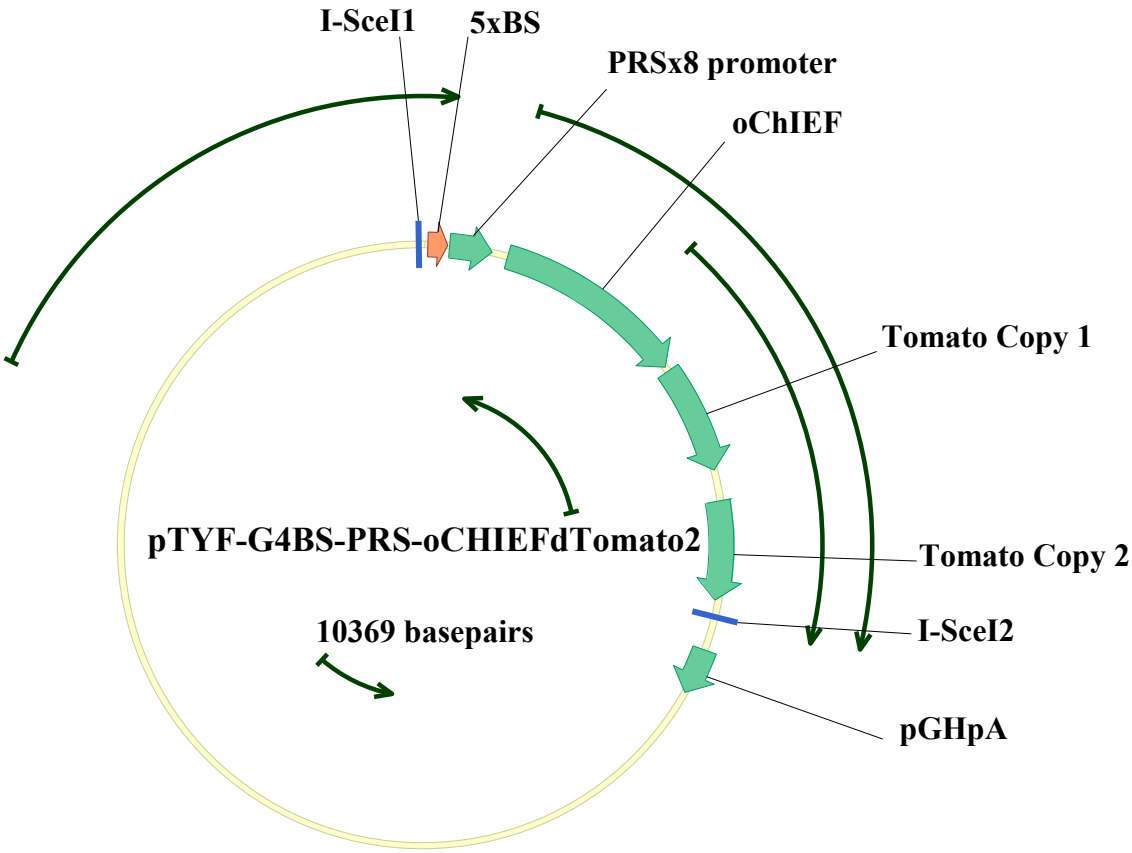

Figure 4-2: PRSx8-ChIEF-tdTomato-LVV Vector circle map

A vector circle map showing the proteins involved in the construction of the viral plasmid.

4.2.6 Cannula and optrode implantations

Three weeks after microinjections of viral vectors into the DVMN (Figure 4-3; Figure 4-4), the animals were anaesthetised with ketamine (60 mg kg^{-1}; i.m.) and medetomidine (250 μg kg^{-1}; i.m.) and either a 26-gauge guide injection cannula (Plastic Products Co., Roanoke, USA; in animals expressing AlstR or eGFP) or a conically tipped optrode (Art Photonics, Berlin, Germany; in animals expressing ChiEF-tdTomato or eGFP) was stereotaxically implanted to reach the dorsal aspect of the *cisterna magna.* Two small screws were placed into the skull, and the implant was secured in place with dental acrylic. The guide cannula was closed with a dummy cannula that extended from the tip of the guide cannula by approximately 0.2 mm. Anaesthesia was reversed with atipemazole (1 mg kg^{-1}; i.m.) and the animals were allowed to recover for at least seven days before the experiments took place.

4.2.7 Knock-in mouse model expressing the phosphorylation-deficient M_3-muscarinic receptors

The knock-in (KI) mouse strain was generated by Professor Andrew Tobin (University of Leicester, UK) via homologous recombination replacing the WT M_3 muscarinic receptor with a phosphorylation deficient form, as described in detail in Kong *et al.* (2010). Previous studies have established that the M_3 receptor is phosphorylated at multiple serines within the third intracellular loop (Budd *et al.*, 2000; Torrecilla *et al.*, 2007). This KI model was generated by replacing 15 of these serine residues with alanine. Body weight and food consumption of M_3 KI animals were not significantly different from their WT counterparts (Kong *et al.*, 2010).

4.2.8 Experiment 1. The effect of unilateral cervical vagotomy on exercise capacity

The resting ABP and exercise capacity were determined in rats five and 32 days after left (n=6) or right (n=6) cervical vagotomy or sham surgery (n=6). The effect of unilateral vagotomy on LV ejection fraction, contractile and HR responses to β-adrenoceptor stimulation (dobutamine, 0.5 mg kg^{-1}; i.p.) were determined five days after the surgery.

4.2.9 Experiment 2. The effects of systemic muscarinic and nNOS blockade on exercise capacity

Exercise capacity was first determined in rats 15 minutes after an acute i.p. injection of saline (n=5) or atropine methyl nitrate (2 mg kg^{-1}; n=5). Then, sustained muscarinic receptor blockade was achieved by infusion of atropine (2 mg kg^{-1} h^{-1}; i.p.) and exercise capacity was determined four hours after the treatment onset. Control animals (n=8) received infusion of saline over the same time period.

To determine the subtype of muscarinic receptors that potentially mediate vagal modulation of exercise capacity, a separate group of rats (n=6) was administered with the M_2 receptor antagonist AFDX116 (2 mg kg^{-1} h^{-1}; i.p.) or vehicle (0.1% DMSO) for four hours. Exercise capacity was also determined in M_3 KI mice (n=6) and their WT counterparts (n=8) before and after systemic treatment with the M_3 receptor antagonist 4-DAMP (2 mg kg^{-1} h; i.p.) or vehicle for four hours.To determine the potential role of NO produced by nNOS, exercise capacity was determined in rats 45 min after an acute i.p. injection of 7-NI (30 mg kg^{-1}) or vehicle (peanut oil) (n=8).

4.2.10 Experiment 3. The effect of systemic muscarinic receptor blockade on cardiovascular response induced by β-adrenoceptor stimulation

To determine the effect of acute and sustained systemic muscarinic receptor blockade on cardiovascular response induced by β-adrenoceptor stimulation, dobutamine was given intravenously (infusion 0.5 mg kg^{-1} min^{-1} for 2 min at a rate of 0.1 ml min^{-1}) 15 minutes and four hours after onset of atropine (2 mg kg^{-1} h^{-1} i.v.; n=5) or saline (n=5) infusion.

4.2.11 Experiment 4. The effect of reduced DVMN activity on exercise capacity

Exercise capacity of animals transduced to express AlstR/eGFP (n=6) or eGFP (n=6) by the DVMN neurones was determined over three consecutive days (Figure 4-3): day one to determine baseline exercise capacity; day two to determine exercise capacity in conditions of reduced DVMN activity (15 minutes following delivery of allatostatin [4 µl of 100 µM solution in aCSF] into the *cisterna magna*); and day three to determine exercise capacity after recovery from the treatment (see

experimental timeline Figure 4-3). Microinjections into the *cisterna magna* were performed via an internal injection cannula connected to PE-20 tubing attached to a 50 µl syringe (Hamilton, Reno, NV) driven by a microinfusion pump (Sp210iw syringe pump, World Precision Instruments). In a separate experiment, changes in blood pressure and HR during and after exercise were determined in six rats expressing AlstR/eGFP and six rats expressing eGFP following allatostatin application.

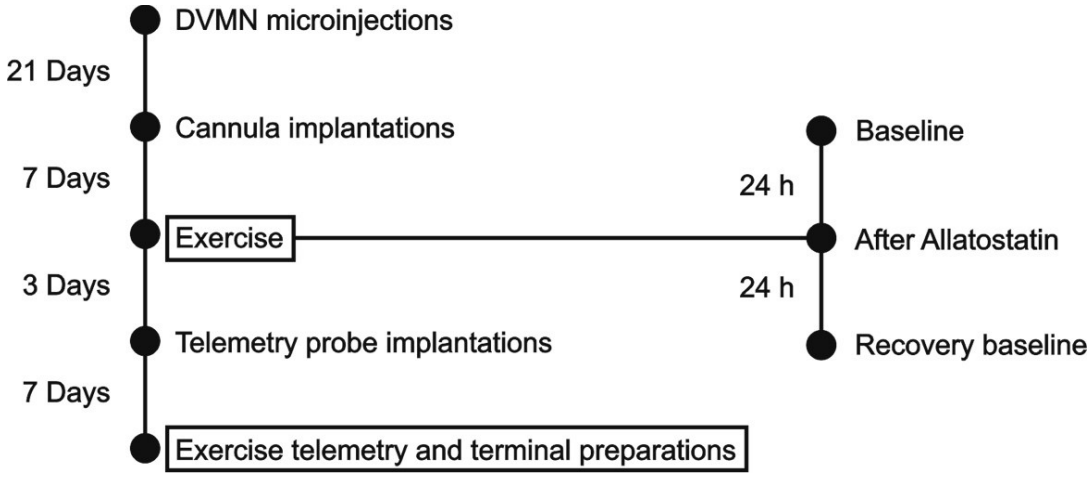

Figure 4-3: Timeline for experiments investing the effect of reduced DVMN activity on exercise capacity.

4.2.12 Experiment 5. The effect of reduced DVMN activity on cardiovascular responses induced by β-adrenoceptor stimulation

The animals transduced to express AlstR/eGFP (n=6) or eGFP (n=6) by the DVMN neurones were anaesthetised with urethane and prepared as described above. They were then left to stabilise for 15-30 min after the preparative surgery. To determine the effect of reduced DVMN activity on cardiovascular response induced by β-adrenoceptor stimulation, dobutamine was given intravenously (infusion 2 mg kg^{-1} min^{-1} i.v.; for two minutes at a rate of 0.1 ml min^{-1}) before and 15 minutes after allatostatin administration into the *cisterna magna*. The heart was paced at 20% above resting HR.

4.2.13 Experiment 6. The effect of DVMN stimulation on exercise contractile responses LV

Exercise capacity of naïve rats (n=10) and animals transduced to express ChiEF-tdTomato (n=9) and eGFP (n=10) by the DVMN neurones was determined twice: on day one to determine baseline exercise capacity and on day six to determine the effect of treatment. In the interim four days (see the timeline illustrated in Figure 4-4), dorsal brainstem of rats expressing ChIEF-tdTomato and eGFP by the DVMN neurones was illuminated via a pre-implanted optrode with blue light (445 nm, 10 ms pulses, 15 Hz) for 15 minutes under mild sedation (1.5 % isoflurane). A group of naïve animals were subjected to four sessions of treadmill exercise, training over four consecutive days with each session lasting up until the defined point of exhaustion. To determine the effect of enhanced DVMN activity and exercise training on inotropic response induced by β-adrenoceptor stimulation, LV ejection fraction and HR was determined using high-resolution ultrasound before and after dobutamine challenge (infusion 2 mg kg^{-1} min^{-1} i.v. for two minutes at a rate of 0.1 ml min^{-1}).

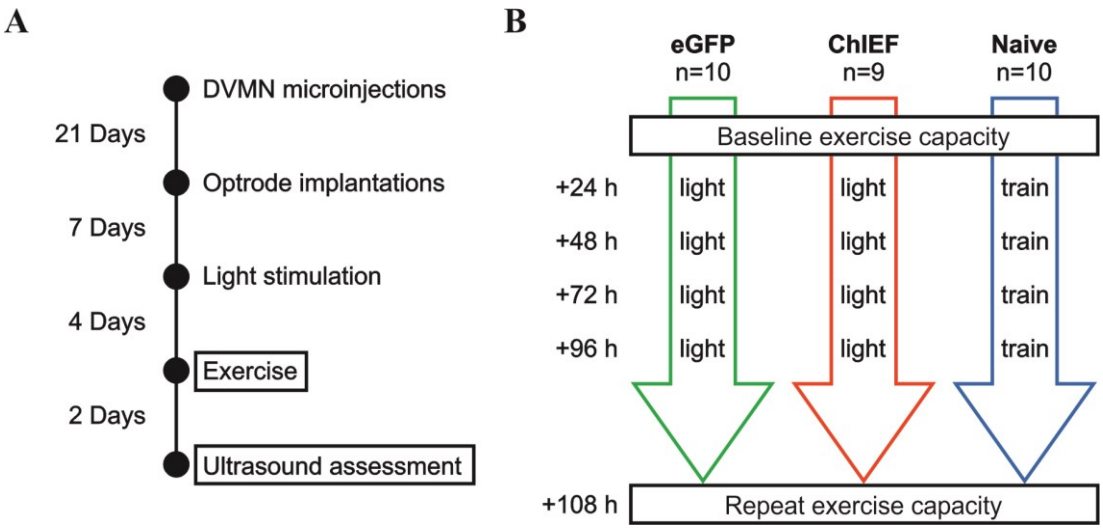

Figure 4-4: Timeline and stimulation paradigm for experiments to determine the effect of DVMN stimulation on exercise capacity

A) Timeline illustrating the intervals between stages of animal preparation and acquisition of exercise data; **B)** Timeline illustrating the optogenetic stimulation paradigm in rats expressing ChIEF-tdtomato and eGFP as well as the naïve rats that underwent exercise training.

4.2.14 Humane end-points

At the end of the experiments the animals were euthanised with an overdose of pentobarbitone sodium (200 mg kg^{-1}, i.p.).

4.2.15 Histology

At the end of the experiments the rats were perfused through the ascending aorta with 0.9% NaCl solution followed by 500 ml 4% phosphate-buffered (0.1 M, pH 7.4) paraformaldehyde. The brains were then removed and stored in the same fixative overnight at 4 °C. After cryoprotection in 30% sucrose, the brainstem was isolated and a sequence of transverse slices (30 μm) was cut. The extent of AlstR/eGFP, ChiEF-tdTomato or eGFP expression was determined using confocal microscopy and mapped using a stereotaxic atlas (Paxinos & Watson, 1998).

4.2.16 Immunoblotting

The blots were performed in collaboration with Dr. Gareth Ackland. Cell lysates prepared from the LV tissue were immunoblotted with specific primary antibodies for GRK2 (C-9; Santa Cruz, sc-13143) and pan-arrestin (Abcam, ab2914) for β-arrestin2. Protein loading was assessed using the housekeeping protein α-tubulin (Santa Cruz, sc53646). Proteins were resolved on SDS-PAGE gels and transferred to polyvinylidene difluoride membranes (Amersham Biosciences, Piscataway, NJ) according to the manufacturer's instructions. After antibody labelling, detection was performed (ECL detection system, Amersham Biosciences, Piscataway, NJ). Densitometry determinations were calculated as the ratio between the protein and α-tubulin (Santa Cruz, sc53646) expression.

4.2.17 Data Analysis

Differences between the experimental groups were analysed using GraphPad Prism six software. Comparisons were made using a two-way ANOVA (followed by Sidak's p value correction for multiple comparisons) or Student's paired test, as appropriate. Data are reported as individual values and means ± s.e.m. Differences with $P<0.05$ were considered to be significant.

4.3 Results

4.3.1 Experiment 1. The effect of unilateral cervical vagotomy on exercise capacity

The rats appeared healthy following unilateral vagotomy. Food and water intake were not different from that of sham-operated animals and all rats gained similar weight over the course of 32 days after the surgery (Figure 4-5A). Exercise capacity was impaired five days after unilateral vagotomy (67±10 vs 134±20 J in sham-operated animals; p=0.006; ANOVA; Figure 4-4B). All groups of animals displayed similar exercise capacity 32 days after unilateral vagotomy or sham surgery (p=0.5; Figure 4-5B). Unilateral vagotomy was not associated with changes in resting LV ejection fraction (p=0.9; ANOVA; Figure 4-5C), HR (p=0.8; ANOVA; Figure 4-5D) or in contractile and HR responses to β-adrenoceptor stimulation (p=0.6; ANOVA; Figure 4-5C and D). Moderate elevation in the systemic ABP was observed in vagotomised animals 32 days after the surgery (137±3 vs 116±9 mmHg in sham-operated animals; p=0.04; ANOVA; Figure 4-5E).

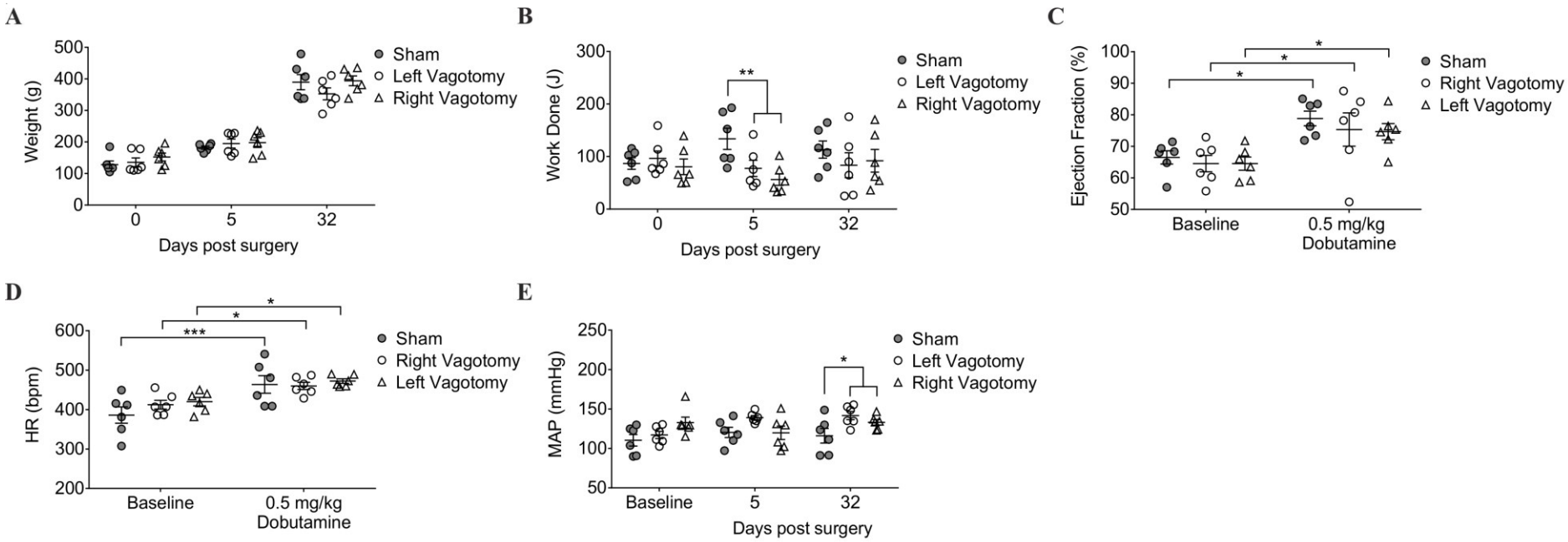

Figure 4-5: The effect of unilateral cervical vagotomy on exercise capacity

A) Summary data illustrating body weights of rats before as well as five and 32 days after left (n=6) or right (n=6) cervical vagotomy or sham surgery (n=6); **B)** Summary data illustrating exercise capacity of rats before as well as five and 32 days after left or right cervical vagotomy or sham surgery**; C)** Summary data illustrating resting ejection fraction and contractile response to dobutamine in rats five days after unilateral vagotomy or sham-surgery; **D)** Summary data illustrating resting heart rate and heart rate response to dobutamine in rats five days after unilateral vagotomy or sham-surgery. **E)** Summary data illustrating mean arterial blood pressure of rats before as well as five and 32 days after left or right cervical vagotomy or sham surgery**.** *P<0.05; **P<0.01; ***P<0.001.

4.3.2 Experiment 2. The effects of systemic muscarinic and nNOS blockade on exercise capacity

Intraperitoneal administration of atropine 15 minutes prior to running tests had no effect on exercise capacity (p=0.865; paired t-test; Figure 4-6A). Sustained muscarinic receptor blockade (atropine infusion over a four hour period) was associated with a significant reduction in exercise capacity (48±10 vs 87±15 J compared to vehicle treatment; paired t-test; p=0.0013; Figure 4-6B). Administration of M_2 receptor antagonist AFDX116 for the same time period had no effect on exercise capacity (93±17 vs 123±18 J compared to vehicle treatment; p=0.15; paired t-test; Figure 4-6C). Mice with global deficiency in M_3 receptor phosphorylation (M_3-KI mice) displayed an impaired exercise capacity as compared to their WT counterparts (130±18 vs 294±36 J; p=0.0006; ANOVA; Figure 4-6D). M_3 receptor blocker 4-DAMP reduced exercise capacity in WT but not in M_3-KI mice, while both groups of animals displayed similar exercise capacity in conditions of systemic 4-DAMP treatment (p>0.9; Figure 4-6D). Exercise capacity was also dramatically reduced following systemic administration of the nNOS inhibitor 7-NI in the rats (31±10 vs 117±18 J after vehicle; p=0.0004; paired t-test; Figure 4-6E).

Biotelemetry recordings confirmed effective systemic muscarinic receptor blockade by atropine, with treated animals displaying higher HR and reduced HRR after cessation of exercise (P<0.0001; Figure 4-7A). Atropine had no effect on the ABP and blood pressure responses to exercise (Figure 4-7B).

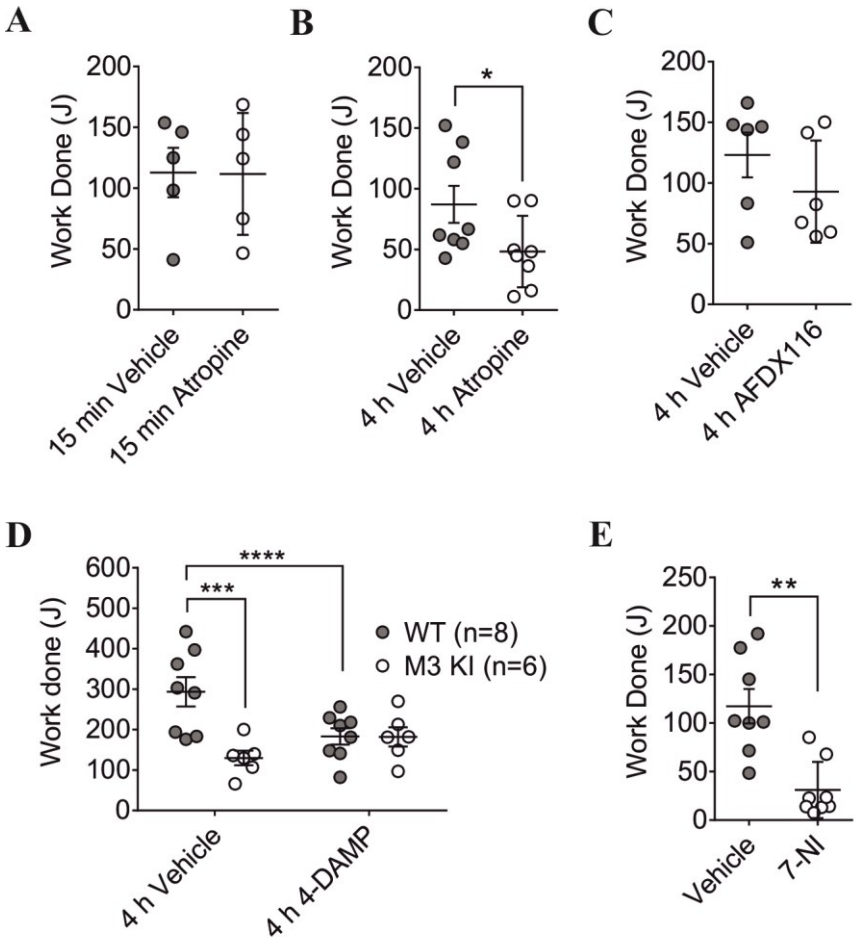

Figure 4-6: The effects of muscarinic and nNOS blockade on exercise capacity

A) Summary data illustrating exercise capacity in rats 15 minutes after an acute i.p. injection of saline (n=5) or atropine methyl nitrate (2 mg kg^{-1}); **B)** Summary data illustrating exercise capacity in conditions of sustained systemic muscarinic receptor blockade (i.p. atropine infusion, 2 mg kg^{-1} h^{-1} for 4 hours). **C)** Summary data illustrating exercise capacity in conditions of systemic M_2 receptor blockade (i.p. infusion of AFDX116, 2 mg kg^{-1} h^{-1}, for 4 hours); **D)** Summary data illustrating exercise capacity of mice with global deficiency in M_3 receptor phosphorylation (M3 KI) and their wild type (WT) counterparts before and in conditions of systemic M_3 receptor blockade (i.p. infusion of 4-DAMP, 2 mg kg^{-1} h^{-1}; for 4 hours). **E)** Summary data illustrating exercise capacity in rats 45 min after an acute i.p. injection of vehicle (peanut oil) (n=8) or nNOS inhibitor 7-NI (30 mg kg^{-1}). *P<0.05; **P<0.01; ***P<0.001; ****P<0.0001.

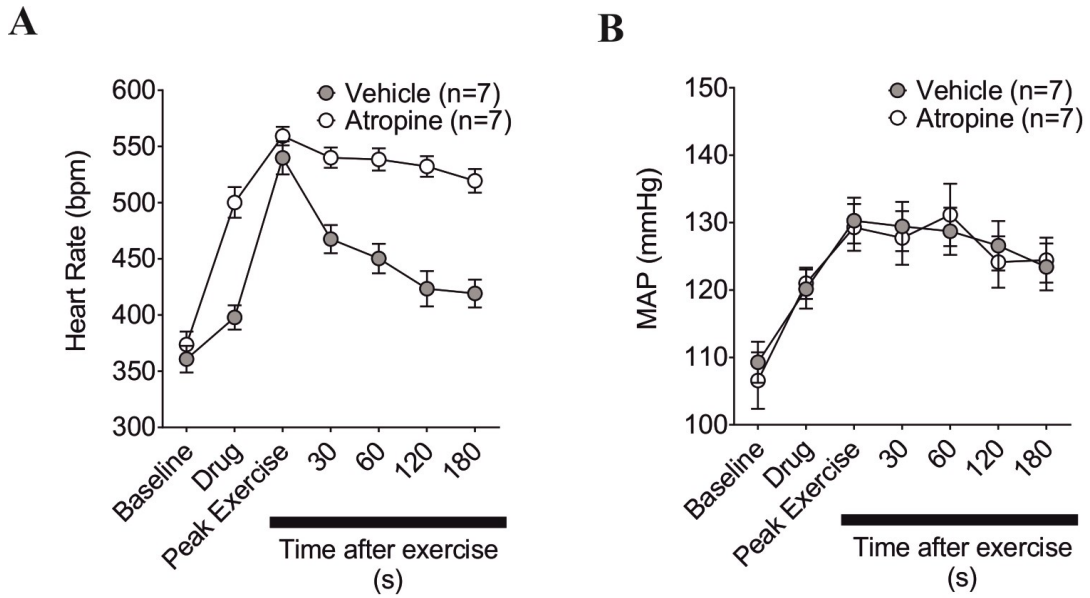

Figure 4-7: The effect systemic muscarinic receptor blockade on heart rate and systemic arterial blood pressure of conscious rats during the course of exercise experiments in rats

A) Summary data illustrating changes in heart rate during exercise in rats following an acute i.p. injection of saline or atropine methyl nitrate (2 mg kg^{-1}); **B)** Summary data illustrating changes in blood pressure during exercise in rats following an acute i.p. injection of saline or atropine methyl nitrate (2 mg kg^{-1}).

4.3.3 Experiment 3. The effect of systemic muscarinic receptor blockade on cardiovascular response induced by β-adrenoceptor stimulation

Systemic muscarinic receptor blockade increased LVd*P*/dt_{max} (11303±160 vs 10011±119 mmHg s^{-1} at baseline; P<0.0001; ANOVA; Figure 4-8A) and LVESP (139±2 vs 132±2 mmHg at baseline; p=0.04; ANOVA; Figure 4-8B). Infusion of the vehicle (saline) over the same period of time had no effect on cardiovascular variables (Figure 4-8A, B). Administration of dobutamine resulted in significant increases in LVd*P*/dt_{max} in control conditions (rats treated with saline) (10806±389 vs 9252±356 mmHg s^{-1} at baseline; p=0.001; ANOVA; Figure 4-8A) as well as in animals following acute injection of atropine (11559±191 vs 10011±119 mmHg s^{-1} at baseline; p=0.008; ANOVA; Figure 4-8A). Dobutamine also increased LVESP in control conditions (rats treated with saline) (135±3 vs 123±2 mmHg at baseline; p=0.0002; ANOVA; Figure 4-8B) as well as in animals following acute injection of atropine (139±5 vs 128±4 mmHg at baseline; p=0.002; ANOVA; Figure 4-8B).

Under chronic (four hour) muscarinic receptor blockade, dobutamine had no further effect on LVd*P*/dt_{max} (11557±145 vs 11304±160 mmHg s^{-1} at baseline; p=0.2; ANOVA; Figure 4-8A) or LVESP (141±3 vs 139±2 mmHg at baseline; p=0.9; ANOVA Figure 4-8B). In addition to β_1-adrenoceptor agonism, dobutamine is also known to acts on β_2- as well as α_1-adrenoceptors (Ruffolo, 1987). This may explain the lack of dobutamine effect on ABP because of the resulting vasodilation counteracting its effect on the LV inotropic state (Figure 4-9A). HR increases induced by dobutamine where similar in control conditions as well as following sustained systemic muscarinic receptor blockade (484±4 vs 463±5 bpm at baseline; p=0.003; ANOVA; Figure 4-9B).

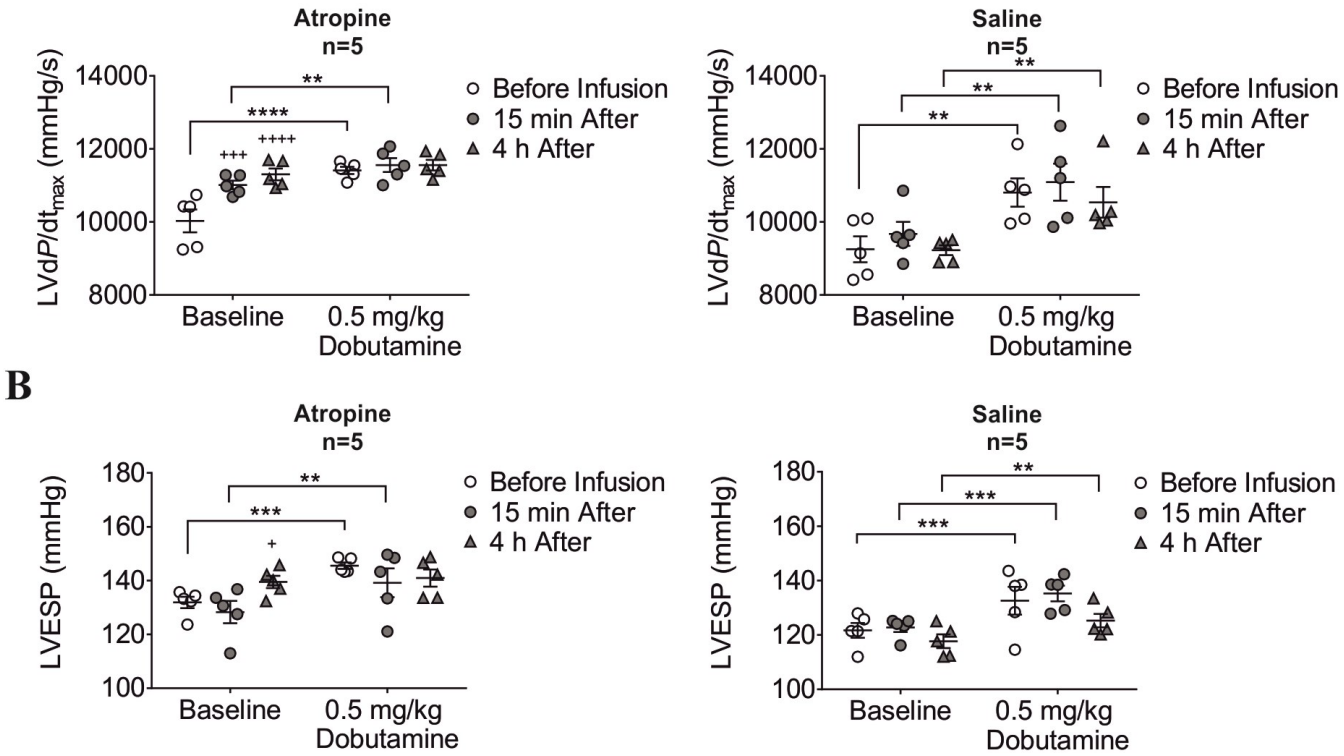

Figure 4-8: The effect of systemic muscarinic receptor blockade on LV contractile response to β-adrenoceptor stimulation

A) Summary data illustrating changes in $LVdP/dt_{max}$ triggered by dobutamine challenge prior to as well as 15 minutes and four hours after the onset of atropine (2 mg kg^{-1} h^{-1} i.v.) or saline infusion. **B)** Summary data illustrating changes in LVESP triggered by dobutamine challenge prior to as well as 15 minutes and four hours after the onset of atropine (2 mg kg^{-1} h i.v.) or saline infusion. *Asterisk* denotes significant effect of dobutamine. *Plus* denotes significant effect of atropine. **P<0.01; ***P<0.001; ****P<0.0001; $^{+}$P<0.05; $^{++}$P<0.01; $^{+++}$P<0.001.

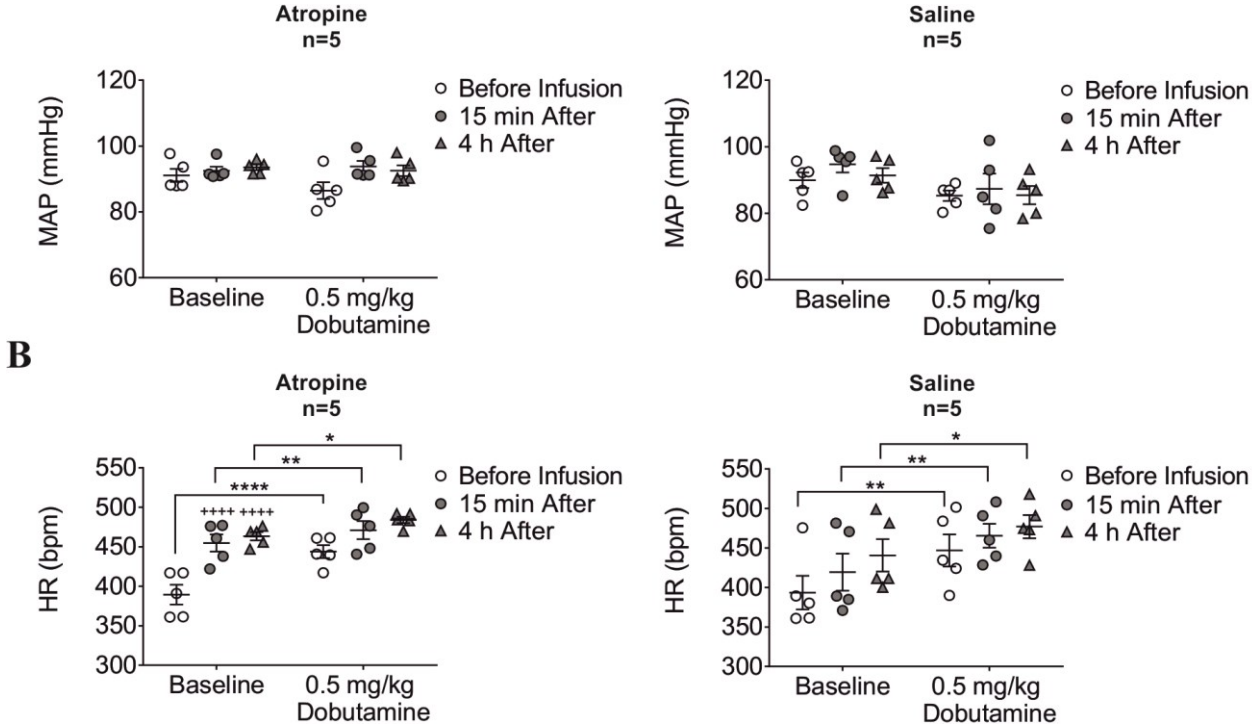

Figure 4-9: The effect of systemic muscarinic receptor blockade on blood pressure and heart rate responses to dobutamine challenge

A) Summary data illustrating values of mean arterial blood pressure during dobutamine challenge prior to as well as 15 minutes and four hours after the onset of atropine (2 mg kg^{-1} h^{-1} i.v.) or saline infusion. **B)** Summary data illustrating changes in HR triggered by dobutamine challenge prior to as well as 15 minutes and four hours after the onset of atropine (2 mg kg^{-1} h^{-1} i.v.) or saline infusion. *Asterisk* denotes significant effect of dobutamine. *Plus* denotes significant effect of atropine. *P<0.05; **P<0.01; ***P<0.001; ****P<0.0001; $^{++++}$P<0.001.

4.3.4 Experiment 4. The effect of reduced DVMN activity on exercise capacity

Histological reconstruction has demonstrated strong expression of AlstR/eGFP along the rostro-caudal extent of both DVM nuclei. Figure 4-10A illustrates AlstR expression in a caudal aspect of the DVMN. Exercise capacity at baseline was similar in rats expressing AlstR/eGFP and eGFP (140±15 vs 191±22 J; p=0.53; ANOVA; Figure 4-10B). Infusion of allatostatin into the *cisterna magna* of rats expressing AlstR in the DVMN resulted in a dramatic reduction in exercise capacity (8±2 vs 202±27 J in rats expressing eGFP; P<0.0001; ANOVA; Figure 4-10B). Exercise capacity of rats in the treatment group recovered within the next 24 hour period (152±15 vs 140±15 J at baseline; p=0.7; ANOVA; Figure 4-10B). Biotelemetry monitoring has demonstrated that reduced DVMN activity results in a small increase in the ABP (111±3 vs 103±4 mmHg at baseline; p=0.03; ANOVA; Figure 4-10C), which was found to be independent of HR changes (364±13 vs 350±12 bpm at baseline; p=0.9; ANOVA; Figure 4-10D). Interestingly, peak increases in ABP during exercise were lower in rats expressing AlstR/eGFP following application of allatostatin (120±2 vs 135±7 mmHg in rats expressing eGFP; p=0.03; ANOVA; Figure 4-10C). Peak HR during exercise was also lower in rats expressing AlstR/eGFP (546±12 vs 510±2 bpm in rats expressing eGFP; p=0.03; ANOVA; Figure 4-10D).

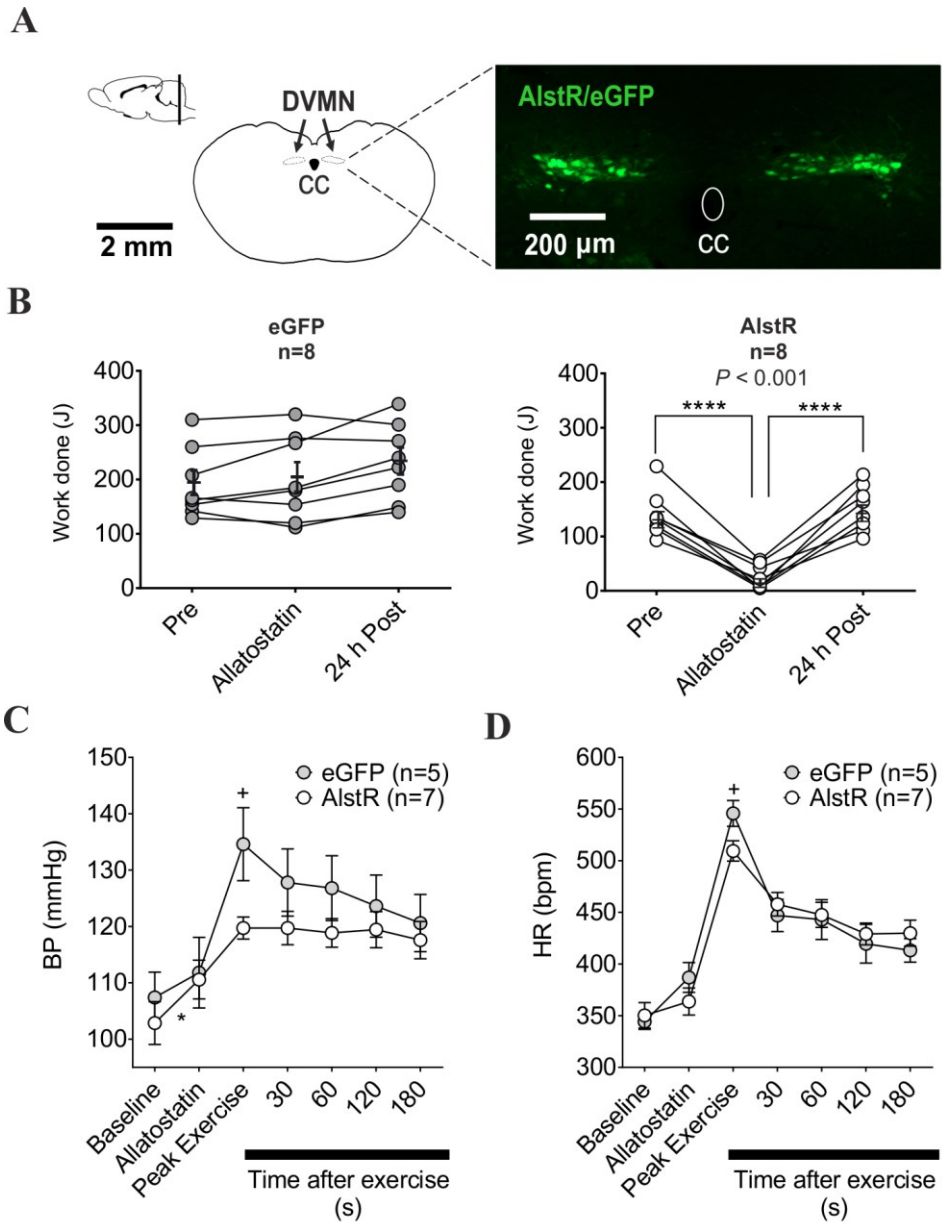

Figure 4-10: The effect of reduced DVMN activity on exercise capacity and cardiovascular response to exercise

Confocal image of a representative coronal section of the rat brainstem showing the distribution of vagal preganglionic neurones transduced to express AlstR/eGFP in the caudal regions of the left and right nuclei. CC, central canal; **B**) Summary data illustrating the effect of allatostatin infusion into the *cisterna magna* on exercise capacity in rats transduced to express eGFP or Alst/eGFP in the DVMN. **C, D**) Summary data illustrating the effect of allatostatin infusion into the *cisterna magna* on exercise-induced changes in the systemic arterial blood pressure and HR in rats transduced to express eGFP or Alst/eGFP in the DVMN. *Asterisk* denotes significant effect of DVMN silencing. *Plus* denotes significance with respect to eGFP. *P<0.05; ****P<0.0001; $^{+}$P<0.01.

4.3.5 Experiment 5. The effect of reduced DVMN activity on cardiovascular response induced by β-adrenoceptor stimulation

Administration of dobutamine triggered significant increases in LVd*P*/dt_{max} in rats expressing eGFP (10304±94 vs 9612±216 mmHg s^{-1} at baseline; p=0.03; ANOVA; Figure 4-11A) and AlstR/eGFP (11808±356 vs 10744±459 mmHg s^{-1} at baseline; p=0.0003; ANOVA; Figure 4-11A) in the DVMN. Dobutamine also triggered significant increases in LVESP in rats expressing eGFP (128±7 vs 119±9 mmHg at baseline; p=0.03; ANOVA; Figure 4-11B) and AlstR/eGFP (169±6 vs 148±6 mmHg s^{-1} at baseline; p<0.0001; ANOVA; Figure 4-11A) in the DVMN.

Dobutamine had a similar effect on LVd*P*/dt_{max} (10535±211 vs 9836±240 mmHg s^{-1} at baseline; p=0.03; ANOVA; Figure 4-11A) and LVESP (143±16 vs 121±10 mmHg at baseline; p=0.02; ANOVA; Figure 4-11B) in rats expressing eGFP following allatostatin infusion. In conditions of reduced DVMN activity (allatostatin application in rats expressing AlstR/eGFP), dobutamine had no effect on LVd*P*/dt_{max} (11234±552 vs 11278±540 mmHg s^{-1} at baseline; p>0.9; ANOVA; Figure 4-11A) and LVESP (164±6 vs 165±7 mmHg at baseline; p>0.9; ANOVA; Figure 4-11B). Dobutamine had no effect on mean ABP in either group of animals prior to and after allatostatin application (p>0.1 for all comparisons; Figure 4-11C).

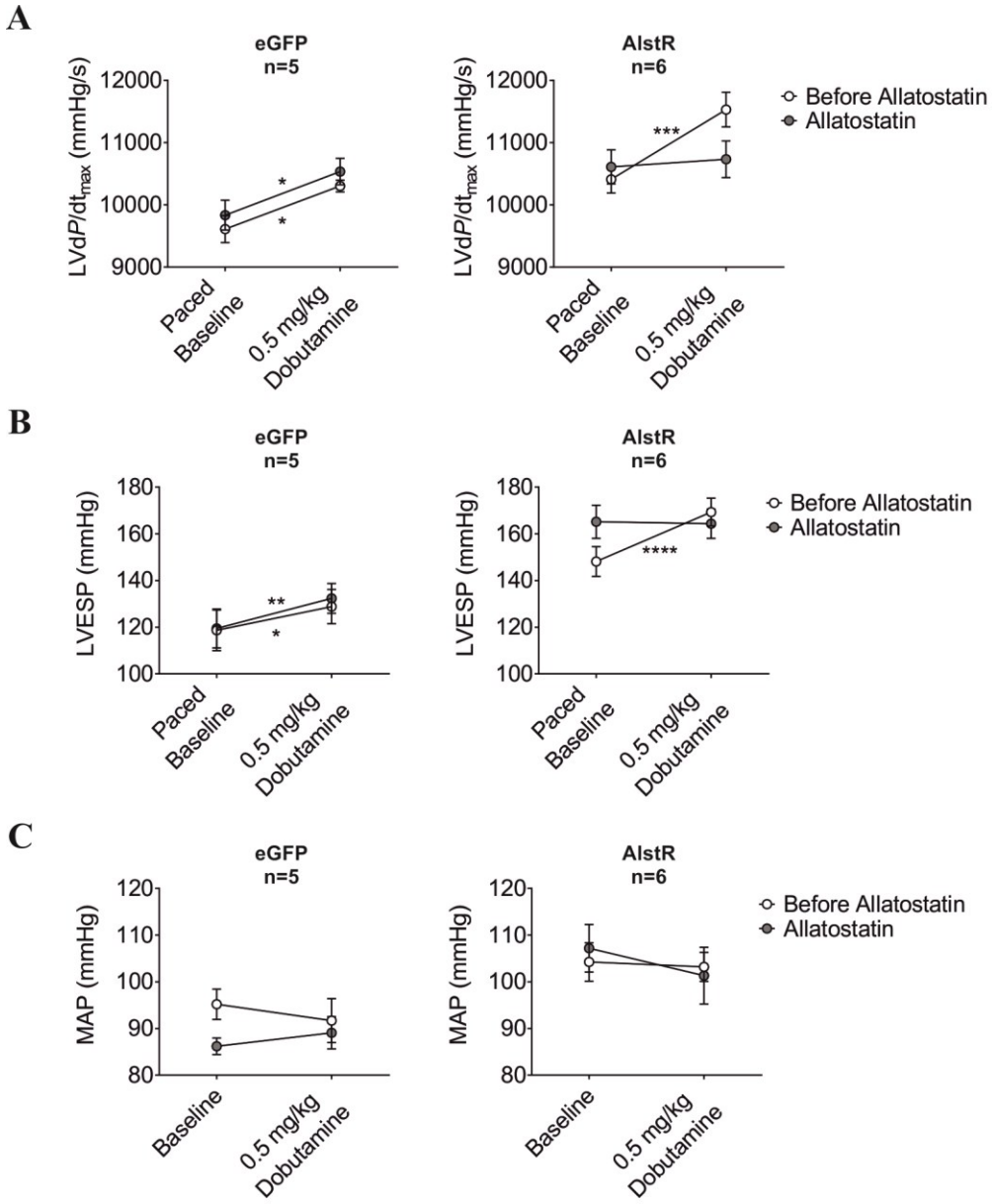

Figure 4-11: The effect of reduced DVMN activity on cardiovascular response induced by β-adrenoceptor stimulation

A) Summary data illustrating changes in LVdP/dt_{max} triggered by dobutamine challenge prior to as well as 15 minutes after allatostatin infusion into the cisterna *magna* of rats expressing eGFP or AlstR/eGFP in the DVMN; **B)** Summary data illustrating changes in LVESP during dobutamine challenge prior to as well as 15 minutes after allatostatin infusion into the *cisterna magna* of rats expressing eGFP or AlstR/eGFP in the DVMN **C)** Summary data illustrating MAP changes triggered by dobutamine challenge prior to as well as 15 minutes after allatostatin infusion into the cisterna magna of rats expressing eGFP or AlstR/eGFP in the DVMN. *Asterisk* denotes significant effect of dobutamine. *P<0.05; **P<0.01; ***P<0.001; ****P<0.0001.

4.3.6 Experiment 6. The effect of DVMN stimulation on exercise capacity and contractile properties of the LV

Strong expression of ChIEF-tdTomato by the DVMN neurones (Figure 4-12A, B) resulted in insertion of light sensitive ChIEF-tdTomato along the length of the neuronal axons reaching the level of the cervical vagus (Figure 4-12C). Rats expressing ChIEF-tdTomato by the DVMN neurones displayed significantly higher exercise capacity of 15 minutes of optogenetic stimulation (daily) after four days (94±11 vs 47±6 J in rats expressing eGFP; p=0.002; ANOVA; Figure 4-13A). This improvement in exercise capacity was similar to that observed in the naïve rats that underwent exercise training to the defined point of exhaustion over the same time period (105±16 vs 47±6 J in rats expressing eGFP; p<0.0001; ANOVA; Figure 4-13A). Thus, optogenetic stimulation of the DVMN neurones and exercise training over the course of four days appear to have a similar effect on exercise capacity (p=0.8; ANOVA).

Furthermore, ultrasound assessment of LV function demonstrated that baseline ejection fraction was increased as a result of four days of optogenetic DVMN stimulation (75±2% in rats expressing ChIEF-tdTomato vs 62±1 % in rats expressing eGFP; p<0.0001; ANOVA; Figure 4-13B). The ejection fraction was unchanged in rats that underwent exercise training to the defined point of exhaustion over the same time period (67±2 vs 62±1 % in rats expressing eGFP; p=0.09; Figure 4-13B). Optogenetic stimulation of the DVMN also resulted in a significantly higher ejection fraction during the dobutamine challenge (93±1 vs 84±2% in rats expressing eGFP; p=0.003; ANOVA; Figure 4-13B). Interestingly there were no significant differences in HR between all groups of animals either at baseline or during dobutamine challenge (Figure 4-13C).

Western blot analysis has demonstrated that optogenetic recruitment of the DVMN activity is associated with downregulation of GRK2 expression in the LV (normalised to the expression of α-tubulin) when compared to that in animals expressing eGFP (0.45±0.42 vs 0.97±0.19; Figure 4-14A) or rats that underwent exercise training (0.45±0.42 vs 1.37±0.15; p=0.004; t-test; Figure 4-14A). Similarly, optogenetic recruitment of the DVMN activity led to downregulation of β-arrestin

expression in the LV when compared to that in animals expressing eGFP (0.49±0.07 vs 0.88±0.07; Figure 4-14B) or rats that underwent exercise training (0.49±0.07 vs 1.10±0.08; p=0.004; t-test; Figure 4-14B).

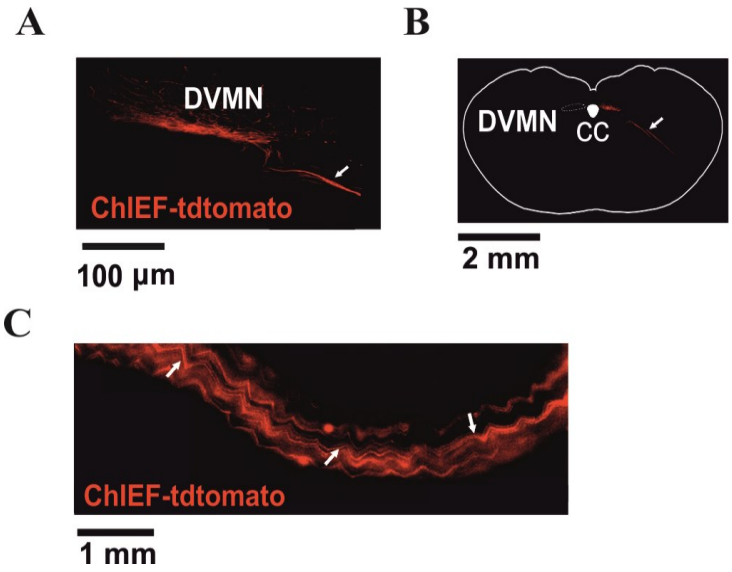

Figure 4-12: Targeting DVMN neurones to express ChIEF-tdTomato

A) Confocal image of a coronal section of the rat brainstem targeted to express ChIEF-tdTomato by the DVMN neurones. Neurones display membrane localisation of the transgene. Ventrally projecting axons (arrow) of the DVMN neurones transduced to express ChIEF-tdTomato; **B)** Low-magnification image illustrating unilateral expression of ChIEF-tdTomato by the DVMN neurones**.** CC, central canal.; **C)** Axons (arrows) of the DVMN neurones transduced to express ChIEF-tdTomato visualised in the whole mount preparation of the left vagus nerve. ChIEF-tdTomato is eventually inserted along the whole length of the neuronal axons.

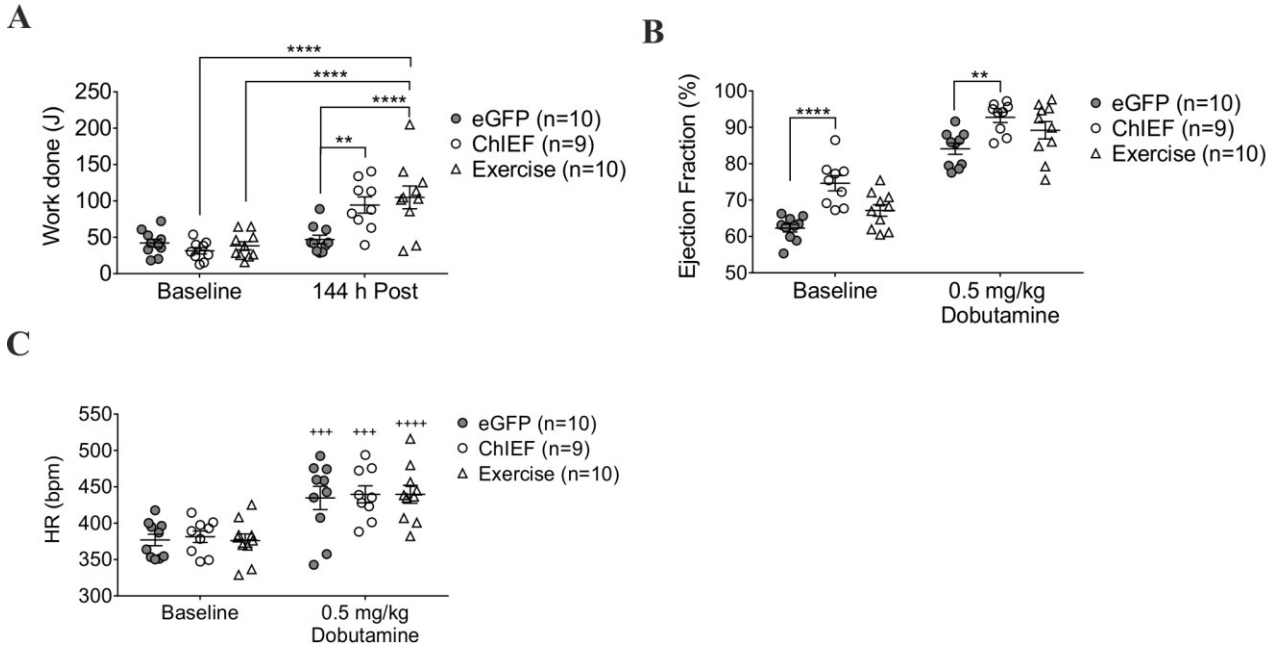

Figure 4-13: The effect of DVMN stimulation on exercise capacity and contractile properties of the LV

A) Summary data illustrating exercise capacity of rats transduced to express ChiEF-tdTomato (n=9) and eGFP (n=10) by the DVMN neurones before and after four days of light stimulation of the dorsal brainstem via a pre-implanted optrode (daily sessions each lasting 15 minutes), as well as of a separate group of naïve animals before and after four daily sessions of treadmill exercise training. **B, C**) Summary data illustrating LV ejection fraction and HR at baseline and during dobutamine challenge (infusion 0.5 mg kg^{-1} min^{-1}, two minutes at a rate of 0.1 ml min^{-1}) in rats transduced to express ChiEF-tdTomato or eGFP by the DVMN neurones before and after four days of light stimulation, as well as in naïve animals before and after four daily sessions of treadmill exercise training. *Asterisk* denotes significant effect of DVMN stimulation. *Plus* denotes significant effect of dobutamine. **P<0.01; ****P<0.0001; $^{+++}$P<0.001; $^{++++}$P<0.0001.

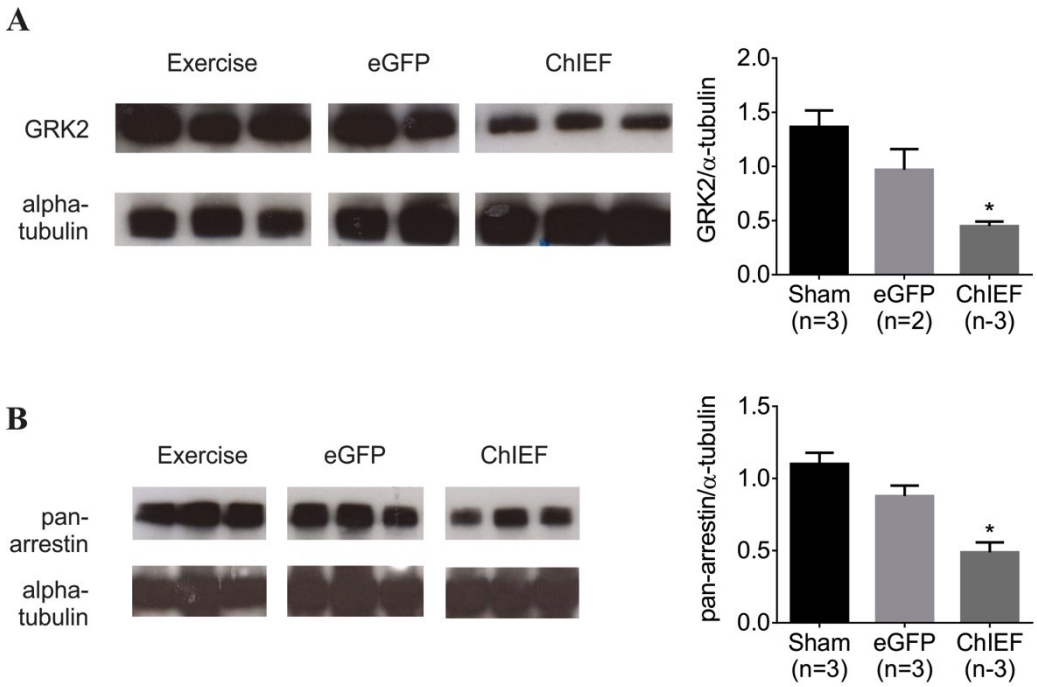

Figure 4-14: The effect of DVMN stimulation on GRK2 and pan-arrestin expression in the LV

Representative immunoblots and summary data illustrating GRK2 **(A)** and pan-arrestin **(B)** (for βarrestin2) expression in the LV of rats transduced to express ChIEF-tdTomato (ChIEF) and eGFP by the DVMN neurones after four days of light delivery to the dorsal brainstem, as well as of naïve animals after four daily sessions of treadmill exercise training. *Asterisk* denotes significant effect of DVMN stimulation. *P<0.01.

4.4 Discussion

4.4.1 The effects of unilateral vagotomy and systemic treatment with atropine

This experimental study was designed to test the hypothesis that the strength of parasympathetic cardiac tone determines exercise capacity. It was predicted that vagal withdrawal decreases and vagal recruitment enhances ability to exercise. Based on the results of the experiments reported in Chapters 1 and 2 suggesting that the DVMN neuronal projections control electrical and contractile properties of the LV, it was therefore hypothesised that the activity of this population of VPNs determines exercise capacity.

A significant reduction in exercise capacity was observed in rats following unilateral vagotomy, sustained (four hours) systemic muscarinic receptor blockade or inhibition of the neuronal NOS. Exercise capacity was also reduced in mice deficient in M_3 muscarinic receptor-mediated signalling and in WT mice in conditions of systemic M_3 muscarinic receptor blockade. Acute reduction in the activity of the DVMN neurones using a pharmacogenetic approach resulted in a dramatic lowering of exercise capacity and inability of the LV to mount a contractile response to β-adrenoceptor stimulation. Optogenetic recruitment of the DVMN activity improved exercise capacity and contractile properties of the LV, and this was associated with downregulation of the ventricular GRK2 and β-arrestin expression.

Unilateral vagotomy reduced exercise capacity in rats by approximately 50% when assessed five days after the surgery. Exercise capacity was similar in vagotomised and sham-operated animals 32 days after the surgery. Ultrasound assessment showed no significant changes in LV ejection fraction or HR as a result of unilateral vagotomy when measured after five days. Recovery of exercise capacity at 32 days post-surgery could be explained by functional compensation by the remaining intact nerve or (partial) re-innervation of the resected side. There is evidence that re-innervation may occur as shown by observations in heart transplant patients who display low amplitude RSA two weeks after the surgery (Zbilut *et al.*, 1988) and exhibit a dramatic (>200%) increase in power of the high frequency component of the HRV (as a measure of cardiac vagal tone) 28 months following

transplantation. Significant recovery of the high frequency component of the HRV cannot be explained by the intrinsic HR response to myocardial wall stretch (Bernardi *et al.*, 1989) and suggests functional parasympathetic innervation of the transplanted heart.

Systemic muscarinic receptor blockade (administration of atropine methyl nitrate) lasting 15 minutes had no effect on exercise capacity. However, administration of atropine for four hours (sustained muscarinic blockade mimicking chronic vagal withdrawal) reduced exercise capacity by approximately 40%. It was hypothesised that sustained muscarinic blockade impairs the ability of LV to mount an appropriate contractile response to sympathetic stimulation. In rats kept under urethane anaesthesia, atropine infusion increased LV contractility (as assessed by recordings of LV$dP/dt_{max}$ and LVESP) and no further increase was observed during dobutamine challenge. Inability of the LV to respond to sympathetic stimulation may be responsible (at least in part) for impaired exercise capacity following four hours of atropine infusion. However, since atropine infusion for four hours was associated with significant increases in HR and LV inotropy at baseline, which may have also resulted in systemic toxic effects (Zhang *et al.*, 2001), a different experimental approach (acute and reversible manipulation of ventricular vagal innervation) was required.

This effect of systemic muscarinic receptor antagonism on exercise capacity was further investigated using the genetic and pharmacological blockade of M_2 and M_3 receptor-mediated signalling. Systemic administration of M_2 receptor blocker AFDX116 for four hours had no effect on exercise capacity suggesting that M_2 receptor antagonism is not responsible for the observed effects of atropine. On the other hand, exercise capacity was found to be significantly impaired in mice with global deficiency in M_3 receptor phosphorylation, with similar reductions in exercise capacity being observed in WT mice in conditions of systemic M_3 receptor blockade (infusion of 4-DAMP for four hours). These data suggest that the detrimental effect of systemic atropine infusion on exercise capacity is likely due to blockade of a mechanism involving M_3 receptor-mediated signalling.

M_2 receptors are Gi-coupled and constitute the most abundant type of cardiac muscarinic receptors. M_3 receptors signal via Gq proteins and have been demonstrated to be involved in smooth muscle relaxation and glandular secretion (Kruse *et al.*, 2012), including insulin secretion (Kong *et al.*, 2010). M_3 receptor expression in the mammalian heart has also been demonstrated (Wang *et al.*, 2004) (Liu *et al.*, 2005; Liu *et al.*, 2008; Pan *et al.*, 2012; Hang *et al.*, 2013).

Potential mechanisms of how M_3 receptor-mediated signalling determines exercise capacity is discussed in terms of its potential role in the control of perfusion, contractile function and metabolism.

4.4.2 Crosstalk between M_3 and β_2-adrenoceptor signalling

Functional interactions between M_3 muscarinic and β_2-adrenoceptor mediated signalling pathways have been demonstrated (Budd *et al.*, 1999) and can provide a plausible explanation for impaired exercise capacity in conditions of either genetic or pharmacological blockade of M3 signalling. G protein-coupled receptor kinase 2 (GRK2) activity is modulated by $G_{\beta\gamma}$ and phosphatidylinositol 4,5-bisphosphate (Krasel *et al.*, 2005), as well as stimulation of β_2-adrenoceptors (Sallese *et al.*, 2000). GRK2 phosphorylation of β_2-adrenoceptor increases the affinity for binding of β-arrestins 1 and 2 with subsequent desensitisation and internalisation of this receptor complex (Krasel *et al.*, 2005).

Under normal conditions, phospholipase C recruitment downstream of M_3 receptor activation increases intracellular Ca^{2+} (Tobin *et al.*, 1992; Willars *et al.*, 1996). Raised intracellular Ca^{2+} activates protein kinase C, which increases GRK2 activity (Sallese *et al.*, 2000). Under conditions of prolonged M_3 receptor blockade, adaptive down-regulation of β_2-adrenoceptor expression could occur given that they exhibit higher constitutive activity (basal cAMP levels are five times higher than that associated with constitutive activity of β_1-adrenoceptors) in addition to robust internalisation (Engelhardt *et al.*, 2001). The lowered threshold would thus reduce the cAMP response, limiting the magnitude of vasodilation due to activation of β_2-adrenoceptors (Ruffolo, 1987). During exercise, sympathetic signalling via vascular

β_2-adrenoceptors is believed to contribute significantantly to coronary vasodilation (Duncker *et al.*, 1998; Gorman *et al.*, 2000). If M_3 receptor blockade impairs the efficacy of β_2-adrenoceptor-mediated signalling (via GRK2 up-regulation) then coronary vascular response may be compromised and insufficient to meet the increased metabolic demands of the myocardium during exercise.

Blockade of M_3-meidated signalling may also be associated with reduced activity of protein kinase D1 (PKD1). There is evidence that uncoupling of M_3 receptor from its cognate proteins upon activation (Kong *et al.*, 2010) may result in recruitment of intracellular signalling pathways independent of those mediated by G-proteins. This occurs predominantly through β-arrestin dependant signalling (Kreienkamp, 2002; Bockaert *et al.*, 2004; Lefkowitz *et al.*, 2006; Reiter & Lefkowitz, 2006) involving activation of PKD1 (Kong *et al.*, 2010). In the cardiac muscle, PKD1 plays an important role in mediating glucose uptake by translocation of the glucose transporter GLUT4 (Dirkx *et al.*, 2012). GLUT4 is responsible for the majority of glucose uptake in both cardiac (Dirkx *et al.*, 2012) and skeletal muscles (Richter & Hargreaves, 2013). Despite being responsible for most of glucose uptake, it is mostly stored within intracellular vesicles due to its high affinity for glucose (Montessuit & Lerch, 2013). Assuming this hypothesis were true, it would be unsurprising that unilateral vagotomy would not affect baseline cardiac parameters given the ventricular capacity for autocrine release of ACh under normal and ischaemic challenge (Akiyama *et al.*, 1994; Kawada *et al.*, 2009).

Brack *et al.* (2009) demonstrated that coronary infusion of ACh triggers NO production from a non-neuronal source, which they suggest to be eNOS. As the endocardial layers are more metabolically demanding (Kainulainen *et al.*, 1990) it would be very interesting to study the metabolic dynamics of this layer with regard to NO, given that the endocardium is subject to the most distension, which can affect the production of NO (Pinsky *et al.*, 1997). The transmural β_2 heterogeneity between the subepicardium and the subendocardium in particular (Hein et al., 2004) results in a somewhat counterintuitive shunting to the less metabolically demanding epicardium in both normal and infarcted hearts (Berdeaux *et al.*, 1979; Domenech & MacLellan, 1980).

Systemic blockade of nNOS (using 7-NI) was found to have the most significant detrimental (reduction by >70%) effect on exercise capacity. NO produced by nNOS expressed by cardiac parasympathetic fibres is known to facilitate presynaptic release of ACh and nNOS blockade was previously found to disrupt muscarinic transmission (Choate *et al.*, 2001; Danson *et al.*, 2004). There is also evidence that exercise training increases nNOS expression at cardiac vagal presynaptic terminals (Danson & Paterson, 2003). Inhibition of endothelial NOS (eNOS) may also (in part) explain the effect of 7-NI on exercise capacity.

Compromised coronary (and possibly skeletal) perfusion (Hein & Kuo, 1999; Paterson, 2001) and glucose uptake could explain the dramatic effects of 7-NI on exercise capacity. NO also appears to have a significant positive lusitropic effect (Pinsky *et al.*, 1997). NO improves ventricular relaxation (Smith *et al.*, 1991) (Shah, 1996), therefore, blockade of NO production may compromise effective ventricular filling required to increase cardiac output during exercise.

4.4.3 The DVMN has a source of acetylcholine and nitric oxide

Acute inhibition of the DVMN VPNs targeted to express AlstR was associated with dramatic (by 87%) reduction of exercise capacity already 15 minutes after allatostatin application. Full recovery of exercise capacity was observed within the next 24 hours. Inhibition of DVMN neurones had no effect on HR but resulted in a small increase in MAP (by 7 mmHg). Importantly, in rats kept under urethane anaesthesia combined with atrial pacing, stimulation of β-adrenoceptors with dobutamine had no effect on LV$dP/dt_{max}$ and LVESP when the activity of DVMN neurones was reduced.

These results, considered together with data obtained in pharmacological experiments involving systemic muscarinic and nNOS blockade, argue in favour of a critical role played by vagal innervation of the ventricle, which maintains the ability of the LV to mount an appropriate contractile response to sympathetic stimulation. Acute nNOS inhibition and acute DVMN silencing were found to have quantitatively similar detrimental effects on exercise capacity. This suggests that the DVMN

neuronal projections control LV function and exercise capacity, using NO as a signalling molecule. The concept of a direct NO-mediated vagal control of the ventricle is supported by the data presented in Chapter 2 of this thesis as well as in previous studies (Brack *et al.*, 2009; Brack *et al.*, 2011). Conflicting with this is a previous exercise study which has shown that mice deficient in nNOS (nNOS-/-) do not appear to have a compromised exercise capacity (Wadley *et al.*, 2007). This could be explained by a compensatory overexpression of the remaining functional isoforms.

Vagal innervation of the LV mediated by muscarinic mechanisms is hypothesised to provide a trophic influence, the significance of which becomes clear over a longer period of time. Optogenetic recruitment of the DVMN neurones (four daily sessions of 15 minute long stimulations) improved exercise capacity and contractile function of the LV. The degree of exercise capacity improvement was quantitatively similar to that observed in a group of naïve rats subjected to exercise training over the same time period. However, no improvement in LV contractile function was observed in the latter group of rats. Changes in LV inotropy following optogenetic DVMN recruitment were not associated with any significant changes in HR. Preliminary blots conducted in collaboration with the research group of Dr. Gareth Ackland have demonstrated that optogenetic stimulation of the DVMN results in down regulation of GRK2 and pan-arrestin expression in the LV myocardium. There is evidence that reduced expression of GRK2 unmasks the significant contractile effect of β_2–adrenoceptor stimulation, which is either weak or absent under normal conditions (Salazar *et al.*, 2013). Increased vagal efferent activity and recruitment of PKD1 via activation of the M_3 receptor had also been shown to promote cardiac hypertrophy and angiogenesis (Rozengurt, 2011). Increased efficacy of β_2–adrenoceptor-mediated signalling in LV cardiomyocytes may therefore explain changes in resting inotropic state underlying the ability of the LV to mount a stronger inotropic response during exercise.

4.4.4 Vagal tone and plasticity

These data show that the strength of vagal tone supplied to the LV by the DVMN neurones determines the ability of cardiomyocytes to respond to sympathetic stimulation and would, therefore, determine exercise capacity. Nevertheless, differences in individual ability to exercise may reflect varying levels of DVMN activity. High vagal tone provided by the DVMN neuronal projections to the LV in elite athletes could make them highly tolerant to intense exercise regimes. Conversely, the loss of exercise capacity with age has been associated with a decline in autonomic function (De Meersman & Stein, 2007). Neurones such as those of the DVMN have long projecting axons with no myelination and require more energy for impulse propagation and are the most susceptible to metabolic stress (Kapfhammer & Schwab, 1994). DVMN dysfunction has already been associated with a host of autonomic abnormalities (Braak *et al.*, 2002; Goldberg *et al.*, 2012) and may contribute to a progressive decline in exercise capacity during aging and in various disease states.

4.5 Study Limitations

With regards to the gene transfer work to silence the DVMN neurones, the viral titres for the constructs used were not reliably known. Acceptable expression was predetermined by injection in test subjects allowing four weeks prior to conducting histology. The extent of expression could have instead been evaluated via polymerase chain reaction as titres would inevitably vary, given the titre loss of the lentiviral constructs immediately after thawing.

In view of the current debate as to whether parasympathetic tone exhibits a certain degree of plasticity (Coote & White, 2015; D'Souza *et al.*, 2015) in such a way that exercise may entrain a high resting vagal tone calls for an additional line of inquiry. It may well be that exercise and/or optogenetic stimulation could be modulating lower vagal interneuron circuitry or even be eliciting changes within the pacemaker itself. It would be important, then, to perform electrophysiological recordings from the DVMN neurones firstly in an anaesthetised preparation during simulated exercise. Such simulations could involve passive limb movement, femoral or sciatic nerve stimulation or dobutamine challenges. To test the hypothesis that regular exercise increases DVMN activity, experimental animals could be provided with an opportunity to exercise (e.g. running wheels in home cages). Running wheels can be used to quantify and correlate exercise capacity with spiking activity and excitability of the DVMN neurones. Voluntary running wheels would also be a superior method of exercising rodents given the additional stress that is inevitably experience with forced running experiments.

In summary, the data reported in this chapter confirms the validity of the hypothesis that the strength of parasympathetic tone determines exercise capacity. The results show that reduced activity of the DVMN VPNs impairs and increased activity of the DVMN enhances exercise capacity and contractile function of the LV. These effects are mediated by the actions of ACh and NO and may involve alterations in the expression of important regulatory proteins, namely GRK2 and β-arrestin, by cardiomyocytes. In his work *Vagus as a regulator of systemic arterial blood pressure* Ivan Pavlov concluded that “the vagus nerve exerts trophic influence

on the ventricle and prepares it for action" (Khaiutin & Lukoshkova, 1995). Indeed, results of this study obtained using pharmacological blockade, M3-KI genetic mouse model, pharmaco- and optogenetic approaches to alter the activity of the DVMN VPNs reveal that vagal supply to the LV maintains the ability of the heart to mount an appropriate inotropic response during increased activity and exercise.

Chapter 5 Enhancing Vagal Activity in Heart Failure

5.1 Introduction

Ischaemic heart disease is one of the most common causes of morbidity and mortality in the developed world. Occlusion of a major coronary artery is followed by myocardial metabolic and functional changes that develop rapidly after cessation of the blood flow (Jennings *et al.*, 1990). Despite rapid reperfusion of the ischaemic area by primary percutaneous coronary intervention (preferred current treatment of an acute MI), many patients develop large infarcts, progress to chronic heart failure and have a poor prognosis. Manifestations of myocardial injury include arrhythmias, contractile and endothelial dysfunction and lethal reperfusion injury of cardiomyocytes (Hearse & Bolli, 1992; Hearse, 1998; Sanada *et al.*, 2011). The latter contributes approximately 50% to the resultant infarct size (Hausenloy & Yellon, 2008).

VNS has been shown to reduce the extent of MI and slow the progression of myocardial remodelling and dysfunction in several animal models of chronic heart failure (Jones *et al.*, 2009; Katare *et al.*, 2009; Calvillo *et al.*, 2011; Shinlapawittayatorn *et al.*, 2013). Although there is a clear clinical association between low (chronotropic) vagal tone and poor cardiovascular outcomes (La Rovere *et al.*, 1998; Nolan *et al.*, 1998; Schwartz, 1998; Schwartz *et al.*, 2004; Schwartz, 2012), the precise mechanisms underlying the beneficial effect of VNS during heart failure are poorly understood.

A potential benefit of VNS has been recently explored in 32 patients with chronic heart failure, using implantable devices capable of delivering low current pulses to stimulate the right vagus nerve. Reported results showed improvements in NYHA class quality of life and LV function (De Ferrari *et al.*, 2011) and led to multicentre clinical trials (NECTAR-HF, INOVATE-HF) designed to test VNS efficacy in large cohorts of patients (Hauptman *et al.*, 2012). However, these trials were initiated without full understanding of the underlying mechanism(s). In the CardioFit preliminary trial (De Ferrari *et al.*, 2011), 26 serious adverse events occurred in 13 of 32 patients enrolled (41%), including three deaths within the first

three months. The NECTAR-HF study (Zannad *et al.*, 2015) was the first randomised controlled trial evaluating the safety and efficacy of VNS applied to the right vagus nerve. Enrolling 96 heart failure patients, no improvements in the objective measures of cardiac function were found after six months of stimulation. However, a marginal improvement in quality of life was reported (Zannad *et al.*, 2015).

The vagus nerve is one of the most complex nerves; it contains sensory and motor fibres which conduct impulses from and to the majority of the internal organs. It is not clear whether the beneficial effects of VNS are due to activation of the efferent or afferent fibres. Recently it was found that stimulation of approximately 300-400 vagal preganglionic DVMN neurones is capable of reducing acute myocardial ischaemia/reperfusion injury in an animal model (Mastitskaya *et al.*, 2012), providing direct evidence of potent cardioprotection via stimulation of the efferent vagus.

Further refinement of VNS allowing selective recruitment of a particular population of vagal fibres is expected to maximise efficacy and limit side effects that include cough, dysphonia, sleep apnoea and others (Parhizgar *et al.*, 2011). It was hypothesised that the beneficial effect of the VNS in heart failure is conferred by the vagal efferent fibres which innervate the LV. The data reported in Chapters 2 to 4 suggest that functionally significant vagal innervation of the ventricle originates in the DVMN. This chapter describes the results of the experiments aimed to determine whether optogenetic recruitment of the DVMN activity slows the remodelling process and improves LV function post-MI in a rat model.

Clinically, the assessment of diastolic function is routinely performed using Doppler echocardiographic recordings of the blood flow velocity across the mitral valve (Poulsen *et al.*, 1999). In this chapter, Doppler recordings of mitral flow were used to assess global, systolic and diastolic function. Diastolic dysfunction contributes to the aetiology of congestive heart failure, being present in approximately 40% of heart failure patients (van Kraaij *et al.*, 2002). LV relaxation is an energy-dependent process that requires dissociation of the bridges formed

between actin and myosin filaments during contraction. This can only occur when cystolic Ca^{2+} is actively removed by sarcoplasmic reticulum calcium transporting ATPase. A mechanism in which function is impaired due to compromised supply of energy substrates in the failing heart (Frank *et al.*, 2002), leading to diastolic dysfunction (Aroesty *et al.*, 1985).

5.2 Methods

All the experiments were performed on rats in accordance with the European Commission Directive 2010/63/EU (European Convention for the Protection of Vertebrate Animals used for Experimental and Other Scientific Purposes) and the UK Home Office (Scientific Procedures) Act (1986) with project approval from the UCL Animal Care and Use Committee.

5.2.1 Genetic targeting of the DVMN vagal preganglionic neurones

Young male Sprague-Dawley rats (100-150 g, n=68) were anaesthetised with ketamine (60 mg kg^{-1}; i.m.) and medetomidine (250 μg kg^{-1}; i.m.). Adequate depth of surgical anaesthesia was confirmed by the absence of a withdrawal response to a paw pinch. With the head fixed prone in a stereotaxic frame, lidocaine (2% solution) was injected subcutaneously for pre-operative analgesia before a midline dorsal neck incision was made to expose the atlanto-occipital membrane and then the dorsal surface of the brainstem. The DVMN was targeted bilaterally with one microinjection per side (0.25 μL at a rate of 0.05 μL min^{-1}) of a solution containing viral particles of PRSx8-ChIEF-tdTomato-LVV or PRSx8-eGFP-LVV. Taking the *calamus scriptorius* as the reference point, the injections were made at 0.5 mm rostral, 0.6 mm lateral, 0.8 mm ventral. Only caudal populations of DVMN neurones were targeted as they have been shown to exert the most significant impact on LV function (Chapter 2 and 3) and their optogenetic stimulation was found to increase LV inotropy and improve exercise capacity (Chapter 4). Anaesthesia was reversed with atipemazole (1 mg kg^{-1}; i.m.). For post-operative analgesia, rats were administered with buprenorphine (0.05 mg kg^{-1} d^{-1}; s.c.) for three days and caprofen (4 mg kg^{-1} d^{-1}; i.p.) for five days. The established titres at the time of production were within the range of 1 x 10^{9} and 1 x 10^{10} transducing units ml^{-1}.

5.2.2 Optrode implantations

Two weeks after microinjections of viral vectors into the DVMN (Figure 5-2), the animals were anaesthetised with ketamine (60 mg kg^{-1}; i.m.) and medetomidine (250 μg kg^{-1}; i.m.), and a conically tipped optrode (Art Photonics) was stereotaxically implanted under the occipital bone to reach the dorsal aspect of the

cisterna magna. Two small screws were placed in the skull, and the implant was secured in place with dental acrylic. Anaesthesia was reversed with atipemazole (1 mg kg^{-1}; i.m.) and the animals were allowed to recover for the next seven days.

5.2.3 Myocardial infarction

Myocardial infarctions were performed with the help of Dr. Svetlana Mastitskaya. Myocardial infarction (MI) leading to LV remodelling and dysfunction was induced using a left anterior descending (LAD) artery occlusion technique described in detail in the scientific literature (Pfeffer *et al.*, 1979). One week following optrode implantations (Figure 5-2), the rats were anaesthetised with ketamine (60 mg kg^{-1}; i.m.) and medetomidine (250 µg kg^{-1}; i.m.). For efficient intubation and in order to minimise trauma to tracheal soft tissue, the rats were pre-treated with atropine methyl nitrate (2 mg^{-1} kg^{-1}; i.p.; 15 minutes before anaesthesia induction) to reduce bronchial secretions and spasms (Wu *et al.*, 1992). In addition, lidocaine (2% solution) was applied to the throat using a cotton bud applicator immediately prior to endotracheal intubation on a custom designed vertical stand (Vet-Tech, UK).

The animals were mechanically ventilated with oxygen-enriched air (tidal volume 0.8 ml/100 g of body weight, 60-80 breaths min^{-1}). A left thoracotomy was performed through the fourth intercostal space to expose the heart, the pericardium was opened and the heart was exteriorised. The LAD coronary artery was ligated below the left atrial appendage using a 4-0 merisilk suture. Successful LAD occlusion was confirmed by pallor of the anterior wall of the LV. Sham surgery involved the same sequence of procedures including exposure of the heart and placement of suture around the LAD artery without occlusion. The heart was then returned to the chest cavity, the incision was closed, and the endotracheal tube was removed. Anaesthesia was reversed with atipemazole (1 mg kg^{-1}; i.m.) and rats were kept for two hours in a recovery chamber set at 30 °C supplied with 1:1 O_2/air mixture. For post-operative analgesia, rats were administered with buprenorphine (0.05 mg kg^{-1} d^{-1}; s.c.) for five days. To prevent infections, the rats were also treated with enrofloxacin one day prior to and three days after the surgery (0.05 mg kg^{-1} d^{-1}; s.c.). Postoperative mortality within the first 48 hours post-MI was 23%. None of the

animals that survived beyond 48 hours died during the remaining study period (six weeks post-MI or sham surgery).

After 48 hours, the distribution of animals between experimental groups were as follows: (1) post-MI/ChiEF-tdTomato (n=19) – animals with permanent LAD occlusion expressing ChiEF-tdTomato in the DVMN; (2) post-MI/eGFP (n=13) – rats with permanent LAD occlusion expressing eGFP in the DVMN; (3) sham-MI/ChiEF-tdTomato (n=10) – sham-operated animals expressing ChiEF-tdTomato in the DVMN; and (4) sham-MI/eGFP (n=8) – sham-operated rats expressing eGFP in the DVMN.

5.2.4 Optogenetic Stimulation

The dorsal brainstem of rats expressing ChiEF-tdTomato or eGFP by the DVMN neurones was illuminated (via a pre-implanted optrode) with blue light (445 nm, 10 ms pulses, 15 Hz) for 15 minutes every 48 hours for four weeks commencing two days after LAD occlusion or sham surgery (Figure 5-2). Light stimulation was performed under mild sedation (1% isoflurane).

5.2.5 Assessment of heart failure phenotype 1: Evaluation of exercise capacity

The exercise capacity of post-MI and sham-MI rats was assessed using a single lane treadmill (Panlab Harvard Apparatus, Cambridge, UK) with an electrical shock grid set at a minimum threshold of 0.1 mA, as described in detail above (Chapter 4). The body weight of each animal was recorded and the rat was placed on a treadmill. To determine exercise capacity, the treadmill speed was raised from the initial 20 cm s^{-1} in increments of 5 cm s^{-1} every 5 min until the animal's hind limbs made contact with the grid four times within a two minute period - the humanely defined point of exhaustion. The distance covered by the animal was recorded and exercise capacity was expressed in joules (J or kg m^2 s^{-2}).

5.2.6 Assessment of heart failure phenotype 2: Ultrasound evaluation of systolic and global function

LV function was assessed using a Vevo® 2100 high-resolution ultrasound system with an MS250 13-24MHz linear array transducer (VisualSonics, Amsterdam, The Netherlands). The rats were kept under isoflurane anaesthesia (2% isoflurane), and baseline ejection fraction and HR (lead II ECG) were first determined. Ejection fraction was determined using B-mode acquisition of a parasternal long-axis view of the LV (in plane so as to dissect across the aorta, (Figure 4-1; Page 84) in order to measure the length of the LV at systole and diastole. Three short axis slice images were also acquired along the length of the ventricle to segment the endocardial border (Figure 4-1; Page 84). Applying Simpson's rule to approximate ventricular volume, ejection fraction was determined as the percentage of blood at diastole ejected at systole (Schiller *et al.*, 1989).

Global LV function was also assessed using the LV myocardial performance index (LV MPI) (Tei *et al.*, 1995). Using Doppler echocardiographic recordings of blood flow velocity across the mitral valve from the apical four-chamber view (Figure 5-1), LV MPI was calculated from the sum of isovolumetric contraction time (IVCT) and the isovolumetric relaxation time (IVRT) divided by the LV ejection time (LV ET):

$$\text{LV MPI} = \frac{\text{IVCT} + \text{IVRT}}{\text{LV ET}}$$

5.2.7 Assessment of heart failure phenotype 3: Ultrasound evaluation of diastolic function

There are two identified filling phases during diastole of the LV. Active relaxation of the LV myocardium and visco-elastic properties of the myocardium (i.e. wall compliance) contribute to early filling (E). The second phase of LV filling (A) is due to atrial contraction. Under normal conditions the transmitral E/A ratio in a healthy heart is >1, i.e. E>A (Galderisi, 2005). Slowing of normal ventricular relaxation contributes to mild forms of diastolic dysfunction (van Kraaij *et al.*, 2002). Less blood entering the ventricle during early filling phase would require a more forceful atrial contraction to compensate. Transmitral E/A ratio of less than 1 (i.e.

E<A) would indicate diastolic dysfunction (van Kraaij *et al.*, 2002). The early wave deceleration time (DT) would also be prolonged as a result, as would the IVRT (Galderisi, 2005). More severe diastolic dysfunction is characterised by restrictive filling pattern and manifested by short, high velocity early phase of filling and reduced atrial filling. Higher filling pressures produce a steep pressure gradient across the mitral valve resulting in its premature opening and allowing for higher early filling velocity (Mandinov *et al.*, 2000). Due to reduced wall compliance as a result of increased collagen content (Zile & Brutsaert, 2002; Zile, 2003), the pressure within the LV rapidly rises equalling that of the atrium. This prevents further filling and produces a short early filling phase (Mandinov *et al.*, 2000). This results in an extreme transmitral E/A ratio of >2 and shortening of both DT and IVRT (van Kraaij *et al.*, 2002).

Doppler echocardiographic recordings of blood flow velocity across the mitral valve were used to determine (Figure 5-1):

- E/A Ratio: The ratio of the early and late phases of diastolic filling (Galderisi, 2005).
- DT: The deceleration time (in ms) of the early phase of filling (Cerisano *et al.*, 1999).
- Deceleration slope: The rate of change in blood velocity (cm s^{-2}) during the early phase of filling. Considered to be a better index of diastolic function compared to the one-dimensional measurement of deceleration time (Mishra *et al.*, 2007).

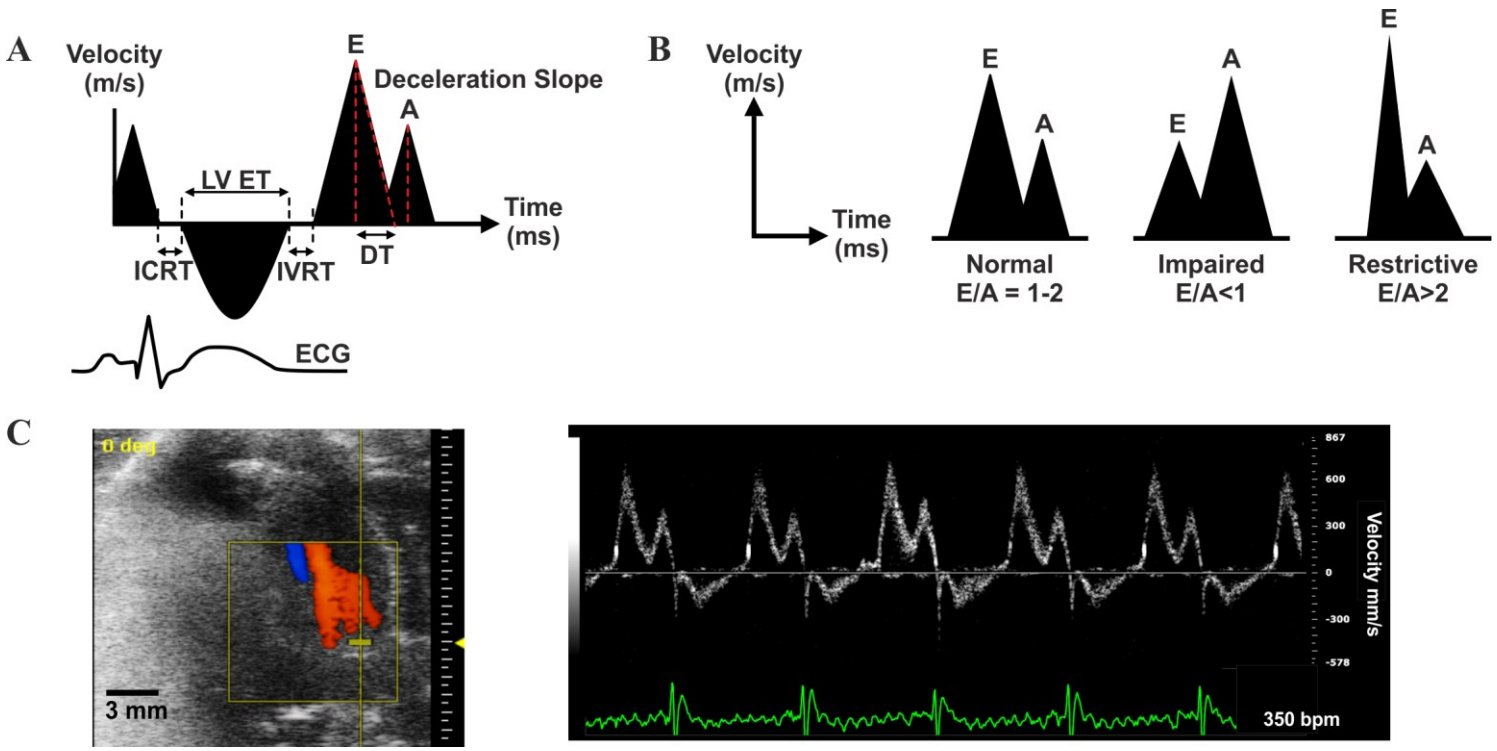

Figure 5-1: Doppler echocardiographic measurements

A) Scheme showing trans-mitral Doppler measurements. **A,** Atrial Filling; **DT**, Deceleration time; **E,** Early Filling; **ICRT,** Isovolumetric contraction time; **IVRT,** Isovolumetric relaxation time; **LV ET,** Left ventricle ejection time; **B)** Scheme of the showing early (E) and atrial (A) filling in normal, impaired diastolic dysfunction and extreme dysfunction restrictive filing patterns. **C) Left**, Coloured Doppler image showing an apical 4 chamber view; **Right**, Ultrasound Doppler showing transmural flow recording.

5.2.8 Assessment of heart failure phenotype 4: Haemodynamic evaluation

Doppler echocardiography does not provide a direct measure of LV pressure changes (Tschope & Paulus, 2009) and degree of LV remodelling cannot be reliably assessed using this method. Therefore, six weeks post MI or sham surgery (Figure 5-2), all animals underwent haemodynamic assessment under urethane (1.3 g kg^{-1}, i.p.) anaesthesia. Adequate anaesthesia was ensured by maintaining stable levels of arterial blood pressure and HR and monitored by the absence of a withdrawal response to a paw pinch. Body temperature was maintained with a servo-controlled heating pad at 37.0±0.5 °C. Partial pressures of O_2 and CO_2 as well as pH of the arterial blood were taken and recorded (RAPIDLab 348EX, Siemens, UK). The femoral artery was cannulated for measurement of ABP. To evaluate LV contractile function, a 2F Millar pressure catheter (SPR-320NR, Millar instruments, USA) was advanced via the right carotid artery and positioned within the chamber of the LV to monitor changes in LVP. After the preparative surgery the animal was left to stabilise for 30 min. LVP, ABP, and standard lead II ECG were then recorded for 15 minutes using a Power1401 interface and *Spike2* software (Cambridge Electronic Design). Average waveforms were used to determine LVESP and LVEDP. LVd*P*/dt was derived from the LVP recording using the slope function. From ABP measurements, average wave forms were used to determine MAP and pulse pressure (PP).

5.2.9 Assessment of heart failure phenotype 5: Ex vivo evaluation of LV pressure-volume relations

Six weeks following LAD occlusion (Figure 5-2), *ex vivo* LV pressure-volume curves were obtained using a method described in Fletcher *et al.* (1981). At the end of the hemodynamic studies, the heart was arrested by KCl, excised and a double-lumen catheter (PE-50 inside PE-200) was inserted into the LV via the ascending aorta. The right ventricle was incised (and weighed), atrioventricular groove was ligated, and isotonic saline was infused into the LV at a rate of 0.7 ml min^{-1} via one lumen, while intraventricular pressure was recorded through the other lumen from 0 to 30 mmHg. At least three measurements of pressure-volume relationships were obtained. The atria were then excised, the weight of LV recorded

and infarct size was measured. The stiffness, constant k, was calculated by fitting one exponential function (Fletcher *et al.*, 1981) of the form using pressure (P) and volume (v) and the additional constant (b):

$$P = be^{kv}$$

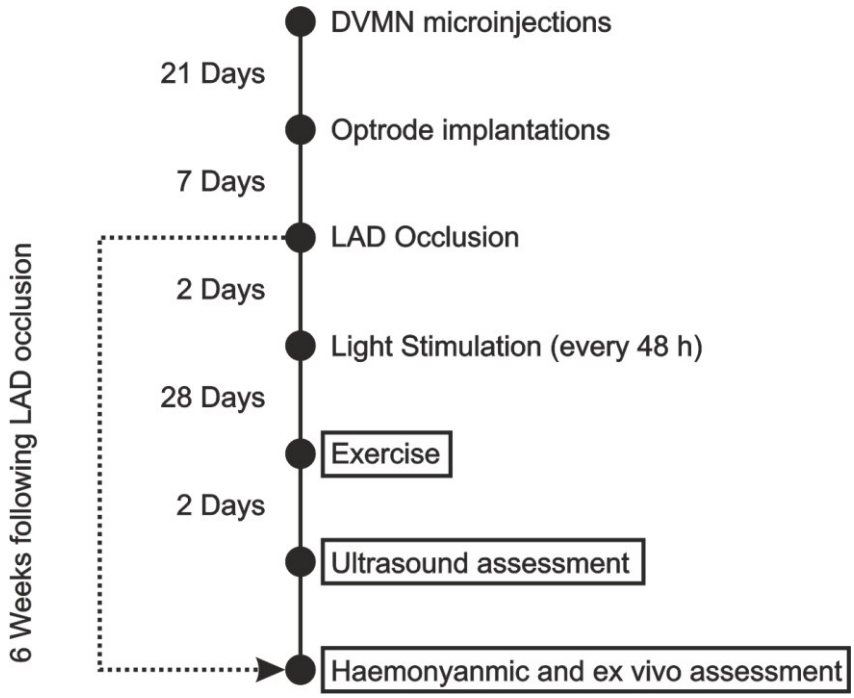

Figure 5-2: Timeline for experiments investing effects of enhanced DVMN activity following myocardial infarction

Timeline illustrating the interval duration between stages of animal preparation and acquisition of data for rats expressing ChIEF-tdTomato or eGFP.

5.2.10 Assessment of heart failure phenotype 6: lung water content, body and ventricles weights

As an additional measurement to assess the degree of LV dysfunction, the lungs were excised and water content was determined to establish the presence of pulmonary oedema (Mullertz *et al.*, 2011). Lungs were weighed immediately after extraction and again after 72 hours of drying at a temperature of 40±1 °C to establish the lung fluid content. Weights of left and right ventricles were expressed as a ratio to body weight (mg kg^{-1}).

5.2.11 Infarct size calculation

After fixation, the extent of MI was determined as described in detail previously (Pfeffer *et al.*, 1979; Fletcher *et al.*, 1981). The LV was cut from the apex to the base into transverse slices of identical thickness (1.5 mm). In each slice, the length of the scar and non-infarcted muscle for endocardial and epicardial surfaces were determined by computerised planimetry. Infarct size (in %) was calculated as an average of infarcted endo- and epicardial surfaces. This method of calculating the infarct size was compared to the infarct estimation using three ultrasound-acquired short axis B-mode images of the LV. The average angle created by the arcs of infarcted circumference out of 360° (Figure 5-11) was used to estimate infarct size (%).

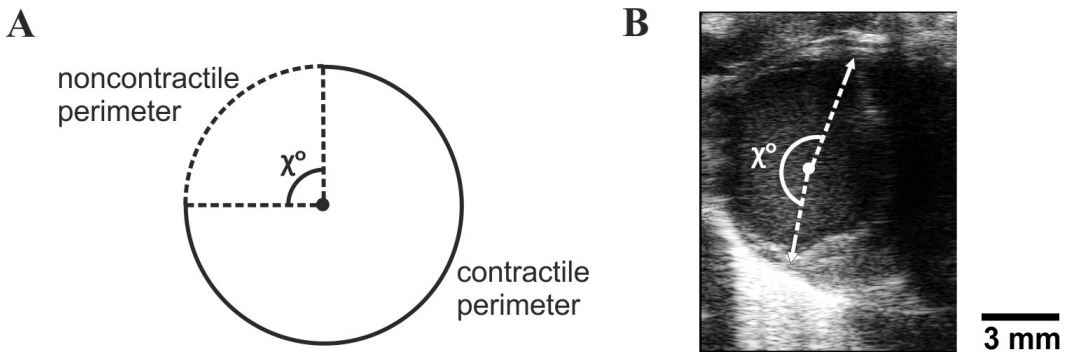

Figure 5-3: Ultrasound estimation of infarct size

A) Scheme of a short axis view of the LV. From the three acquired slices, the average angle created by the arcs of infarcted circumference out of 360° were used to estimate infarct size (%); **B)** Example of angular measurement on a B-mode slice.

5.2.12 Data Analysis

Differences between the experimental groups were assessed for statistical significance using GraphPad Prism 6 software. Comparisons were made using a one-way ANOVA (followed by Sidak's p value correction for multiple comparisons) or Student's t-test, as appropriate. To compare how accurate ultrasound measurements could estimate the actual infarct size, a correlation analysis was conducted to compute the value of Pearson's correlation coefficient. The results are reported as individual values and means ± s.e.m. Differences with $p<0.05$ were considered to be significant.

5.3 Results

5.3.1 Infarct size calculation and comparison

Infarct sizes ranged between 17% and 40% (n=19) in post-MI/ChiEF-tdTomato group and between 19% and 43% (n=13) in post-MI/eGFP group when assessed using computerised planimetry. No infarcts were noted in sham-operated animals.

A significant correlation was found between infract size values obtained using ultrasound and computerised planimetry (Figure 5-4C; r=0.54; p=0.001). A linear regression analysis has demonstrated that the ultrasound method used overestimated the actual infarct size by approximately 10%, producing the following equation where x is the percentage of non-contractile perimeter measured using ultrasound and y is the planimetry-derived infarct size:

$$y = 0.8968\,x + 0$$

The data obtained in animals with infarct sizes >30% were taken for subsequent analysis (Zhang *et al.*, 2001). Nine animals with infarct sizes of 30-40% formed post-MI/eGFP group (average infarct size 36±1%), and twelve rats with infarct sizes of 30-40% formed post-MI/ChiEF-tdTomato group (average infract size 33±1%). There were no differences in infarct sizes between these two experimental groups of animals (p=0.1; t-test; Figure 5-4B).

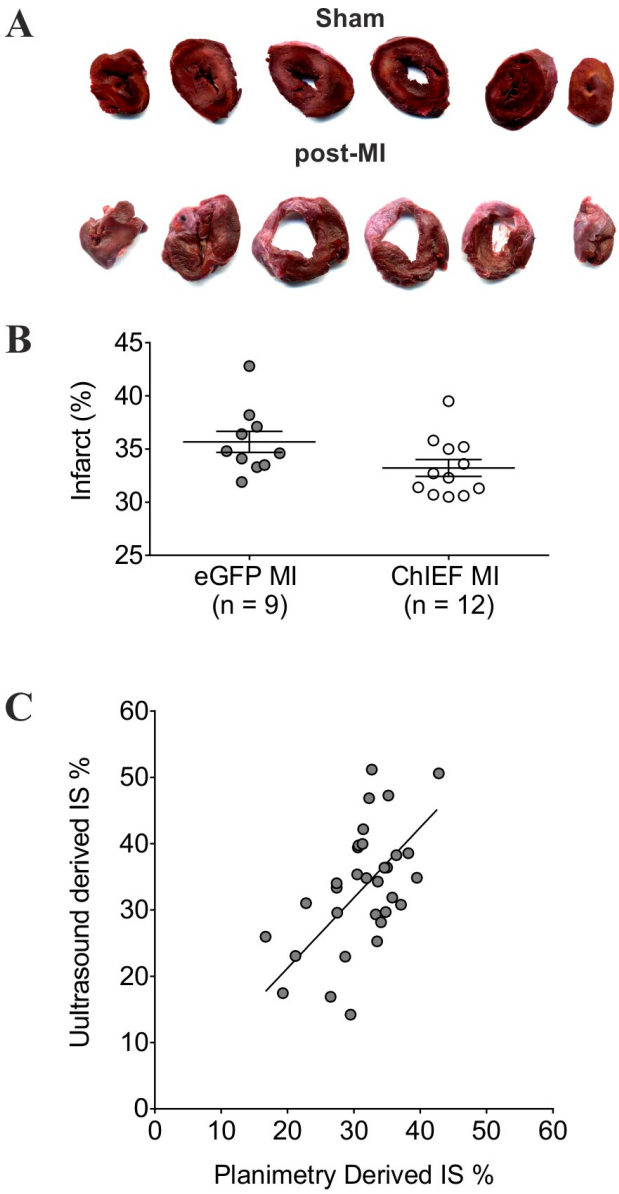

Figure 5-4: Assessment of infarct size

A) Images illustrate representative sections of the LV from a sham-operated animal and an animal six weeks after LAD occlusion. Computerised planimetry was used to calculate infarct size as described in detail in the Methods; **B**) Summary data illustrating infarct sizes determined using computerised planimetry of LV sections of rats transduced to express eGFP or ChiEF-tdTomato by the DVMN neurones six weeks after LAD occlusion; **C)** Correlation between infract size (IS) values obtained using analysis of three short axis B-mode images acquired using ultrasound and computerised planimetry.

5.3.2 Assessment of heart failure phenotype 1: evaluation of exercise capacity

Strong expression of ChIEF-tdTomato by the DVMN neurones in the caudal aspect of the left and right nuclei was observed six weeks after microinjections of the virus (Figure 5-5). Exercise capacity was reduced six weeks post-MI in rats expressing eGFP in the DVMN when compared to sham-operated animals (28±3 vs 56±8 J; p=0.04; ANOVA; Figure 5-6). Optogenetic stimulation of the DVMN neurones expressing ChIEF-tdTomato enhanced exercise capacity in sham-operated animals (105±11 vs 56±8 J in sham-operated rats expressing eGFP; p=0.001; ANOVA; Figure 5-6) and improved exercise capacity in post-MI animals (56±4 vs 28±3 J in post-MI rats expressing eGFP; p=0.02; ANOVA; Figure 5-6). Thus, in rats, optogenetic recruitment of the DVMN activity for 15 minutes every 48 hours for four weeks after LAD occlusion restores exercise capacity to the level of sham-operated animals.

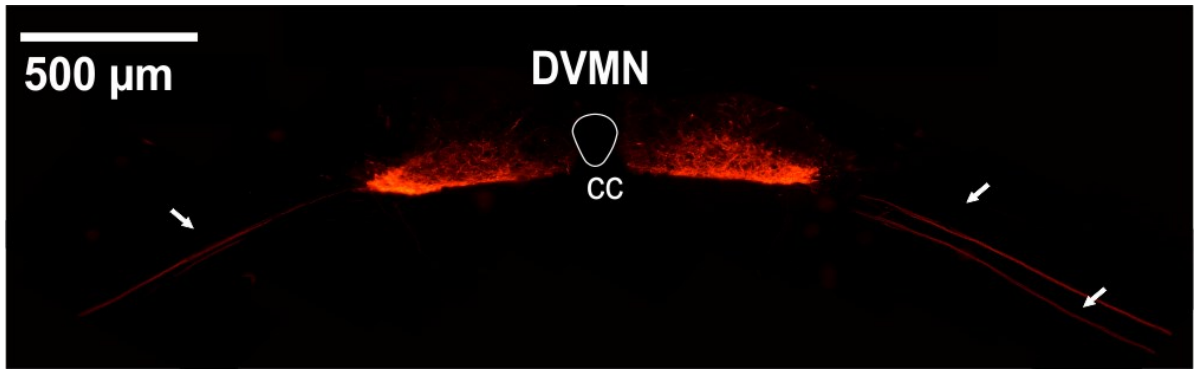

Figure 5-5: Targeting DVMN neurones to express ChIEF-tdTomato

Confocal image of a coronal section of the rat brainstem targeted to express ChIEF-tdTomato by the DVMN neurones. Ventrally projecting axons (arrow) of the DVMN neurones transduced to express ChIEF-tdTomato. CC, central canal.

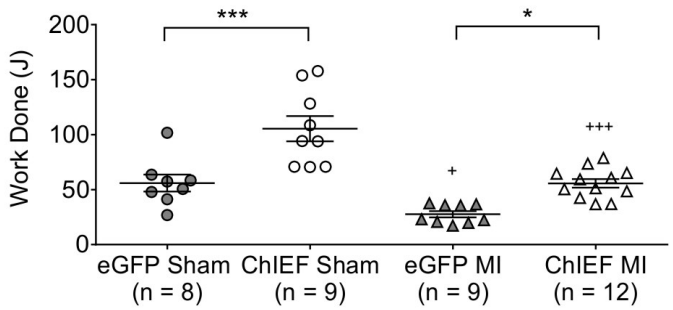

Figure 5-6: The effect of enhanced DVMN activity on exercise capacity of rats six weeks after LAD occlusion or sham-surgery

Summary data illustrating exercise capacity of rats transduced to express ChIEF-tdTomato (ChIEF) or eGFP by the DVMN neurones after four weeks of light (445 nm, 10 ms pulses, 15 Hz) delivery to the dorsal brainstem for 15 minutes every 48 hours commencing two days after LAD occlusion (MI) or sham surgery. *Asterisk* denotes significant effect of optogenetic DVMN stimulation. *Plus* denotes significant effect of LAD occlusion. *P<0.05; ***P<0.001; $^{+}$P<0.01; $^{+++}$P<0.001.

5.3.3 Assessment of heart failure phenotype 2: Ultrasound evaluation of systolic and global function

LV ejection fraction was reduced six weeks post-MI in rats expressing eGFP in the DVMN when compared to sham-operated animals (33±3 vs 50±5%; p=0.01; ANOVA Figure 5-7A**)**. Optogenetic stimulation of the DVMN neurones expressing ChIEF-tdTomato increased ejection fraction both in sham-operated animals (76±2 vs 50±5% in sham-operated rats expressing eGFP; p<0.0001; ANOVA; Figure 5-7A) and in post-MI rats (49±3 vs 33±3% in post-MI rats expressing eGFP; p=0.005; ANOVA; Figure 5-7A).

Isovolumetric contraction time (IVCT) was found to be prolonged six weeks post-MI in rats expressing eGFP in the DVMN when compared to sham-operated animals (24±1 vs 15±1 ms; p<0.0001; ANOVA; Figure 5-7B). Optogenetic stimulation of the DVMN neurones expressing ChIEF-tdTomato shortened IVCT both in sham-operated animals (13±1 vs 15±1 ms in rats expressing eGFP; p=0.04; ANOVA; Figure 5-7B) and in post-MI rats (15±1 vs 24±1 ms in post-MI rats expressing eGFP; p<0.0001; ANOVA; Figure 5-7B).

LV myocardial performance index (LV MPI) (an established method for assessing global myocardial function through the ratio of isovolumetric times to left ventricular ejection time) (Tei *et al.*, 1995) was increased post-MI in rats expressing eGFP (0.74±0.03 vs 0.53±0.03 in sham-operated rats; p<0.0001; ANOVA; Figure 5-7C**)**. Optogenetic stimulation of the DVMN resulted in a significant lowering of LV MPI both in sham-operated animals (0.41±0.02 vs 0.53±0.03 in rats expressing eGFP; p=0.006; ANOVA; Figure 5-7C) and in rats post-MI (0.57±0.02 vs 0.74±0.03 in post-MI rats expressing eGFP; p<0.0001; ANOVA; Figure 5-7C).

Under isoflurane anaesthesia, HR was similar in all four experimental groups (p=0.4; ANOVA; Figure 5-7D). These data suggest that in rats, optogenetic recruitment of the DVMN activity for 15 minutes every 48 hours for four weeks after LAD occlusion is sufficient to maintain a normal ejection fraction, reduce IVCT and improve LV-MPI to the levels of sham-operated animals. Significant improvement

of LV function as a result of DVMN recruitment was also observed in sham-operated animals.

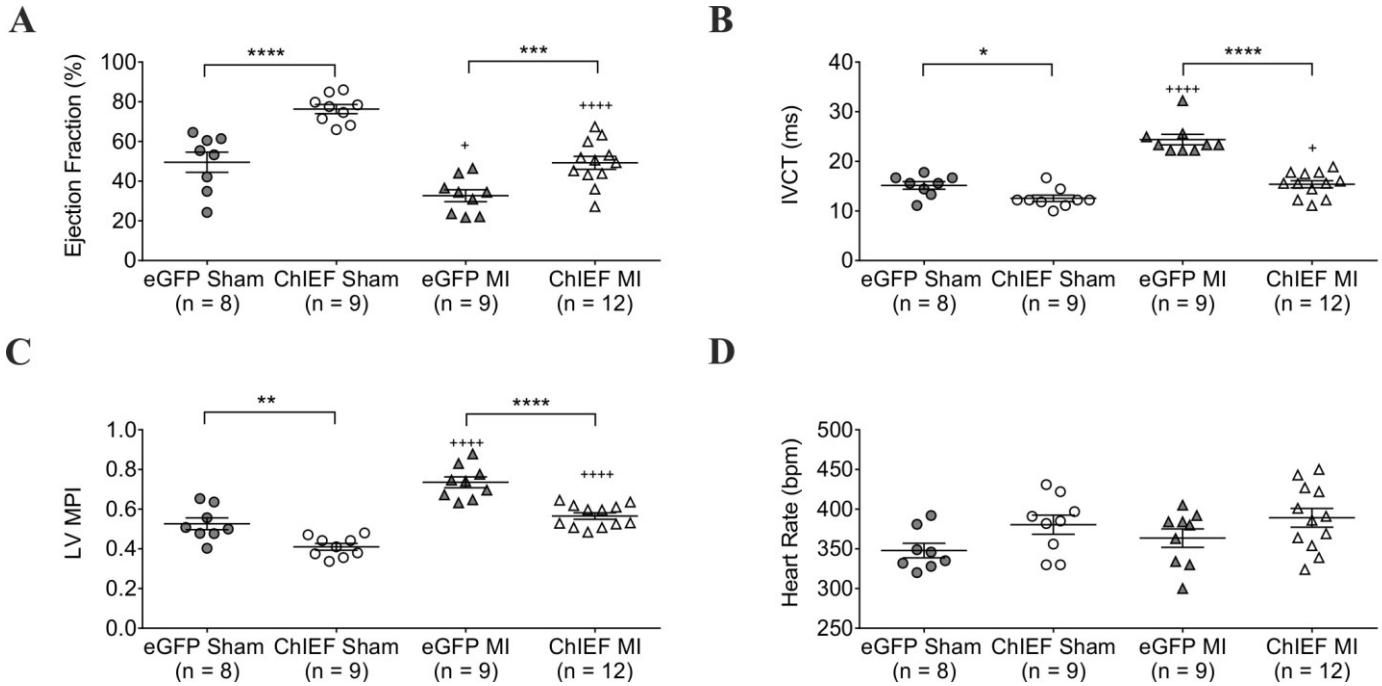

Figure 5-7: The effect of enhanced DVMN activity on indices of LV systolic and global function in rats six weeks after LAD occlusion or sham-surgery (isoflurane anaesthesia)

Summary data illustrating **A)** LV ejection fraction; **B**) IVCT; **C**) LV-MPI; and **D**) HR of rats transduced to express ChIEF-tdTomato (ChIEF) or eGFP by the DVMN neurones after four weeks of light (445 nm, 10 ms pulses, 15 Hz) delivery to the dorsal brainstem for 15 minutes every 48 hours, commencing two days after LAD occlusion (MI) or sham surgery. *Asterisk* denotes significant effect of optogenetic DVMN stimulation. *Plus* denotes significant effect of LAD occlusion. *P<0.05; **P<0.01; ***P<0.001; ****P<0.0001; $^{+}$P<0.01; $^{++++}$P<0.0001.

5.3.4 Assessment of heart failure phenotype 3: ultrasound evaluation of diastolic function

LV diastolic function was assessed using pulsed wave Doppler of transmitral flow velocities in the apical four-chamber view (Figure 5-1C). Six weeks post-MI the E/A ratio was reduced both in rats expressing eGFP (0.88±0.09 vs 1.21±0.12 in sham-operated rats; p=0.04; ANOVA; Figure 5-8A) and ChIEF-tdTomato (1.20±0.10 vs 1.57±0.09 in sham-operated rats; p=0.02; ANOVA; Figure 5-8A) indicative of an "impaired" filling (van Kraaij *et al.*, 2002). Optogenetic stimulation of the DVMN (rats expressing ChIEF-tdTomato in the DVMN) increased E/A ratio both in sham-operated animals (1.57±0.09 vs 1.21±0.12 in rats expressing eGFP in the DVMN; p=0.03; ANOVA; Figure 5-8A) and in rats post-MI (1.20±0.10 vs 0.88±0.09 in rats expressing eGFP in the DVMN; p=0.03; ANOVA; Figure 5-8A).

DT was similar six weeks post-MI in rats expressing eGFP in the DVMN when compared to sham-operated animals (24±3 vs 27±3 ms in sham-operated rats; p=0.1; ANOVA; Figure 5-8B**).** Optogenetic stimulation of the DVMN neurones expressing ChiEF-tdTomato increased DT in sham-operated animals only (28±3 vs 36±3 in sham operated rats; p=0.03; ANOVA; Figure 5-8B).

The deceleration slope was steeper six weeks post-MI in rats expressing eGFP in the DVMN when compared to sham-operated animals (-3581±352 vs -2473±286 mm s^{-2} in sham-operated rats; p=0.02; ANOVA; Figure 5-8A). Optogenetic stimulation of the DVMN neurones expressing ChIEF-tdTomato did not affect the deceleration slope in sham-operated animals (-1885±102 vs -2473±286 mm s^{-2} in rats expressing eGFP; p=0.3; ANOVA; Figure 5-8C), but broadened the slope in rats post-MI (-2690±256 vs -3581±352 mm s^{-2} in rats expressing eGFP; p=0.04; ANOVA; Figure 5-8C).

IVRT was similar six weeks post-MI in rats expressing eGFP in the DVMN when compared to sham-operated animals (21±2 vs 21±2 in sham-operated rats; p>0.9; ANOVA; Figure 5-8D). Optogenetic stimulation of the DVMN neurones expressing ChIEF-tdTomato reduced IVRT in sham-operated animals only (15±2 vs 21±2 in rats expressing eGFP; p=0.03; ANOVA; Figure 5-8D), with no effect on rats

post-MI (23±2 vs 21±2 in rats expressing eGFP; p=0.8; ANOVA; Figure 5-8D). These data suggest that in rats, optogenetic recruitment of the DVMN activity for 15 minutes every 48 hours for four weeks after LAD occlusion is sufficient to maintain normal diastolic function of the LV.

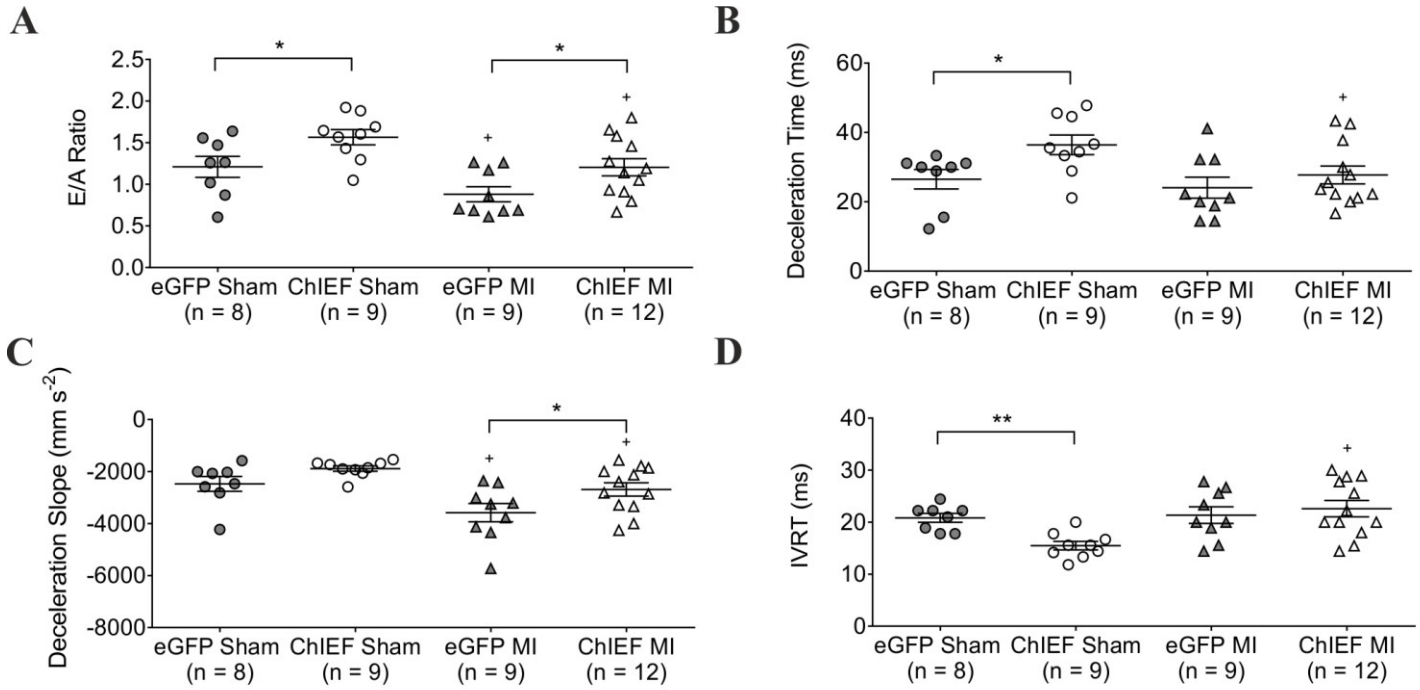

Figure 5-8: The effect of enhanced DVMN activity on indices of left ventricular diastolic function in rats six weeks after LAD occlusion or sham-surgery (isoflurane anaesthesia)

Summary data illustrating **A)** ratio of early (E) and atrial (A) filling velocities during diastole; **B**) the early wave deceleration time; **C**) the early wave deceleration slope; and **D**) the isovolumetric relaxation time (IVRT) of rats transduced to express ChIEF-tdTomato (ChIEF) or eGFP by the DVMN neurones after four weeks of light (445 nm, 10 ms pulses, 15 Hz) delivery to the dorsal brainstem for 15 minutes every 48 hours, commencing two days after LAD occlusion (MI) or sham surgery. *Asterisk* denotes significant effect of optogenetic DVMN stimulation. *Plus* denotes significant effect of LAD occlusion. *P<0.05; **P<0.01; $^{+}$P<0.01.

5.3.5 Assessment of heart failure phenotype 4: Haemodynamic evaluation

LV dP/dt$_{max}$ was reduced six weeks post-MI in rats expressing eGFP in the DVMN when compared to sham-operated animals (5690±444 vs 7472±381 mmHg s^{-1} in sham-operated rats; p=0.009; ANOVA; Figure 5-9A). Optogenetic stimulation of the DVMN neurones expressing ChIEF-tdTomato increased LV dP/dt$_{max}$ both in sham-operated animals (8980±411 vs 7472±381 mmHg s^{-1} in rats expressing eGFP; p=0.04; ANOVA; Figure 5-9A) and in rats post-MI (7673±332 vs 5690±444 mmHg s^{-1} in rats expressing eGFP; p=0.001; ANOVA; Figure 5-9A).

LVESP reduced six weeks post-MI in rats expressing eGFP in the DVMN when compared to sham-operated animals (106±3 vs 122±4 mmHg in sham-operated rats; p=0.04; ANOVA; Figure 5-9B). Optogenetic stimulation of the DVMN neurones expressing ChIEF-tdTomato increased LVESP both in sham-operated animals (138±4 vs 122±4 mmHg in rats expressing eGFP; p=0.04; ANOVA; Figure 5-9B) and in rats post-MI (122±4 vs 106±3 mmHg in rats expressing eGFP; p=0.02; ANOVA; Figure 5-9B).

LV dP/dt$_{min}$ was reduced six weeks post-MI in rats expressing eGFP in the DVMN when compared to sham-operated animals (-4348±275 vs -6136±269 mmHg s^{-1} in sham-operated rats; p=0.0004; ANOVA; Figure 5-9C). Optogenetic stimulation of the DVMN neurones expressing ChIEF-tdTomato did not affect LV dP/dt$_{min}$ in sham-operated animals (-6774±391 vs -6136±269 mmHg s^{-1} in rats expressing eGFP; p=0.5; ANOVA; Figure 5-9A), but was improved in rats post-MI (-5550±176 vs -4348±274 mmHg s^{-1} in rats expressing eGFP; p=0.003; ANOVA; Figure 5-9C).

LVEDP was increased six weeks post-MI in rats expressing eGFP in the DVMN when compared to sham-operated animals (7±1 vs 4±1 mmHg in sham-operated rats; p=0.004; ANOVA; Figure 5-9D). Optogenetic stimulation of the DVMN neurones expressing ChIEF-tdTomato had no effect on sham-operated animals (3±2 vs 4±1 mmHg in rats expressing eGFP; p=0.2; ANOVA; Figure 5-9D), but decreased LVEDP in rats post-MI (5±2 vs 7±1 mmHg in rats expressing eGFP; p=0.01; ANOVA; Figure 5-9D).

These data suggest that in rats, optogenetic recruitment of DVMN activity for 15 minutes every 48 hours for four weeks after LAD occlusion reduces LVEDP and maintains normal levels of LVdP/dt_{max}, LVESP and LVdP/dt_{min}.

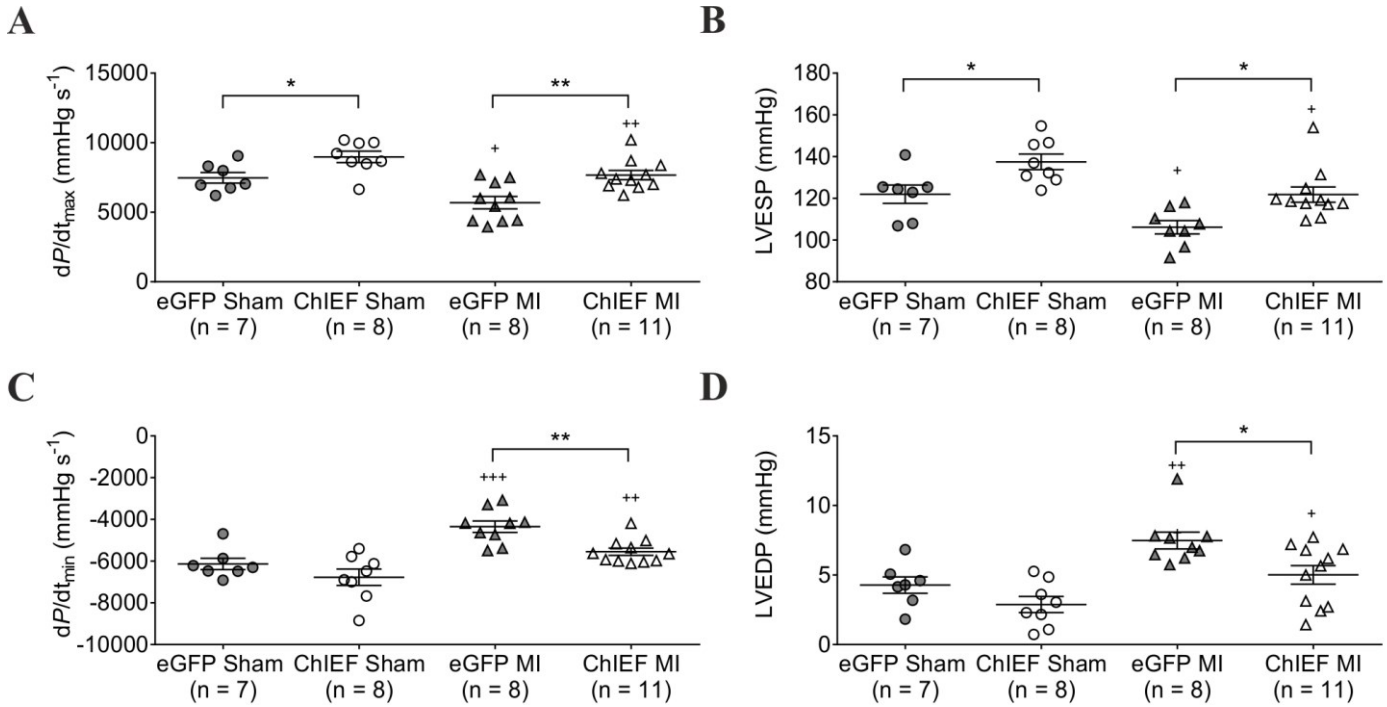

Figure 5-9: The effect of enhanced DVMN activity on indices of left ventricular systolic and diastolic function in rats six weeks after LAD occlusion or sham-surgery under urethane anaesthesia

Summary data illustrating values of the **A)** maximum first differential of left ventricular pressure (LVd*P*/dt_{max}); **B**) left ventricular end systolic pressure (LVESP); **C**) the minimum first differential of left ventricular pressure (LVdP/dt_{min}); and **D**) left ventricular end diastolic pressure (LVEDP) in rats transduced to express ChIEF-tdTomato (ChIEF) or eGFP by the DVMN neurones after four weeks of light (445 nm, 10 ms pulses, 15 Hz) delivery to the dorsal brainstem for 15 minutes every 48 hours, commencing two days after LAD occlusion (MI) or sham surgery. *Asterisk* denotes significant effect of optogenetic DVMN stimulation. *Plus* denotes significant effect of LAD occlusion. *P<0.05; **P<0.01; $^{+}$P<0.01; $^{++}$P<0.01; $^{+++}$P<0.01.

MAP was reduced six weeks post-MI in rats expressing eGFP in the DVMN when compared to sham-operated animals (66±3 vs 78±3 mmHg in sham-operated rats; p=0.04; ANOVA; Figure 5-10A). Optogenetic stimulation of the DVMN neurones expressing ChIEF-tdTomato had no effect on sham-operated animals (84±4 vs 78±3 mmHg in rats expressing eGFP; p=0.6; ANOVA; Figure 5-10A), but was higher in rats post-MI (78±3 vs 66±3 mmHg in rats expressing eGFP; p=0.03; ANOVA; Figure 5-10A).

PP was reduced six weeks post-MI in rats expressing eGFP in the DVMN when compared to sham-operated animals (36±4 vs 52±4 mmHg in sham-operated rats; p=0.04; ANOVA; Figure 5-10B). Optogenetic stimulation of the DVMN neurones expressing ChIEF-tdTomato had no effect on sham-operated animals (51±2 vs 52±4 mmHg in rats expressing eGFP; p>0.9; ANOVA; Figure 5-10B), but was higher in rats post-MI (51±5 vs 36±4 mmHg in rats expressing eGFP; p=0.03; ANOVA; Figure 5-10B).

HRs were not affected six weeks post-MI in rats expressing eGFP in the DVMN when compared to sham-operated animals (362±17 vs 371±15 bpm in sham-operated rats; p>0.9; ANOVA; Figure 5-10C). Optogenetic stimulation of the DVMN neurones expressing ChIEF-tdTomato did not affect HR in sham-operated animals (380±19 vs 371±15 bpm in rats expressing eGFP; p>0.9; ANOVA; Figure 5-10C) or post-MI rats (380±13 vs 362±17 bpm in rats expressing eGFP; p>0.9; ANOVA; Figure 5-10C). These data suggest that in rats, optogenetic recruitment of DVMN activity for 15 minutes every 48 hours for four weeks after LAD occlusion is sufficient to maintain normal MAP and normal PP.

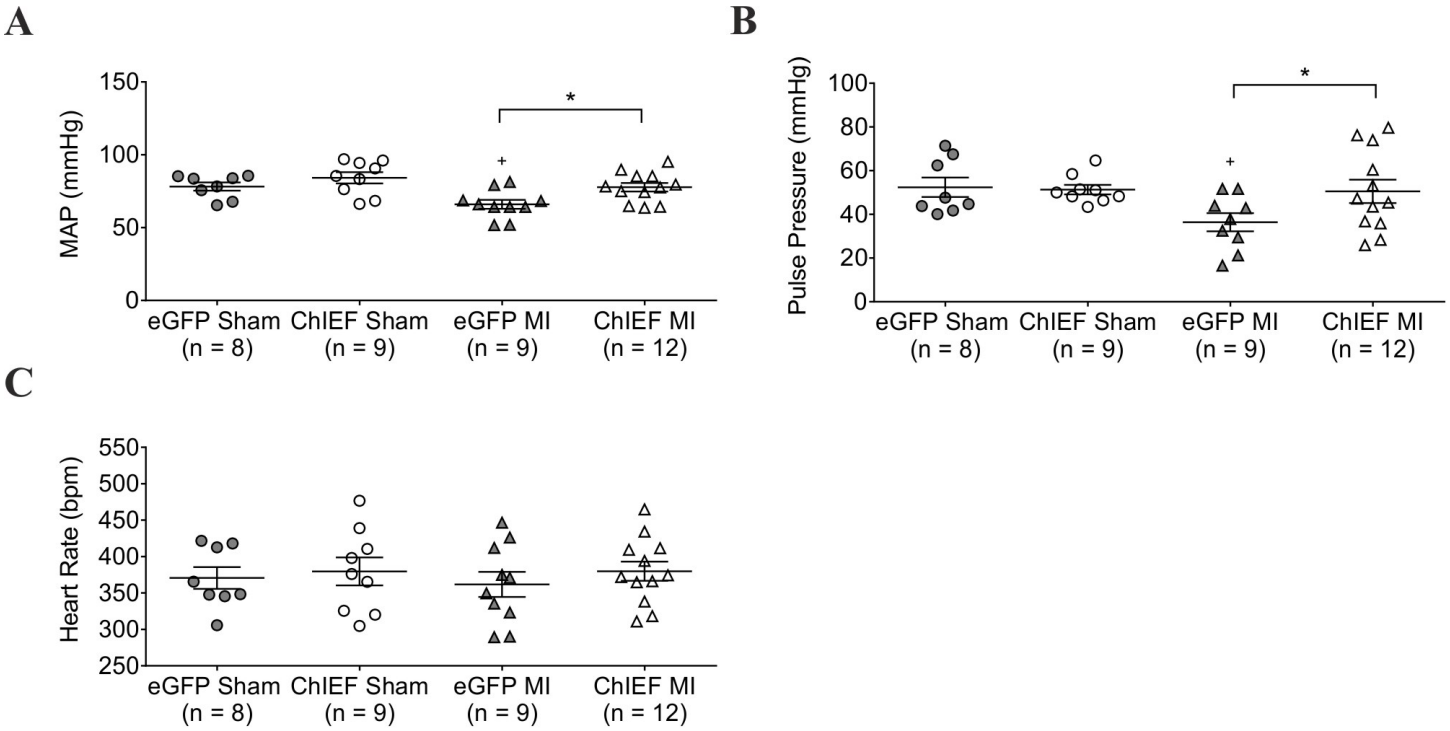

Figure 5-10: The effect of enhanced DVMN activity on systemic arterial blood pressure and heart rates in rats six weeks after LAD occlusion or sham-surgery (urethane anaesthesia)

Summary data illustrating values of mean arterial pressure (MAP, **A**), pulse pressure (**B**) and heart rate (**C**) in rats transduced to express ChIEF-tdTomato (ChIEF) or eGFP by the DVMN neurones after four weeks of light (445 nm, 10 ms pulses, 15 Hz) delivery to the dorsal brainstem for 15 minutes every 48 hours, commencing two days after LAD occlusion (MI) or sham surgery. *Asterisk* denotes significant effect of optogenetic DVMN stimulation. *Plus* denotes significant effect of LAD occlusion. *$P<0.05; $^{+}P<0.01$.

5.3.6 Assessment of heart failure phenotype 5: *ex vivo* evaluation of LV pressure-volume relations

The index of myocardial wall compliance, the stiffness (constant k) was not changed six weeks post-MI in rats expressing eGFP in the DVMN when compared to sham-operated animals (3.9±0.3 vs 3.4±0.1 in sham-operated rats; p=0.4; ANOVA; Figure 5-8D). Optogenetic stimulation of the DVMN neurones expressing ChIEF-tdTomato increased k in sham-operated animals (4.8±0.3 vs 3.8±0.3 in rats expressing eGFP; p=0.01; ANOVA; Figure 5-8D), but did not affect rats post-MI (3.2±0.1 vs 3.4±0.1 in rats expressing eGFP; p=0.9; ANOVA; Figure 5-8D).

These data suggest that in rat hearts excised six weeks following LAD occlusion, optogenetic recruitment of DVMN activity for 15 minutes every 48 hours for four weeks improves stiffness constants in sham-operated animals only.

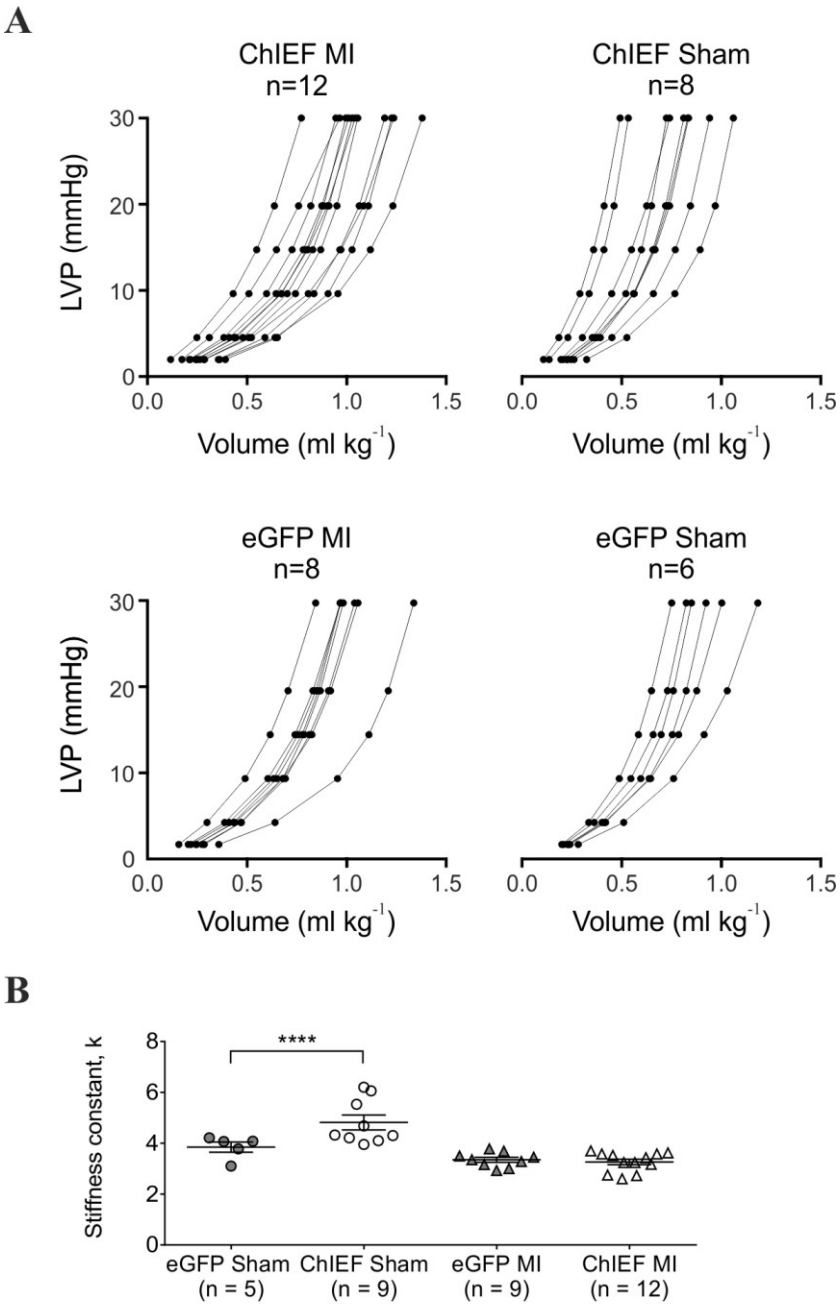

Figure 5-11: The effect of enhanced DVMN activity after six weeks in sham and post-MI operated rats on LV pressure-volume relations

A) Summary data illustrating the pressure volume relations of the left ventricle (LV) immediately after excision in rats transduced to express ChiEF-tdTomato and eGFP by the DVMN neurones after one month of light stimulation of the dorsal brainstem via a pre-implanted optrode (for 15 minutes every 48 hours for four weeks commencing two days after LAD occlusion or sham surgery); **B)** Summary data illustrating the pressure constant, k. *Asterisk* denotes significant effect of optogenetic DVMN stimulation. *Plus* denotes significant effect of optogenetic stimulation. ****P<0.0001; $^{+}$P<0.01.

5.3.7 Assessment of heart failure phenotype 6: lung water content, body and ventricles weights

Body weights were not affected six weeks post-MI in rats expressing eGFP in the DVMN when compared to sham-operated animals (453±18 vs 431±18 kg in sham-operated rats; p=0.9; ANOVA; Figure 5-12A**)**. Optogenetic stimulation of the DVMN neurones expressing ChIEF-tdTomato reduced body weights in rats post-MI only (391±5 vs 453±19 mg kg^{-1} in rats expressing eGFP; p=0.04; ANOVA; Figure 5-12A**)**. There were no differences in lung water content between all the experimental groups (p>0.9; ANOVA; Figure 5-12B).

LV to body mass ratios were not different six weeks post-MI in rats expressing eGFP in the DVMN when compared to sham-operated animals (2.19±0.08 vs 2.12±0.07 mg kg-1 in sham-operated rats; p=0.5; ANOVA; Figure 5-12C). Optogenetic stimulation of the DVMN neurones expressing ChIEF-tdTomato increased LV to body mass ratios in sham-operated animals (1.91±0.06 vs 2.12±0.07 mg kg-1 in rats expressing eGFP; p=0.04; ANOVA; Figure 5-12C), but did not in rats post-MI (2.24±0.05 vs 2.19±0.08 mg kg-1 in rats expressing eGFP; p=0.03; ANOVA; Figure 5-12C).

RV to body mass ratios were not different six weeks post-MI in rats expressing eGFP in the DVMN when compared to sham-operated animals (0.42±0.02 vs 0.38±0.01 mg kg-1 in sham-operated rats; p=0.4; ANOVA; Figure 5-12D). Optogenetic stimulation of the DVMN neurones expressing ChIEF-tdTomato had no effect on sham-operated animals (0.37±0.01 vs 0.38±0.01 mg kg-1 in rats expressing eGFP; p=0.7; ANOVA; Figure 5-12D), but increased RV to body mass ratio in rats post-MI (0.36±0.02 vs 0.42±0.02 mg kg-1 in rats expressing eGFP; p=0.03; ANOVA; Figure 5-12D).

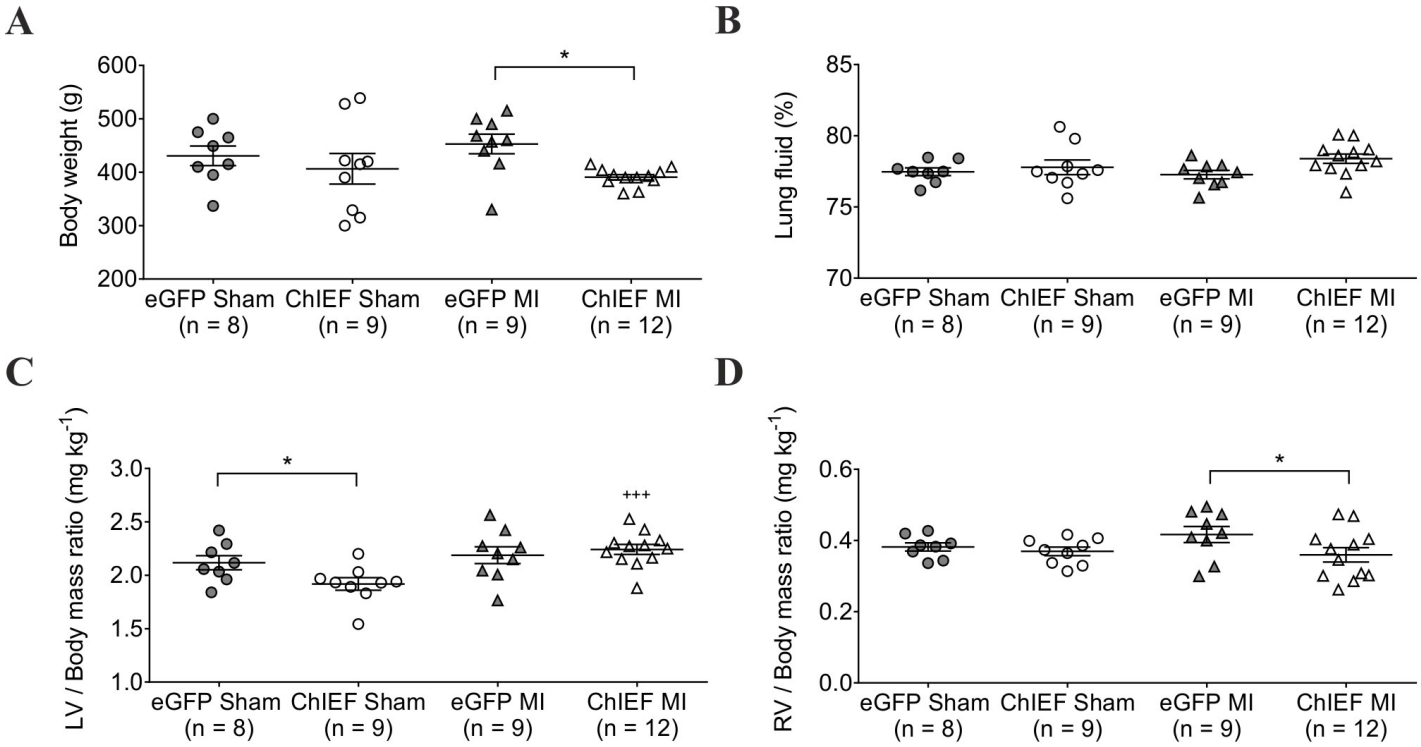

Figure 5-12: The effect of enhanced DVMN activity on body weight, lung fluid content, left and right ventricular weights in rats six weeks after LAD occlusion or sham-surgery

Summary data illustrating the **A)** body weights; **B)** lung fluid content (in %); **C)** LV to body weight ratio and **D)** RV to body weight ratio in rats transduced to express ChIEF-tdTomato (ChIEF) or eGFP by the DVMN neurones after four weeks of light (445 nm, 10 ms pulses, 15 Hz) delivery to the dorsal brainstem for 15 minutes every 48 hours, commencing two days after LAD occlusion (MI) or sham surgery. *Asterisk* denotes significant effect of optogenetic DVMN stimulation. *Plus* denotes significant effect of LAD occlusion. *P<0.05; $^{+++}$P<0.01.

5.4 Discussion

This study was designed to test the hypothesis that experimental (optogenetic) enhancement of DVMN activity would be sufficient to slow left ventricular dysfunction and remodelling developing after a MI. This study builds upon the results of the experiments presented in Chapters 2 and 3, suggesting that DVMN neurones provide functional innervation of the left cardiac ventricle and control its electrical and contractile properties. Results of the experiments described in Chapter 4 also demonstrated that the activity of this population of VPNs determines LV responsiveness to β-adrenoceptor stimulation and exercise capacity. Clear improvement in exercise capacity and LV contractility after four daily sessions (15 minutes each) of DVMN stimulations (Chapter 4) suggested that the same treatment delivered over a longer period of time may slow or even prevent LV dysfunction and heart failure development after permanent coronary artery occlusion.

To test this hypothesis an experiment was designed involving four groups of animals. Rats transduced to express either eGFP (control) or ChIEF-tdTomato (optogenetic construct) by the DVMN neurones underwent LAD occlusion or sham surgery. All animals were subjected to four weeks of light stimulation of the dorsal brainstem via a pre-implanted optrode for 15 minutes every 48 hours commencing two days after LAD occlusion or sham surgery. LV systolic and diastolic functions were then assessed using different methods, including high-resolution ultrasound. Only rats with infarct sizes of more than 30% were included in this study to allow comparisons between control (post-MI/eGFP) and experimental (post-MI/ChIEF-tdTomato) groups with similar infarcts. Permanent LAD occlusion with infarct sizes of 30-40% reduced exercise capacity and impaired LV function when assessed six weeks after the infarction (Figure 5-4A; Figure 5-6). Ventricular chamber to body weight ratios and lung fluid percentages were then used to assess hypertrophy (Lamas, 1993) and pulmonary oedema (Mullertz *et al.*, 2011).

It was found that optogenetic stimulation of DVMN over the course of four weeks following LAD occlusion maintained exercise capacity at the level exhibited by sham-operated animals expressing eGFP. Significant improvement in exercise

capacity was also noted in sham-operated rats as a result of optogenetic stimulation, an observation concordant with the data reported in Chapter 4.

Ultrasound assessment of cardiac performance and, more precisely, of LV systolic and diastolic function reflected these significant improvements in exercise capacity. Optogenetic stimulation of the DVMN increased ejection fraction of the infarcted myocardium by approximately 20%. A 20% improvement is highly significant given that the average baseline ejection fraction is approximately 30% in rats expressing eGFP post-MI. The LV IVCT was also significantly reduced (by approximately 9 ms).

The LV myocardial global performance index (LV MPI) is used to quantify energetics of ventricular wall contraction and relaxation during systole and diastole of each cardiac cycle, assessed independently of (although potentially dependant on) HR. Optogenetic DVMN stimulation resulted in a clear beneficial effect on LV contractility in post-MI rats, with significant improvements also noted in sham-operated animals. Doppler measurements of transmitral blood flow velocities were made to comprehensively evaluate the LV diastolic function. Optogenetic DVMN stimulation was sufficient for maintaining a normal E/A ratio (i.e. >1), while in post-MI rats expressing eGFP in the DVMN the average ratio was 0.9 (and would be considered in a clinical setting as evidence of a mild diastolic dysfunction). These observations were interpreted as rats expressing ChIEF-tdTomato post-MI having a normal E/A ratio, as opposed to a pseudo-normalised E/A filling pattern, an unlikely scenario in the context of other ultrasound assessments (in a clinical setting, this would be differentiated using the Valsalva manoeuvre and ultrasound Doppler of the pulmonary vein (Paulus, 1998) to reveal an impaired filling pattern).

In addition to E/A ratio, other parameters of the early filling wave were assessed as indices of myocardial wall compliance and lusitropic function. Optogenetic stimulation of the DVMN improved early wave DT in sham-operated animals only. The negative gradient of the E wave, i.e. the deceleration, is clinically shown to be a better index of diastolic function and predictor of cardiovascular outcomes than one of its constitutive one-dimensional components, such as

deceleration time (Mishra *et al.*, 2007). Optogenetic stimulation of the DVMN in post-MI rats was found to significantly improve the deceleration slope. Ultrasound assessment of LV function is clinically useful and allows for longitudinal studies. Ultrasound measurements are based on the assumptions of a "normal" LV shape allowing the use of Simpson's rule for calculating ejection fraction from b-mode acquisitions (Schiller *et al.*, 1989). This may become less reliable in pathological conditions as ventricular hypertrophy and wall thinning can result in an abnormal chamber shape. However, good concordance has been found between non-invasive and invasive assessment of LV function in animal models (Schober *et al.*, 2003) and humans (Sarma *et al.*, 1974; Sokolski *et al.*, 2011).

Following MI, optogenetic stimulation of the DVMN in rats expressing ChiEF-tdTomato preserved inotropic function as assessed by LVdP/dt$_{max}$. This was in agreement with peak LV end systolic pressures, which were higher in rats expressing ChIEF-tdTomato both in the sham and post-MI groups. Optogenetic stimulation of the DVMN lowered LVEDP and also normalised LVdP/dt$_{min,}$ indicative of the beneficial effect of the treatment on LV lusitropy.

It was noted that in all the animals the consistent induction of surgical anaesthesia required a higher dose of urethane (1.4 g kg^{-1}, i.p.). As a result, the mean arterial pressures in animals of all experimental groups were below 100 mmHg. Nevertheless, optogenetic stimulation of the DVMN of infarcted rats resulted in a MAP of a more normotensive range possibly reflecting maintained inotropic function. Pulse pressures were also compared. Clinically, a narrow pulse pressure is used as a prognostic marker of poor cardiovascular outcomes (Yildiran *et al.*, 2010). Optogenetic stimulation of the DVMN was found to maintain normal pulse pressure in post-MI rats, which is suggestive of a preserved systolic function as also reflected by the maintained LVESP.

An *ex vivo* analysis of LV pressure volume curves demonstrates that optogenetic stimulation of DVMN enhanced myocardial wall compliance in sham-operated animals only. No significant shift of the LV pressure-volume curve was observed as a result of MI when assessed six weeks after LAD occlusion. Classical

earlier studies assessing LV remodelling in rats have found that generally more severe infarctions are required to produce significant rightward shifts in LV pressure volume curves (Pfeffer *et al.*, 1991). However, previous work conducted in this laboratory (Marina *et al.*, 2013) involving male Sprague-Dawley rats obtained from UCL colony which underwent LAD occlusion, resulting in a marginally lower average infarct size (approximately 30%), reported a significant rightward shift of LV pressure volume curves. An important difference between these two studies was that in this experiment the animals had recurrent (every 48 hours) exposure to isoflurane anaesthesia required for optogenetic DVMN stimulation. Moderate LV remodelling observed in both groups of post-MI animals could be explained by potent cardioprotective action of isoflurane (Belhomme *et al.*, 1999). Collectively these data indicate that optogenetic stimulation of the DVMN over the course of four weeks post-MI prevents cardiac dysfunction, as is evident from improved/maintained exercise capacity and LV systolic and diastolic function. Concordant improvements were observed in most of the assessed indices of contractile (ejection fraction, IVCT, LVdP/dt$_{max}$ and LVESP) and diastolic (E/A ratio, deceleration slope, LVdP/dt$_{min}$ and LVEDP) function. DT and IVRT were not significant between animals post-MI, likely due to the inherent lack of sensitivity of these measurements (Mishra *et al.*, 2007).

Normalised LV MPI reflected the improvements in the aforementioned systolic and diastolic indices as a result of optogenetic stimulation of the DVMN after the MI. No differences in HR were observed between all four experimental groups either under urethane or isoflurane anaesthesia. This is relevant to the assessment of LV inotropy and lusitropy due to strong force-frequency relations in the rat's heart (Nalivaiko *et al.*, 2010). No significant differences in lung water content were observed between sham-operated and post-MI rats, consistent with previous work involving similar infarct sizes (Marina *et al.*, 2013). There was, however, evidence of right ventricular hypertrophy in post-MI rats expressing eGFP in the DVMN, which was prevented by optogenetic stimulation of this population of VPNs.

As discussed in Chapter 4, preliminary blots conducted in collaboration with the research group of Dr. Gareth Ackland demonstrate that optogenetic stimulation of the DVMN results in down regulation of GRK2 and pan-arrestin expression in the LV. Reduced expression of GRK2 had been shown previously to unmask the significant contractile effect of β_2–adrenoceptor stimulation, which is either weak or absent under normal conditions (Salazar *et al.*, 2013). Increased activity of β_2–adrenoceptor in the intact myocardium may therefore explain preserved inotropic function post-MI. It is also possible that this mechanism unlocks the angiogenic potential of β_2–adrenoceptor (Rengo *et al.*, 2012).

Stimulation of β_2-adrenoceptors also specifically elicits dilation of coronary high resistance vessels (subendocardial and subepicardial arterioles) through the opening of ATP-sensitive potassium channels (Hein et al., 2004). Hence, optogenetic stimulation of the DVMN may increase/improve myocardial perfusion via downregulation of important intracellular proteins which control signalling mediated by β-adrenoceptors.

A direct parasympathetic effect on coronary blood flow may also underlie beneficial effects of DVMN stimulation of LV function. Vagal innervation of the coronary vessels has been a subject of scientific scrutiny since the mid-1800s (Panum, 1858). Parasympathetic fibres were found to follow the coronary vessels into the myocardium (Woollard, 1926). Both electrical stimulation of the vagus nerve and coronary ACh perfusion have been shown to trigger the release of nitric oxide within the ventricles (Brack *et al.*, 2009). NO was found to be produced within the heart by either constitutive or inducible NO synthases (Schulz *et al.*, 1992; Balligand *et al.*, 1993; Pinsky *et al.*, 1994; Sessa, 1994). Since NO is also produced in response to distension (Pinsky *et al.*, 1997), it is less surprising that the subendocardium, subject to the most stretch, may have lower β_2–adrenoceptor expression (Hein et al., 2004) and, therefore, more NO mediated vasodilation. There is also evidence that β_2-adrenoceptor stimulation leading to K_{ATP} channel opening (Hein et al., 2004) may contribute to NO production (Ming *et al.*, 1997). These potential mechanisms are hypothesised to improve cardiac perfusion during periods

of DVMN optogenetic stimulation – this may have a significant beneficial effect on the contractile properties of the viable myocardium in the long term.

A dramatic improvement of the LV function as a result of optogenetic stimulation of the DVMN in rats allows informed criticisms of on-going clinical trials of VNS efficiency in heart failure. Recently published results of NECTAR-HF trial demonstrated no effect of VNS on any objective measures of LV function, although a marginal improvement in the quality of life was reported (Zannad *et al.*, 2015).

Both NECTAR-HF and the on-going INOVATE-HF were designed to determine whether VNS would attenuate cardiac remodelling, improve cardiac function and increase exercise capacity in symptomatic heart failure patients. NECTAR-HF trial recruited patients with ejection fraction of ≤35% and VNS was applied to the right vagus nerve. Right VNS was chosen as having a more profound effect on HR (via strong innervation of the SA node by the right vagus) with the resulting bradycardia having a therapeutic effect. Indeed, lowering HR was found to be beneficial in heart failure patients in clinical trials with ivabradine that typically excluded patients with HR ranges of <70 bpm (SHIFT study, (Swedberg *et al.*, 2010) (Zugck *et al.*, 2014). Both NECTAR-HF and INOVATE-HF trials did not exclude patients with low resting heart rates and allowed normal medication including β blockers.

Collectively, the data presented in this thesis demonstrate significant functional innervation of the LV by the neuronal projections of the DVMN. DVMN neurones control electrical and contractile properties of the LV and provide crucial trophic innervation of the LV, which is required to mount an appropriate contractile response to β-adrenoceptor stimulation. Selective optogenetic recruitment of these projections has a dramatic beneficial effect on healthy ventricles (*enhanced* function) as well as ventricular myocardium compromised by occlusion of a major coronary artery (*preserved/restored* function). These data suggest that the design of future clinical trials of VNS in heart failure could be significantly improved by targeting the

left vagus nerve with additional modifications allowing selective recruitment of C fibre efferents originating from the DVMN.

Chapter 6 General Discussion and Summary

The experimental studies described in this thesis aimed to determine the functional significance of cardiac innervation provided by projections of VPNs residing in the dorsal vagal motor nucleus (DVMN). The parasympathetic nervous system develops first in evolution of vertebrates, with the sympathetic nervous system appearing relatively late (cardiac sympathetic innervation is not present in elasmobranch fish) (Taylor *et al.*, 1999). Therefore, the DVMN is probably the most (evolutionary) ancient central nervous structure that harbours autonomic motor neurones. During transition from water to air breathing, a group of DVMN neurones migrate ventrally and give rise to compact formation of the NA, which acquires respiratory modulation of activity from the neighbouring respiratory network (Burggren & Infantino, 1994; Burggren, 1995; Taylor *et al.*, 1999; Jones, 2001). Given the evolutionary origin of the cardiorespiratory system it is inconceivable that the DVMN has no role in autonomic control of the heart, although the functional significance of cardiac innervation by the DVMN has been repeatedly questioned (Jones *et al.*, 1998; Jones, 2001). This study used contemporary methods of molecular neuroscience (including pharmaco- and optogenetics) applied in carefully designed and executed physiological experiments conducted using animal (rat and mouse) models. Collectively, this thesis demonstrates that the DVMN neuronal projections control electrical and contractile properties of the LV, determine exercise capacity and have a major impact on the progression of left ventricular dysfunction post-MI.

Experiments described in Chapter 2 were designed to determine the role of DVMN neurones in controlling electrical properties of the ventricle. The preliminary aims of the experiments for this chapter were:

- To determine the effect of systemic muscarinic and neuronal NO synthase (nNOS) blockade on the electrical properties of nodal and ventricular tissue
- To determine the effect of DVMN silencing on the electrical properties of nodal and ventricular tissue
- To determine the effect of synuclein pathology on DVMN activity and ventricular electrical stability.

The data obtained demonstrates that the DVMN VPNs provide functional, tonic innervation of the ventricle. The experiments on rats under urethane anaesthesia in conditions of systemic β-adrenoceptor blockade with subsequent muscarinic and nNOS synthase blockade confirmed the existence of a tonic parasympathetic control of cardiac excitability mediated by the actions of ACh and NO. Acute DVMN silencing led to shortening of the ventricular effective refractory period, lowering threshold for triggered ventricular tachycardia and prolonging the corrected QT interval. Lower resting activity of the DVMN neurones in aging synuclein deficient mice was found to be associated with ventricular effective refractory period shortening and corrected QT interval prolongation.

These findings imply that the activity of the DVMN VPNs is responsible for tonic parasympathetic control of ventricular excitability, likely to be mediated by NO. Vagal influence on the atria and conductive tissue is assumed to be mediated via a muscarinic mechanism from a neuronal source other than the DVMN. These findings provided the first insight into the central nervous substrate that underlies functional parasympathetic innervation of the ventricles and highlighted its vulnerability in neurodegenerative disease(s).

Having established the presence of functional innervation of the ventricle by the DVMN neuronal projections, the experiments described in Chapter 3 were designed to determine the functional significance of this innervation concerning the control of left ventricular contractility. The preliminary aims of the experiments for Chapter 3 were:

- To determine the effects of systemic muscarinic blockade on left ventricular contractility
- To determine the effect of reduced DVMN activity on left ventricular contractility
- To identify the anatomical location of DVMN neurones that control left ventricular contractility.

It was found that under systemic β-adrenoceptor blockade combined with spinal cord transection (to remove sympathetic influences), intravenous

administration of atropine increases left ventricular contractility in rats anaesthetised with urethane, but not in animals anaesthetised with pentobarbital. These observations are consistent with the previously published data showing that cardiac vagal tone is preserved under urethane anaesthesia and abolished by pentobarbital (O'Leary & Jones, 2003).

Increased left ventricular contractility in rats anaesthetised with urethane was observed when the activity of DVMN neurones, targeted bilaterally to express an inhibitory *Drosophila* allatostatin receptor, was reduced by application of an insect peptide allatostatin. No significant changes in heart rate were observed following DVMN inhibition, an observation concordant with the large body of evidence indicating that chronotropic vagal tone is provided by VPNs of the NA (Spyer, 1994).

Microinjections of glutamate and muscimol to activate or inhibit neuronal cell bodies in distinct locations along the rostro-caudal extent of the left and right DVMN demonstrate that VPNs that have an impact on left ventricular contractility are located in the caudal region of the left DVMN. Changes in left ventricular contractility were only observed when this subpopulation of DVMN neurones was activated or inhibited. These data confirmed the existence of a tonic inhibitory muscarinic influence on ventricular inotropy. The results obtained also suggest that the activity of this subpopulation of DVMN neurones provides functionally significant parasympathetic control of the left ventricular contractile function. Therefore, the subsequent experiments described in Chapters 3 and 4 targeted VPNs residing in the caudal aspects of the DVMN.

Having demonstrated that DVMN neurones contribute to the autonomic control of the electrical and contractile properties of the LV, subsequent experiments described in Chapter 3 were designed to test the hypothesis that the strength of cardiac parasympathetic tone determines exercise capacity. It was hypothesised that vagal withdrawal decreases and vagal recruitment enhances the ability to exercise. Previous studies conducted in this laboratory demonstrated that DVMN activity mediates the phenomenon of remote ischaemic preconditioning (when cycles of

ischaemia/reperfusion applied to the tissue/organ remote from the heart protect cardiomyocytes from lethal ischaemia/reperfusion injury) (Mastitskaya *et al.*, 2012). Increasing DVMN activity mimics the effect of remote preconditioning on the heart (Mastitskaya *et al.*, 2012), while remote preconditioning was found to improve both aerobic and anaerobic exercise capacity in humans (Salvador *et al.*, 2015). Combined, these data suggest that recruitment of common mechanisms may underlie the effect of remote ischaemia/reperfusion on myocardial injury and ventricular performance. An experimental model of forced exercise in rodents was used and exercise capacity was determined in conditions of

- Unilateral cervical vagotomy
- Acute and chronic systemic muscarinic receptor blockade
- Systemic M_2 and M_3 muscarinic receptor blockade
- nNOS blockade
- Genetic targeting and silencing of DVMN neurones
- Optogenetic activation of the DVMN neurones.

Significant reduction in exercise capacity was observed in rats following unilateral vagotomy, sustained (four hours) systemic muscarinic receptor blockade or inhibition of the neuronal NOS. Exercise capacity was also reduced in mice deficient in M3 muscarinic receptor-mediated signalling and in WT mice in conditions of systemic M3 muscarinic receptor blockade. Acute reduction in the activity of the DVMN neurones using a pharmacogenetic approach resulted in a dramatic lowering of exercise capacity and inability of the LV to mount a contractile response to β-adrenoceptor stimulation.

These results argue in favour of an essential role played by vagal innervation of the ventricle which maintains the ability of the LV to mount an appropriate contractile response to sympathetic stimulation. Acute nNOS inhibition and acute DVMN silencing were found to have quantitatively similar detrimental effects on exercise capacity, suggesting that the DVMN neuronal projections control left ventricular function and exercise capacity using NO as a signalling molecule. The concept of a direct nitrergic NO-mediated vagal control of the ventricle input is supported both by the data presented in Chapter 2 of this thesis and available

literature data (Brack et al., 2009, 2011). Vagal innervation of the LV mediated by muscarinic mechanisms is hypothesised to provide trophic influences, the significance of which becomes clear over a longer time period. Optogenetic recruitment of the DVMN neurones (four daily sessions of 15 minute-long stimulations) markedly improved exercise capacity and contractile properties of the LV. The degree of exercise capacity improvement was quantitatively similar to that observed in a group of naïve animals subjected to exercise training over the same time period. However, no improvement in ventricular contractile function was observed in the latter group of rats.

Changes in left ventricular inotropy following optogenetic DVMN recruitment were not associated with any significant changes in heart rate. It was also found that optogenetic stimulation of the DVMN results in down regulation of GRK2 and pan-arrestin expression in the LV. Reduced expression of GRK2 had previously been shown to unmask a significant contractile effect of β_2–adrenoceptor stimulation, which is either weak or absent under normal conditions (Salazar et al., 2013). Increased vagal efferent activity and potentially enhanced recruitment of PKD1, via activation of the M_3 receptor, had also been shown to promote cardiac hypertrophy and angiogenesis (Rozengurt, 2011). Increased efficacy of β_2–adrenoceptor mediated signalling in ventricular cardiomyocytes may therefore explain changes in resting inotropic state and the ability of the LV to mount a stronger inotropic response during exercise.

Together, the results in Chapter 4, obtained using pharmacological blockade, M_3-KI genetic mouse model, pharmaco- and optogenetic approaches to alter the activity of the DVMN VPNs, have demonstrated that the vagal supply to the LV maintains the ability of the heart to mount an appropriate inotropic response and determines exercise capacity. Experimental studies described in Chapter 5 were designed to test the hypothesis that increasing activity of DVMN neurones might be sufficient to slow left ventricular dysfunction and remodelling developing after a MI. This hypothesis was based on the results of the experiments presented in Chapters 2 and 3, suggesting that DVMN neurones provide functional innervation of the left cardiac ventricle, controlling its electrical and contractile properties. The results of

the experiments described in Chapter 4 have also demonstrated a clear improvement in exercise capacity and left ventricular contractility after four daily sessions (15 minutes each) of DVMN stimulations, suggesting that the same treatment delivered over a longer period of time may slow or even prevent left ventricular dysfunction and heart failure development after permanent coronary artery occlusion.

To test this hypothesis an experimental design was created involving four groups of animals: rats transduced to express either eGFP (control) or ChIEF-tdTomato (optogenetic construct) by the DVMN neurones that underwent left anterior descending artery occlusion or sham surgery. All animals were subjected to four weeks of light stimulation of the dorsal brainstem via a pre-implanted optrode for 15 minutes every 48 hours, commencing two days after left anterior descending occlusion or sham surgery. Left ventricular systolic and diastolic functions were then assessed using different methods, including high-resolution ultrasound.

The data obtained has demonstrated that optogenetic stimulation of the DVMN over the course of four weeks post-MI prevents cardiac dysfunction, as evident from improved/maintained exercise capacity and left ventricular systolic and diastolic function. Concordant improvements were observed in most of the assessed indices of contractile (ejection fraction, IVCT, LV$dP/dt_{max}$ and LVESP) and diastolic (E/A ratio, deceleration slope, LV$dP/dt_{min}$ and LVEDP) function.

Collectively, the data presented in this thesis has demonstrated significant functional innervation of the LV by projections of VPNs residing in the DVMN (Figure 6-1). DVMN controls the electrical and contractile properties of the LV and provide crucial trophic innervation, which is required to mount an appropriate contractile response to β-adrenoceptor stimulation.

Strength of vagal tone supplied to the LV by the DVMN neurones determines the ability of cardiomyocytes to respond to sympathetic stimulation and, therefore, determines exercise capacity. These data imply that differences in individual ability to exercise may reflect varying levels of DVMN activity due to multitude of genetic and environmental factors. High vagal tone provided by the DVMN neuronal projections to the ventricular system in elite athletes could make them highly tolerant

to intense exercise regimes. On the other side of the spectrum, loss of exercise capacity with age has been found to be associated with a progressive decline in autonomic function (De Meersman & Stein, 2007). Neurones such as those of the DVMN have long projecting axons with no myelination and require more energy for impulse propagation and are susceptible to metabolic stress (Kapfhammer & Schwab, 1994). DVMN dysfunction has already been associated with a host of autonomic abnormalities (Braak et al., 2002; Goldberg et al., 2012) and may contribute to progressing decline in exercise capacity during aging and in various disease states.

In practical terms, the data showing that relatively very short (15 minutes) sessions of optogenetic DVMN stimulation delivered every 48 hours are sufficient to preserve left ventricular function and exercise capacity post-MI may inform further development of VNS technology for heart failure treatment. Selective optogenetic recruitment of DVMN projections has a dramatic beneficial effect on healthy ventricles as well as ventricular myocardium compromised by occlusion of a major coronary artery. This thesis thus identifies the source and provides a comprehensive analysis of the functional role of ventricular vagal innervation. It further suggests that the design of future clinical trials of VNS in heart failure could be significantly improved by targeting the left vagus nerve with additional modifications allowing selective recruitment of C fibre efferents originating from the DVMN.

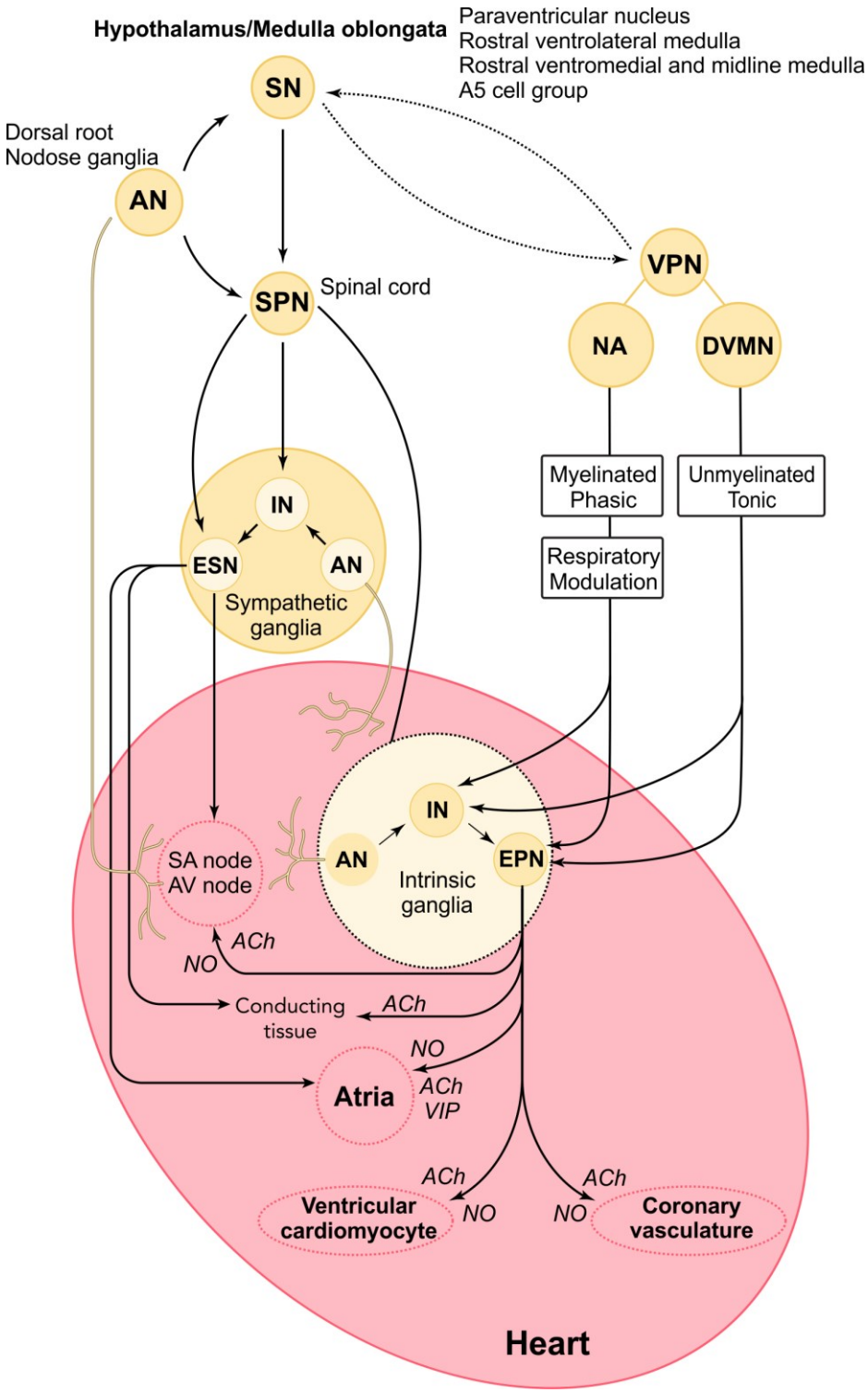

Figure 6-1: Scheme of sensory and efferent neural pathways controlling the heart

Dashed lines represent hypothesised projections. AN, afferent (sensory) neurones; DVMN, dorsal vagal motor nucleus; EPN, efferent parasympathetic neurones; ESN, efferent sympathetic neurones; IN, interneurones; NA, nucleus ambiguus, SN, sympathoexcitatory neurones; VPN, vagal (parasympathetic) preganglionic neurones.

Bibliography

Akiyama T & Yamazaki T. (2001). Effects of right and left vagal stimulation on left ventricular acetylcholine levels in the cat. *Acta Physiol Scand* **172,** 11-16.

Akiyama T, Yamazaki T & Ninomiya I. (1994). In vivo detection of endogenous acetylcholine release in cat ventricles. *Am J Physiol* **266,** H854-860.

al-Ani M, Munir SM, White M, Townend J & Coote JH. (1996). Changes in R-R variability before and after endurance training measured by power spectral analysis and by the effect of isometric muscle contraction. *Eur J Appl Physiol* **74,** 397-403.

Al-Wandi A, Ninkina N, Millership S, Williamson SJ, Jones PA & Buchman VL. (2010). Absence of alpha-synuclein affects dopamine metabolism and synaptic markers in the striatum of aging mice. *Neurobiol Aging* **31,** 796-804.

Anwar S, Peters O, Millership S, Ninkina N, Doig N, Connor-Robson N, Threlfell S, Kooner G, Deacon RM, Bannerman DM, Bolam JP, Chandra SS, Cragg SJ, Wade-Martins R & Buchman VL. (2011). Functional alterations to the nigrostriatal system in mice lacking all three members of the synuclein family. *J Neurosci* **31,** 7264-7274.

Ardell JL. (1994). *Structure and function of mammalian intrinsic cardiac neurons.* In Neurocardiology, ed. Armour JA & Ardell JL, pp. 95-114. Oxford Univeristy Press, New York.

Armbruster BN, Li X, Pausch MH, Herlitze S & Roth BL. (2007). Evolving the lock to fit the key to create a family of G protein-coupled receptors potently activated by an inert ligand. *Proc Natl Acad Sci U S A* **104,** 5163-5168.

Armour JA. (1994). *Peripheral autonomic neuronal interactions in cardiac regulation.* In Neurocardiology, ed. Armour JA & Ardell JL, pp. 219-244. Oxford Univeristy Press, New York.

Aroesty JM, McKay RG, Heller GV, Royal HD, Als AV & Grossman W. (1985). Simultaneous assessment of left ventricular systolic and diastolic dysfunction during pacing-induced ischemia. *Circulation* **71,** 889-900.

Ashley EA, Sears CE, Bryant SM, Watkins HC & Casadei B. (2002). Cardiac nitric oxide synthase 1 regulates basal and β-adrenergic contractility in murine ventricular myocytes. *Circulation* **105,** 3011-3016.

Aubert AE, Seps B & Beckers F. (2003). Heart rate variability in athletes. *Sports Med* **33,** 889-919.

Ball RM, Bache RJ, Cobb FR & Greenfield JC, Jr. (1975). Regional myocardial blood flow during graded treadmill exercise in the dog. *J Clin Invest* **55,** 43-49.

Balligand JL, Kelly RA, Marsden PA, Smith TW & Michel T. (1993). Control of cardiac muscle cell function by an endogenous nitric oxide signaling system. *Proc Natl Acad Sci U S A* **90,** 347-351.

Balligand JL, Kobzik L, Han X, Kaye DM, Belhassen L, O'Hara DS, Kelly RA, Smith TW & Michel T. (1995). Nitric oxide-dependent parasympathetic signaling is due to activation of constitutive endothelial (type III) nitric oxide synthase in cardiac myocytes. *J Biol Chem* **270,** 14582-14586.

Barouch LA, Harrison RW, Skaf MW, Rosas GO, Cappola TP, Kobeissi ZA, Hobai IA, Lemmon CA, Burnett AL, O'Rourke B, Rodriguez ER, Huang PL, Lima JA, Berkowitz DE & Hare JM. (2002). Nitric oxide regulates the heart by spatial confinement of nitric oxide synthase isoforms. *Nature* **416,** 337-339.

Bartfai T, Iverfeldt K, Fisone G & Serfozo P. (1988). Regulation of the release of coexisting neurotransmitters. *Annu Rev Pharmacol Toxicol* **28,** 285-310.

Bayliss W & Starling E. (1902). The mechanism of pancreatic secretion. *J Physiol* **28,** 1-29.

Bayliss WM & Starling EH. (1892). On some Points in the Innervation of the Mammalian Heart. *J Physiol* **13,** 407-418 403.

Belardinelli L, Shryock JC, Song Y, Wang D & Srinivas M. (1995). Ionic basis of the electrophysiological actions of adenosine on cardiomyocytes. *Faseb J* **9,** 359-365.

Belhomme D, Peynet J, Louzy M, Launay JM, Kitakaze M & Menasche P. (1999). Evidence for preconditioning by isoflurane in coronary artery bypass graft surgery. *Circulation* **100,** II340-344.

Bennett JA, Kidd C, Latif AB & McWilliam PN. (1981). A horseradish peroxidase study of vagal motoneurones with axons in cardiac and pulmonary branches of the cat and dog. *Q J Exp Physiol* **66,** 145-154.

Berdeaux A, Garnier M, Boissier JR & Giudicelli JF. (1979). The role of β-adrenoceptors in coronary blood flow distribution in normal and ischemic canine myocardium. *Eur J Pharmacol* **53,** 261-271.

Bernardi L, Keller F, Sanders M, Reddy PS, Griffith B, Meno F & Pinsky MR. (1989). Respiratory sinus arrhythmia in the denervated human heart. *J Appl Physiol (1985)* **67,** 1447-1455.

Blackhall-Morison A. (1926). Note on the innervation of the ventricle of the human heart. *J Anat* **60,** 143.

Bockaert J, Roussignol G, Becamel C, Gavarini S, Joubert L, Dumuis A, Fagni L & Marin P. (2004). GPCR-interacting proteins (GIPs): nature and functions. *Biochem Soc Trans* **32,** 851-855.

Boutcher SH & Stein P. (1995). Association between heart rate variability and training response in sedentary middle-aged men. *Eur J Appl Physiol* **70,** 75-80.

Braak H, Del Tredici K, Bratzke H, Hamm-Clement J, Sandmann-Keil D & Rub U. (2002). Staging of the intracerebral inclusion body pathology associated with idiopathic Parkinson's disease (preclinical and clinical stages). *J Neurol* **249 Suppl 3,** III/1-5.

Brack KE, Coote JH & Ng GA. (2011). Vagus nerve stimulation protects against ventricular fibrillation independent of muscarinic receptor activation. *Cardiovasc Res* **91,** 437-446.

Brack KE, Patel VH, Mantravardi R, Coote JH & Ng GA. (2009). Direct evidence of nitric oxide release from neuronal nitric oxide synthase activation in the left ventricle as a result of cervical vagus nerve stimulation. *J Physiol* **587,** 3045-3054.

Broderson SH, Westrum LE & Sutton AE. (1974). Studies of the direct coloring thiocholine method for localizing cholinesterase activity. *Histochemistry* **40,** 13-23.

Budd DC, Challiss RA, Young KW & Tobin AB. (1999). Cross talk between m3-muscarinic and β(2)-adrenergic receptors at the level of receptor phosphorylation and desensitization. *Mol Pharmacol* **56,** 813-823.

Budd DC, McDonald JE & Tobin AB. (2000). Phosphorylation and regulation of a Gq/11-coupled receptor by casein kinase 1alpha. *J Biol Chem* **275,** 19667-19675.

Burggren WW. (1995). Central Cardiovascular Function in Amphibians: Qualitative Influences of Phylogeny, Ontogeny, and Season. In *Mechanisms of Systemic Regulation*, ed. Heisler N, pp. 175-197. Springer Berlin Heidelberg, New York.

Burggren WW & Infantino RL. (1994). The Respiratory Transition from Water to Air-Breathing during Amphibian Metamorphosis. *Am Zool* **34,** 238-246.

Calvillo L, Vanoli E, Andreoli E, Besana A, Omodeo E, Gnecchi M, Zerbi P, Vago G, Busca G & Schwartz PJ. (2011). Vagal stimulation, through its nicotinic action, limits infarct size and the inflammatory response to myocardial ischemia and reperfusion. *J Cardiovasc Pharmacol* **58,** 500-507.

Carbonell LM. (1956). Esterases of the conductive system of the heart. *J Histochem Cytochem* **4,** 87-95.

Carlson MD, Geha AS, Hsu J, Martin PJ, Levy MN, Jacobs G & Waldo AL. (1992). Selective stimulation of parasympathetic nerve fibers to the human sinoatrial node. *Circulation* **85,** 1311-1317.

Carlsten A, Folkow B & Hamberger CA. (1957). Cardiovascular effects of direct vagal stimulation in man. *Acta Physiol Scand* **41,** 68-76.

Carter JB, Banister EW & Blaber AP. (2003). Effect of endurance exercise on autonomic control of heart rate. *Sports Med* **33,** 33-46.

Cerisano G, Bolognese L, Carrabba N, Buonamici P, Santoro GM, Antoniucci D, Santini A, Moschi G & Fazzini PF. (1999). Doppler-derived mitral deceleration time: an early strong predictor of left ventricular remodeling after reperfused anterior acute myocardial infarction. *Circulation* **99,** 230-236.

Ceroni A, Chaar LJ, Bombein RL & Michelini LC. (2009). Chronic absence of baroreceptor inputs prevents training-induced cardiovascular adjustments in normotensive and spontaneously hypertensive rats. *Exp Physiol* **94,** 630-640.

Cerrone M, Colombi B, Santoro M, di Barletta MR, Scelsi M, Villani L, Napolitano C & Priori SG. (2005). Bidirectional ventricular tachycardia and fibrillation elicited in a knock-in mouse model carrier of a mutation in the cardiac ryanodine receptor. *Circ Res* **96,** e77-82.

Cheng Z & Powley TL. (2000). Nucleus ambiguus projections to cardiac ganglia of rat atria: an anterograde tracing study. *J Comp Neurol* **424,** 588-606.

Cheng Z, Powley TL, Schwaber JS & Doyle FJ, 3rd. (1999). Projections of the dorsal motor nucleus of the vagus to cardiac ganglia of rat atria: an anterograde tracing study. *J Comp Neurol* **410,** 320-341.

Choate JK, Danson EJ, Morris JF & Paterson DJ. (2001). Peripheral vagal control of heart rate is impaired in neuronal NOS knockout mice. *Am J Physiol Heart Circ Physiol* **281,** H2310-2317.

Chowdhary S & Townend JN. (1999). Role of nitric oxide in the regulation of cardiovascular autonomic control. *Clin Sci (Lond)* **97,** 5-17.

Christophe J, Waelbroeck M, Chatelain P & Robberecht P. (1984). Heart receptors for VIP, PHI and secretin are able to activate adenylate cyclase and to mediate inotropic and chronotropic effects. Species variations and physiopathology. *Peptides* **5,** 341-353.

Ciriello J & Calaresu FR. (1980). Distribution of vagal cardioinhibitory neurons in the medulla of the cat. *Am J Physiol* **238,** R57-64.

Ciriello J & Calaresu FR. (1982). Medullary origin of vagal preganglionic axons to the heart of the cat. *J Auton Nerv Syst* **5,** 9-22.

Cohen MV, Yang XM, Liu GS, Heusch G & Downey JM. (2001). Acetylcholine, bradykinin, opioids, and phenylephrine, but not adenosine, trigger preconditioning by generating free radicals and opening mitochondrial K(ATP) channels. *Circ Res* **89,** 273-278.

Cohn AE. (1912). On the Differences in the Effects of Stimulation of the Two Vagus Nerves on Rate and Conduction of the Dog's Heart. *J Exp Med* **16,** 732-757.

Conlon K, Collins T & Kidd C. (1998). The role of nitric oxide in the control by the vagal nerves of the heart of the ferret. *Exp Physiol* **83,** 469-480.

Conlon K & Kidd C. (1999). Neuronal nitric oxide facilitates vagal chronotropic and dromotropic actions on the heart. *J Auton Nerv Syst* **75,** 136-146.

Coote JH. (2013). Myths and realities of the cardiac vagus. *J Physiol* **591,** 4073-4085.

Coote JH & White MJ. (2015). CrossTalk proposal: bradycardia in the trained athlete is attributable to high vagal tone. *J Physiol* **593,** 1745-1747.

Coronel R, Janse MJ, Opthof T, Wilde AA & Taggart P. (2012). Postrepolarization refractoriness in acute ischemia and after antiarrhythmic drug administration: action potential duration is not always an index of the refractory period. *Heart Rhythm* **9,** 977-982.

Coumel P, Attuel P, Lavallée J, Flammang D, Leclercq JF & Slama R. (1978). The syndrome of atrial arrhythmia of vagal origin. *Arch Mal Coeur Vaiss* **71,** 645-656.

Crick SJ, Anderson RH, Ho SY & Sheppard MN. (1999). Localisation and quantitation of autonomic innervation in the porcine heart II: endocardium, myocardium and epicardium. *J Anat* **195 (Pt 3),** 359-373.

Cullis W & Tribe EM. (1913). Distribution of nerves in the heart. *J Physiol* **46,** 141-150.

D'Souza A, Bucchi A, Johnsen AB, Logantha SJ, Monfredi O, Yanni J, Prehar S, Hart G, Cartwright E, Wisloff U, Dobryznski H, DiFrancesco D, Morris GM & Boyett MR. (2014). Exercise training reduces resting heart rate via downregulation of the funny channel HCN4. *Nat Commun* **5,** 3775.

D'Souza A, Sharma S & Boyett MR. (2015). CrossTalk opposing view: bradycardia in the trained athlete is attributable to a downregulation of a pacemaker channel in the sinus node. *J Physiol* **593,** 1749-1751.

Dale H. (1934a). Chemical Transmission of the Effects of Nerve Impulses. *Br Med J* **1,** 835-841.

Dale HH. (1934b). The Chemical Transmission of Nerve Impulses. *Science* **80,** 450.

Dale HH & Feldberg W. (1934). The chemical transmitter of vagus effects to the stomach. *J Physiol* **81,** 320-334.

Danson EJ, Mankia KS, Golding S, Dawson T, Everatt L, Cai S, Channon KM & Paterson DJ. (2004). Impaired regulation of neuronal nitric oxide synthase and heart rate during exercise in mice lacking one nNOS allele. *J Physiol* **558,** 963-974.

Danson EJ & Paterson DJ. (2003). Enhanced neuronal nitric oxide synthase expression is central to cardiac vagal phenotype in exercise-trained mice. *J Physiol* **546,** 225-232.

Danson EJ & Paterson DJ. (2005). Cardiac neurobiology of nitric oxide synthases. *Ann N Y Acad Sci* **1047,** 183-196.

Davies F, Francis E & King T. (1952). Neurological studies of the cardiac ventricles of mammals. *J Anat* **86,** 130.

Davis RP, van den Berg CW, Casini S, Braam SR & Mummery CL. (2011). Pluripotent stem cell models of cardiac disease and their implication for drug discovery and development. *Trends Mol Med* **17,** 475-484.

De Ferrari GM, Crijns HJ, Borggrefe M, Milasinovic G, Smid J, Zabel M, Gavazzi A, Sanzo A, Dennert R, Kuschyk J, Raspopovic S, Klein H, Swedberg K, Schwartz PJ & CardioFit Multicenter Trial I. (2011). Chronic vagus nerve stimulation: a new and promising therapeutic approach for chronic heart failure. *Eur Heart J* **32,** 847-855.

De Geus EJ, Boomsma DI & Snieder H. (2003). Genetic correlation of exercise with heart rate and respiratory sinus arrhythmia. *Med Sci Sports Exerc* **35,** 1287-1295.

de Lau LM & Breteler MM. (2006). Epidemiology of Parkinson's disease. *Lancet Neurol* **5,** 525-535.

De Meersman RE & Stein PK. (2007). Vagal modulation and aging. *Biol Psychol* **74,** 165-173.

Degeest H, Levy MN & Zieske H. (1964). Negative inotropic effect of the vagus nerves upon the canine ventricle. *Science (New York, NY)* **144,** 1223-1225.

Degeest H, Levy MN & Zieske H. (1965a). Carotid Chemoreceptor Stimulation and Ventricular Performance. *American Journal of Physiology* **209,** 564-570.

Degeest H, Levy MN & Zieske H. (1965b). Reflex Effects of Cephalic Hypoxia Hypercapnia and Ischemia Upon Ventricular Contractility. *Circ Res* **17,** 349-358.

Degeest H, Levy MN, Zieske H & Lipman RI. (1965c). Depression of Ventricular Contractility by Stimulation of the Vagus Nerves. *Circ Res* **17,** 222-235.

Denison AB, Jr. & Green HD. (1958). Effects of autonomic nerves and their mediators on the coronary circulation and myocardial contraction. *Circulation Research* **6,** 633-643.

Dirkx E, Schwenk RW, Coumans WA, Hoebers N, Angin Y, Viollet B, Bonen A, van Eys GJ, Glatz JF & Luiken JJ. (2012). Protein kinase D1 is essential for contraction-induced glucose uptake but is not involved in fatty acid uptake into cardiomyocytes. *J Biol Chem* **287,** 5871-5881.

Dixon AF. (1906). "a Sidelight on Medical Education.". *Br Med J* **2,** 1137-1140.

Dixon WE. (1907). The action of alcohol on the circulation. *J Physiol* **35,** 346-366.

Dobrzynski H, Janvier NC, Leach R, Findlay JB & Boyett MR. (2002). Effects of ACh and adenosine mediated by Kir3.1 and Kir3.4 on ferret ventricular cells. *Am J Physiol Heart Circ Physiol* **283,** H615-630.

Dobrzynski H, Marples DD, Musa H, Yamanushi TT, Henderson Z, Takagishi Y, Honjo H, Kodama I & Boyett MR. (2001). Distribution of the muscarinic K+ channel proteins Kir3.1 and Kir3.4 in the ventricle, atrium, and sinoatrial node of heart. *J Histochem Cytochem* **49,** 1221-1234.

Domenech RJ & MacLellan PR. (1980). Transmural ventricular distribution of coronary blood flow during coronary β 2-adrenergic receptor activation in dogs. *Circ Res* **46,** 29-36.

Drury AN. (1923). The influence of vagal stimulation upon the force of contraction, and the refractory period of ventricular muscle in the dog's heart. *Heart* **10,** 405.

Duncker DJ, Stubenitsky R & Verdouw PD. (1998). Autonomic control of vasomotion in the porcine coronary circulation during treadmill exercise: evidence for feed-forward β-adrenergic control. *Circ Res* **82,** 1312-1322.

Eliakim M, Bellet S, Tawil E & Muller O. (1961). Effect of vagal stimulation and acetylcholine on the ventricle. Studies in dogs with complete atrioventricular block. *Circ Res* **9,** 1372-1379.

Elvan A, Rubart M & Zipes DP. (1997). NO modulates autonomic effects on sinus discharge rate and AV nodal conduction in open-chest dogs. *Am J Physiol* **272,** H263-271.

Engelhardt S, Grimmer Y, Fan GH & Lohse MJ. (2001). Constitutive activity of the human β(1)-adrenergic receptor in β(1)-receptor transgenic mice. *Mol Pharmacol* **60,** 712-717.

Filliau C, Younes M, Blanchard AL, Piscione J, Van de Louw A, Seguret C, Israel J & Cottin F. (2015). Effect of "Touch Rugby" Training on the Cardiovascular Autonomic Control In Sedentary Subjects. *Int J Sports Med* **36,** 567-572.

Fletcher PJ, Pfeffer JM, Pfeffer MA & Braunwald E. (1981). Left ventricular diastolic pressure-volume relations in rats with healed myocardial infarction. Effects on systolic function. *Circ Res* **49,** 618-626.

Francillon M. (1928). Zur topographie der Ganglien des menschlichen Herzens. *Anat Embryol (Berl)* **85,** 131-165.

Frank KF, Bolck B, Brixius K, Kranias EG & Schwinger RH. (2002). Modulation of SERCA: implications for the failing human heart. *Basic Res Cardiol* **97 Suppl 1,** I72-78.

Furchgott RF & Vanhoutte PM. (1989). Endothelium-derived relaxing and contracting factors. *Faseb J* **3,** 2007-2018.

Galderisi M. (2005). Diastolic dysfunction and diastolic heart failure: diagnostic, prognostic and therapeutic aspects. *Cardiovasc Ultrasound* **3,** 9.

Garcia Perez M & Jordan D. (2001). Effect of stimulating non-myelinated vagal axons on atrio-ventricular conduction and left ventricular function in anaesthetized rabbits. *Auton Neurosci* **86,** 183-191.

Gaskell WH. (1882). The Croonian Lecture: On the Rhythm of the Heart of the Frog, and on the Nature of the Action of the Vagus Nerve. *Philos T Roy* **173,** 993-1033.

Gatti PJ, Johnson TA, McKenzie J, Lauenstein JM, Gray A & Massari VJ. (1997). Vagal control of left ventricular contractility is selectively mediated by a cranioventricular intracardiac ganglion in the cat. *J Auton Nerv Syst* **66,** 138-144.

Geis GS, Kozelka JW & Wurster RD. (1981). Organization and reflex control of vagal cardiomotor neurons. *J Auton Nerv Syst* **3,** 437-450.

Geis GS & Wurster RD. (1980a). Cardiac responses during stimulation of the dorsal motor nucleus and nucleus ambiguus in the cat. *Circ Res* **46,** 606-611.

Geis GS & Wurster RD. (1980b). Horseradish peroxidase localization of cardiac vagal preganglionic somata. *Brain Res* **182,** 19-30.

Gesell RA. (1916). Cardiodynamics in heart block as affected by auricular systole, auricular fibrillation and stimulation of the vagus nerve. *Am J Physiol* **40,** 267-313.

Gilbey MP. (2007). Sympathetic rhythms and nervous integration. *Clin Exp Pharmacol Physiol* **34,** 356-361.

Gilbey MP, Jordan D, Richter DW & Spyer KM. (1984). Synaptic mechanisms involved in the inspiratory modulation of vagal cardio-inhibitory neurones in the cat. *J Physiol* **356,** 65-78.

Goldberg JA, Guzman JN, Estep CM, Ilijic E, Kondapalli J, Sanchez-Padilla J & Surmeier DJ. (2012). Calcium entry induces mitochondrial oxidant stress in vagal neurons at risk in Parkinson's disease. *Nat Neurosci* **15,** 1414-1421.

Goldsmith RL, Bigger JT, Jr., Bloomfield DM & Steinman RC. (1997). Physical fitness as a determinant of vagal modulation. *Med Sci Sports Exerc* **29,** 812-817.

Gonzalas-Serrato H & Alanis J. (1962). La accion de los nervios cardiacos y de la acetilacolina sobre el automatiomc del corazon. *Acta physiologica latino americana* **12,** 139-152.

Goodchild A, Dampney R & Bandler R. (1982). A method for evoking physiological responses by stimulation of cell bodies, but not

axons of passage, within localized regions of the central nervous system. *J Neurosci Methods* **6,** 351-363.

Gorman MW, Tune JD, Richmond KN & Feigl EO. (2000). Feedforward sympathetic coronary vasodilation in exercising dogs. *J Appl Physiol (1985)* **89,** 1892-1902.

Greene JG. (2014). Causes and consequences of degeneration of the dorsal motor nucleus of the vagus nerve in Parkinson's disease. *Antioxid Redox Signal* **21,** 649-667.

Haney H, Lindgren A, Karstens A & Youmans W. (1943). Responses of the heart to reflex activation of the right and left vagus nerves by the pressor compounds, neosynephrin and pitressin. *American Journal of Physiology -- Legacy Content* **139,** 675-685.

Hang P, Zhao J, Qi J, Wang Y, Wu J & Du Z. (2013). Novel insights into the pervasive role of M(3) muscarinic receptor in cardiac diseases. *Curr Drug Targets* **14,** 372-377.

Harvey W. (1928). Exercitatio anatomica de motu cordis et sanguinis in animalibus. *Frankfurt am Main* **1628**.

Hauptman PJ, Schwartz PJ, Gold MR, Borggrefe M, Van Veldhuisen DJ, Starling RC & Mann DL. (2012). Rationale and study design of the increase of vagal tone in heart failure study: INOVATE-HF. *Am Heart J* **163,** 954-962 e951.

Hausenloy DJ & Yellon DM. (2008). Remote ischaemic preconditioning: underlying mechanisms and clinical application. *Cardiovasc Res* **79,** 377-386.

Hayes E, Pugsley MK, Penz WP, Adaikan G & Walker MJA. (1994). Relationship between Qat and Rr Intervals in Rats, Guinea-Pigs, Rabbits, and Primates. *J Pharmacol Toxicol* **32,** 201-207.

Hearse DJ. (1998). Myocardial protection during ischemia and reperfusion. *Mol Cell Biochem* **186,** 177-184.

Hearse DJ & Bolli R. (1992). Reperfusion induced injury: manifestations, mechanisms, and clinical relevance. *Cardiovasc Res* **26,** 101-108.

Hebeiss K & Kilbinger H. (1996). Differential effects of nitric oxide donors on basal and electrically evoked release of acetylcholine from guinea-pig myenteric neurones. *Br J Pharmacol* **118,** 2073-2078.

Hein TW & Kuo L. (1999). cAMP-independent dilation of coronary arterioles to adenosine : role of nitric oxide, G proteins, and K(ATP) channels. *Circ Res* **85,** 634-642.

Hein TW, Zhang C, Wang W & Kuo L. (2004). Heterogeneous β2-adrenoceptor expression and dilation in coronary arterioles across the left ventricular wall. *Circulation* **110,** 2708-2712.

Henderson Y & Barringer T. (1913). The conditions determining the volume of the arterial blood stream. *Am J Physiol* **31,** 288-299.

Henning RJ. (1992). Vagal stimulation during muscarinic and β-adrenergic blockade increases atrial contractility and heart rate. *J Auton Nerv Syst* **40,** 121-129.

Hepburn H, Fletcher J, Rosengarten TH & Coote JH. (2005). Cardiac vagal tone, exercise performance and the effect of respiratory training. *Eur J Appl Physiol* **94,** 681-689.

Herring N, Golding S & Paterson DJ. (2000). Pre-synaptic NO-cGMP pathway modulates vagal control of heart rate in isolated adult guinea pig atria. *J Mol Cell Cardiol* **32,** 1795-1804.

Herring N & Paterson DJ. (2001). Nitric oxide-cGMP pathway facilitates acetylcholine release and bradycardia during vagal nerve stimulation in the guinea-pig in vitro. *J Physiol* **535,** 507-518.

Higgins C, Vatner S & Braunwald E. (1973). Parasympathetic Control of the Heart. *Pharmacol Rev* **25,** 119-155.

Hommers LG, Lohse MJ & Bunemann M. (2003). Regulation of the inward rectifying properties of G-protein-activated inwardly rectifying K+ (GIRK) channels by Gβ gamma subunits. *J Biol Chem* **278,** 1037-1043.

Hopkins DA & Armour JA. (1982). Medullary cells of origin of physiologically identified cardiac nerves in the dog. *Brain Res Bull* **8,** 359-365.

Hopkins DA & Armour JA. (1984). Localization of sympathetic postganglionic and parasympathetic preganglionic neurons which innervate different regions of the dog heart. *J Comp Neurol* **229,** 186-198.

Hopkins DA, Gootman PM, Gootman N & Armour JA. (1997). Anatomy of medullary and peripheral autonomic neurons innervating the neonatal porcine heart. *J Auton Nerv Syst* **64,** 74-84.

Hopkins DA, Gootman PM, Gootman N, Di Russo SM & Zeballos ME. (1984). Brainstem cells of origin of the cervical vagus and cardiopulmonary nerves in the neonatal pig (Sus scrofa). *Brain Res* **306,** 63-72.

Howell W & Duke W. (1906). Experiments on the isolated mammalian heart to show the relation of the inorganic salts to the action of the accelerator and inhibitory nerves. *J Physiol* **35,** 131-150.

Ignarro LJ. (1991). Signal transduction mechanisms involving nitric oxide. *Biochem Pharmacol* **41,** 485-490.

Ito H, Hosoya Y, Inanobe A, Tomoike H & Endoh M. (1995). Acetylcholine and adenosine activate the G protein-gated muscarinic K+ channel in ferret ventricular myocytes. *Naunyn Schmiedebergs Arch Pharmacol* **351,** 610-617.

Izzo PN, Deuchars J & Spyer KM. (1993). Localization of cardiac vagal preganglionic motoneurones in the rat: immunocytochemical evidence of synaptic inputs containing 5-hydroxytryptamine. *J Comp Neurol* **327,** 572-583.

James TN. (1967). Cardiac innervation: anatomic and pharmacologic relations. *Bull N Y Acad Med* **43,** 1041-1086.

Jennings RB, Murry CE, Steenbergen C, Jr. & Reimer KA. (1990). Development of cell injury in sustained acute ischemia. *Circulation* **82,** II2-12.

Jones JF. (2001). Vagal control of the rat heart. *Exp Physiol* **86,** 797-801.

Jones JF, Wang Y & Jordan D. (1995). Heart rate responses to selective stimulation of cardiac vagal C fibres in anaesthetized cats, rats and rabbits. *J Physiol* **489 (Pt 1),** 203-214.

Jones JF, Wang Y & Jordan D. (1998). Activity of C fibre cardiac vagal efferents in anaesthetized cats and rats. *J Physiol* **507 (Pt 3),** 869-880.

Jones WK, Fan GC, Liao S, Zhang JM, Wang Y, Weintraub NL, Kranias EG, Schultz JE, Lorenz J & Ren X. (2009). Peripheral nociception associated with surgical incision elicits remote nonischemic cardioprotection via neurogenic activation of protein kinase C signaling. *Circulation* **120,** S1-9.

Kainulainen H, Komulainen J, Leinonen A, Rusko H & Vihko V. (1990). Regional differences of substrate oxidation capacity in rat hearts: effects of extra load and endurance training. *Basic Res Cardiol* **85,** 630-639.

Kakinuma Y, Akiyama T, Okazaki K, Arikawa M, Noguchi T & Sato T. (2012). A non-neuronal cardiac cholinergic system plays a protective role in myocardium salvage during ischemic insults. *PLoS ONE* **7,** e50761.

Kakinuma Y, Akiyama T & Sato T. (2009). Cholinoceptive and cholinergic properties of cardiomyocytes involving an amplification mechanism for vagal efferent effects in sparsely innervated ventricular myocardium. *The FEBS journal* **276,** 5111-5125.

Kalia M & Mesulam MM. (1980). Brain stem projections of sensory and motor components of the vagus complex in the cat: II. Laryngeal, tracheobronchial, pulmonary, cardiac, and gastrointestinal branches. *J Comp Neurol* **193,** 467-508.

Kapfhammer JP & Schwab ME. (1994). Inverse Patterns of Myelination and Gap-43 Expression in the Adult Cns - Neurite Growth-Inhibitors as Regulators of Neuronal Plasticity. *J Comp Neurol* **340,** 194-206.

Karjalainen J, Viitasalo M, Manttari M & Manninen V. (1994). Relation between Qt Intervals and Heart-Rates from 40 to 120 Beats/Min in Rest Electrocardiograms of Men and a Simple Method to Adjust Qt Interval Values. *J Am Coll Cardiol* **23,** 1547-1553.

Karnovsky MJ & Roots L. (1964). A "Direct-Coloring" Thiocholine Method for Cholinesterases. *J Histochem Cytochem* **12,** 219-221.

Katare RG, Ando M, Kakinuma Y, Arikawa M, Handa T, Yamasaki F & Sato T. (2009). Vagal nerve stimulation prevents reperfusion injury through inhibition of opening of mitochondrial permeability transition pore independent of the bradycardiac effect. *J Thorac Cardiovasc Surg* **137,** 223-231.

Kawada T, Akiyama T, Shimizu S, Kamiya A, Uemura K, Li M, Shirai M & Sugimachi M. (2009). Detection of endogenous acetylcholine release during brief ischemia in the rabbit ventricle: a possible trigger for ischemic preconditioning. *Life Sci* **85,** 597-601.

Kaye DM, Wiviott SD, Balligand JL, Simmons WW, Smith TW & Kelly RA. (1996). Frequency-dependent activation of a constitutive nitric oxide synthase and regulation of contractile function in adult rat ventricular myocytes. *Circ Res* **78,** 217-224.

Kent KM, Epstein SE, Cooper T & Jacobowitz DM. (1974). Cholinergic innervation of the canine and human ventricular conducting system. Anatomic and electrophysiologic correlations. *Circulation* **50,** 948-955.

Khaiutin VM & Lukoshkova EV. (1995). [The early studies of I. P. Pavlov: the neural regulation of the blood circulation (1875-1883)]. *Fiziol Zh Im I M Sechenova* **81,** 43-55.

King TS & Coakley J. (1958). The intrinsic nerve cells of the cardiac atria of mammals and man. *J Anat* **92,** 353.

Klimaschewski L, Kummer W, Mayer B, Couraud JY, Preissler U, Philippin B & Heym C. (1992). Nitric oxide synthase in cardiac nerve fibers and neurons of rat and guinea pig heart. *Circ Res* **71,** 1533-1537.

Kmecova J & Klimas J. (2010). Heart rate correction of the QT duration in rats. *Eur J Pharmacol* **641,** 187-192.

Kobayashi Y, Okuda T, Fujioka Y, Matsumura G, Nishimura Y & Haga T. (2002). Distribution of the high-affinity choline transporter in the human and macaque monkey spinal cord. *Neuroscience Letters* **317,** 25-28.

Kojda G, Kottenberg K & Noack E. (1997). Inhibition of nitric oxide synthase and soluble guanylate cyclase induces cardiodepressive effects in normal rat hearts. *Eur J Pharmacol* **334,** 181-190.

Kong KC, Butcher AJ, McWilliams P, Jones D, Wess J, Hamdan FF, Werry T, Rosethorne EM, Charlton SJ, Munson SE, Cragg HA, Smart AD & Tobin AB. (2010). M3-muscarinic receptor promotes insulin release via receptor phosphorylation/arrestin-dependent activation of protein kinase D1. *Proc Natl Acad Sci U S A* **107,** 21181-21186.

Krasel C, Bunemann M, Lorenz K & Lohse MJ. (2005). B-arrestin binding to the β2-adrenergic receptor requires both receptor phosphorylation and receptor activation. *J Biol Chem* **280,** 9528-9535.

Kreienkamp HJ. (2002). Organisation of G-protein-coupled receptor signalling complexes by scaffolding proteins. *Curr Opin Pharmacol* **2,** 581-586.

Kruse AC, Hu J, Pan AC, Arlow DH, Rosenbaum DM, Rosemond E, Green HF, Liu T, Chae PS, Dror RO, Shaw DE, Weis WI, Wess J & Kobilka BK. (2012). Structure and dynamics of the M3 muscarinic acetylcholine receptor. *Nature* **482,** 552-556.

Kuhar MJ & Murrin LC. (1978). Sodium-dependent, high affinity choline uptake. *J Neurochem* **30,** 15-21.

Kuntz A. (1911). The evolution of the sympathetic nervous system in vertebrates. *J Comp Neurol* **21,** 215-236.

La Rovere MT, Bigger JT, Jr., Marcus FI, Mortara A & Schwartz PJ. (1998). Baroreflex sensitivity and heart-rate variability in

prediction of total cardiac mortality after myocardial infarction. ATRAMI (Autonomic Tone and Reflexes After Myocardial Infarction) Investigators. *Lancet* **351,** 478-484.

Lamas GA. (1993). Left ventricular hypertrophy in post-myocardial infarction left ventricular remodelling and in hypertension; similarities and contrasts. *Eur Heart J* **14 Suppl J,** 15-21.

Landzberg JS, Parker JD, Gauthier DF & Colucci WS. (1994). Effects of intracoronary acetylcholine and atropine on basal and dobutamine-stimulated left ventricular contractility. *Circulation* **89,** 164-168.

Lee R. (1849). On the Ganglia and Nerves of the Heart. *Philos T Roy* **139,** 43-46.

Lefkowitz RJ, Rajagopal K & Whalen EJ. (2006). New roles for β-arrestins in cell signaling: not just for seven-transmembrane receptors. *Mol Cell* **24,** 643-652.

Leonhardt H. (1986). *Internal organs. (3rd ed)* Georg Thieme Verlag, Stuttgart**.**

Levy MN. (1971a). Sympathetic-parasympathetic interactions in the heart. *Circ Res* **29,** 437-445.

Levy MN. (1971b). Sympathetic-parasympathetic interactions in the heart. *Circ Res* **29,** 437-445.

Levy MN & Martin P. (1984). Parasympathetic control of the heart. *Nervous control of cardiovascular function*. Oxford University Press (NY)**.**

Lewis ME, Al-Khalidi AH, Bonser RS, Clutton-Brock T, Morton D, Paterson D, Townend JN & Coote JH. (2001). Vagus nerve stimulation decreases left ventricular contractility in vivo in the human and pig heart. *J Physiol* **534,** 547-552.

Lin JY, Lin MZ, Steinbach P & Tsien RY. (2009). Characterization of engineered channelrhodopsin variants with improved properties and kinetics. *Biophys J* **96,** 1803-1814.

Lips KS, Pfeil U, Haberberger RV & Kummer W. (2002). Localisation of the high-affinity choline transporter-1 in the rat skeletal motor unit. *Cell Tissue Res* **307,** 275-280.

Liu JL, Murakami H & Zucker IH. (1996). Effects of NO on baroreflex control of heart rate and renal nerve activity in conscious rabbits. *Am J Physiol* **270,** R1361-1370.

Liu Y, Sun HL, Li DL, Wang LY, Gao Y, Wang YP, Du ZM, Lu YJ & Yang BF. (2008). Choline produces antiarrhythmic actions in animal models by cardiac M3 receptors: improvement of intracellular Ca2+ handling as a common mechanism. *Can J Physiol Pharmacol* **86,** 860-865.

Liu Y, Xu CQ, Jiao JD, Wang HZ, Dong DL & Yang BF. (2005). M3-R/IK(M3)-a new target of antiarrhythmic agents. *Yao Xue Xue Bao* **40,** 8-12.

Loewi O. (1921). Über humorale übertragbarkeit der herznervenwirkung. *Pflügers Archiv European Journal of Physiology* **189,** 239-242

Loewi O. (1926). Über den Vagusstoff. *Naturwissenschaften* **14,** 994-995.

Loewi O. (1936). The chemical transmission of nerve action. *Nobel Lecture*.

Loewi O & Navratil E. (1926). Über humorale Übertragbarkeit der Herznervenwirkung. *Pflüger's Archiv für die Gesamte Physiologie des Menschen und der Tiere* **214-214,** 678-688.

Lonergan T, Teschemacher AG, Hwang DY, Kim KS, Pickering AE & Kasparov S. (2005). Targeting brain stem centers of cardiovascular control using adenoviral vectors: impact of promoters on transgene expression. *Physiol Genomics* **20,** 165-172.

Lorente P, Lacampagne A, Pouzeratte Y, Richards S, Malitschek B, Kuhn R, Bettler B & Vassort G. (2000). gamma-aminobutyric acid type B receptors are expressed and functional in mammalian cardiomyocytes. *Proc Natl Acad Sci U S A* **97,** 8664-8669.

Lundberg J, Hökfelt T, Schultzberg M, Uvnäs-Wallensten K, Köhler C & Said S. (1979). Occurrence of vasoactive intestinal polypeptide (VIP)-like immunoreactivity in certain cholinergic neurons of the cat: evidence from combined immunohistochemistry and acetylcholinesterase staining. *Neuroscience* **4,** 1539-1559.

Lundberg JM & Hökfelt T. (1986). Multiple co-existence of peptides and classical transmitters in peripheral autonomic and sensory neurons-functional and pharmacological implications. *Prog Brain Res* **68,** 241.

Machhada A, Ang R, Ackland GL, Ninkina N, Buchman VL, Lythgoe MF, Trapp S, Tinker A, Marina N & Gourine AV. (2015). Control of ventricular excitability by neurons of the dorsal motor nucleus of the vagus nerve. *Heart Rhythm* **In Press**.

Mandinov L, Eberli FR, Seiler C & Hess OM. (2000). Diastolic heart failure. *Cardiovasc Res* **45,** 813-825.

Marcus H. (1909). Ueber den Sympathicus. *Sitzungsb d Gesell f Morphol u Physiol in München,* pp. 1–13.

Marina N, Abdala AP, Korsak A, Simms AE, Allen AM, Paton JF & Gourine AV. (2011). Control of sympathetic vasomotor tone by catecholaminergic C1 neurones of the rostral ventrolateral medulla oblongata. *Cardiovasc Res* **91,** 703-710.

Marina N, Abdala AP, Trapp S, Li A, Nattie EE, Hewinson J, Smith JC, Paton JF & Gourine AV. (2010). Essential role of Phox2b-expressing ventrolateral brainstem neurons in the chemosensory control of inspiration and expiration. *J Neurosci* **30,** 12466-12473.

Marina N, Tang F, Figueiredo M, Mastitskaya S, Kasimov V, Mohamed-Ali V, Roloff E, Teschemacher AG, Gourine AV & Kasparov S. (2013). Purinergic signalling in the rostral ventro-lateral medulla controls sympathetic drive and contributes to the progression of heart failure following myocardial infarction in rats. *Basic Res Cardiol* **108,** 317.

Mastitskaya S, Marina N, Gourine A, Gilbey MP, Spyer KM, Teschemacher AG, Kasparov S, Trapp S, Ackland GL & Gourine

AV. (2012). Cardioprotection evoked by remote ischaemic preconditioning is critically dependent on the activity of vagal pre-ganglionic neurones. *Cardiovasc Res* **95,** 487-494.

Mawe GM, Talmage EK, Lee KP & Parsons RL. (1996). Expression of choline acetyltransferase immunoreactivity in guinea pig cardiac ganglia. *Cell Tissue Res* **285,** 281-286.

McAllen RM & Spyer KM. (1976). The location of cardiac vagal preganglionic motoneurones in the medulla of the cat. *J Physiol* **258,** 187-204.

McAllen RM & Spyer KM. (1978a). The baroreceptor input to cardiac vagal motoneurones. *J Physiol* **282,** 365-374.

McAllen RM & Spyer KM. (1978b). Two types of vagal preganglionic motoneurones projecting to the heart and lungs. *J Physiol* **282,** 353-364.

McFarland J & Anders A. (1913). The morbid histology of the cardiac nervous ganglia. *J Medical Res* **27,** 425.

McMorn SO, Harrison SM, Zang WJ, Yu XJ & Boyett MR. (1993). A direct negative inotropic effect of acetylcholine on rat ventricular myocytes. *Am J Physiol* **265,** H1393-1400.

McWilliam JA. (1888). On the Phenomena of inhibition in the Mammalian Heart. *J Physiol* **9,** 345-i316.

Merati G, Maggioni MA, Invernizzi PL, Ciapparelli C, Agnello L, Veicsteinas A & Castiglioni P. (2015). Autonomic modulations of heart rate variability and performances in short-distance elite swimmers. *Eur J Appl Physiol* **115,** 825-835.

Ming Z, Parent R & Lavallee M. (1997). B 2-adrenergic dilation of resistance coronary vessels involves KATP channels and nitric oxide in conscious dogs. *Circulation* **95,** 1568-1576.

Misawa H, Nakata K, Matsuura J, Nagao M, Okuda T & Haga T. (2001). Distribution of the high-affinity choline transporter in the central nervous system of the rat. *Neuroscience* **105,** 87-98.

Mishra RK, Galloway JM, Lee ET, Best LG, Russell M, Roman MJ & Devereux RB. (2007). The ratio of mitral deceleration time to E-wave velocity and mitral deceleration slope outperform deceleration time alone in predicting cardiovascular outcomes: the Strong Heart Study. *J Am Soc Echocardiogr* **20,** 1300-1306.

Miura M & Okada J. (1981). Cardiac and non-cardiac preganglionic neurones of the thoracic vagus nerve: an HRP study in the cat. *Jpn J Physiol* **31,** 53-66.

Mizumaki K, Nishida K, Iwamoto J, Nakatani Y, Yamaguchi Y, Sakamoto T, Tsuneda T, Kataoka N & Inoue H. (2012). Vagal activity modulates spontaneous augmentation of J-wave elevation in patients with idiopathic ventricular fibrillation. *Heart Rhythm* **9,** 249-255.

Moncada S, Palmer RM & Higgs EA. (1991). Nitric oxide: physiology, pathophysiology, and pharmacology. *Pharmacol Rev* **43,** 109-142.

Montessuit C & Lerch R. (2013). Regulation and dysregulation of glucose transport in cardiomyocytes. *Biochim Biophys Acta* **1833,** 848-856.

Morot Gaudry-Talarmain Y, Moulian N, Meunier FA, Blanchard B, Angaut-Petit D, Faille L & Ducrocq C. (1997). Nitric oxide and peroxynitrite affect differently acetylcholine release, choline acetyltransferase activity, synthesis, and compartmentation of newly formed acetylcholine in Torpedo marmorata synaptosomes. *Nitric Oxide* **1,** 330-345.

Mullertz KM, Strom C, Trautner S, Amtorp O, Nielsen S, Christensen S, Haunso S & Jonassen TE. (2011). Downregulation of aquaporin-1 in alveolar microvessels in lungs adapted to chronic heart failure. *Lung* **189,** 157-166.

Musialek P, Lei M, Brown HF, Paterson DJ & Casadei B. (1997). Nitric oxide can increase heart rate by stimulating the hyperpolarization-activated inward current, I(f). *Circ Res* **81,** 60-68.

Nalivaiko E, Antunes VR & Paton JF. (2010). Control of cardiac contractility in the rat working heart-brainstem preparation. *Exp Physiol* **95,** 107-119.

Navaratnam V. (1965). Development of the nerve supply to the human heart. *Br Heart J* **27,** 640.

Neff RA, Wang J, Baxi S, Evans C & Mendelowitz D. (2003). Respiratory sinus arrhythmia: endogenous activation of nicotinic receptors mediates respiratory modulation of brainstem cardioinhibitory parasympathetic neurons. *Circ Res* **93,** 565-572.

Ng GA, Brack KE, Patel VH & Coote JH. (2007). Autonomic modulation of electrical restitution, alternans and ventricular fibrillation initiation in the isolated heart. *Cardiovasc Res* **73,** 750-760.

Niemela TH, Kiviniemi AM, Hautala AJ, Salmi JA, Linnamo V & Tulppo MP. (2008). Recovery pattern of baroreflex sensitivity after exercise. *Med Sci Sports Exerc* **40,** 864-870.

Nilsson S. (1976). Fluorescent Histochemistry and Cholinesterase Staining of Sympathetic Ganglia in a Teleost, Gadus morrhua. *Acta Zoologica* **57,** 69-77.

Nolan J, Batin PD, Andrews R, Lindsay SJ, Brooksby P, Mullen M, Baig W, Flapan AD, Cowley A, Prescott RJ, Neilson JM & Fox KA. (1998). Prospective study of heart rate variability and mortality in chronic heart failure: results of the United Kingdom heart failure evaluation and assessment of risk trial (UK-heart). *Circulation* **98,** 1510-1516.

Nonidez J. (1939). Studies on the innervation of the heart. I. Distribution of the cardiac nerves, with special reference to the identification of the sympathetic and parasympathetic postganglionics. *Am J Anat* **65,** 361-413.

Nonidez J. (1941). Studies on the innervation of the heart. II. Afferent nerve endings in the large arteries and veins. *Am J Anat* **68,** 151-189.

Nosaka S, Yamamoto T & Yasunaga K. (1979). Localization of vagal cardioinhibitory preganglionic neurons with rat brain stem. *J Comp Neurol* **186,** 79-92.

Nosaka S, Yasunaga K & Tamai S. (1982). Vagal cardiac preganglionic neurons: distribution, cell types, and reflex discharges. *Am J Physiol* **243,** R92-98.

O'Leary DM & Jones JF. (2003). Discharge patterns of preganglionic neurones with axons in a cardiac vagal branch in the rat. *Exp Physiol* **88,** 711-723.

Okuda T & Haga T. (2003). High-affinity choline transporter. *Neurochem Res* **28,** 483-488.

Olshansky B, Sabbah HN, Hauptman PJ & Colucci WS. (2008). Parasympathetic nervous system and heart failure - Pathophysiology and potential implications for therapy. *Circulation* **118,** 863-871.

Ondicova K & Mravec B. (2010). Multilevel interactions between the sympathetic and parasympathetic nervous systems: a minireview. *Endocr Regul* **44,** 69-75.

Ordway GA, Charles JB, Randall DC, Billman GE & Wekstein DR. (1982). Heart rate adaptation to exercise training in cardiac-denervated dogs. *J Appl Physiol Respir Environ Exerc Physiol* **52,** 1586-1590.

Pan Z, Guo Y, Qi H, Fan K, Wang S, Zhao H, Fan Y, Xie J, Guo F, Hou Y, Wang N, Huo R, Zhang Y, Liu Y & Du Z. (2012). M3 subtype of muscarinic acetylcholine receptor promotes cardioprotection via the suppression of miR-376b-5p. *PLoS One* **7,** e32571.

Panum PL. (1858). Untersuchungen iiber einige von den Moinenten, welche Einfluss auf die Herzbewegungen, auf den Stillstand und auf das Aufhoren des Contraktionsvermogens des Herzens haben. *Schmidt's Jahrb* **100,** 148.

Parhizgar F, Nugent K & Raj R. (2011). Obstructive sleep apnea and respiratory complications associated with vagus nerve stimulators. *J Clin Sleep Med* **7,** 401-407.

Patel VH, Brack KE, Coote JH & Ng GA. (2008). A novel method of measuring nitric-oxide-dependent fluorescence using 4,5-

diaminofluorescein (DAF-2) in the isolated Langendorff-perfused rabbit heart. *Pflugers Arch* **456,** 635-645.

Paterson D. (2001). Nitric oxide and the autonomic regulation of cardiac excitability. The G.L. Brown Prize Lecture. *Exp Physiol* **86,** 1-12.

Patterson S, Piper H & Starling E. (1914). The regulation of the heart beat. *J Physiol* **48,** 465-513.

Paulus WJ. (1998). How to diagnose diastolic heart failure. European Study Group on Diastolic Heart Failure. *Eur Heart J* **19,** 990-1003.

Pauza DH, Rysevaite-Kyguoliene K, Vismantaite J, Brack KE, Inokaitis H, Pauza AG, Rimasauskaite-Petraitiene V, Pauzaite JI & Pauziene N. (2014). A combined acetylcholinesterase and immunohistochemical method for precise anatomical analysis of intrinsic cardiac neural structures. *Ann Anat* **196,** 430-440.

Pauza DH, Skripka V, Pauziene N & Stropus R. (2000). Morphology, distribution, and variability of the epicardiac neural ganglionated subplexuses in the human heart. *Anat Rec* **259,** 353-382.

Paxinos G & Watson C. (1998). *The Rat Brain in Stereotaxic Coordinates*. Academic Press, San Diego.

Pfeffer JM, Pfeffer MA, Fletcher PJ & Braunwald E. (1991). Progressive ventricular remodeling in rat with myocardial infarction. *Am J Physiol* **260,** H1406-1414.

Pfeffer MA, Pfeffer JM, Fishbein MC, Fletcher PJ, Spadaro J, Kloner RA & Braunwald E. (1979). Myocardial infarct size and ventricular function in rats. *Circ Res* **44,** 503-512.

Pinsky DJ, Oz MC, Koga S, Taha Z, Broekman MJ, Marcus AJ, Liao H, Naka Y, Brett J, Cannon PJ & et al. (1994). Cardiac preservation is enhanced in a heterotopic rat transplant model by supplementing the nitric oxide pathway. *J Clin Invest* **93,** 2291-2297.

Pinsky DJ, Patton S, Mesaros S, Brovkovych V, Kubaszewski E, Grunfeld S & Malinski T. (1997). Mechanical transduction of nitric oxide synthesis in the beating heart. *Circ Res* **81,** 372-379.

Plecha DM, Randall WC, Geis GS & Wurster RD. (1988). Localization of vagal preganglionic somata controlling sinoatrial and atrioventricular nodes. *Am J Physiol* **255,** R703-708.

Polak RL. (1969). The influence of drugs on the uptake of acetylcholine by slices of rat cerebral cortex. *Br J Pharmacol* **36,** 144-152.

Porges SW. (2009). The polyvagal theory: new insights into adaptive reactions of the autonomic nervous system. *Cleve Clin J Med* **76 Suppl 2,** S86-90.

Poulsen SH, Jensen SE & Egstrup K. (1999). Longitudinal changes and prognostic implications of left ventricular diastolic function in first acute myocardial infarction. *Am Heart J* **137,** 910-918.

Priestley J. (1775). *Experiments and Observations on Different Kinds of Air: Vol. II. By Joseph Priestley*. J. Johnson.

Qian YZ, Levasseur JE, Yoshida K & Kukreja RC. (1996). KATP channels in rat heart: blockade of ischemic and acetylcholine-mediated preconditioning by glibenclamide. *Am J Physiol* **271,** H23-28.

Randall W & Wurster R. (1994). Peripheral cardiac innervation of the heart. *Vagal control of the heart: experimental basis and clinical implications Armonk (NY): Futura Publishing***,** 613-636.

Rastaldo R, Pagliaro P, Cappello S, Penna C, Mancardi D, Westerhof N & Losano G. (2007). Nitric oxide and cardiac function. *Life Sci* **81,** 779-793.

Reeves TJ & Hefner LL. (1961). The effect of vagal stimulation on ventricular contractility. *Trans Assoc Am Physicians* **74,** 260-270.

Reiter E & Lefkowitz RJ. (2006). GRKs and β-arrestins: roles in receptor silencing, trafficking and signaling. *Trends Endocrinol Metab* **17,** 159-165.

Rengo G, Zincarelli C, Femminella GD, Liccardo D, Pagano G, de Lucia C, Altobelli GG, Cimini V, Ruggiero D, Perrone-Filardi P, Gao E, Ferrara N, Lymperopoulos A, Koch WJ & Leosco D. (2012). Myocardial β(2) -adrenoceptor gene delivery promotes coordinated cardiac adaptive remodelling and angiogenesis in heart failure. *Br J Pharmacol* **166,** 2348-2361.

Richard V, Blanc T, Kaeffer N, Tron C & Thuillez C. (1995). Myocardial and coronary endothelial protective effects of acetylcholine after myocardial ischaemia and reperfusion in rats: role of nitric oxide. *Br J Pharmacol* **115,** 1532-1538.

Richter EA & Hargreaves M. (2013). Exercise, GLUT4, and skeletal muscle glucose uptake. *Physiol Rev* **93,** 993-1017.

Ringer S. (1883). A further contribution regarding the influence of the different constituents of the blood on the contraction of the heart. *J Physiol* **4,** 29-42.

Robb J & Kaylor C. (1945). The A-V Conduction System in the Heart of the Guinea Pig. *Proceedings of the Society for Experimental Biology and Medicine Society for Experimental Biology and Medicine (New York, NY)* **59,** 92-93.

Rossi L. (1994). Histlogy of cardiac vagal innervation in man. *Vagal control of the heart: experimental basis and clinical implications Armonk (NY): Futura Publishing***,** 3-20.

Rothberger CJ & Scherf D. (1930). Wirkt der Vagus auf die Kontraktionsstärke der Kammern des Säugetierherzens? *Z Ges Exp Med* **71,** 274-283.

Roy CS & Adami JG. (1891). Contributions to the Physiology and Pathology of the Mammalian Heart. *P Roy Soc Lond* **50,** 435-442.

Rozengurt E. (2011). Protein kinase D signaling: multiple biological functions in health and disease. *Physiology (Bethesda)* **26,** 23-33.

Ruffolo RR, Jr. (1987). The pharmacology of dobutamine. *Am J Med Sci* **294,** 244-248.

Sacknoff DM, Gleim GW, Stachenfeld N & Coplan NL. (1994). Effect of athletic training on heart rate variability. *Am Heart J* **127,** 1275-1278.

Salazar NC, Vallejos X, Siryk A, Rengo G, Cannavo A, Liccardo D, De Lucia C, Gao E, Leosco D, Koch WJ & Lymperopoulos A. (2013). GRK2 blockade with βARKct is essential for cardiac β2-adrenergic receptor signaling towards increased contractility. *Cell Commun Signal* **11,** 64.

Sallese M, Iacovelli L, Cumashi A, Capobianco L, Cuomo L & De Blasi A. (2000). Regulation of G protein-coupled receptor kinase subtypes by calcium sensor proteins. *Biochim Biophys Acta* **1498,** 112-121.

Salvador AF, De Aguiar RA, Lisboa FD, Pereira KL, Cruz RS & Caputo F. (2015). Ischemic Preconditioning and Exercise Performance: A Systematic Review and Meta-Analysis. *Int J Sports Physiol Perform*.

Sampaio KN, Mauad H, Spyer KM & Ford TW. (2003). Differential chronotropic and dromotropic responses to focal stimulation of cardiac vagal ganglia in the rat. *Exp Physiol* **88,** 315-327.

Sanada S, Komuro I & Kitakaze M. (2011). Pathophysiology of myocardial reperfusion injury: preconditioning, postconditioning, and translational aspects of protective measures. *Am J Physiol Heart Circ Physiol* **301,** H1723-1741.

Sarma R, Ishikawa K, Getzen JH, McNair JD, Buggs H, Johnson JL & Bing RJ. (1974). Comparison of the invasive and noninvasive measurements in coronary artery disease. *Cardiology* **59,** 114-122.

Sarnoff SJ, Brockman SK, Gilmore JP, Linden RJ & Mitchell JH. (1960). Regulation of ventricular contraction. Influence of cardiac sympathetic and vagal nerve stimulation on atrial and ventricular dynamics. *Circ Res* **8,** 1108-1122.

Schiller NB, Shah PM, Crawford M, DeMaria A, Devereux R, Feigenbaum H, Gutgesell H, Reichek N, Sahn D, Schnittger I & et al. (1989). Recommendations for quantitation of the left ventricle by two-dimensional echocardiography. American Society of

Echocardiography Committee on Standards, Subcommittee on Quantitation of Two-Dimensional Echocardiograms. *J Am Soc Echocardiogr* **2,** 358-367.

Schober KE, Fuentes VL & Bonagura JD. (2003). Comparison between invasive hemodynamic measurements and noninvasive assessment of left ventricular diastolic function by use of Doppler echocardiography in healthy anesthetized cats. *Am J Vet Res* **64,** 93-103.

Schreiner GL, Berglund E, Borst HG & Monroe RG. (1957). Effects of vagus simulation and of acetylcholine on myocardial contractility, O2 consumption and coronary flow in dogs. *Circ Res* **5,** 562-567.

Schulz R, Nava E & Moncada S. (1992). Induction and potential biological relevance of a Ca(2+)-independent nitric oxide synthase in the myocardium. *Br J Pharmacol* **105,** 575-580.

Schwartz PJ. (1998). The autonomic nervous system and sudden death. *Eur Heart J* **19 Suppl F,** F72-80.

Schwartz PJ. (2012). Autonomic modulation for chronic heart failure: a new kid on the block? *Eur J Heart Fail* **14,** 1316-1318.

Schwartz PJ, Priori SG, Cerrone M, Spazzolini C, Odero A, Napolitano C, Bloise R, De Ferrari GM, Klersy C, Moss AJ, Zareba W, Robinson JL, Hall WJ, Brink PA, Toivonen L, Epstein AE, Li C & Hu D. (2004). Left cardiac sympathetic denervation in the management of high-risk patients affected by the long-QT syndrome. *Circulation* **109,** 1826-1833.

Schwartz PJ, Verrier RL & Lown B. (1977). Effect of stellectomy and vagotomy on ventricular refractoriness in dogs. *Circ Res* **40,** 536-540.

Sears CE, Bryant SM, Ashley EA, Lygate CA, Rakovic S, Wallis HL, Neubauer S, Terrar DA & Casadei B. (2003). Cardiac neuronal nitric oxide synthase isoform regulates myocardial contraction and calcium handling. *Circ Res* **92,** e52-59.

Sears CE, Choate JK & Paterson DJ. (1998). Effect of nitric oxide synthase inhibition on the sympatho-vagal contol of heart rate. *J Auton Nerv Syst* **73,** 63-73.

Sears CE, Choate JK & Paterson DJ. (1999). NO-cGMP pathway accentuates the decrease in heart rate caused by cardiac vagal nerve stimulation. *J Appl Physiol (1985)* **86,** 510-516.

Sessa WC. (1994). The nitric oxide synthase family of proteins. *J Vasc Res* **31,** 131-143.

Shah AM. (1996). Paracrine modulation of heart cell function by endothelial cells. *Cardiovasc Res* **31,** 847-867.

Shen MJ & Zipes DP. (2014). Role of the autonomic nervous system in modulating cardiac arrhythmias. *Circ Res* **114,** 1004-1021.

Shinlapawittayatorn K, Chinda K, Palee S, Surinkaew S, Thunsiri K, Weerateerangkul P, Chattipakorn S, KenKnight BH & Chattipakorn N. (2013). Low-amplitude, left vagus nerve stimulation significantly attenuates ventricular dysfunction and infarct size through prevention of mitochondrial dysfunction during acute ischemia-reperfusion injury. *Heart Rhythm* **10,** 1700-1707.

Shusterman V, Aysin B, Gottipaty V, Weiss R, Brode S, Schwartzman D & Anderson KP. (1998). Autonomic nervous system activity and the spontaneous initiation of ventricular tachycardia. ESVEM Investigators. Electrophysiologic Study Versus Electrocardiographic Monitoring Trial. *J Am Coll Cardiol* **32,** 1891-1899.

Shvilkin A, Danilo P, Jr., Chevalier P, Chang F, Cohen IS & Rosen MR. (1994). Vagal release of vasoactive intestinal peptide can promote vagotonic tachycardia in the isolated innervated rat heart. *Cardiovasc Res* **28,** 1769-1773.

Singh S, Johnson PI, Lee RE, Orfei E, Lonchyna VA, Sullivan HJ, Montoya A, Tran H, Wehrmacher WH & Wurster RD. (1996). Topography of cardiac ganglia in the adult human heart. *J Thorac Cardiovasc Surg* **112,** 943-953.

Smatresk NJ. (1994). Respiratory Control in the Transition from Water to Air-Breathing in Vertebrates. *Am Zool* **34,** 264-279.

Smith JA, Shah AM & Lewis MJ. (1991). Factors released from endocardium of the ferret and pig modulate myocardial contraction. *J Physiol* **439,** 1-14.

Smith R. (1971a). Observations on nerve cells in human, mammalian and avian cardiac ventricles. *Anatomischer Anzeiger* **129,** 437.

Smith R. (1971b). The occurrence and location of intrinsic cardiac ganglia and nerve plexuses in the human neonate. *Anat Rec* **169,** 33-40.

Sokolski M, Rydlewska A, Krakowiak B, Biegus J, Zymlinski R, Banasiak W, Jankowska EA & Ponikowski P. (2011). Comparison of invasive and non-invasive measurements of haemodynamic parameters in patients with advanced heart failure. *J Cardiovasc Med (Hagerstown)* **12,** 773-778.

SoRelle R. (1998). Nobel prize awarded to scientists for nitric oxide discoveries. *Circulation* **98,** 2365-2366.

Spyer KM. (1994). Annual review prize lecture. Central nervous mechanisms contributing to cardiovascular control. *J Physiol* **474,** 1-19.

Spyer KM, Brooks PA & Izzo PN. (1994). Vagal preganglionic neurons supply the heart. *Vagal control of the heart: experimental basis and clinical implications Armonk (NY): Futura Publishing***,** 45-64.

Stecker EC, Reinier K, Marijon E, Narayanan K, Teodorescu C, Uy-Evanado A, Gunson K, Jui J & Chugh SS. (2014). Public health burden of sudden cardiac death in the United States. *Circ Arrhythm Electrophysiol* **7,** 212-217.

Stotler WA & Mc MR. (1947). The innervation and structure of the conductive system of the human heart. *J Comp Neurol* **87,** 57-83.

Stuesse SL. (1982). Origins of cardiac vagal preganglionic fibers: a retrograde transport study. *Brain Res* **236,** 15-25.

Sugimoto T, Itoh K, Mizuno N, Nomura S & Konishi A. (1979). The site of origin of cardiac preganglionic fibers of the vagus nerve: an HRP study in the cat. *Neurosci Lett* **12,** 53-58.

Sun Z, Tong G, Ma N, Li J, Li X, Li S, Zhou J, Xiong L, Cao F, Yao L, Wang H & Shen L. (2013). NDRG2: a newly identified mediator of insulin cardioprotection against myocardial ischemia-reperfusion injury. *Basic Res Cardiol* **108,** 341.

Swedberg K, Komajda M, Bohm M, Borer JS, Ford I, Dubost-Brama A, Lerebours G, Tavazzi L & Investigators S. (2010). Ivabradine and outcomes in chronic heart failure (SHIFT): a randomised placebo-controlled study. *Lancet* **376,** 875-885.

Szerb J. (1979). Autoregulation of acetylcholine release. In *Presynaptic receptors*, ed. Langer SZ, Starke K & Dubocovich ML, pp. 293-298. Pergamon Press, Oxford.

Tanaka K, Ohshima H, Esumi H & Chiba T. (1993). Direct synaptic contacts of nitric oxide synthase-immunoreactive nerve terminals on the neurons of the intracardiac ganglia of the guinea pig. *Neurosci Lett* **158,** 67-70.

Taylor EW. (1994). The evolution of efferent vagal control of the heart in vertebrates. *Cardioscience* **5,** 173-182.

Taylor EW, Jordan D & Coote JH. (1999). Central control of the cardiovascular and respiratory systems and their interactions in vertebrates. *Physiol Rev* **79,** 855-916.

Tcheng KT. (1951). Innervation of the dog's heart. *Am Heart J* **41,** 512-524.

Tei C, Ling LH, Hodge DO, Bailey KR, Oh JK, Rodeheffer RJ, Tajik AJ & Seward JB. (1995). New index of combined systolic and diastolic myocardial performance: a simple and reproducible measure of cardiac function--a study in normals and dilated cardiomyopathy. *J Cardiol* **26,** 357-366.

Tobin AB, Lambert DG & Nahorski SR. (1992). Rapid desensitization of muscarinic m3 receptor-stimulated polyphosphoinositide responses. *Mol Pharmacol* **42,** 1042-1048.

Torrecilla I, Spragg EJ, Poulin B, McWilliams PJ, Mistry SC, Blaukat A & Tobin AB. (2007). Phosphorylation and regulation of a G protein-coupled receptor by protein kinase CK2. *J Cell Biol* **177,** 127-137.

Tschope C & Paulus WJ. (2009). Is echocardiographic evaluation of diastolic function useful in determining clinical care? Doppler echocardiography yields dubious estimates of left ventricular diastolic pressures. *Circulation* **120,** 810-820; discussion 820.

Ullrich KJ, Riecker G & Kramer K. (1954). [Cardiac pressure-volume diagram of warm-blooded animals; isometric balance curves]. *Pflugers Arch* **259,** 481-498.

Ulphani JS, Cain JH, Inderyas F, Gordon D, Gikas PV, Shade G, Mayor D, Arora R, Kadish AH & Goldberger JJ. (2010). Quantitative analysis of parasympathetic innervation of the porcine heart. *Heart Rhythm* **7,** 1113-1119.

Van den Bos GC, Elzinga C, Westerhof N & Noble MI. (1973). Problems in the use of indices of myocardial contractility. *Cardiovasc Res* **7,** 834-848.

van Kraaij DJ, van Pol PE, Ruiters AW, de Swart JB, Lips DJ, Lencer N & Doevendans PA. (2002). Diagnosing diastolic heart failure. *Eur J Heart Fail* **4,** 419-430.

Vandecasteele G, Eschenhagen T, Scholz H, Stein B, Verde I & Fischmeister R. (1999). Muscarinic and β-adrenergic regulation of heart rate, force of contraction and calcium current is preserved in mice lacking endothelial nitric oxide synthase. *Nat Med* **5,** 331-334.

Vanoli E, Ferrari G, Stramba-Badiale M, Hull S, Foreman R, Schwartz P, Vanoli E, Ferrari G, Stramba-Badiale M, Hull S, Foreman R & Schwartz P. (1991). Vagal stimulation and prevention of sudden death in conscious dogs with a healed myocardial infarction. *Circ Res* **68,** 1471-1481.

Vassalle M, Caress DL, Slovin AJ & Stuckey JH. (1967). On the cause of ventricular asystole during vagal stimulation. *Circ Res* **20,** 228-241.

Wadley GD, Choate J & McConell GK. (2007). NOS isoform-specific regulation of basal but not exercise-induced mitochondrial biogenesis in mouse skeletal muscle. *J Physiol* **585,** 253-262.

Wang Y, Jones J, Jeggo R, Daly M, Jordan D & Ramage A. (2000). Effect of pulmonary C-fibre afferent stimulation on cardiac vagal neurones in the nucleus ambiguus in anaesthetized cats. *J Physiol* **526,** 157-165.

Wang Z, Shi H & Wang H. (2004). Functional M3 muscarinic acetylcholine receptors in mammalian hearts. *Br J Pharmacol* **142,** 395-408.

Waxman MB, Cupps CL & Cameron DA. (1988). Modulation of an idioventricular rhythm by vagal tone. *J Am Coll Cardiol* **11,** 1052-1060.

Waxman MB, Sharma AD, Asta J, Cameron DA & Wald RW. (1989). The protective effect of vagus nerve stimulation on catecholamine-halothane-induced ventricular fibrillation in dogs. *Can J Physiol Pharmacol* **67,** 801-809.

Weihe E & Reinecke M. (1981). Peptidergic innervation of the mammalian sinus nodes: vasoactive intestinal polypeptide, neurotensin, substance P. *Neuroscience letters* **26,** 283-288.

Weihe E, Reinecke M & Forssmann W. (1984). Distribution of vasoactive intestinal polypeptide-like immunoreactivity in the mammalian heart. *Cell Tissue Res* **236,** 527-540.

Wiggers CJ & Katz LN. (1922). The contour of the ventricular volume curves under different conditions. *Am J Physiol* **58,** 439-475.

Willars GB, Challiss RA & Nahorski SR. (1996). Acute regulation of the receptor-mediated phosphoinositide signal transduction pathway. *J Lipid Mediat Cell Signal* **14,** 157-168.

Wong KC, Schafer PG & Schultz JR. (1993). Hypokalemia and anesthetic implications. *Anesth Analg* **77,** 1238-1260.

Woollard HH. (1926). The Innervation of the Heart. *J Anat* **60,** 345-373.

Wu SC, Hildebrandt J, Isner PD, Pierson DJ & Bishop MJ. (1992). Efficacy of anticholinergic and β-adrenergic agonist treatment of maximal cholinergic bronchospasm in tracheally intubated rabbits. *Anesth Analg* **75,** 777-783.

Xu KY, Huso DL, Dawson TM, Bredt DS & Becker LC. (1999). Nitric oxide synthase in cardiac sarcoplasmic reticulum. *Proc Natl Acad Sci U S A* **96,** 657-662.

Yamaguchi F, Nasa Y, Yabe K, Ohba S, Hashizume Y, Ohaku H, Furuhama K & Takeo S. (1997). Activation of cardiac muscarinic receptor and ischemic preconditioning effects in in situ rat heart. *Heart Vessels* **12,** 74-83.

Yildiran T, Koc M, Bozkurt A, Sahin DY, Unal I & Acarturk E. (2010). Low pulse pressure as a predictor of death in patients with mild to advanced heart failure. *Tex Heart Inst J* **37,** 284-290.

Yutzey KE & Robbins J. (2007). Principles of genetic murine models for cardiac disease. *Circulation* **115,** 792-799.

Zang WJ, Chen LN & Yu XJ. (2005a). Progress in the study of vagal control of cardiac ventricles. *Sheng Li Xue Bao* **57,** 659-672.

Zang WJ, Chen LN, Yu XJ, Fang P, Lu J & Sun Q. (2005b). Comparison of effects of acetylcholine on electromechanical characteristics in guinea-pig atrium and ventricle. *Exp Physiol* **90,** 123-130.

Zannad F, De Ferrari GM, Tuinenburg AE, Wright D, Brugada J, Butter C, Klein H, Stolen C, Meyer S, Stein KM, Ramuzat A, Schubert B, Daum D, Neuzil P, Botman C, Castel MA, D'Onofrio A, Solomon SD, Wold N & Ruble SB. (2015). Chronic vagal stimulation for the treatment of low ejection fraction heart failure: results of the NEural Cardiac TherApy foR Heart Failure (NECTAR-HF) randomized controlled trial. *Eur Heart J* **36,** 425-433.

Zbilut JP, Murdock DK, Lawson L, Lawless CE, Von Dreele MM & Porges SW. (1988). Use of power spectral analysis of respiratory sinus arrhythmia to detect graft rejection. *J Heart Transplant* **7,** 280-288.

Zhang K, Li YF & Patel KP. (2001). Blunted nitric oxide-mediated inhibition of renal nerve discharge within PVN of rats with heart failure. *Am J Physiol Heart Circ Physiol* **281,** H995-1004.

Zhang Y, Wu J, King JH, Huang CL & Fraser JA. (2014). Measurement and interpretation of electrocardiographic QT intervals in murine hearts. *Am J Physiol Heart Circ Physiol* **306,** H1553-1557.

Zhou S, Jung BC, Tan AY, Trang VQ, Gholmieh G, Han SW, Lin SF, Fishbein MC, Chen PS & Chen LS. (2008). Spontaneous stellate ganglion nerve activity and ventricular arrhythmia in a canine model of sudden death. *Heart Rhythm* **5,** 131-139.

Zile MR. (2003). Heart failure with preserved ejection fraction: is this diastolic heart failure? *J Am Coll Cardiol* **41,** 1519-1522.

Zile MR & Brutsaert DL. (2002). New concepts in diastolic dysfunction and diastolic heart failure: Part II: causal mechanisms and treatment. *Circulation* **105,** 1503-1508.

Zuanetti G, De Ferrari GM, Priori SG & Schwartz PJ. (1987). Protective effect of vagal stimulation on reperfusion arrhythmias in cats. *Circ Res* **61,** 429-435.

Zuberi Z, Nobles M, Sebastian S, Dyson A, Lim SY, Breckenridge R, Birnbaumer L & Tinker A. (2010). Absence of the inhibitory G-protein Galphai2 predisposes to ventricular cardiac arrhythmia. *Circ Arrhythm Electrophysiol* **3,** 391-400.

Zugck C, Martinka P & Stockl G. (2014). Ivabradine treatment in a chronic heart failure patient cohort: symptom reduction and improvement in quality of life in clinical practice. *Adv Ther* **31,** 961-974.